“Deriving biodiversity-relevant forest structure parameters: The value of aerial imagery from state surveys”

Thesis submitted in partial fulfilment of the requirements
of the degree Doctor rer. nat.
of the Faculty of Environment and Natural Resources,
Albert-Ludwigs-Universität
Freiburg im Breisgau, Germany

by

Katarzyna Zielewska-Büttner

Freiburg im Breisgau, Germany
2020

Name of Dean:	Prof. Dr. Heiner Schanz
Name of 1st Supervisor and Reviewer:	Prof. Dr. Barbara Koch
Name of 2nd Supervisor:	Prof. Dr. Ilse Storch
Name of 2nd Reviewer:	Prof. Dr. Jürgen Bauhus
External advisors:	Dr. Veronika Braunisch Dr. Petra Adler
Date of thesis' defense:	25. November 2020

SUMMARY

The growing demand for bio-resources, expanding and diversifying human impacts on multiple use forests, together with effects of climate change and aerial nitrification permanently alter forests and their structure with consequences for forest biodiversity. The need to integrate forest biodiversity conservation into forest management in order to halt biodiversity loss is of highest relevance.

Given the limitations in assessing and monitoring species diversity at extensive spatial scales, the development of structural indicators linking biodiversity components (e.g. indicator species) to forest structure parameters and enabling monitoring of structural conditions is a widely discussed approach. Until recently this approach has been hampered by the lack of area-wide forest structural data. The growing availability of remotely sensed information now offers the possibility to assess forest structures across different spatial scales, from single trees to the landscape level. However, this requires the development of methods and metrics to assess and describe structural gradients and quantify the links between these metrics and selected biodiversity components.

Until recently the assessment of forest structures used mostly in forest nature conservation research was based either on terrestrial sampling and forest inventory or on visual interpretation of stereo aerial images or orthophotos. Nowadays, with changes from analogue to digital aerial imagery and a growing diversity of remote sensing (RS) data varying in resolution and extent, the processing methods focus primarily on automatic computing. This allows for the processing a large amount of data with objective and reproducible data analyses methods, and for adjustable algorithm parameters depending on the aim of the study.

In my doctoral thesis I focus on the value of remote sensing data and techniques for forest ecology research, combining the methodological development of forest structure detection methods and their application in habitat modelling for forest focal species. The methodological focus of the thesis lies on the detection of two forest structures considered highly relevant for forest biodiversity: canopy gaps (Chapter I) and standing deadwood (Chapter III). Regularly updated digital stereo aerial imagery data of state surveys (subsequently referred to as aerial imagery) and the derivatives thereof produced by Image Matching (Digital Surface Models (DSMs) and orthophotos) were used and evaluated as primary input data, as they could support a cost-efficient long-term monitoring of structural conditions and their changes. An emphasis however was put on the development of algorithms that could also be fed with data of another origin, and flexibly adjusted to the different ecological thresholds required by different taxa.

In the first study (Chapter I) an automatized gap mapping method based on Canopy Height Models (CHMs) derived from DSMs from aerial imagery and a Digital Terrain Model (DTM) based on Aerial Laser Scanning (ALS) is presented. Gaps were detected and delineated in relation to height and cover of the surrounding forest using a hybrid pixel and neighborhood based hierarchic procedure for data from two public flight campaigns (2009 and 2012). Gaps were detected with high overall accuracy (OA) of 0.9 (2009) and 0.82 (2012) and a producer's accuracy (PA) of more than 0.95 (both years), as validated by visual stereo-interpretation. Lower user's accuracy (UA) of 0.84 (2009) and 0.73 (2012)

indicated an omission error (as some gaps were not detected) that could be attributed to shadow occurrence and the height of the surrounding forest stands, with UA dropping to 0.70 (2009) and 0.52 (2012) in stands with mean vegetation heights of ≥ 8m. Open forest stands were mapped as an important interim step and side-product, as they also may be of importance for photophilic species. With an OA = 0.92 and uncertainties occurring mostly in areas of intermediate forest cover, the models for detecting this forest structure class showed high reliability. Shadow occurrence and geometric limitations of the central perspective of the aerial imagery, with resulting restrictions regarding e.g. viewing angle and image distortions towards the outer parts of an image, were recognized as the main sources of errors. To achieve a potential improvement I recommended using stereo imagery with higher overlap and resolution together with enhanced image-matching algorithms.

In Chapter II I provide a greater in-depth analysis of this topic, by explicitly addressing the limitations of aerial imagery when used as input for the detection of canopy gaps based on the method described in Chapter I. The limitations of aerial imagery become obvious when attempting to accurately map fine structures as well as areas between trees or close to the ground. To evaluate the factors affecting the mapping accuracy, gap detection maps based on data from three flight campaigns differing in image overlap and spatial and radiometric resolution were compared, each covering an approx. 1000-ha study area in the Black Forest, Germany. Gap mapping based on aerial imagery of higher spatial resolution and overlap delivered more detailed gap maps and showed higher detection accuracies. The results confirmed shadow occurrence and geometric limitations of the aerial imagery as serious issues influencing the accuracy of a CHM and consequentially the gap mapping results. Both of them can be improved by harmonizing flight times and associated solar altitude when planning flight campaigns over forested areas. Increasing the spatial resolution and overlap of the aerial imagery could considerably enhance gap detectability especially in the transition areas between high and low vegetation.

In the third study (Chapter III) I present a method for detecting standing deadwood from orthophotos and CHMs using the same aerial imagery data, with a special focus on solving the problem of misclassification between deadwood and bare ground pixels. Due to deadwood mainly occurring in extensively managed forests, as well as its frequent association with canopy openings and open and complex structured stands located in rugged terrain, bare ground is often visible nearby. Having a similar spectral signature both classes are thus prone to misclassifications. Both spectral (orthophoto) and structural (CHM) predictor variables were tested for detecting standing deadwood of more than 5 m in height. The method was calibrated in a mountain forest area encompassing strictly protected and managed forests with a significant amount of deadwood in different decay stages. In a first step, Random Forest (RF) classification was employed to assign forest pixels to one of four classes: live, declining and dead trees as well as bare ground. Two enhancing procedures, aiming at eliminating misclassifications, were then developed and compared 1) post-processing, based on morphological rules filtering out potentially misclassified deadwood pixels and isolated pixels of all classes and 2) a “deadwood-uncertainty” model quantifying and predicting the probability of a deadwood-pixel to be correctly classified based on the environmental conditions and

image texture in its neighborhood. Validation of the RF model based on data partitioning delivered both UA and PA over 0.9. Independent validation on stratified random sample, however, revealed a high commission error for deadwood mainly in areas with bare ground (UA = 0.60, PA = 0.87). Both enhancement-procedures, post-processing (1) and the "uncertainty filter" (2) improved the differentiation between the two classes and led to a more balanced relation between UA and PA of deadwood (UA = 0.69 and PA = 0.79 for (1) and UA = 0.74 and PA = 0.80 for (2)), with the filtering based on the uncertainty model (2) resulting in a substantially greater improvement.

The final chapter (Chapter IV) presents a case study on employing deadwood detection in habitat selection modelling. RS data is increasingly used for generating habitat variables that describe forest structures relevant for protected forest species, as it offers the unique potential to provide high resolution information over large geographic extents. We generated RS-based variables, especially information on standing deadwood, to model habitat suitability of the Three-toed woodpecker (*Picoides tridactylus*) in the Bavarian Forest National Park. Combined information from ALS and color-infrared (CIR) aerial imagery delivered tree-based information, such as tree type (broadleaved, coniferous), status (living, dead), as well as several tree-related metrics (e.g. tree height, projected crown area, tree volume, diameter at breast height and basal area). Generalized Additive Models (GAM) based on the single tree polygon-data, aggregated across multiple, species-relevant scales, showed that at least 8 dying or recently dead trees (the latter indicated by an average branch length of at least 2 m) within a 100 m surrounding were necessary to support woodpecker presence. In addition, and for the first time, an adverse effect of very large deadwood amounts (more than 40 - 55 dead trees within 100 m) on woodpecker occurrence was shown, making a significant contribution to the knowledge about Three-toed woodpecker ecology. The case study illustrated the great potential of the RS data to deliver reliable and meaningful input parameters for habitat models and to derive habitat thresholds that are easily applicable in forest management.

In summary, this thesis addressing several novel aspects of using the aerial imagery data in ecology research, confirms that public aerial imagery and the data products thereof, such as orthophotos and CHMs, enable the detection of forest structures and deriving ecologically relevant variables valuable for biodiversity studies. However, the methodological studies (Chapters I, II and III) showed limitations with regard to the accuracy of the vegetation heights derived from image matching and the detectability of forest gaps and standing deadwood structures in areas between tall trees and between high and low vegetation. In my thesis, I analyze these emerging problems, propose potential solutions (e.g. two alternative approaches for detecting and correcting deadwood and bare ground misclassifications, Chapter III) and discuss future research needs that would enable successful habitat modelling and deriving meaningful thresholds for forest structures to support forest biodiversity conservation (Chapter IV) based on data from aerial imagery and ALS .

ZUSAMMENFASSUNG

Die steigende Nachfrage nach biologischen Ressourcen, wachsende Ansprüche an multifunktional genutzte Wälder, die Folgen der Klimaveränderung sowie der Nitrateinträge aus der Luft, führen zu Veränderungen von Wäldern und ihrer Struktur, mit Auswirkungen auf ihre Biodiversität. Um den Artenverlust zu stoppen, ist es unerlässlich den Schutz der biologischen Vielfalt in die Waldbewirtschaftung zu integrieren. Angesichts der eingeschränkten Möglichkeiten der großflächigen Erfassung bzw. dem großflächigem Monitoring von Arten, wird die Entwicklung von Strukturindikatoren, über die Zielarten mit bestimmten Waldstrukturen verknüpft werden können, breit diskutiert. Bisher fehlten hierfür jedoch flächendeckende Waldstrukturdaten. Die wachsende Verfügbarkeit von Informationen aus der Fernerkundung bietet nun zunehmend die Möglichkeit, Waldstrukturen auf unterschiedlichen räumlichen Maßstabsebenen (vom Einzelbaum bis zur Landschaftsebene) zu erfassen. Dies erfordert jedoch die Entwicklung von Methoden und Kennzahlen für die Beurteilung und Charakterisierung von Strukturgradienten und für die Quantifizierung von Zusammenhängen zwischen Parametern und ausgewählten Biodiversitätskomponenten.

Im Rahmen der Waldnaturschutzforschung wurden Waldstrukturen bisher in der Regel mittels Forstinventuren an terrestrischen Stichprobenpunkten aufgenommen. Daneben spielte die visuelle Auswertung von Stereoluftbildern bzw. Orthophotos eine Rolle. Im Zuge der Umstellung von analogen auf digitale Luftbilder und der stetig wachsenden Vielfalt an Fernerkundungsdaten unterschiedlicher Auflösung und Ausdehnung, werden heute vorwiegend moderne, automatisierte Auswerteverfahren entwickelt. Sie ermöglichen eine objektive und reproduzierbare Verarbeitung von großen Datenmengen mit Algorithmen, deren Berechnungsparameter abhängig vom Studienziel angepasst werden können.

Thema meiner Dissertation ist die Bedeutung von Fernerkundungsdaten und -methoden für die waldökologische Forschung. Zu diesem Zweck wurden Algorithmen zur Erfassung von Waldstrukturen entwickelt, die für die Habitatmodellierung von Waldzielarten Verwendung finden können. Der methodologische Schwerpunkt der Dissertation liegt auf der Erkennung von zwei verschiedenen Waldstrukturen mit anerkannt großer Bedeutung für die Waldbiodiversität: Waldlücken (Kapitel I) und stehendes Totholz (Kapitel III). Dabei lag der Fokus auf der Nutzung von in regelmäßigen Abständen aufgenommenen digitalen Stereoluftbilder der öffentlichen Behörden (später Luftbilder genannt) und den aus ihnen mittels Image Matching erstellten Produkte, digitale Oberflächenmodelle (Digital Surface Models, DSM) und Orthophotos, da sie sich potenziell für ein kosteneffizientes langfristiges Monitoring von Waldstrukturen und deren Veränderungen eignen. Sie wurden im Rahmen der Methodenentwicklung genutzt und in ihrer Rolle als primäre Inputdaten evaluiert. Ein Ziel war jedoch die Entwicklung von Algorithmen, die mit Daten aus unterschiedlichen Quellen gespeist werden können und flexibel an ökologische Schwellenwerte und Bedürfnisse von unterschiedlichen Arten angepasst werden können.

In der ersten Studie der Dissertation (Kapitel I) wird eine automatisierte Methode zur Erkennung von Waldlücken präsentiert. Sie beruht auf Kronenhöhenmodellen (Canopy Height Models, CHMs), die

aus luftbildbasierten digitalen Oberflächenmodellen und einem digitalen Geländemodell (Digital Terrain Model, DTM) auf der Basis von ALS (Aerial Laser Scanning)-Daten berechnet wurden. Die Lücken wurden in Abhängigkeit von Höhe und Überschirmungsgrad des umliegenden Bestandes mittels eines hybriden pixel- und nachbarschaftsbasierten hierarchischen Auswertungsverfahren auf der Grundlage von zwei amtlichen Befliegungskampagnen (2009 und 2012) berechnet. Die Lückenerkennung wurde mit Hilfe einer visuellen Stereoluftbildinterpretation validiert und ergab hohe Gesamtgenauigkeiten (Overall Accuracy, OA) für beide Jahre (0.9 für 2009 und 0.82 für 2012). Die Produzentengenauigkeit (Producer's Accuracy, PA) betrug mehr als 0.95 für beide Jahre. Niedrigere Nutzergenauigkeiten (User's Accuracy, UA) von 0.84 (2009) und 0.73 (2012) deuteten auf das Nicht-Erkennen einiger Lücken hin. Dies kann mit dem Auftreten von Schatten und mit der Höhe des umliegenden Bestandes zusammenhängen, denn in Beständen mit einer mittleren Vegetationshöhe ≥ 8m wurden geringere OA=0.7 (2009) und OA=0.52 (2012) gemessen. Neben Lücken wurden als Zwischenprodukt auch lichte Waldflächen wegen ihrer Bedeutung für lichtliebende Arten mitkartiert. Mit einer OA=0.92 und Unsicherheiten, die vor allem in Bereichen mittlerer Kronenbedeckung auftraten, zeigten die Modelle eine hohe Zuverlässigkeit bei der Erkennung dieser Strukturklasse. Die Hauptursache von Fehlinterpretationen waren das Auftreten von Schatten und die geometrischen Eigenschaften der Zentralperspektive von Luftbildern mit den resultierenden Restriktionen in Bezug auf z B. unterschiedliche Blickwinkel oder Verzerrungen in den Randbereichen der Bilder. Um die Genauigkeit der Ergebnisse zu erhöhen, empfehle ich deshalb die Nutzung von Stereo Luftbildern mit größerer Überlappung und höherer Auflösung in Kombination mit verbesserten Image Matching Algorithmen.

In Kapitel II wird das Thema von Kapitel I vertieft, indem explizit auf die Limitierungen von Luftbilddaten bei der Erkennung von Waldlücken eingegangen wird. Besonders deutlich werden ihre eingeschränkten Möglichkeiten bei der Erkennung von Kleinstrukturen in Bereichen zwischen den Bäumen oder in Bodennähe. Die Einflussfaktoren auf die Kartiergenauigkeit wurden anhand von Luftbilddaten aus drei Befliegungskampagnen eines ca. 1000 ha großen Untersuchungsgebietes im Schwarzwald, Deutschland evaluiert: Dabei wurden aus Luftbilddaten, die sich hinsichtlich ihrer Bild-Überlappung sowie ihrer räumlichen und radiometrischen Auflösung unterschieden, Lückenkarten berechnet und miteinander verglichen. Luftbilder mit höherer räumlicher Auflösung und größerer Bildüberlappung lieferten detailliertere Karten und wiesen höhere Kartiergenauigkeiten auf. Die Ergebnisse bestätigten den großen Einfluss von Schatten sowie der Luftbildqualität auf die Genauigkeit von Kronenhöhenmodellen und somit auch auf die Lückenerkennung. Beides kann verbessert werden, wenn schon bei der Planung von Flugkampagnen über Waldgebieten die Flugzeiten an den Sonnenstand angepasst werden. Auch eine höhere räumliche Auflösung und größere Überlappung der Luftbilder kann die Lückenerkennung insbesondere in den Übergangsbereichen zwischen niedriger und hoher Vegetation erheblich verbessern.

Im dritten Teil der Dissertation (Kapitel III) stelle ich eine Methode zur Erfassung von stehendem Totholz aus Orthophotos und Kronenhöhenmodellen, die beide aus denselben Luftbilddaten generiert wurden, vor. Der Fokus lag hierbei auf der Suche nach Lösungen für das Problem fehlerhafter Klassifizierungen von Totholz- und Bodenpixeln. In der Umgebung von Totholz ist oft der

nackte Boden zu sehen, da Totholz im Allgemeinen häufiger in extensiv bewirtschafteten Wäldern mit Kronendachöffnungen sowie in offenen und komplex strukturierten Beständen in steilem Gelände vorkommt. Totholz- und Bodenpixel weisen eine ähnliche spektrale Signatur auf, so dass es zu Fehlklassifizierungen zwischen beiden Klassen kommen kann. In dieser Studie wurden sowohl spektrale (Orthophoto) als auch strukturelle (CHM) Prädiktorvariablen für die Erkennung von stehendem Totholz ab 5m Höhe getestet. Die Methode wurde in einem Bergwaldgebiet, an unbewirtschafteten und bewirtschafteten Waldflächen kalibriert, in denen jeweils erhebliche Mengen an Totholz in unterschiedlichen Zersetzungsstadien vorkamen. Im ersten Modellierungsschritt wurde der Random Forest (RF) Klassifizierungsalgorithmus verwendet, um die Waldpixel in vier Klassen zu klassifizieren: lebende und absterbende Bäume, stehendes Totholz sowie sichtbarer Boden. Um falsche Klassifizierungen zu korrigieren wurden zwei Optimierungsverfahren entwickelt und miteinander verglichen: 1) ein Post-Processing Verfahren basierend auf morphologischen Regeln zur Filterung von potenziell fehlklassifizierten Totholzpixeln und isoliert vorkommenden Pixeln der anderen Klassen und 2) ein „Totholz-Unsicherheits-Model“ zur Quantifizierung und Vorhersage der Wahrscheinlichkeit einer korrekten Klassifizierung der Totholzpixel in Abhängigkeit von Umweltbedingungen und der Bildtextur in der Nachbarschaft. Die Validierung des RF-Models mittels eines Evaluierungsdatensatzes, der auf einer Datenpartitionierung basierte, lieferte UA- und PA-Werte über 0.9. Eine unabhängige Validierung anhand eines Evaluierungsdatensatzes basierend auf einer stratifizierten Zufallsstichprobe zeigte jedoch einen großen Anteil falsch-positiv bestimmter Totholzpixel, meistens in Bereichen mit sichtbarem Boden (UA=0.60, PA=0.87). Beide Verfahren, Post-Processing (1) und “Totholz-Unsicherheits-Filter“ (2), führten zu einer besseren Unterscheidung zwischen den beiden Klassen und zu einem ausgewogeneren Verhältnis zwischen UA und PA für Totholz (UA = 0,69 und PA = 0,79 für (1) und UA = 0,74 und PA = 0,80 für (2)), wobei der „Totholz-Unsicherheits-Filter“ (2) zu wesentlich besseren Resultaten führte.

Im letzten Kapitel (Kapitel IV) wird eine Fall-Studie für die Verwendung fernerkundungsbasierter Totholzdaten in Habitatmodellen vorgestellt. Fernerkundungsdaten werden immer häufiger für die Herleitung von Habitatvariablen eingesetzt, die relevante Strukturen für geschützte Waldarten beschreiben. Sie haben den großen Vorteil, dass sie großflächige und zugleich hochaufgelöste Informationen liefern. Aus einer Kombination von ALS-Daten und Colorinfrarot-Luftbildern aus dem Nationalpark Bayerischer Wald, Deutschland, wurden Einzelbaum-Parameter wie Baumart (Nadel- oder Laubbaum), Status (Lebend, Tot) und weitere Baum-bezogene Attribute (z.B. Baumhöhe, projizierte Kronenfläche, Baumvolumen, Brusthöhendurchmesser oder Grundfläche) hergeleitet. Diese Variablen, insbesondere die über stehendes Totholz, wurden zur Modellierung der Habitateignung für den Dreizehenspecht (*Picoides tridactylus*) im Nationalpark Bayerischer Wald genutzt. Dabei wurden Informationen aus den Polygondaten von Einzelbäumen auf mehreren artrelevanten räumlichen Ebenen aggregiert und als Prädiktoren in einem Generalisierten Additiven Model (GAM) getestet. Es zeigte, dass mindestens acht stehende tote Bäume (Hier definiert als Totholz mit einer durchschnittlichen Astlänge ≥ 2 m) innerhalb eines 100 m Radius nötig sind, um die Wahrscheinlichkeit für das Vorkommen des der Art signifikant zu erhöhen. Als neuer und

bedeutsamer Beitrag zur Ökologie des Dreizehenspechts konnte zum ersten Mal zusätzlich auch ein oberer Totholz-Schwellenwert für das Vorkommen des Dreizehenspechts ermittelt werden: Ab 40-55 Totholzbäumen pro Hektar innerhalb des 100 m Radius um den Beobachtungspunkt, sank die Vorkommenswahrscheinlichkeit wieder. Diese Fall-Studie unterstreicht das große Potenzial von Fernerkundungsdaten für ökologische Studien: Sie liefern verlässliche und aussagekräftige Variablen für die Habitatmodellierung und können zur Ableitung ökologischer Schwellenwerte genutzt werden, die direkt in der Waldbewirtschaftung Verwendung finden können.

Zusammenfassend bestätigt diese Arbeit, die sich mit verschiedenen Aspekten der Nutzung von Luftbilddaten für die ökologische Forschung beschäftigt, dass auf Grundlage von amtlichen Luftbildern und Produkten daraus (Orthophotos und Kronenhöhenmodelle) sowohl die automatisierte Erfassung von Waldstrukturen, als auch die Ableitung von ökologisch relevanten, und wertvollen Variablen für die Biodiversitätsforschung möglich ist. Die methodischen Studien (Kapitel I, II und III) zeigten jedoch auch die Grenzen von Fernerkundungsdaten auf, hinsichtlich der Genauigkeit der Vorhersage von Vegetationshöhen aus dem Image Matching, der Erkennbarkeit von Waldlücken sowie von stehendem Totholz, insbesondere in hohen Beständen und im Grenzbereich zwischen hoher und niedriger Vegetation. In meiner Dissertation analysiere ich diese Probleme, schlage mögliche Lösungen vor (z.B. zwei alternative Ansätze zur Erkennung und Korrektur von Fehlklassifizierungen zwischen Totholz und Bodenpixel (Kapitel III)) und diskutiere den zukünftigen Forschungsbedarf. Der Einsatz von Luftbild- und ALS-Daten (Kapitel IV) für Habitatmodelle und zur Identifikation bedeutsamer ökologischer Schwellenwerte für Waldstrukturen könnte so den Biodiversitäts- und Waldnaturschutz voranbringen.

To my husband

To my girls

To my parents

PREFACE

The idea for this dissertation grew over the last 10 years, during which time I worked on various applied projects in the field of remote sensing and nature conservation all over Europe. It evolved fully after I came back to the FVA to work on the development of automated remote sensing methods for the detection of selected biodiversity-relevant forest structure parameters.

My earlier work experience both in research and monitoring in protected areas, including visual aerial imagery interpretation for nature protection purposes, was advantageous for designing the framework of this Thesis. Having already an idea about the needs of forest nature conservation regarding forest structure parameters and knowing the potential of remote sensing data and the techniques to acquire meaningful information, my aim was to elucidate the value of publicly acquired aerial imagery for deriving forest structure parameters as input for species habitat modelling and other forestry applications.

The study was carried out as a part of my work at the Forest Research Institute (FVA), in the Department of Forest Nature Conservation, Forest Nature Reserves Research Group under internal scientific supervision of Dr. Veronika Braunisch and Dr. Petra Adler. This was possible due to the cooperation between the FVA and Freiburg University, supporting the scientific exchange between these organizations.

Scientific and formal supervision was assured by Prof. Dr. Barbara Koch, Chair of Remote Sensing and Landscape Information Systems (FELIS), as principal supervisor, and Prof. Dr. Ilse Storch, Chair of Wildlife Ecology and Management, as second supervisor. The last chapter of the thesis (Chapter IV) resulted from a scientific cooperation with Prof. Dr. Jörg Müller, Biocenter, University of Würzburg and Deputy Head of the Bavarian Forest National Park and Head of the conservation and research department and Associate Prof. Dr. Marco Heurich, Chair of Wildlife Ecology and Management, University of Freiburg and Head of the Department of Visitor Management and National Park Monitoring, Bavarian Forest National Park.

AKNOWLEDGMENTS

I thank Prof. Dr. Barbara Koch, the head of the Chair of Remote Sensing and Landscape Information Systems (FELIS) at the Albert-Ludwigs-University of Freiburg, for the scientific and academic supervision of my work. Your support of my project also in times of my maternity leave and acceptance of my independent way of work while giving valuable advices meant very much to me.

I would also like to thank Prof. Dr. Ilse Storch for being the second supervisor of this thesis and Prof. Dr. Jürgen Bauhus for agreeing to be the second examiner.

My greatest “thank you” I address to Dr. Vero Braunisch for your constant support, both scientific and organizational throughout the time of our collaboration. Thank you for your always positive motivation that gave me energy to give my best. I appreciate to be a part of your research group, benefiting and learning from your broad ecological knowledge, scientific experience and your leading skills creating highly enjoyable and supportive working environment while keeping high working standards.

My deep gratitude also extends to Dr. Petra Adler, the second external advisor of this thesis, who supported me very much with her broad remote sensing and photogrammetry knowledge and research experience related closely to forest practice. Your wise advises on solution finding during our methodological discussions and your always cool view on my overall working and family situation helped me at multiple times to clarify my mind and to find a good way forward, without losing track of the important things of life on the way.

Dr. Jörg Kleinschmit, the head of the Department of Forest Nature Conservation (WNS) at the FVA, I thank for the support to my dissertation carried within a framework of the FVA project. To my colleagues from the WSG-research group and the WNS Department, “Thanks a lot” for very friendly and motivating working atmosphere that made me coming to work with pleasure every day. Special “thanks” to Anne, Marlotte, Lucia, Flici, Vanessa, Charalambos, Hans-Gerd and Julia for your faith in me and interest in my work and my state of mind. Anne, thank you also for proofreading of the german “Zusammenfassung”.

To all who contributed to this work (if not mentioned yet): Michaela Ehmann, Ruben Beck, Joao Paulo Pereira, Sven Kolbe, Johannes Brändle, Lisa Ganter, and Miguel Kohling I express my big gratitude. You were all a huge support with your hard work on method development, validation or adaptation of the processing algorithms to tile-wise large dataset processing. Thank you! It was enrichment for me to work with you!

Thanks to the remote sensing team der FVA for sharing your knowledge and interest to work with remote sensing data with me. Selina, thank you also for your contribution to Figure 1-2 of this dissertation and Melanie, for your advice regarding image matching methodology.

Graduate School of the University of Freiburg I thank for the opportunity to use its supportive and motivating events in the final phase of my dissertation.

Dr. Jana Chmielewski and Dr. Franka Brüchert I thank for being great supervisors during my previous employments showing me the fun and sense of the scientific work. Prof. Dr. Jörg Müller and ass. Prof. Dr. Marco Heurich from the National Park Bavarian Forest I thank for very constructive and uncomplicated cooperation on Chapter IV of this thesis and your inspiring enthusiasm for the nature conservation and research in that field.

Finally and most importantly I would like to thank my husband, Matthias, for your full support and faith in me, your flexibility and for keeping my other duties to a minimum so that I could work as much as necessary to finish this dissertation. To my daughters, Ana Malina and Helen: Thank you for your patience and your endless love that gave me new energy every day. To my loving parents, extended family and my friends, especially to Alicia, Corinna, Franziska und Sałatka: Many, many thanks for being there for me, distracting me, chilling with me and motivating me when I needed it. Lastly, thank you, Heidi, for your support in these Corona-times.

ABBREVIATIONS

Abbreviation	Description
2D, 3D	Two-dimensional, Three-dimensional
AIC	Akaikes Information Criterion
ALS	Airborne Laser Scanning
AUC	Area Under the Receiver Operating Characteristic (ROC) Curve
BA	Basal Area
BRDF	Bidirectional Reflectance Distribution Function
B_I_ratio	Blue to all bands ratio
CCR	Correct Classification Rate
CHM	Canopy Height Model (synonym to nDSM in forested areas)
CI	Confidence Interval
CIR	Color-Infrared
CNN	Convolutional Neural Networks
CTREE	Conditional Inference Trees
DBH	Diameter at the Breast Height
DEM	Digital Elevation Model (synonym for DTM)
DL	Deep Learning
DSM	Digital Surface Model
DTM	Digital Terrain Model
FAO	Food and Agriculture Organization of the United Nations
FELIS	Dept. of Remote Sensing and Landscape Information Systems, Albert-Ludwigs University Freiburg, Germany
FVA	Forest Research Institute Baden-Württemberg in Freiburg, Germany
GAM	Generalized Additive Model
GIS	Geographical Information System
GLM	Generalized Linear Model
GLCM	Grey-Level Co-occurrence Matrix
HSM	Habitat Suitability Model
HSV	Hue, Saturation, Value
IDW	Inverse Distance Weighting
IPBES	Intergovernmental Platform on Biodiversity and Ecosystem Services
LAS	Data file format containing LiDAR point data records
LFV	State Forest Administration of Baden-Württemberg, Germany
LGL	State Agency of Spatial Information and Rural Development of Baden-Württemberg, Germany
LiDAR	Light Detection and Ranging
ML	Machine Learning
N	Amount of observations

NA	Not Applicable / Not Available (i.e. no data)
NATURA 2000	European (European Union's) network of protected areas
nDSM	normalized Digital Surface Model
NDVI	Normalised Difference Vegetation Index
NIR	Near Infrared
NPV	Negative Prediction Value
OA	Overall Accuracy
OBIA	Object-Oriented Image Analysis
PA	Producer's Accuracy
PPV	Positive Prediction Value
R	R statistic software
R_ratio	Red to all bands ratio
RF	Random Forest
RGBI	Red, Green, Blue, Infrared spectral bands
ROC	Receiver Operator Curve
RS	Remote Sensing
RQ	Research Question
SD	Standard Deviation
SDM	Species Distribution Model
SGM	Semi-Global Matching
SVM	Support Vector Machine
SWIR	Short Wave Infrared
TreMs	Tree Related Microhabitats
TTW	Three-toed woodpecker
UA	User´s Accuracy
UAV	Unmanned Aerial Vehicle
VHR	Very High Resolution (satellite data of resolution of 1m or less)
VOL	Tree volume

LIST OF PAPERS

The chapters presented in this doctoral thesis represent four original papers that were written as stand-alone scientific papers. Chapters I, III and IV were published or are currently under review at international research journals for publication as open-source papers under open access common rights. Chapter II was published as a conference paper and is presented in this thesis with the agreement of the conference organizer. All papers are included in full length in the paper section of this dissertation and formatted according to the style of this thesis.

Chapter I: *Zielewska-Büttner, K.; Adler, P.; Ehmann, M.; Braunisch, V. (2016). Automated Detection of Forest Gaps in Spruce Dominated Stands Using Canopy Height Models Derived from Stereo Aerial Imagery. Remote Sens., 8, 175.*

Zielewska-Büttner, K.; Adler, P.; Ehmann, M.; Braunisch, V. (2017). Erratum: Zielewska-Büttner, K.; Adler, P.; Ehmann, M.; Braunisch, V. (2016). Automated Detection of Forest Gaps in Spruce Dominated Stands Using Canopy Height Models Derived from Stereo Aerial Imagery. Remote Sens., 8, 175. Remote Sens. 9, 471.

Chapter II: *Zielewska-Büttner, K., Adler, P., Peteresen, M., Braunisch, V. (2016). Parameters Influencing Forest Gap Detection Using Canopy Height Models Derived From Stereo Aerial Imagery. In: Kersten, T.P. (Ed.), 3. Wissenschaftlich-Technische Jahrestagung der DGPF. Dreiländertagung der DGPF, der OVG und der SGPF. Publikationen der DGPF, Bern, Schweiz, pp. 405-416.*

Chapter III: *Zielewska-Büttner, K., Adler, P., Kolbe, S., Beck, R., Ganter, L., Koch, B., Braunisch, V.. Detection of Standing Deadwood from Aerial Imagery Products: Two Methods for Addressing the Bare Ground Misclassification Issue. Forests 2020, 11, 801.*

Chapter IV: *Zielewska-Büttner, K.; Heurich, M.; Müller, J.; Braunisch, V. (2018). Remotely Sensed Single Tree Data Enable the Determination of Habitat Thresholds for the Three-Toed Woodpecker (Picoides tridactylus). Remote Sens., 10, 1972.*

In addition, some work conducted in the framework of this doctoral thesis fed into the publication below:

Ackermann, J.; Adler, P.; Aufreiter, C.; Bauerhansl, C.; Bucher, T.; Franz, S.; Engels, F.; Ginzler, C.; Hoffmann, K.; Jütte, K.; Kenneweg, H.; Koukal, T.; Martin, K.; Oehmichen, K.; Rüffer, O.; Sagischewski, H.; Seitz, R.; Straub, C.; Tintrup, G.; Waser, L.; Zielewska-Büttner, K., (2020): Oberflächenmodelle aus Luftbildern für forstliche Anwendungen. Leitfaden. AFL 2020. WSL Bern. 87. p. 60.

CONTENTS

1 INTRODUCTION

1.1 Fundamental idea

"Nature and its vital contributions to people, which together embody biodiversity and ecosystem functions and services, are deteriorating worldwide" (IPBES, 2019). Forest ecosystems cover 30.6 % of the world's land area and are among the most important repositories of biodiversity and providers of ecosystem services on earth (FAO, 2018). However, forests have been exploited continuously throughout history leading to simplification in forest structure, deterioration of the biomass resources and shrinking area of the natural forests. These changes have altered forest biodiversity and contributed a growing list of rare, endangered or even extinct forest species across the globe.

To save the remaining forest species dedicated conservation efforts are needed. However, the conservation of forest biodiversity is challenging and often seen as a competitor for other uses, as the large part of the world's forests are managed for wood production or other economic, environmental, or cultural values (Felton *et al.*, 2019). Effective forest biodiversity conservation requires reliable information at relevant spatial scales pertaining to species' occurrence, their habitat requirements and the forest structures that species rely on. From a broader perspective, conservation measures must therefore target forest structural elements at different spatial scales, and provide large and medium-sized protected areas or smaller, integrative conservation elements, within forests actively managed for economic goals (Lindenmayer and Franklin, 2002).

In recent years, two main research pathways on the assessment of biodiversity relevant forest structures have been observed: Defining and mapping of visible forest structures such as crown cover, forest gaps or deadwood occurrence, which are tangible from a human perceptive; and the development of statistical indices that capture the structures in a mathematical or geometrical way, but are not necessary easily understandable for human perception (Frey *et al.*, 2019). Such statistical indices may correlate with species occurrence and be important for gaining new knowledge; but are not easily transferable into practice. From the perspective of a forest manager clear and simple indicators for the quality and quantity of well-definable structures are needed.

Due to the rapid technical development in RS in the past two decades, a wide variety of data with different qualities and specialties are now offered, with continuously growing capacities for faster and larger data acquisition, evaluation and storage. Despite the broad variety of available RS data, the focus of this thesis is on the use of digital stereo aerial imagery (hereafter referred to as aerial imagery) and the evaluation of its suitability for biodiversity studies, with the aim to develop widely

applicable methods for forest research and management. Aerial imagery data has been used for decades in the planning of forestry operations (Ackermann *et al.*, 2012), is often available for free to research and forest administration, and provides high resolution (0.1 - 0.2 m) information on vegetation cover across large areas.

Combining these two aspects is difficult as often a gain in area coverage is at the cost of the image resolution. With the very fast technical and methodological development e.g. some very high resolution (VHR) satellite imagery provides a large-scale resolution of 0.5 - 1 m, but not free of charge) data quality is often not standardized. Moreover, it is not always possible for satellites to deliver cloud free data, whereas the airplanes can schedule their flights on demand and acquire images below clouds. It is also important to mention data from Airborne Laser Scanning (ALS, also referred to as airborne Light Detection and Ranging or LiDAR), as it is used as a standard in many countries (e.g. Scandinavia) in forest applications and delivers very precise surface heights. This data is often referred to in this thesis as an alternative or complementary to aerial imagery.

Two forest structures, forest gaps (1) and deadwood (2), are frequently in the focus of forest ecological studies as they play a key role in forest regeneration processes (Getzin *et al.*, 2014; Meyer *et al.*, 2017) and are considered key habitat elements for many forest species depending of semi open habitats (1) (Sierro *et al.*, 2001; Zellweger *et al.*, 2013), saproxylic species (2) (Müller *et al.*, 2005), birds and bats (Bouvet *et al.*, 2016). In addition there are several remote sensing studies related to mapping these structures (Bütler and Schlaepfer, 2004; Hobi *et al.*, 2015; Polewski *et al.*, 2015c; White *et al.*, 2018). They often focus, however, on small to regional project-specific scales encompassing on the most part an area from few hectares up to several hundreds of square kilometers in size, with the latter usually being large protected areas e.g. National Parks (Krzystek *et al.*, 2020)

The aim of this thesis is to develop automated, standardized but also flexible and adjustable methods allowing the detection of forest gaps and standing deadwood across large spatial scales (thousands of square km) and at high spatial resolution. Another aim of this doctoral thesis is to evaluate the suitability of the aerial imagery based mapping results for ecological studies. In a case study on the deadwood requirements of the Three-toed woodpecker, the applicability of deadwood parameters derived from the remote sensing was tested and compared to the results of several studies based on terrestrial data.

1.2 Forest structures and biodiversity

Forests are important ecosystems that on one hand accommodate a vast number of terrestrial species and provide non-economic ecosystem services to the society, and on the other hand deliver timber and other products of high monetary values. Combining the different economic, ecological and societal functions of forests puts them and the biodiversity they host under pressure (Messier *et al.*, 2015). This is one of the reasons forest successional phases that are economically unviable (e.g. old-growth and decay stages), have become rare in western European forest landscapes (Scherzinger, 1996), are becoming rare around the world, and with them the species that depend on their specific structures (Barlow *et al.*, 2016; Betts *et al.*, 2017). As a consequence, a multitude of nature conservation programs for rare or endangered forest species, have been developed in the past decades at local, regional (Schaber-Schoor *et al.*, 2015), country (Bundesministerium für Umwelt Naturschutz, Bau und Reaktorsicherheit, 2007) and international scale (Beatty *et al.*, 2018).

Every species requires specific habitat conditions that consist of abiotic and biotic factors (ecological niche concept (Guisan and Thuiller, 2005; Hirzel and Le Lay, 2008)). Many of these factors cannot be changed (e.g. climate, terrain) or are difficult to influence (e.g. air quality, species interactions), thus – to promote a given species – conservation programs focus on changing the parameters that are easiest to influence. With regard to forest species, forest management including forest nature conservation practices can alter the situation in the field and improve habitat conditions (Gustafsson *et al.*, 2012; Leberger *et al.*, 2020). As the development of conservation programs is not possible for all species, surrogate species, for example species with supposed umbrella (Lambeck, 1997) or key-stone function (sensu Thompson and Angelstam (1999)), are often chosen as focal species. The intention is to support several other species of the associated species community through habitat enhancement and management for the selected species (Magg *et al.*, 2019). To achieve this aim, precise, area-wide information on the abundance, distribution and main characteristics of the key habitat structures for the focal species is required at relevant spatial scales.

1.2.1 The investigated forest structure parameters

Forest species require stand structures that differ in terms of type, quantity and quality. In past decades a close relationship has been identified between endangered forest species and forest structures representing forest development phases that are rare in current European forests due to the prevailing management regime, such as late successional stages with large old trees (habitat, veteran trees), standing and lying deadwood, or open forest structures and forest gaps with regeneration, as produced by natural disturbance regimes (Müller *et al.*, 2005; Seibold *et al.*, 2014;

Bässler, 2015). Recently, there has been an increase in interest in other landscape-scale structures such as vertical and horizontal forest heterogeneity (Zellweger *et al.*, 2013; Hofstetter *et al.*, 2015) or forest edges (Pfeifer *et al.*, 2017) and smaller and dispersed structural elements such as trees with micro habitats (TREMs) (Bütler *et al.*, 2013; Regnery *et al.*, 2013) as their importance for biodiversity has become widely recognized.

Forest structure can be mapped and quantified at different spatial scales ranging from tree-related micro-structures to stand- or landscape-scale characteristics. It is however not always easy or even possible to map, quantify and characterize structures at a relevant (e.g. species-relevant) level of detail and required spatial extent, i.e. at fine resolution over big areas. Depending on the extent and characteristics of the structural element, different mapping methods are required. Remote sensing might be a good solution for area-wide mapping of structures detectable from the air (e.g. to assess the canopy cover percentage and the canopy cover heterogeneity or the occurrence of forest gaps), whereas field sampling methods currently offer the only feasible way to inventory TreMs.

The methodological part of this work focuses on the tree-scale (in other words: on the object scale) when aiming at the detection of deadwood and forest gaps. This is in line with the forest manager's unit, the tree, and with his or her wish for tangible, understandable and easily identifiable forest structures, that can be incorporated into the planning of forest operations and nature conservation measures.

1.2.1.1 Forest gaps

Canopy cover and forest gaps are forest structure elements that are considered important for photophilic components of forest biodiversity, i.e. for animal and plant species that depend on (semi) open habitats (Sierro *et al.*, 2001; Müller and Brandl, 2009; Zellweger *et al.*, 2013). The simplification of forest structures with the establishment of even-aged forest stands in the nineteen and twentieth century (Boncina, 2011), and the shift towards close-to-nature forestry with continuous forest cover at the end of twentieth century (Johann, 2006) led to the underrepresentation of the early and late phases of succession, where canopy gaps and open stands naturally occur (Scherzinger, 1996). This trend was supported by the cessation – or even legal prohibition – of historical forest use practices, such as forest pasturing, litter raking or coppicing.

Various photophilic forest focal species thus require the active creation of open stands or forest gaps with abundant sun light on the ground. Gaps in the canopy also create inner forest edges, which, for example, bats use for foraging and as guiding structures for navigation during the flight (Patriquin and Barclay, 2003; Runkel, 2008). Canopy openings also play a key role in stand regeneration

processes where the light regime is the main driver for the composition and the diversity of the understory biota (Getzin *et al.*, 2014).

Many forest biodiversity and nature conservation programs (Braunisch and Suchant, 2013; Schaber-Schoor *et al.*, 2015), developed in the recent years therefore underline the importance of canopy gaps and list their creation and maintenance as one of the objectives for promoting forest focal species and natural forest regeneration. Since the quality and quantity of the structural elements are of importance, effective species conservation management requires taxon-specific information on the required size, form, distribution and connectivity of gaps.

1.2.1.2 Standing deadwood

Deadwood is a forest structure parameter with long-recognized significance for forest biodiversity (Thorn *et al.*, 2019), (Hahn and Christensen, 2004), (Schuck *et al.*, 2004), (Paillet *et al.*, 2010). Among forest species, 20-25 % depend on deadwood (Herrmann and Bauhus, 2010). Similar to forest gaps deadwood is typical for late development phases and as a result of natural disturbances, which are rarely tolerated under most forestry regimes. Deadwood is thus underrepresented in managed forest ecosystems.

As a consequence, many deadwood enrichment programs in managed forest landscapes have been initiated in the past 30 years, e.g. in Europe and Germany in recent 30 years (Schaber-Schoor, 2010). An effective implementation of these programs, however, requires knowledge regarding the amount and distribution of deadwood elements in forests at relevant scales (Braunisch, 2008; Stighäll *et al.*, 2011; Kortmann *et al.*, 2018a). Mapping of deadwood and delivering information on its quantity is thus essential, while complementary information on tree species and stages of decay is also desirable in order to address the species requirements more precisely.

Standing or lying, fresh or in progressive stage of decay, deadwood provides habitat for a considerable number of species. Deadwood delivers microhabitats, substrate for lichens, bryophytes (Djupstrom *et al.*, 2010) and fungi (Bader *et al.*, 1995; Baldrian *et al.*, 2016; Olchowik *et al.*, 2019) and releases nutrients for the growth of a new generation of trees Albrecht (1991). In various stages of decay it hosts various rare species of saproxylic beetles (Müller *et al.*, 2005; Seibold *et al.*, 2014) and in the early decay stages it is an attractive resource for woodpeckers that feed on bark beetles dwelling in weakened, dead or dying trees (Fayt, 2003; Pechacek and Krištín, 2004; Balasso, 2016). Numerous cavity nesters such as forest birds, fat dormice or bats (Virkkala, 2006) use cavities in deadwood, natural or created by woodpeckers, as shelter. Bats also utilize the cracks in dying or dead trees or bark straps as their roosting places (Kortmann *et al.*, 2018b).

Depending on the size of species' home range, different spatial scales of deadwood occurrence may be of relevance. Moreover, the species' specific requirements regarding deadwood-quality define the necessary detail of deadwood mapping. For some species a rough approximation of the deadwood amount is a sufficient proxy while for others a precise detection of a particular deadwood type (e.g. standing or lying, in a certain decay stage or of a particular tree species) is needed for accurately targeting the species needs (Balasso, 2016; Vogel *et al.*, 2020).

1.3 Remote sensing in forest ecology studies

Remote sensing data and techniques have become a common source of information in forest research and management, including a variety of topics from forest growth and timber production (Holopainen *et al.*, 2014; White *et al.*, 2016) to habitat modelling for selected species (Imbeau and Desrochers, 2002; Graf *et al.*, 2009) and nature conservation purposes (Bässler *et al.*, 2010; Corbane *et al.*, 2015).

They offer numerous advantages for the collection of data on forest structures detectable from the air such as standing canopy deadwood, canopy cover or forest gaps. Main assets are continuous area-wide information, large spatial coverage as well as automated and standardized detection methods (Wulder *et al.*, 2006; Heurich *et al.*, 2015) founded on a long tradition and established standards of visual interpretation of orthophotos and stereo aerial imagery (AFL, 2003; Ackermann *et al.*, 2012).

1.3.1 Data requirements

When mapping of biodiversity relevant forest structure parameters matters, the level of detail is of importance. Many species rely on very specific structures, sometimes of very small size that need to be mapped with high level of detail (Basile *et al.*, 2020), whereas for other species a magnitude of the occurrence of a given structure in large area units is sufficient (Økland *et al.*, 1996). In contrast, international or global applications, e.g. forest cover mapping or land cover change detection require generalized data across large geographical scales (Seebach, 2013). Most forestry applications and biodiversity research require trade-off between resolution and extent, as the highest possible detail is desired for an extensive area-coverage.

Such area-wide information on relevant forest structures is important especially for predicting species' habitats, or identifying areas for nature conservation measures (Rechsteiner *et al.*, 2017). In this respect the continuous digital data and automated mapping methods from remote sensing have an advantage over inventory procedures, which deliver only punctual information. The latter

however are crucial as training and validation data to complement the remote sensing data to reveal its full potential.

1.3.2 Structure information for practical application

Effective biodiversity conservation requires solid information on species requirements accompanied with information on the structures the species are dependent on. Assessing the occurrence, quantity and quality of biodiversity-relevant forest structures helps to target the nature conservation goals.

Recently new indices have been developed based on remote sensing data and purely mathematical concepts to describe forest structure richness and diversity (Ehbrecht *et al.*, 2017; Frey *et al.*, 2019). They are important to open new research perspectives and acquire new knowledge on general relationships between species and forest structural patterns. From the forest or conservation manager's perspective, however, well measurable and definable goals for structures that can be identified during planning of forest operations are necessary to assure an effective implementation in practice.

1.3.3 Potential and limitations of remote sensing data

RS data of different spatial resolutions offer different levels of detail and generalization (Figure 1-1).

Frey (2019) categorized the opportunities of remote sensing by its range into: 1) long-range spaceborne remote sensing, usually based on instruments carried by satellites, with flight altitudes of hundreds to thousands of kilometers and resolutions from below 1 m to several hundred meters, 2) medium-range remote sensing, usually airborne (carried by airplanes or larger Unmanned Aerial Vehicles (UAVs)) at altitudes between hundreds of meters to some kilometers, resulting in products of decimal resolution, 3) close-range remote sensors (laser scanning or digital photogrammetry systems), based on the ground or mounted on mobile vehicles or UAVs, covering small ranges, e.g. single forest sites of up to few hectares and delivering very detailed products with resolutions of some centimeters or even millimeters.

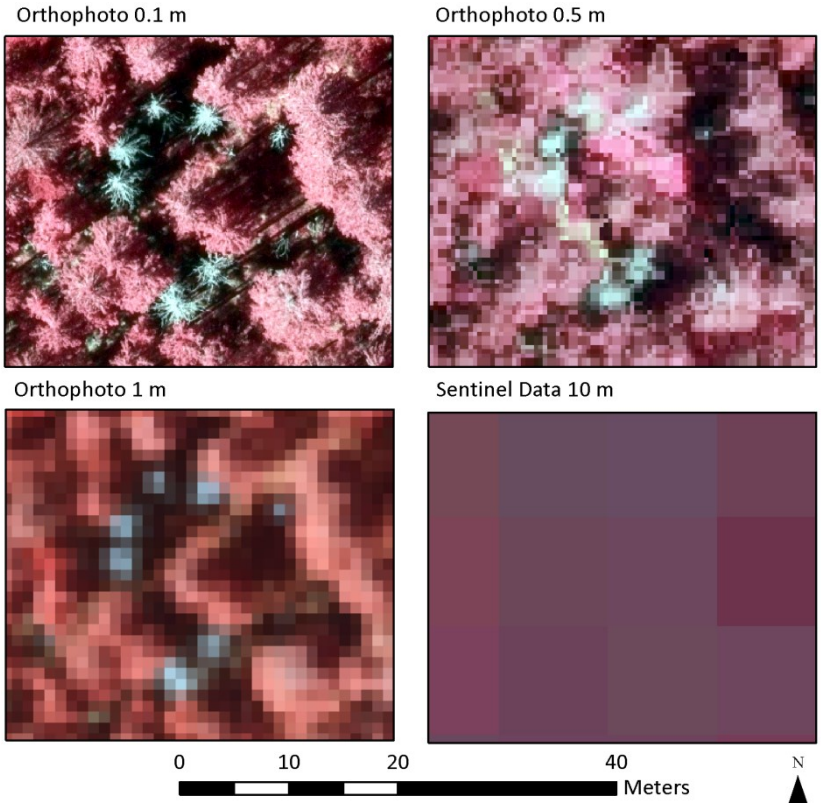

Figure 1-1 Examples of deadwood, shown by optical remote sensing data of different resolution: orthophoto - 0.1 m (Black Forest National Park), orthophoto - 0.5 m (State Agency of Spatial Information and Rural Development, LGL), orthophoto - 1 m (resampled from exemplary data of 0.1 m resolution), sentinel Satellite 2 data - 10 m resolution (ESA, 2020). All examples display the same area in color-infrared (CIR) band combination.

The various RS data products thus represent different possibilities for answering research questions related to forest ecology and biodiversity. There is no “ideal” data but rather various datasets that are suitable for different research questions.

Nowadays remote sensing delivers optical data suitable for spectral analyses (e.g. of the vegetation type and health status) (Wulder *et al.*, 2006) and imagery or point cloud data suitable for deriving structural information on vegetation heights (Hobi and Ginzler, 2012; Dietmaier *et al.*, 2019).

Modern imaging instruments record spectral signatures of the land cover not only in three bands of the visible light (red, green and blue - RGB) and in the near-infrared (NIR) (e.g. as in the aerial imagery (RGBI), but also in short-wave infrared (SWIR), and even thermal infrared in multi- or hyperspectral air- or spaceborne sensors, measuring the radiation in multiple bands (Jones and Vaughan, 2010). Aerial RGBI images are the standard products of many public mapping agencies. They deliver standardized data with high resolution of 0.1 - 0.2 m and an image-overlap between 60 % / 30 % - 80 % / 60 % (end/side lap), which allow for the derivation of vegetation heights by

image matching (Landesamt für Geoinformation und Landentwicklung Baden-Württemberg, 2020b). Since the technique is well known and the public mapping services cover large areas, the flight plans are scheduled for many years in advance to reliably deliver updated data products for the use in public services, including forestry. Certain satellite imagery products are also already available at very high resolution (VHR) of 0.5 - 1m, with advantages for forestry applications, especially deadwood detection (Pluto-Kossakowska *et al.*, 2017). Generating large scale structural information from this data requires however, complex processing methods and workflows, which often hinder a fast uptake into practice, although there are some successful examples of area-wide forest damage mapping in Canada (Wulder *et al.*, 2005; Wulder *et al.*, 2006) and of tree species differentiation in Switzerland (Ginzler *et al.*, 2019).

In the case of ALS, an active technique that produces very high resolution point clouds (currently up to 200 points/m² (Amiri *et al.*, 2019)) and depicts object surfaces in high detail, high costs and the complexity of the data processing are considered to be the limiting factors for frequent use (White *et al.*, 2016). Although this data delivers forest structure information with a level of detail that is not achievable with other techniques and can be beneficial for countless applications, ALS is only used to a limited extent e.g. for the generation of a new accurate Digital Terrain Model (DTM) every few years or every decade. Only in some forest-rich countries, such as those of Scandinavia (Kangas *et al.*, 2018) , in the state of Thuringia in Germany (Thüringer Landesamt für Bodenmanagement und Geoinformation, 2020) or for some smaller organizational units (e.g. National Parks (Heurich *et al.*, 2015)) is ALS in operational use and provides area-wide data for digital remote sensing based forest inventories. Economic cost-benefit analyses (Holopainen *et al.*, 2014; Bergseng *et al.*, 2015) could help to weigh all potential benefits of the different data types for different applications against the costs for large scale mapping to deliver sound arguments on whether supplementing public surveys with ALS data at regular interval would be cost-efficient for providing a more accurate detection of forest structures.

1.3.4 Remote sensing applications in biodiversity studies

Rapidly developing remote sensing techniques and new automated data processing make RS data particularly interesting for biodiversity studies. The main advantage is the wide area coverage, a high level of detail (defined by the resolution of the data) and the automatization of the data processing allowing efficient and standardized analyses. Traditionally forest structures were described based on plot-based terrestrial inventories or visual mapping from orthophotos (Ahrens, 2001; Ahrens *et al.*, 2004), which is in both cases costly (White *et al.*, 2016), limited to small areas, strongly dependent on

the interpreter and prone to inaccuracies when extrapolating the plot-based data into the neighboring area.

In recent years many biodiversity studies based on remote sensing data incorporated the information on vertical vegetation structure into the analyses. With its ability to penetrate through the canopy ALS is usually the first choice as it provides precise information on vegetation heights at and below the forest surface, allowing the quantification of vertical forest structure (Latifi *et al.*, 2016). The structural variables based on ALS data proved to be suitable predictors for habitat selection of many forest species, especially birds (Lesak *et al.*, 2011; Zellweger, 2013; Braunisch *et al.*, 2014; Rechsteiner *et al.*, 2017) and bats (Froidevaux *et al.*, 2016; Carr *et al.*, 2018; Kortmann *et al.*, 2018b).

Beside the well-known, advantageous qualities of ALS, the recent technical advances in digital photogrammetry demonstrate major potential for the derivation of Digital Surface Models (DSMs) from the stereo aerial imagery. In the next step the Canopy Height Models (CHMs) providing vegetation heights can be calculated through normalization of the DSMs against the DTM. CHM data on vegetation heights have been shown to deliver good proxy variables for forest structures at the plot level, stand level, e.g. for top height and periodic yearly increments of tree height (Straub *et al.*, 2013; Stepper *et al.*, 2014) or landscape level e.g. for tree and forest cover, forest type and growing stock (Ginzler *et al.*, 2019).

The fusion of data from different sensors, e.g. ALS delivering the accurate structural information and aerial imagery or satellite data providing spectral information in multiple bands including NIR, allows combining both advantages. This has been shown to work well in mapping of tree species (Persson *et al.*, 2004; Dalponte *et al.*, 2008; Heinzel and Koch, 2012), in deadwood detection (Polewski *et al.*, 2015c, a; Krzystek *et al.*, 2020) or in analyzing forest structure complexity (Jayathunga *et al.*, 2018).

In this dissertation I investigated new aspects of aerial imagery data utilization for applications in biodiversity studies. The usability of CHMs derived from aerial imagery, is evaluated for detection of forest gaps on the object level. The combination of the spectral and structural (CHM) information derived both from the same digital stereo aerial imagery data is tested for the detection of standing deadwood. Finally, I evaluate variables derived from a combination of ALS and aerial imagery for predicting the habitat suitability for the Three-toed woodpecker.

1.4 Aerial imagery and digital surface models

1.4.1 Aerial Imagery

Remote sensing has been successfully used for forestry applications for more than one hundred years. In the beginning, it were primarily analogue aerial photographs and orthophotos thereof that were used for forest cover and forest type mapping (Canada 1919, USA 1920), forest fire and damage studies (Canada 1920), forest enterprise inventory and mapping (Germany 1920, Sweden 1921) and vegetation studies in the tropical forests (Burma 1924) Hildebrandt (1996). Since then, aerial photography have been the main remote sensing technique used for various applications in forestry until today. In addition, research on natural forest development and nature reserves regularly applied stereo aerial photographs and orthophotos e.g. for deadwood detection or estimation of forest development phases (AFL, 2003; Ahrens *et al.*, 2004), (Ahrens *et al.*, 2004). Today digital stereo aerial imagery, usually acquired as RGBI imagery, is still the most popular RS data, as they are intuitive for visual interpretation with standardized interpretation keys (European Commission, 2000; AFL, 2003). Moreover, by recording the spectral signatures of trees in the visible spectral range (RGB - red, green, blue), aerial imagery provides information on leaf pigments especially chlorophyll (Hildebrandt, 1996). The spectral curves in the NIR spectral region indicate the status of the leaf inner structure and therefore the health condition of the tree (Adamczyk and Bedkowski, 2006). Aerial imagery acquisition can respond quickly to forest damage events and cover large areas. The quality standards of both the acquisition and processing techniques of the aerial imagery data are well established (Ackermann *et al.*, 2012).

Over the years, digital stereo aerial imagery has become a standard product of public mapping agencies and state administrations in many countries or regions (Stepper *et al.*, 2014; Landesamt für Geoinformation und Landentwicklung Baden-Württemberg, 2020b). The advantages that it offers, such as regular acquisition intervals, large spatial coverage, proven quality and a fine spatial resolution of 20 cm or less at relatively low or no cost (for public administration and research purposes) (Straub *et al.*, 2013; Ginzler and Hobi, 2015; Ginzler *et al.*, 2019), make it particularly interesting for long-term forest monitoring.

Since an important aim of my thesis is to provide methods and products suitable for a broad application in forestry purposes, I have only used data from state surveys. All data sources were products of the State Agency of Spatial Information and Rural Development of Baden-Württemberg (LGL) (Landesamt für Geoinformation und Landentwicklung Baden-Württemberg, 2020b) or internal data of the State Forest Administration of Baden-Württemberg (LFV). The RGBI stereo aerial imagery evaluated in this doctoral thesis in Chapters I - III had a resolution of 20 cm and overlap of 60 % (end lap) and 30 % (side lap). Additional datasets of RGBI stereo aerial imagery of 10cm resolution and 80 % and 60 % overlap originating from Black Forest National Park (Chapter II) and an ALS (30 - 40

points/m² at 0.32 m footprint) based data on canopy heights and deadwood polygons from the remote sensing based forest inventory in the Bavarian Forest National Park (Heurich *et al.*, 2015) (Chapter IV) were used for methodological comparison.

1.4.2 Image Matching and Digital Surface Models (DSMs)

Technical advances in the field of digital photogrammetry in recent years revealed the potential of automatic image matching for deriving high-resolution surface measurements of the forest canopy (Straub *et al.*, 2013; Stepper *et al.*, 2014). In the first step of an image matching algorithm, the same points are searched for pixel by pixel in two or more overlapping images. Knowing the geographical location, flight height and the viewing angle of the camera, the absolute height of these points in two or more overlapping images is calculated based on trigonometric principles (Ackermann *et al.*, 2020). At first, an irregular point cloud is generated, with the accuracy and completeness depending on the algorithm and software used, but also on site conditions, camera properties, flight parameters and many other factors as listed by White *et al.* (2013) after Baltsavias *et al.* (2008).

Raster DSMs are generated from point clouds by rasterizing the results on a selected resolution, normally at least two times lower than the resolution of the input aerial imagery (Ackermann *et al.*, 2020). Depending on the density of matched points for a given area unit the surface heights differ in accuracy. With low point density the surface height information is interpolated between available points, with very high density filtering of points is applied. The occurrence of cells without surface height information ("no-data" cells) can be an expression of multiple sources of problems in image matching. To identify and analyze these was one of the aims of this thesis (Chapter I - II).

Image matching success depends on the quality of the aerial imagery with high resolution and high image overlap producing more complete and denser point clouds and more accurate point matches between the neighboring images (Zimmermann and Hoffmann, 2017; Ganz *et al.*, 2019) (Figure 1-2).

Topography and forest structure also influence the image matching success (Hobi and Ginzler, 2012; Adler *et al.*, 2014; Wang *et al.*, 2015a). Together with technical camera and flight parameters e.g. time and date of the data acquisition, which affects sun inclination and angle and the resulting shadow occurrence, the many influential factors make the image matching process complex and prone to errors, especially in areas with varying canopy heights. Different algorithms and settings deliver surface heights of diverging quality, e.g. some are more accurate for tree tops, some may be more suited for lower surface areas and other give the best overall results when the heights are averaged for the stand area. Thus, the suitability of the different algorithms for derivation of different forest parameters varies. Generally, the results of image matching are better in flat terrain

compared to rugged mountainous topography (Ginzler and Hobi, 2016) or in highly structured forests (Adler et al., 2014) (Figure 1-2).

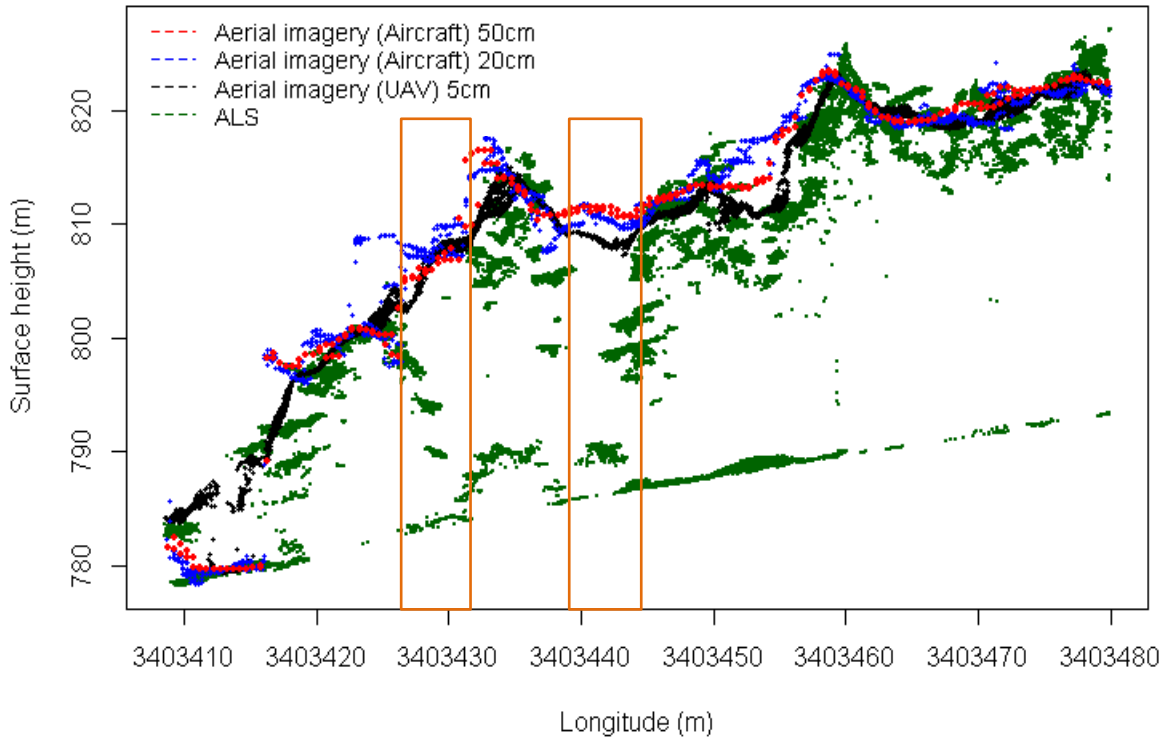

Figure 1-2 Examples of point clouds and the differences in obtained surface heights (m) generated for the same 80m long and 1m wide forest stripe by: photogrammetric airborne systems acquiring aerial imagery of different resolution (UAV – 5 cm (in black), aircraft – 20 cm (in blue), aircraft – 50 cm (in red)) in comparison to a point cloud generated for the same area by the UAV LiDAR system (in green). The orange boxes indicate problematic areas between trees for which the optical systems often deliver false surface heights. Data: ProQualTools Project, FVA, 2018. Figure K. Zielewska-Büttner, S. Ganz.

Many forest ecological studies, however, focus on stands with high structural complexity as often the case in protected areas. Thus, investigation of the reliability of the aerial imagery derived CHMs for derivation of key forest structure parameters in difficult terrain and complex structured stands, is a central aspect of this doctoral thesis.

Compared to ALS-data, CHMs from aerial imagery are less accurate particularly in transition areas between low and high surfaces, e.g. between trees, at the forest edges or in forest gaps (White *et al.*, 2018). However, as aerial imagery are the most affordable and accessible area-wide RS data in many regions, generating accurate CHMs from image matching is a worth-while challenge to produce valuable information on vegetation heights for forestry purposes. In addition, they are spatially compatible with the orthophotos derived from the same aerial imagery data and therefore suitable for combined analyses. Considering these advantages, one of the aims of this thesis (Chapter III) is to

explore the usability of the combined spectral and structural information from the same aerial imagery data.

1.4.3 True-orthophotos

Spectral information from aerial imagery is mainly utilized in form of orthophotos (also known as ortho-imagery) where it is attributed to the correct geographical location on the earth surface. Orthophotos were first generated based on DTMs, so some location errors were possible and image distortions occurred frequently as the image pixels were attributed not to the surface heights but to the ground elevation. With the newer DSMs based on aerial imagery, deriving true-orthophotos with correctly attributed surface heights based on the same data became possible.

Correct co-registration of different data sources is of highest importance for analyses based on data fusion. When data differ greatly in terms of positional accuracy and resolution, the point correspondences are often wrong (Lanaras *et al.*, 2015). Combining data of different type and resolution with even small location errors might cause major errors especially for analyses of small objects or object classes. Thus using the data products generated from the same RS data (as tested in my deadwood detection method utilizing the four orthophoto bands and the vegetation heights from the CHM derived from the same aerial imagery data (Chapter III)), should be advantageous because of the correct match of the spectral and structural information at a given point.

1.4.4 Aerial imagery in forest ecology research

Aerial imagery data and its derivatives play a large role in biodiversity and ecology studies, due to their broad accessibility and widespread familiarity with the data. Color-infrared (CIR) aerial imagery, being combination of: 1) near-infrared, 2) red and 3) green bands, and derived orthophotos have been the main data source for deadwood detection for decades in studies related to forest development and dynamics (Rall and Martin, 2002; Ahrens *et al.*, 2004), forest disturbance and regeneration (Wulder *et al.*, 2006; Zielewska, 2012) and forest biodiversity (Bütler and Schlaepfer, 2004).

The spectral properties of the NIR region of the light spectrum (0.7 -1.3 µm) (Hildebrandt, 1996) reflect the differences in the cell structure of a leaf particularly well, enabling differentiation between the different health status of trees (Commission, 2000) and live and dead vegetation (Kenneweg, 1970; Adamczyk and Bedkowski, 2006). Thus the CIR or RGBI aerial imagery and orthophotos are often used as primary data for deadwood recognition.

DSMs delivering the information on vegetation heights are important e.g. for delineation of forest stands and calculation of the canopy cover. Diversification (also called hetero- or homogeneity or roughness) of the canopy surface, the existence of forest gaps, open forest stands, and structures such as inner and outer forest edges can also be calculated. In addition in single tree and deadwood detection the information on the surface heights are crucial as the physical dimensions and forms of different tree species or live and dead trees differ. Fusion of the spectral information from aerial imagery with surface height information from ALS was already used frequently for the detection of single dead trees (Polewski *et al.*, 2015a) or deadwood of different tree species (Amiri *et al.*, 2016; Kamińska *et al.*, 2018; Krzystek *et al.*, 2020). Examining the value of fusion of the spectral and structural data originating exclusively from the aerial imagery is an aim of Chapter III.

1.5 Methods for the analysis of remote sensing data

1.5.1 Image analysis

To derive information on forests from remote sensing data visual interpretation and manual delineation of objects were initially applied to analyze analogue aerial photographs and orthophotos (Hildebrandt, 1996). These methods are based on the cognitive capabilities of the human eyes and brain and their life-long experience and training. Automated computer classification methods are however much more efficient in processing large datasets and repeatable algorithms make them standardized and objective. With the rapid technical development in remote sensing technology in the last 20 years, including the transition from analogue aerial photography to digital aerial imagery, the automated methods outperformed the visual analyses, with the latter still remaining valuable for special small-scale applications (Rugani *et al.*, 2013) or validation purposes (Waser *et al.*, 2014a; Hamdi *et al.*, 2019).

Digital image analysis is grounded in two main techniques: image classification (1) and segmentation (2). Both aim to assign the single image cells to different image classes. Whereas the image classification is performed pixel by pixel, image segmentation additionally groups the pixels into disjoint, spatially continuous and homogenous regions representing objects of a given class (Seebach, 2013).

1.5.1.1 Image classification

Pixel-based image classification based on machine learning (ML) became a standard tool image analysis in the field of remote sensing and forest ecology in recent years (Liu et al., 2018).

Non-parametric classifiers among which the Maximum Likelihood, Random Forest (RF) or Supported Vector Machines (SVM) are well known from various forestry (Gosh, 2014) and deadwood detection studies (Fassnacht, 2013; Stereńczak et al., 2017; Kamińska et al., 2018). They have the advantage of performing well with different types of input data and without the need to specify the data distribution (Wegmann et al., 2016). Deep learning (DL) algorithms continue to gain in popularity for analyzing remote sensing and show a great potential for image classification (Paoletti et al., 2019).

The RF algorithm as originally developed by Breiman (2001) and implemented in R in Caret package (Kuhn et al., 2018) is an ensemble classifier making use of a large number of decision trees combined into a forest of decision trees. It can deal with correlated variables, produce robust results for large datasets and is known to both classify and predict well as it is not prone to overfitting (Wegmann *et al.*, 2016), all of the above are important assets for area-wide deadwood mapping (Chapter III).

1.5.1.2 Image segmentation

Image segmentation also called segment-based or object-based analysis (OBIA) is an image processing technique that is frequently used in thematic mapping with high resolution remote sensing data. Segmentation algorithms group image elements following the principles of neighborhood and value of similarity, homo- or heterogeneity (Schiewe, 2012).

This processing technique was initially carried out manually (Kenneweg, 1970; Rall and Martin, 2002). Following further technical developments semi-automatic and automatic segmentation methods became very popular (Blaschke *et al.*, 2004). It has been commonly applied in RS applications for forestry, e.g. for forest cover mapping (Pekkarinen *et al.*, 2009), forest type mapping (Kempeneers *et al.*, 2012), stand delineation (Hernando *et al.*, 2012) forest change analysis (Conchedda *et al.*, 2008; Chehata *et al.*, 2011), delineating forest damage or disturbance areas (Kenneweg, 1970; Rall and Martin, 2002; Zielewska, 2012), forest nature conservation purposes (Mitchell *et al.*, 2016), and estimating forest parameters such as basal area or timber volume at stand level (Hernando *et al.*, 2012; Straub *et al.*, 2013).

Various classification methods such as threshold value analyses, supervised and unsupervised classification organized as hierarchic or hybrid classification procedures (Hildebrandt, 1996) can be applied in image segmentation processing steps. Depending on the research question and the targeted results, different algorithmic approaches, i.e. point-based, edge-based, region-based and combined approaches (Schiewe, 2012) can be chosen.

Dealing with under- or over-segmentation of the classified objects, morphological rules need to be set to build the model regions, detailed enough to reflect the variability in the image classes well, but

also generalized enough in order to get a clear picture of the classes' distribution. The formulation of the definitions and rules for segmenting and clustering image elements into objects of different classes including interim objects at different levels of the decision tree is challenging and requires careful considerations to achieve the desired results, especially when a flexible detection tool with modifiable object classes is developed (Chapter I).

1.5.1.3 Model variables

Various variables can be used to analyze remote sensing data and to derive thematic maps. Variables used during the methodological developments within this thesis (Papers I - III) can be divided into following classes based on the data type:

A) Pure spectral bands

B) Spectral ratios and indices

C) Hue-Saturation-Value (HSV)

D) Vegetation height information

E) Image texture

Objects on the earth surface reflect the visible light and the near-infrared radiation in different wavelengths that can be captured by optical cameras in RGBI, CIR or multi- and hyperspectral images. Different characteristics of the photographed objects then become visible in different spectral bands, e.g. chlorophyll content in the red and green bands and the different plant cell structure and water content in the near-infrared region of the light spectrum (Hildebrandt, 1996). These properties of the pure spectral bands (A) can be used directly for modelling. In such cases, however it is necessary to consider the atmospheric and terrain conditions of the acquired aerial imagery and the compatibility of the images from different flights with each other.

Spectral indices (B) developed with the aim of recognizing vegetation types or forms are called vegetation indices. They are widely known in remote sensing analyses, because - depending on the formula and spectral bands included - they can improve the ability to measure object or vegetation properties and reflect them for human visual perception (Fassnacht, 2013). Combining different bands into one measure is also expected to reduce the atmospheric and Bidirectional Reflectance Distribution Function (BRDF) (Nicodemus *et al.*, 1977; Fassnacht and Koch, 2012) noise in the imagery and to overcome the differences in light conditions between different scenes to make the results of studies from different areas based on flights by different weather and light conditions comparable with each other (Jones and Vaughan, 2010).

The Normalized Difference Vegetation Index NDVI (Eq. 1) is one of the most famous among many other formulas (Bannari *et al.*, 1995; Silleos *et al.*, 2006). Developed by (Jackson and Huete, 1991), using the red (strongly reflecting live vegetation) and infrared (stronger reflecting the dead compared to the live vegetation) bands, NDVI is especially efficient for differentiating between vital and non-vital vegetation and other materials and is therefore broadly applied in forest health and damage studies (Hildebrandt, 1996; Fassnacht, 2013) and deadwood recognition (Pluto-Kossakowska *et al.*, 2017; Kamińska *et al.*, 2018).

$$NDVI = (I - R) / (I + R) \qquad \textit{(Eq. 1)}$$

The use of the HSV (Hue = color, Saturation = saturation of the color, Value = lightness or darkness of the color) (C) transformed values (from RGB) proved to contribute positively to increasing the information content of the remote sensing data and became a steady part in remote sensing applications in geology and soil science (Hildebrandt, 1996). Forestry-applications also used HSV transformations and showed a significant contribution to separating conifer tree species (Ganz, 2016) and to shadow detection for deriving shadow masks (Shahtahmassebi *et al.*, 2013; Ginzler *et al.*, 2019).

Vegetation height information (D) originating from the CHMs can be used either directly per pixel or indirectly through the derivation of neighborhood based values e.g. height canopy cover percentage or canopy height heterogeneity that can also be directly used as predictors for ecological modelling (Braunisch *et al.*, 2014; Zellweger *et al.*, 2015). The accuracy of the CHM plays a key role especially for pixel-based analyses. Plot or area-based values are normally less prone to errors as erroneous information is smoothed by the remaining correct values (Ullah *et al.*, 2019). For more details regarding CHM please see section 1.4.2.

Image texture (E) is known to provide additional information suitable for remote sensing image analysis (Irons and Petersen, 1981; Heinzel and Koch, 2012). Textural energy can be measured based on different mathematic formulas describing spatial relationship patterns in the grey-level co-occurrence matrix (GLCM) introduced by (Haralick *et al.*, 1973), or of pixel values of single spectral bands or combinations of bands (Law, 1980; Irons and Petersen, 1981). Observing different gradients of spectral signatures at different pixel aggregation levels, I assumed texture features to be meaningful for deadwood detection (Chapter III).

Based on the specifications and expected benefits of the different data types described above I combined RGBI pure bands, NDVI and several other indices including some self-developed ones, the HSV transformed color scale, vegetation height and image texture information for standing

deadwood detection (Chapter III). The vegetation height information was also the main input for the forest gap mapping (Chapter I) and the HSV information was used for the generation of shadow masks (Chapter II and III).

1.5.1.4 Role of training data (sample)

To ensure successful classification of remote sensing data when using a supervised method the training sample needs to represent all relevant model classes with their intra-class heterogeneity, while accounting for inter-class similarities (Adamczyk and Bedkowski, 2006). To account for viewing angle, light condition bias and spatial autocorrelation (Jones and Vaughan, 2010; Fassnacht *et al.*, 2012) the reference data should originate from different geographical locations within the analyzed image or sequence of images.

Various sampling approaches can be applied, with the five basic strategies being: random, random stratified, systematic, clustered and transect sampling, all of them having advantages and disadvantages (Congalton, 1991; Fassnacht, 2013). For the generation of training and validation data stratified random sampling was preferred in this thesis, as it is often the most efficient method to avoid an operator bias and reduce the chance of under sampling of underrepresented classes.

1.5.2 Postprocessing

In pixel based image classification inter-class variability within an image often leads to misclassifications of similar pixels (Adamczyk and Bedkowski, 2006). A fraction of these misclassified pixels occurs isolated between pixels of the respective correct class. This so-called “salt and pepper effect” (Kelly *et al.*, 2011) blurs the image and can cause confusion in image interpretation. Neighborhood analysis can be used to single out such problematic pixel with the values of the neighboring pixels, their mean, median, modus or majority value assigned to the isolated pixels to obtain a smoother image and clearly delineated classes. I used the majority filter to smoothen the results of the deadwood detection method by reclassifying groups of 1 - 2 pixels to improve interpretability for forest practitioners. This procedure might, however, be prone to introducing errors as it may also misclassify correctly classified pixels. For that reason I developed and tested an alternative approach with the modelling of the probability of the correct deadwood classification based on additional structural and textural variables in the neighborhood of deadwood pixels.

While deriving objects in the course of the image segmentation not only single pixels but also bigger groups of pixels may not fulfil the requirements of a defined class (e.g. when a small patch with low height pixels is located within a high forest stand). To achieve compact objects and to deliver clear

maps with all classes fulfilling the defined rules a morphological clean-up is necessary. In Chapter I reclassification rules were defined based on predefined thresholds and neighborhood analysis.

The format (raster, vector or point) in which the results of the image analysis are stored, the data resolution and the amount of attributed information need to be specified before the processing of the remote sensing data in order to produce data products suitable for further analyses, applications and different users' groups. RS input data (amount, resolution, quality and format), the targeted results (resolution, format), the available software and computer power are to be carefully considered. Aiming at the development of wide-area methods, also data storage for all interim- and final products of the analyses is an important issue requiring consideration (Chapter I and III).

1.5.3 Model validation

Validation is an inevitable element in the development of methods. However, depending on the validation data and method it can deliver either reliable results or misleading ones, when the validation sample is biased. The data sampling method (See 1.5.1.4), the sampling unit (e.g. point (Chapter III) or areas (Chapter I and II)) and the response design used to select the reference sample and its classification are crucial to obtain validation data which enable quantifying mapping accuracies and errors (Stehman and Czaplewski, 1998).

A confusion matrix and associated accuracy measures are frequently used to evaluate multi-class classifications (Chapters I - III). The accuracy measures include: overall accuracy (OA, expressing the partition of correctly classified samples in all classes), producer's accuracy (PA, referring to the probability that a certain pixel has the same real value on the ground), user's accuracy (UA, referring to the probability that a pixel of a given class in the map really is this class) (Congalton, 1991) and Cohen´s Kappa reflecting the overall reliability of the map (Cohen, 1960).

For binary classifications (Chapter I and III) the following model diagnostics measures (as implemented in "Caret" R package (Kuhn *et al.*, 2015)) can be chosen: OA, sensitivity (equal to PA, measuring the proportion of actual positives of a given class to be classified as such), specificity (measuring the proportion of actual negatives that are correctly classified as such), as well as positive (PPV) and negative prediction values (NPV) (measuring the proportion of true (PPV) or false (NPV) classifications among all positive (PPV) or negative (NPV) classifications, respectively. In addition to these and Cohen´s Kappa some variant of pseudo R squared statistics can estimate the goodness of fit of the logistic regression (e.g. McFadden's pseudo R-Square). Finally, the area under the receiver operating characteristic (ROC) curve, shortly called "area under curve" (AUC) (Hosmer and

Lemeshow, 2000) can estimate the probability that a model will rank a randomly chosen positive case higher than randomly chosen negative case.

1.6 Modelling species habitat suitability using remote sensing data

RS-based information is often used in ecological modelling, especially for species distribution models (SDM), often also referred to as habitat suitability models (HSM). Such models aim at explaining the distribution of different taxa and predicting their likely response to changes in the environment in relation to the habitat conditions (Guisan *et al.*, 2017). Precise, area-wide information on the occurrence and distribution of key habitat features at relevant spatial scales is thus essential for assessing species' habitat selection and for effective conservation planning and management (Stighäll *et al.*, 2011). High resolution remote sensing data delivering continuous structural and spectral information on land cover and vegetation facilitate deriving meaningful habitat variables to which species occurrence data can be related.

1.6.1 Species data

The availability of appropriate species occurrence data is crucial for building a reliable HSM. Numerous research papers have reviewed the effect of the sample size on the model fit and reliability, and recommend a minimum of 30, but ideally at least 50 presence observations for HSMs (Thibaud *et al.*, 2014; Guisan *et al.*, 2017).

Depending on the available data "presence-absence" vs. "presence-only" models can be generated. For "presence-only" models, when absence data is not available, exclusively actual species observations are used for modelling and contrasted against the "background" i.e. the available conditions in the study area (Guisan *et al.*, 2017) or an additional dataset of "pseudo-absence" samples is generated to use statistical approaches for binary data (Barbet-Massin *et al.*, 2012). I used the latter approach in Chapter IV to supplement the Three-toed woodpecker occurrence data with pseudo-absence points randomly sampled in the areas without confirmed species presence and in a predefined distance between each other to avoid spatial clustering.

Depending on the species and sampling design it might not be possible to mark or recognize single individuals in the presence data. This can result in pseudo replication in the response dataset when two or several observations of the same individual are considered as two different samples (Guisan *et al.*, 2017). Spatial data filtering (i.e. selecting only one location within a predefined area) can be done based on the species' home range or seasonal activity range as applied in Chapter IV of this thesis. The home range size, reflecting the average area which an individual of the focal species uses,

is also relevant for choosing an appropriate spatial resolution for the HSM (Braunisch and Suchant, 2010).

1.6.2 Predictor variables

In recent years, the technical developments in the field of digital photogrammetry and image matching of aerial imagery also led to an increase in research that addresses their possible application in ecology (Wang *et al.*, 2015a; White *et al.*, 2018). ALS-derived gap information (Braunisch *et al.*, 2014; Kortmann *et al.*, 2018b) and habitat variables describing deadwood based on visual interpretation of orthophotos or field inventories (Bütler *et al.*, 2004c; Müller and Bütler, 2010) has been frequently used in habitat modelling.

Referring to this, one of the main research questions of this thesis is, whether similar variables can be extracted solely from the top of the canopy surface (i.e. derived by image matching of aerial imagery) (Chapters I - III) and whether this information is useful for conservation research and application. To estimate the general potential of vegetation heights from RS (CHMs) for derivation of deadwood variables that are relevant for habitat modelling, ALS and aerial imagery based digital inventory data (Heurich *et al.*, 2015) is examined as input for HSM for an important forest focal species of boreal and temperate mountainous forest, Three-toed woodpecker (Chapter IV).

1.6.3 Modelling approaches

In the past two decades, with the increase in computer power and the development of new automated statistical and modelling techniques, the use of HSMs in ecological studies has increased immensely (Guisan *et al.*, 2017). There are many statistical modelling approaches used in habitat suitability modelling, each of them having different advantages and disadvantages, e.g. related to the degree of model complexity, requirements towards the data distribution, predisposition to overfitting or data-driven behavior. In general HSMs can be divided into descriptive, explanatory or predictive, focusing on different aspects of the modelling process. It is crucial to identify the most appropriate method according to the goal of the study and the type of the response variable (Guisan *et al.*, 2017).

In this doctoral thesis three model types were used to: 1) explain and predict the probability of deadwood occurrence (GLM, Chapter III); 2) explain and predict the habitat suitability (Dormann *et al.*, 2004) of the Three-toed woodpecker (GAM, Chapter IV) and 3) to derive critical thresholds for its key habitat variables (CTREE, Chapter IV).

The **Generalized linear model (GLM)** is a model-driven regression technique based on the general linear model enhanced with an implemented maximum likelihood approach (Dormann and Kühn, 2012). It requires an assumption regarding the data distribution with a binomial data distribution (function "logit") used for binary (e.g. true-false, presence-absence or 1 / 0) data (Chapters III and IV). In contrast to data-driven methods that fit the model as close as possible to the data, GLM requires to specify the expected shape (linear or quadratic) of the response variable as a function of the predictors. GLMs deliver generalized results suitable for predicting general trends. However, their lack of complexity may also limit their application for complex, non-linear response types.

The **Generalized Additive Model (GAM)** is a model type building upon GLMs combined with smoothing splines (Dormann and Kühn, 2012), which enable fitting response curves "as closely as possible" to the data. GAMs do not require predefining the shape of the response curve and can deliver answers for non-linear dependencies between response and explaining variables. Being data-driven GAMs are prone to overfitting, but also have the advantage of giving the user the opportunity to explore the general shape of the response functions, especially when species–habitat relationships are complex and cannot be easily fitted with the standard parametric functions (Guisan et al., 2017). The application of a tensor smooth for the spatial location furthermore allows accounting for spatial patterns in species locations, which was tested in Chapter IV for examining the expected spatial clustering of Three-toed woodpecker observations.

Conditional Inference Trees (CTREE) (Hothorn *et al.*, 2006; Hothorn *et al.*, 2017) are decision tree based regression models frequently used in forest and wildlife ecology (Müller et al., 2009). Applicable to all kinds of regression problems, simple with regard to the underlying statistical methods and with a useful visualization of the results they have been found to be particularly useful to derive ecological thresholds (Müller and Bütler, 2010). The model trees split the data into significantly different partitions with each node of the tree representing one data split. The variables are ranked according to their importance until no further split is possible with the significance of the split being indicated in the splitting nodes. The variable values splitting the datasets are labeled on the branches of the tree and the final results are displayed as boxplots showing the predicted probability of the response variable under the given combination of variable values. CTREEs were applied in Chapter IV to derive ecological thresholds for habitat variables that explain Three-toed woodpecker presence.

1.6.4 Validation

In habitat selection studies, especially of rare species, the amount of species data is often not large enough to generate an independent validation dataset. In this case the most frequently used method to evaluate the model results is the k-fold cross-validation. In this method a set of validation data is split into k equal folds, iteratively using k-1 folds for model training and the remaining one for validation. For each combination of the folds the model is trained and validated using evaluation metrics for binary classifications such as: OA, sensitivity, specificity, PPV, NPV, Cohen´s Kappa, McFadden's pseudo R-Square and AUC (as described in p. 2.4.1.).

This validation scheme was used in Chapter IV. Additionally, averaged results of all k validation runs were calculated to show the variance in the achieved accuracies.

1.6.5 Predictive mapping of species occurrence probability

Remote sensing data and methods, allow detailed, area-wide, large scale structural analyses that are useful for deriving habitat suitability maps and predictive maps of species occurrence (Guisan and Thuiller, 2005; Farrell *et al.*, 2013). These maps, as generated in Chapter IV, carry continuous information and are thus helpful in setting targets and selecting suitable areas for conservation measures based on clearly defined criteria and thresholds. In addition, area-wide success-control of the conservation measures can be supported by evaluating data of time series using the same model algorithms.

1.7 Objectives and research questions

The first main aim of this doctoral thesis is to develop automated and standardized methods (Figure 1-3, METHODS) for mapping two selected forest structures: canopy gaps and standing deadwood. These structures are well-studied in the field of forest ecology and their high value for forest biodiversity is confirmed. The second aim is to evaluate the potential of public aerial imagery as a source of information for mapping these structures (Figure 1-3, EVALUATION) and to derive meaningful variables from the data for use in forest and conservation research and practice (Figure 1-3, APPLICATION). Each of the thesis' aims is addressed by one or several research question (RQ) defined below, with the four chapters (Chapter I–IV) answering these research questions on selected examples. The interrelationships between the different parts of this thesis are illustrated in Figure 1-3.

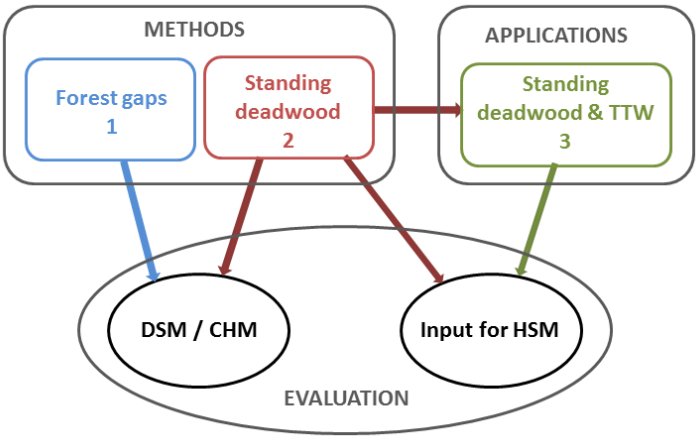

Figure 1-3 Structure of the doctoral thesis showing how the three main thesis sections (research areas: 1, 2, 3) are embedded in the overall aims of the thesis (METHODS – method development, APPLICATIONS – applied ecology research and EVALUATION – evaluating the potential of aerial imagery data) are interconnected with each other. (DSM: digital surface model, CHM: canopy height model, HSM: habitat suitability model, TTW: Tree-toed woodpecker).

The following research questions were formulated (how they are interlinked is illustrated in Figure 1-3):

RQ1: Are stereo aerial imagery from state surveys and the orthophotos and CHMs thereof reliable primary sources of information for the detection of open forest structures and single standing deadwood objects, for which deep insight between the trees to the ground is required?

RQ2: What are the parameters influencing the derivation of structural information and vegetation heights from CHMs based on aerial imagery? What alternative data sources or parameters can be used to enhance them?

RQ3: Are aerial imagery based forest structure parameters (using solely aerial imagery data or in fusion with ALS data) suitable to derive meaningful, reliable and practicable habitat variables to explain and predict the habitat requirements of a selected forest species?

The research questions are addressed in the individual chapters of the thesis, with each chapter addressing a specific objective:

Chapter I: To develop and validate a standardized adjustable automated method for the detection of canopy cover and forest gaps based on aerial imagery derived CHMs (RQ1-2)

Chapter II: To compare and evaluate the results of the forest gap mapping method when using CHMs from different aerial imagery datasets varying in spatial and radiometric resolution and image overlap (RQ2)

Chapter III: To develop an automated and standardized method for the detection of standing deadwood (height > 5m) combining structural (CHM) and spectral (orthophoto) information from the same aerial imagery data source (RQ1-2)

Chapter IV: To develop and evaluate a species habitat model, derive thresholds for key habitat variables and generate area-wide predictions of species occurrence for the Three-toed woodpecker, a focal species of boreal and temperate mountain forests, based on the remote sensing derived variables (RQ3)

The first three chapters address methodological questions regarding the detection of biodiversity relevant forest structures at a fine single-object scale. While the focus of Chapter I and III is the development of methods and their validation in form of accuracy assessment, the topic of Chapter II is to evaluate the hypothesized benefit for structure detection when using aerial imagery data with higher resolution and overlap. Finally, evaluating the suitability of standing deadwood information mapped from ALS and CIR aerial imagery data in a species ecological study and inferring requirements towards standing deadwood mapping for this purpose is the focus of Chapter IV.

1.8 Outline of the thesis

The chapters are grouped into three main thesis sections related to: 1) forest gap detection, 2) standing deadwood mapping and 3) habitat suitability analysis based on remote sensing derived variables (Table 1-1). The content of each section with the numbers of chapters included, their thematic focus, the research questions methodology and remote sensing data sources used is summarized in Table 1-1.

Chapter I present the development of a method for the detection of forest gaps. It includes: CHM generation with image matching and point cloud processing, an analysis of vegetation heights for the delineation of open and dense forest, the identification of low and high stands and gap extraction in different types of stands. In order to quantify mapping accuracy, open and dense forest and different gap types were validated based on a stratified random sample. As I hypothesized an effect of terrain and gap characteristics on the model results the influence of these variables on mapping accuracy is explored.

Table 1-1 Overview over the thesis sections with their main aims, methods as well as the types of remote sensing data used.

	AIM		
Thesis section	**1**	**2**	**3**
Thematic focus	Gap detection	Deadwood detection	Three-toad woodpecker habitat suitability model
Research question	RQ1, RQ2	RQ1, RQ2	RQ3
Chapter	I, II	III	IV
	METHODS		
Methodological focus	REMOTE SENSING	REMOTE SENSING	HABITAT MODELLING
Activity	DEVELOPMENT	DEVELOPMENT	CASE STUDY, ANALYSIS
	MATERIAL		
Aerial imagery	Primary input, Validation	Primary input, Validation	Primary input
Orthophoto	Validation	Model input, Validation	Model input
Aerial imagery based CHM	Model input	Model input	-
ALS CHM	-	-	Model input (Structure analysis)

Chapter II is based on the results of Chapter I, testing the hypothesis whether CHMs from aerial imagery of higher resolution and overlap deliver better results in the mapping of forest gaps. In this study the gap model developed in Chapter I was run on three aerial imagery datasets of different spatial and radiometric resolution and varying image overlap. The validation was performed by visual validation on a stratified sample similar to the methodology used in Chapter I. The gap mapping results obtained with the three test datasets were compared and the effects of shadow occurrence and geometric limitations of the stereo aerial imagery on mapping accuracy were evaluated.

Chapter III describes the development and evaluation of an automated method for detecting standing deadwood in complex structured mountain forest stands. The aim is to evaluate the potential of the stereo RGBI aerial imagery data to deliver suitable spectral and structural (from image matching) information for deadwood prediction. Due to the fact that standing deadwood frequently occurs in well-structured open stands and difficult mountainous terrain the emphasis is on addressing the “deadwood versus bare ground misclassification” issue. This is a well-known problem which has rarely been addressed, and suitable solutions are lacking. I developed and evaluated two

possible solutions to enhance the image classification results of a RF model, 1) postprocessing with a morphological clean-up of the results and 2) using a deadwood uncertainty model (GLM) for reclassifying misclassified deadwood pixels. The accuracy of predicting standing deadwood occurrence based on an RGBI orthophoto and a CHM, both derived from the same aerial imagery, as well as the two enhancement methods are evaluated. The limitations of the input data are analyzed and possibilities for further development are discussed.

Chapter IV evaluates the suitability of RS-based habitat variables, especially deadwood-variables, for modelling and predicting the habitat suitability for a selected forest species, the Three-toed woodpecker (TTW). A multivariate GAM is used to identify the decisive habitat variables and a CTREE model is used to find critical, species specific variables' thresholds. Model input variables are based on deadwood polygon mapping using a combination of ALS and CIR aerial imagery data. I introduce a novel differentiation between dead trees and snags based on the mapped crown area to explore the TTW's preference for trees of a particular decay stage. Based on literature I hypothesize a preference for freshly dead trees with large crown sizes. In addition, I hypothesize an adverse effect of very large amounts deadwood at the home range-scale, which I tested using data from an area with very high deadwood abundances. From the results, area-wide predictive habitat suitability maps and management recommendations for forestry and species conservation practice are drawn.

The Chapters I, III and IV were published as stand-alone papers in international peer reviewed journals. Chapter II was published as a conference paper and was reprinted in this thesis with the agreement of the conference organizer. All papers are included in full length in the paper section (paragraphs 2 - 5) of this thesis. Their format has been adapted to the format of this dissertation.

2 CHAPTER I: AUTOMATED DETECTION OF FOREST GAPS IN SPRUCE DOMINATED STANDS USING CANOPY HEIGHT MODELS DERIVED FROM STEREO AERIAL IMAGERY

Chapter I is based on Paper I published as research article of Zielewska-Büttner *et al.* (2016a) and Erratum to the Paper I (Zielewska-Büttner *et al.*, 2017):

Zielewska-Büttner, K.; Adler, P.; Ehmann, M.; Braunisch, V. (2016). Automated detection of forest gaps in spruce dominated stands using canopy height models derived from stereo aerial imagery. Remote Sens. , 8, 175. DOI: https://doi.org/10.3390/rs8030175

Zielewska-Büttner, K.; Adler, P.; Ehmann, M.; Braunisch, V. Erratum: Zielewska-Büttner, K.; Adler, P.; Ehmann, M.; Braunisch, V. (2017). Automated Detection Of Forest Gaps In Spruce Dominated Stands Using Canopy Height Models Derived From Stereo Aerial Imagery. Remote Sens. 2016, 8, 175. Remote Sens., 9, 471. DOI: https://Doi.Org/10.3390/Rs9050471

Tables 6 and 8 and the relevant text of the Paper I, as the column values in the tables were unintentionally exchanged, have been corrected in this chapter (Tables 2-6 and 2-8) in line with the content of the Erratum.

Abstract: Forest gaps are important structural elements in forest ecology to which various conservation-relevant, photophilic species are associated. To automatically map forest gaps and detect their changes over time, we developed a method based on Digital Surface Models (DSM) derived from stereoscopic aerial imagery and a LiDAR-based Digital Elevation Model (LiDAR DEM). Gaps were detected and delineated in relation to height and cover of the surrounding forest comparing data from two public flight campaigns (2009 and 2012) in a 1023-ha model region in the Northern Black Forest, Southwest Germany. The method was evaluated using an independent validation dataset obtained by visual stereo-interpretation. Gaps were automatically detected with an overall accuracy of 0.90 (2009) and 0.82 (2012). However, a very high user's accuracy of more than 0.95 (both years) was counterbalanced by a producer's accuracy of 0.84 (2009) and 0.72 (2012) as some gaps were not automatically detected. Accuracy was mainly dependent on the shadow occurrence and height of the surrounding forest with producer's accuracies dropping to 0.70 (2009) and 0.52 (2012) in high stands (>8 m tree

height). As one important step in the workflow, the class of open forest, an important feature for many forest species, was delineated with a very good overall accuracy of 0.92 (both years) with uncertainties occurring mostly in areas with intermediate canopy cover. Presence of complete or partial shadow and geometric limitations of stereo image matching were identified as the main sources of errors in the method performance, suggesting that images with a higher overlap and resolution and ameliorated image-matching algorithms provide the greatest potential for improvement.

Keywords: aerial imagery, RGBI, photogrammetry, DSM, nDSM, CHM, LiDAR DEM, forest gap, canopy opening, canopy cover

2.1 Introduction

Structural complexity and niche diversity within forest habitats are important predictors for forest biodiversity (Noss, 1990; Lindenmayer et al., 2000; Lindenmayer et al., 2006). Canopy cover (Smith et al., 2008), vertical variation of the canopy height (Müller and Brandl, 2009) and forest gaps (Zellweger et al., 2013) are considered important structural elements in forest ecology to which various conservation relevant forest species are associated (Koukoulas and Blackburn, 2004). Presence or absence of many animal species such as European nightjar (Caprimulgus europaeus) (Sierro et al., 2001), Capercaillie (Tetrao urogallus) (Braunisch, 2008), Grey-headed woodpecker (Picus canus) (Hölzinger and Mahler, 2001), various chiroptera (Patriquin and Barclay, 2003; Aschoff et al., 2006; Runkel, 2008), saproxylic beetles (Seibold et al., 2014) or bird species assemblages (Zellweger et al., 2013; Braunisch et al., 2014) are expected to depend on semi-open forest habitats. Gaps in forest canopies also play a key role in various ecological processes such as the regeneration of trees and ground vegetation development, with the associated light regime being a main driver for composition and diversity of understory biota (Getzin et al., 2014). The establishment of an economically sustainable forest management with even-aged stands, as introduced by Hartig and Cotta in Europe at the beginning of 19th century (Boncina, 2011), resulted in the simplification of the forest structure (Noss, 1999) and an underrepresentation of the early and late phases of the forest succession (Scherzinger, 1996) which are characterized by a discontinuous canopy cover and the occurrence of forest gaps. The shift towards ecologically sustainable close-to nature forestry (Johann, 2006) has additionally led in recent decades in many European temperate forests to a progressive increase of growing stocks, with detrimental effects on many photophilic species. Species conservation programs and habitat restoration measures in temperate forests are therefore often directed towards the creation of canopy openings and gaps; yet this requires quantitative, taxon-

specific information about the required size, shape, distribution and connectivity of gaps. To generate such information, to develop appropriate management strategies and to monitor their success, precise information on spatial distribution of organisms and on forest structures at relevant - often broad - spatial scales are necessary (Bässler et al., 2010). While such data were long missing, given the impossibility to derive area-wide mosaic-structures from plot-based forest inventories or the huge effort to visually assess and manually map such structures based on aerial photographs, the rapid development of remote sensing now offers the potential to deliver forest structural information across large spatial scales at an unprecedented degree of precision.

Size and spatial distribution are the most commonly mapped gap parameters for which various remote sensing data and techniques have been used (Kathke and Bruelheide, 2010). Gap size and distribution pattern were mapped from satellite imagery by Garbarino et al. (2012) and Hobi et al. (2015). (Vepakomma et al., 2010); Vepakomma (2012) used LiDAR to assess spatial contiguity and continuity of canopy gaps over time in mixed wood boreal forests. Rugani et al. (2013) based a similar research question using visual stereo interpretation of scanned color-infrared CIR aerial photographs. Getzin et al. (2012) showed that very high-resolution images from unmanned aerial vehicles (UAV) can be used to effectively assess forest gaps and associated plant biodiversity in temperate forests. In recent years many studies confirmed the benefit from including forest structure parameters such as canopy cover and forest gaps derived from Light Detection and Ranging (LiDAR) into habitat models showing LiDAR to deliver precise, reproducible and high resolution information for answering a variety of ecological questions (Müller and Brandl, 2009; Zellweger et al., 2013; Zellweger, 2013; Braunisch et al., 2014).

Despite the well-known, advantageous qualities of LiDAR and emerging possibilities of UAVs, digital aerial images currently represent the most cost-effective and accessible input data for operative forest remote sensing applications. Digital aerial images with large spatial coverage, consistent quality and a spatial resolution of 20 cm or less became standard products of regional mapping agencies in recent years (Waser et al., 2011; Straub et al., 2013; Ginzler and Hobi, 2015; Wang et al., 2015b). Acquired in regular time intervals and available at relative low costs they are particularly interesting for forest monitoring and change-detection purposes.

Recent technical advances in the field of digital photogrammetry demonstrate the great potential of automatic image matching for deriving Digital Surface Models (DSMs) that can be used for an accurate characterization of the forest canopy structure (Straub et al., 2013). Height measurements from the DSMs normalized versus DEM (nDSMs) also called canopy height models (CHMs) have been shown to perform very well when estimating timber volume or basal area on the plot, stand or

country level (Straub et al., 2013; Kotremba, 2014; Ginzler and Hobi, 2015) and might thus be also well suited for gap detection (Betts et al., 2005; Kotremba, 2014).

To map forest gaps and detect their changes over time in a cost-efficient way, we developed a method based on CHMs derived from stereo aerial imagery from public standard flight campaigns. We aimed for a gap mapping tool that would deliver reliable and replicable results when applied to available data either in form of original aerial imagery, point cloud or a raster DSM. One important scope thereby was to assess the viability of gap assessment based on publicly available, standard products of mapping agencies so as to evaluate their potential to deliver reliable forest structure information for monitoring programmes at various spatial scales. Our method involves several steps: (1) the derivation of a CHM from stereo aerial imagery, (2) the quantification of canopy cover and height for pre-stratification, (3) the mapping of forest gaps and their changes, (4) the detection of gaps in specific locations (i.e. on forest roads), (5) the evaluation of the mapping accuracy and finally (6) the identification of the main sources of error. In addition to the main aim, the mapping of forest gaps, the intermediate processing steps deliver other important forest structure parameters such as canopy cover and forest height diversity that are frequently required as predictor variables for species-habitat studies in forest ecosystems (Braunisch and Suchant, 2008; Zellweger et al., 2015).

2.2 Material and methods

2.2.1 Study Area

The study area of 1023 ha is located in the State of Baden-Württemberg, Southwestern Germany, in the northern Black Forest (8° 34’ E, 48° 58’ N). A lake covers 1.8 ha of the area, which reduces the effective study area to 1021.2 ha. The area was chosen due to its high diversity with regard to topography, forest successional stage, protection status and consequential different management regime.

The elevation within the study area ranges from 493 to 941 m. According to the classification of the AG Boden (1996) most slopes (77.5 %) are very steep (> 20°) or strongly inclined (10 - 20°). The Northern Black Forest belongs to the most forested regions in the state of Baden-Württemberg (forest cover of 69 % (Landesamt für Geoinformation und Landentwicklung Baden-Württemberg, 2015c)) and has been used for litter and timber extraction over centuries (Moosmayer, 1972; Mantel, 1990). The dominant tree species is Norway spruce (*Picea abies* L.) with admixture of Silver fir (*Abies alba* Mill.) and Scots pine (*Pinus sylvestris*). In 82 % of the forest stands the broadleaves tree species

account for less than 30 %. In addition, the area is characterized by a dense forest road network of 187 m/ha (19 km in total).

At the time of the acquisition of the aerial photographs used for this study (2009, 2012) the southern part of the study area was protected according to the European law as a NATURA 2000 site (391.6 ha) completely overlapping with a forest reserve managed for conservation purposes (172.7 ha).

2.2.2 Material

2.2.2.1 Aerial imagery

As a primary input data, two aerial imagery data sets from the two flight campaigns, of 2009 and 2012, were used (Figure 2-1, Table 2-1). The data (including the absolute orientation of the images) was provided by the state agency of spatial information and rural development of Baden-Württemberg (LGL) with 4 channels (red, green, blue and near-infrared (RGBI)) and radiometric resolution of 8 (2009) and 16 (2012) bit. The overall spatial resolution of the imagery was 20 cm with an overlap of 60 % (end lap) and 30 % (side lap).

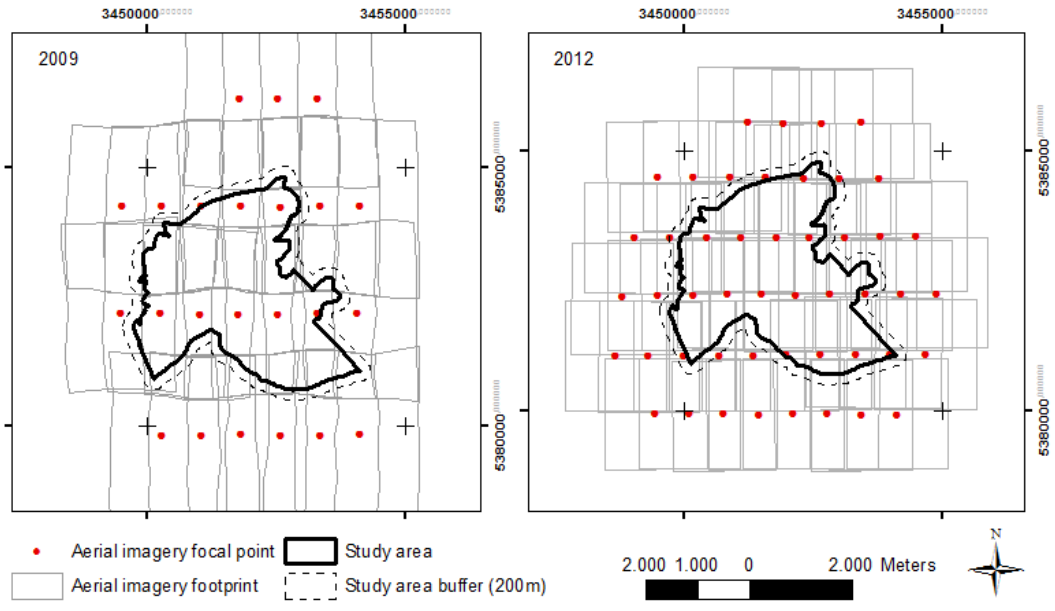

Figure 2-1 Photogrammetry blocks of aerial imagery covering the study area (23 images in 2009 and 48 images in 2012) used for image-matching and generation of Digital Surface Models (DSMs)

Table 2-1 Technical characteristics of the aerial image data used in the study

Year	2009	2012
Camera	UltraCamXp	DMC II 140 – 006
Panchromatic / color lens focal length	100 / 33 mm	92 mm
Resolution	20 cm	20 cm
Overlap	60 % / 30 %	60 % / 30 %
Image type	Digital color infrared (RGB NIR)	Digital color infrared (RGB NIR)
Angle-of-view from vertical, cross track (along track)	55° (37°)	50.7° (47.3°)
No. of stripes in the block file	3	6
No. of images	23	48
Flight height	3890 m	2850 m
Flight date	23.05.2009	01.08.2012

2.2.2.2 Additional data sources

In line with our goal to use only publicly available data we limited the additional data sources also to the products of the LGL or internal data of the forestry administration. A DEM with 1 m resolution (DEM01) derived from LiDAR-data (Landesamt für Geoinformation und Landentwicklung Baden-Württemberg, 2015b) was used as a ground surface for the generation of the CHMs. Slope and aspect were derived from a DEM with 50 m resolution (DEM50) (Landesamt für Geoinformation und Landentwicklung Baden-Württemberg, 2015b). In addition, for identifying gaps along or influenced by forest roads, we used the forest road network datasets of the State Authority Topographical and Cartographical Information System (ATKIS) (Landesamt für Geoinformation und Landentwicklung Baden-Württemberg, 2015a) and the Department of Forest Geoinformation of Baden-Württemberg (Mathow, 2015).

2.2.3 Methods

2.2.3.1 Forest gap definition

In the literature, there are inconsistencies with regard to terminology, methods for gap identification and modelling gap dynamics (Schliemann and Bockheim, 2011). Two main definitions of forest gaps can be found. The first defines a canopy gap as a ‘hole’ in the forest canopy cover down to a predefined height (e.g. 2 m) above ground (Brokaw, 1982). According to the second definition the gap additionally includes the ground surface below the canopy extending to the base of the trees which surround the canopy opening (Runkle, 1981). Definitions also vary depending on the assessment method and research objective: A terrestrial “bottom-up” approach, mostly used in field surveys (Brokaw, 1982) predefines a fixed maximum vegetation height within the gap while the aerial

"top-down" approach considers in the first place the technical capabilities of the sensor penetration through the tree canopy to forest ground and therefore defines a maximum vegetation height in a gap in relation to the height of the surrounding trees (Qinghong and Hytteborn, 1991; Hytteborn and Verwijst, 2013). Often the gap is passively mapped as the area remaining between the actively mapped trees.

The definition used in this study was based on a combination of the above mentioned definitions: We define forest gap as a canopy opening of at least $10m^2$ in dense forest (≥ 60% canopy cover) reaching through all forest strata down to maximum 2 m vegetation height in high forest stands (≥ 8 m height) and down to maximum 1 m in low forest stands (<8 m height).

We considered a minimum stand size of 0.3 ha, which corresponds to the conventional minimum stand size in Baden-Württemberg (Mathow, 2015). Areas with canopy cover less than 60 % and exceeding 0.5 ha were classified in line with Ahrens *et al.* (2004) as "open forest". Open spaces within this forest type were considered as inherent stand characteristic and thus not mapped as gaps. The minimum size of a gap was set to 10 m² according to Müller and Wagner (2003) and Schliemann and Bockheim (2011). The maximum gap-vegetation height of 2 m was chosen compliant with Brokaw (1982) and adapted to 1 m in the lower stands after the first mapping tests, which revealed that gaps within the lower stands were not significantly distinct when using the 2 m threshold.

2.2.3.2 Calculation of Canopy Height Models (CHM)

Canopy Height Models were generated in two steps: (1) image matching and (2) point cloud processing (Figure 2-2).

Image matching

DSMs with a spatial resolution of 1 m were calculated from the stereo imagery. To avoid artefacts at the borders of the study area, both during the image matching process and during the subsequent raster analysis using a moving window, the study area was buffered with 200 m. For each study year two point clouds were generated using Leica Photogrammetry Suite enhanced Automatic Terrain Extraction (LPS eATE (ERDAS, 2012)) and Semi Global Matching (SGM XPro (Hexagon Geospatial, 2014)) algorithms. Both algorithms returned different point clouds partially complementing each other (Figure 2-3).

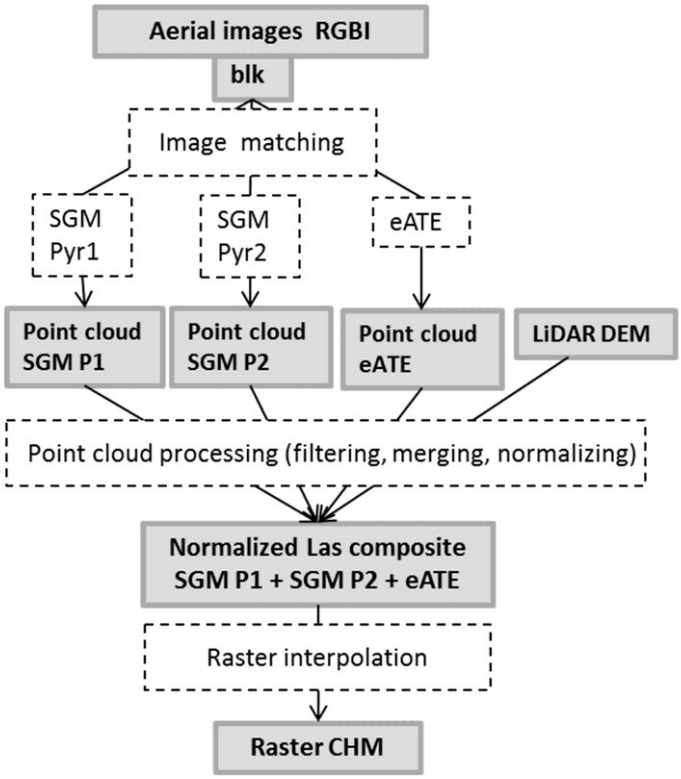

Figure 2-2 Workflow for deriving of canopy height models (CHMs) from stereo aerial imagery and LiDAR DEM

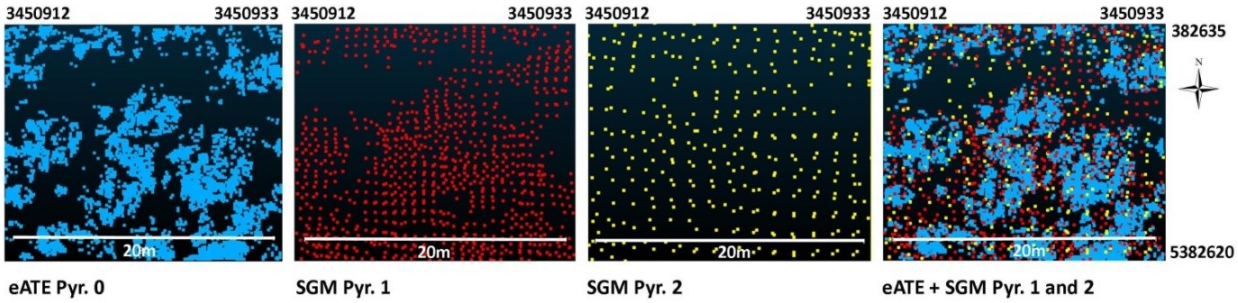

Figure 2-3 Exemplary differences in point cloud structures generated with different algorithms and settings from aerial imagery dated 2009

Image matching for terrain extraction result in a first step in an irregular point cloud depending on the algorithm, site conditions and camera properties and situation (Adler *et al.*, 2014). Consequently not every cell of a DSM raster is covered by a matched point and the generated DSMs consist of a certain percentage of cells without original height information ("no-data" cells).

The input pyramid layer was identified as one of the key factors affecting point density and distribution of the generated point cloud. It also influences the point resolution and accuracy as the coarser (higher) image level delivers points with lower accuracy, especially in situations of irregular canopy surface. Based on visual assessment, we decided for a combination of 3 point clouds from

eATE and SGM processed with the pyramid levels 0, 1 and 2 respectively which provided good point coverage in reasonable processing time. The detailed settings of both algorithms are listed in Table 2-2.

Table 2-2 Settings of the image matching algorithms for point cloud generation

Settings eATE
Minimum images: 2; Maximum images: 2; Overlap min.: 50%; Correlator: NCC; Window size: 13; Coefficient start/end: 0.2 / 0.5; Interpolation: Spike; Point threshold: 5; Search window: 50; Blunder Type: PCA; St. Dev. Tolerance: 3; LSQ Refinement: 2; Edge constraint: 3; Reverse matching tolerance: 1; Smoothing: Low; Low contrast: Yes; Stop at pyramid layer: 0; Point sampling distance: 1; Pixel block size: 100; Most nadir: Yes; Gradient threshold: 0; Premier correlation band: 4; Use all spectral data: Yes; create radiometric layer: No
Settings SGM
Band: G; Last pyramid layer: 1 or 2; Disparity Difference: 1; Urban processing: 0; Keep vertical surfaces: Y; Thinning: Mild

Point cloud processing

In the next processing step only LAS points between -1 and 55 m height in relation to the DEM01 point cloud filtered with LAStools (Isenburg, 2014) were retained, which removed most of the outliers and resulted in the normalized land cover surface heights (Figure 2-2). The "LasDataset to Raster" transformation (Data Management Toolbox in ArcGIS) with the inverse difference weighting (IDW) for interpolation and the natural neighbor void fill method was applied to calculate CHMs with a 1m resolution as a basis for subsequent height analysis and forest gaps extraction.

2.2.3.3 Gap extraction

Forest gap extraction based on the CHM was performed in ArcGIS 10.3 (ESRI, 2014) (raster and vector based) in three steps (Figure 2-4): (1) identification of open and dense forest, (2) classification of dense forest into height classes of low and high forest and (3) gap extraction in the latter two classes. In an additional post-processing step (4) gaps on and next to forest roads were located.

Open and dense forest

In the first step of the object based raster analysis (Figure 2-4.1), open (OF) and dense forest (DF) areas were identified based on the CHM (Figure 2-4.2). Based on the proportion of vegetation higher than 1 m within a circular moving window (r = 25 m), directly adjacent neighbouring cells with values of canopy cover percentage (CC) of 60 % or less were aggregated (Spatial Analyst function: region group, 4 neighbors) to open forest patches when aggregations were greater than 0.5 ha. The remaining cells representing either gaps or dense forest were submitted to further gap extraction.

Low and high stands

Within dense forest, cells with CHM-values < 8 m were identified and grouped (region group, 4 neighbors) into low forest (LF) stands, when their size exceeded 0.3 ha (Figure 2-4.3). The remaining cells were classified as high forest (HF).

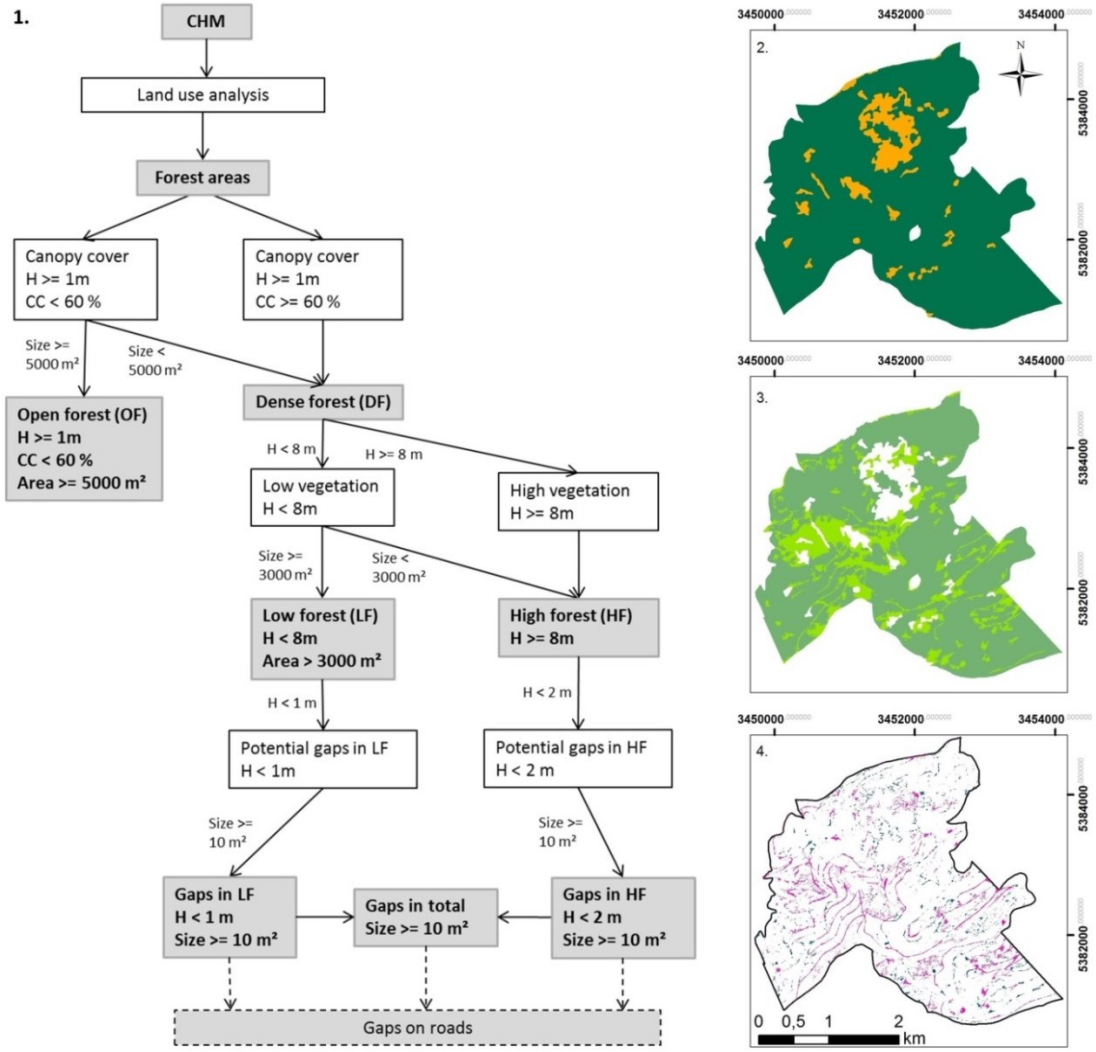

Figure 2-4 Workflow of the CHM analysis for forest gap extraction based on the following parameters: vegetation height (H), canopy cover (CC) and area size (1). Grey boxes indicate important in- or outputs, dashed lines represent an additional post-processing step. On the right, exemplary results for 2009 are shown: (2) discrimination between open forest (OF, yellow) and dense forest (DF, green), (3) classification of DF into low (LF, light green) and high (HF, dark green) and forest stands and (4) gap extraction in LF (pink) and HF (blue).

Forest gaps

Forest gaps were identified separately for LF and HF. All cells with canopy heights less than 1 m within LF were identified and grouped using the function region group with 8 neighbours, i.e.

including not only neighboring cells with adjacent border but also diagonal neighbours. The same procedure was carried out for raster cells less than 2 m height within HF. In both classes, LF and HF, groups with a minimum size of 10 m² were retained and reclassified into forest gaps.

Gaps on and next to forest roads

Gaps on and next to forest roads and skidding trails were identified in a post-processing step using 2D reference vector data from ATKIS and Forest Geoinformation databases. Since both files contained minor errors (i.e. missing data, location inaccuracies) features missing in the more comprehensive ATKIS file were added from the Forest Geoinformation database. Gaps located on or adjacent to roads were selected within a 5m buffer to both sides of the road or skidding trail (Figure A 2-1).

2.2.3.4 Validation

The discrimination between open and dense forest and the detection of gaps were evaluated by a comparison with visual stereo-interpretation of the original aerial imagery using Stereo Analyst for ArcGIS 10.2 (GEOSYSTEMS GmbH, 2014). Therefore we generated independent evaluation data at circular sampling plots (r = 25 m, corresponding to the window-size used for open and dense forest classification). Two sets of evaluation plots were generated. For testing the accuracy of the classification into open and dense forest an equal amount of plots was placed randomly in both forest types. The plots for evaluating the performance of the forest-gap detection were selected according to a stratified random design.

Open-dense forest

For evaluating the accuracy of the classification into open and dense forest 40 plots were randomly placed in each of the two classes (Figure 2-5.a). With a plot size of 1962.5 m², the total evaluation area per class amounted to 7.9 ha, corresponding to 9.5 % and 27.0 % of the open forest of 2009 and 2012 respectively. A change of the forest type from open to dense between 2009 and 2012 was allowed for additional validation of the change-recognition performance. The set of sample plots located in open forest of 2009 was therefore also kept in 2012. However, since 30 of the evaluation plots in the open forest changed to dense forest in 2012 additional 30 sample plots were generated within the open forest of this year to maintain a balanced verification dataset. Within the evaluation plots canopy cover was visually estimated in 5 % steps, aided by schematic illustrations (AFL, 2003; Ahrens *et al.*, 2004), and the forest class was assigned accordingly. The agreement between visual and automatic mapping was assessed using different evaluation indices based on a confusion matrix.

Overall, producer's (probability that the automatically mapped class was also visually confirmed) and user´s (Story and Congalton, 1986) (probability that visually interpreted class was also automatically classified as such) accuracy (Congalton, 1991; Stehman and Czaplewski, 1998; Rossiter, 2014) as well as Cohen's kappa (Cohen, 1960) were calculated using the package "caret" in R (Kuhn *et al.*, 2015).

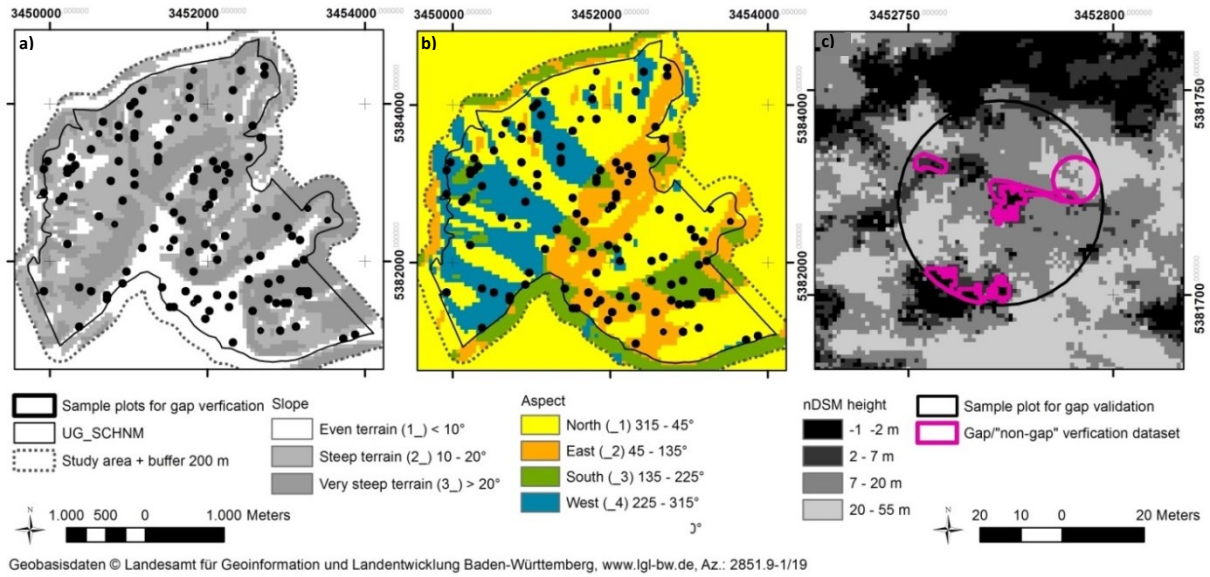

Figure 2-5 Sampling design of the evaluation dataset: Location of sample plots for gap verification with regard to the strata defined by slope (a) and aspect (b); Example of an evaluation plot with visually identified gaps and "non-gap" evaluation circle indicated in pink (c).

Gaps

Since the gap-mapping accuracy was expected to vary in relation to two terrain parameters, slope and aspect, evaluation plots were stratified along these two gradients: Three classes of slope (0 – 10° plane, 10 – 20° strong inclined or steep, > 20° very steep, according to the definition of AG Boden (1996) and in line with Wrbka *et al.* (1997)) and 4 classes of aspect (north 315 - 45°, east 45 – 135°, south 135 – 225°, west 225 - 315°) resulted in 12 terrain situations that were extracted from the DEM50 (Figure 2-5.a, b). The focal point of each 50x50 m cell represented a possible center of an evaluation plot (r = 25 m).

Forest gaps were evaluated on 120 evaluation plots (10 per terrain stratum) (Figure 2-5.a, b) covering a total area of 23.6 ha, which corresponds to 2.4 % of the dense forest in each study year. Within the evaluation plots gaps with an area of at least 10 m^2 inside the plot (168 in 2009 and 171 in 2012) were visually assessed, delineated and (Figure 2-5.c) compared with the automatically mapped gaps located with at least 10 m^2 inside the evaluation plot. To assess the correct classification of gap–absence, we randomly placed circles in the dense forest areas within the sampling plots, equal in

amount to the visually verified gaps and in size corresponding to their mean size per year (95 m² in both years).

Correct agreement between visually and automatically mapped gaps was assigned if there was an overlap of at least 80%. “Non-gap” circles were attributed as “wrongly classified” when a gap of at least 8 m² (80% of the minimum gap size) was identified within it. The agreement between visual and automatic mapping was again assessed by means of overall, producers´ and users´ accuracy and Cohen’s Kappa.

Variables affecting mapping accuracy

Since we expected the accuracy of the method to be affected by external factors, selected characteristics of the viewed gaps were visually assessed for each of the gaps mapped in the evaluation plots (Table 2-3). Effects of the recorded variables such as gap size, height of the surrounding forest, presence of shadow, slope, aspect and gap location were tested using Conditional Inference Trees (ctree) vignette of R-package ‘partykit’ (Hothorn *et al.*, 2006; Hothorn and Zeileis, 2015).

Table 2-3 List of variables tested in ctree for having an effect on gap mapping accuracy

Variable	Characteristics	Source	Input format in ctree
Gap size	Area (m²)	Automated mapping, Visual interpretation	numeric
Height of the surrounding forest	1=Low forest (LF<8 m) 2=High forest (HF>= 8m)	Automated mapping	factor
Shadow occurrence	0=none 1=complete 2=partial	Visual interpretation	factor
Slope (degree)	1= plane (0–10°) 2=strongly inclined or steep (10–20°) 3=very steep (>20°)	DEM50 (LGL)	factor
Aspect	Easting (sine of aspect) Northing (cosine of aspect)	DEM50 (LGL)	numeric
Gap type (gap location)	0=inner forest stand, 1=on storm throw 2=on a forest road 3=next to open forest 4=on a skidding trail 5=next to a road or a skidding trail	Visual interpretation	factor

We also evaluated whether missing information in some raster cells (“no-data” cells) could be a reason for a fraction of the undetected gaps. In a DSM created from an eATE point cloud “no-data” cells amounted to 10-15% whereas in a DSM generated from the SGM point cloud this percentage

was much lower (2-3%). This difference was caused by an internal interpolation used by the SGM algorithm during the matching process resulting in an artificial assignment of values to cells, where no points were directly matched.

2.3 Results

2.3.1 Mapping of open and dense forest

Mapping of open forest areas resulted in 82.7 ha (8 % of the study area) and 28.8 ha (3 %) in 2009 and 2012 respectively. The number of open forest patches decreased from 31 to 28. This includes also open forest patches smaller than 0.5 ha located at the border of the study area but being part of larger open forest areas. The mean size of the open forest patches within the study area changed from 3.5 ha to 1.6 ha, which illustrates the closure of open forest areas from their borders inwards. Dense forest amounted to 938.5 ha (92 % of the study area) in 2009 and 992.5 ha (97 %) in 2012.

The classification obtained with the chosen settings agreed well with the results of the visual assessment (Table 2-4, Figure A 2-2, Table A 2-1) with accuracy measures between 0.85 and 1.00 confirming a very good performance of the method. An assessment of the 12 erroneous classifications revealed that deviations between automatic and visual estimation occurred in plots with canopy cover estimates ranging between 30 and 80 %, with most (75%) of the errors occurring within a narrow 10 % buffer (50-70%) around the canopy cover threshold of 60 %. In 9 of the 12 cases the automated method overestimated the canopy cover. An increased rate of deviation (20%) was found in the 30 plots that changed from open forest in 2009 to dense forest in 2012, which confirms that areas with canopy cover close to the threshold are particularly prone to misclassification.

Table 2-4 Mapping accuracies of the open (positive class) and dense forest (accessed with 95 % confidence interval (CI))

	Producer´s accuracy	User´s accuracy	Producer´s accuracy	User´s accuracy	Kappa	Overall accuracy
	OF	OF	DF	DF		with 95 % CI
2009	0.92	0.92	0.92	0.92	0.85	0.92
2012	0.87	1.00	1.00	0.85	0.85	0.92

2.3.2 Identification of low and high forest

Patches with low (LF) and high (HF) forest amounted to 82 (175.0 ha) and 18 (763.6 ha) respectively in 2009, versus 70 (211.3 ha) and 22 (781.3 ha) in 2012 (Table A 2-2). Within the dense forest, high forest stands dominated with a share of about 80 % forming large compact patches with a mean size

of 42.4 ha (2009) and 35.5 ha (2012). The total area of both low and high dense forest increased from 2009 to 2012 to the disadvantage of the open forest. Low stands - on average much smaller than high stands - got consolidated and increased significantly in area and size, from a mean size of 1.8 ha in 2009 to 2.9 ha in 2012.

2.3.3 Forest gaps mapping

The automated mapping approach detected 4575 (2009) and 4667 (2012) gaps in the dense forest. Total gap density was 4.9 gaps per ha (7.2 % of the dense forest area) in 2009 and 4.7 gaps per ha (6.3 %) in 2012 (Table A 2-3). Generally, many more (13.7 – 14.6 N/ha) gaps were mapped in the low forest than in the high forest (2.0 – 2.8 N/ha).

2.3.3.1 Mapping accuracy

The comparison of automatic gap-detection with the visually identified gaps revealed good agreement (Table 2-5 and Table 2-6) with an overall accuracy of 0.90 and 0.82 in 2009 and 2012, respectively, and corresponding Kappa values of 0.80 and 0.66. User's accuracies greater than 0.96 show that almost all automatically detected gaps were correctly classified. However, a fraction of the visually identified gaps were not captured during the automated mapping process, which is reflected in omission errors of 0.16 (2009) and 0.28 (2012). Method performance for the "non-gap" areas showed an opposite pattern with producer's accuracies greater than user's accuracies.

Table 2-5 Evaluation results: Comparison of the automated mapping with the results of visual stereo interpretation

	Visual reference					
	2009			2012		
Automated mapping	"Non-gap"	Gap	Total	"Non-gap"	Gap	Total
"Non-gap"	166	31	197	164	63	227
Gap	3	166	171	7	167	174
Total	171	197	368	171	230	401

Table 2-6 Mapping accuracies of automatically generated gaps derived from a comparison with the results of visual interpretation (accessed with 95 % confidence interval (CI))

	Producer's Accuracy	User's Accuracy	Producer's Accuracy	User's Accuracy	Kappa	Overall Accuracy
	Gap	Gap	"Non-Gap"	"Non-Gap"		with 95% CI
2009	0.84	0.97	0.97	0.84	0.80	0.90
2012	0.72	0.96	0.96	0.73	0.66	0.82

However, 71 % (2009) and 73 % (2012) of the visually but not automatically identified gaps were adjacent to automatically mapped gaps indicating that a significant proportion of the gaps have been captured correctly, but the extent delineated was too small.

2.3.3.2 Variables affecting mapping accuracy

Among the tested variables, shadow occurrence and forest height class affected mapping accuracy (Figure 2-6), while no significant effect was found in relation to the other variables tested (Table 2-3). Presence of shadow strongly limits the penetrability of an optical sensor into the lower parts of the canopy. In both study years the occurrence of full shadow in the incision in the forest canopy was the main cause for the erroneous delineation of gaps. The effect of shadow was also confirmed directly during visual verification, as the most of the visually identified but not automatically mapped gaps (70 - 87 %) were identified in areas of total or partial shadow (Table A 2-4).

The height of the surrounding forest stand (LF and HF) determining the depth in the canopy, to which the light can penetrate, is also strongly linked to shadow occurrence. While in 2012 the height of the surrounding forest caused increased failure in gap mapping in HF, in 2009 this tendency was not pronounced. Generally the gaps in locations without or with partial shadow occurrence were mapped with a high accuracy in LF and less reliability in HF, whereas the complete shadow occurrence hinders the gap mapping performance in all stand types.

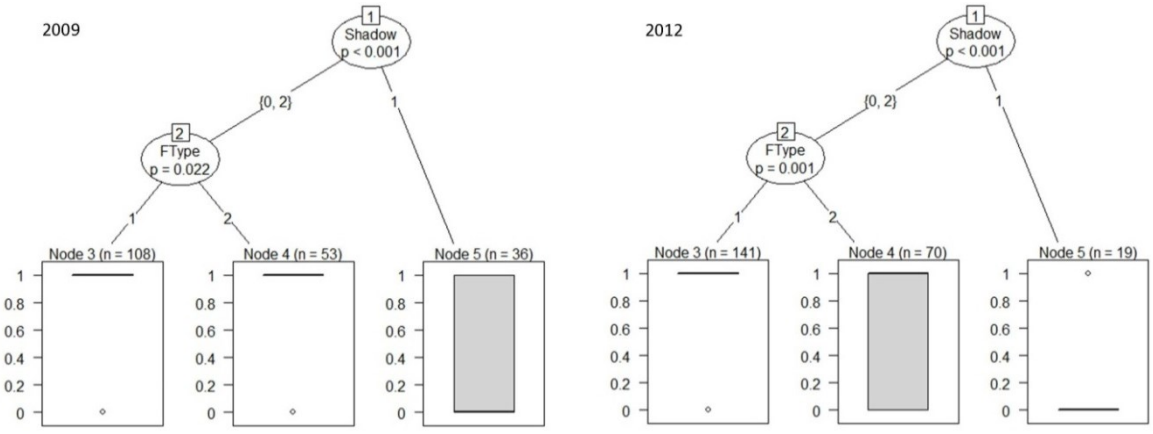

Figure 2-6 Conditional inference tree showing the variables that affected the user´s accuracy of gap-prediction in the evaluation plots in 2009 and 2012. Each node of the tree plot represents one split of the data into significantly different partitions, with variables ranked according to their importance, until no further split is possible (nodes 3, 4, 5). The significance of the split (p-values after Bonferroni correction) is indicated in the splitting nodes. The Y-axis shows the predicted probability of correct gap detection under the given combination of variable values. The variable values splitting the datasets are indicated on the tree branches: Shadow (0=none, 1=complete, 2=partial), Ftype: Forest height class (1=low and 2=high forest).

Despite similar user's accuracies of 0.96–0.98 and overall accuracies higher than 0.79, producer's accuracy in high forest was much lower than in low forest with 0.70 in 2009 and 0.52 in 2012 (Table 2-7 and Table 2-8)

The analysis of the "no-data" cells revealed that they did not only occur in shadowy incisions in the canopy cover, e.g. along roads or in stands with a highly heterogeneous vertical structure but also in low forest stands and on hilltops where aerial photographs should theoretically deliver good material. Such "no-data" cells were mostly located along flight strips (2009), particularly in the outer parts of the lateral and longitudinal overlapping zone of the images (2009, 2012) ().

Table 2-7 Confusion matrix comparing the automated gap mapping results with visually verified gaps and "non-gap" areas in low forest (LF) and high forest (HF) in 2009 and 2012

Automated mapping		Visual interpretation			
		2009		2012	
		"Non-gap"	Gap	"Non-gap"	Gap
LF	"Non-gap"	17	8	32	22
	Gap	2	112	2	122
HF	"Non-gap"	149	23	132	41
	Gap	3	54	5	45

Table 2-8 Accuracy of the automated mapping of gap and "non-gap" areas assessed visually (with 95 % of confidence interval (CI)) in low forest (LF) and high forest (HF) in 2009 and 2012

	Forest Height Class	Producer's Accuracy	User's Accuracy	Producer's Accuracy	User's Accuracy	Kappa	Overall Accuracy
		Gap	Gap	"Non-Gap"	"Non-Gap"		with 95% CI
2009	LF	0.93	0.98	0.89	0.68	0.73	0.93
	HF	0.70	0.98	0.98	0.87	0.73	0.88
2012	LF	0.85	0.98	0.94	0.59	0.93	0.86
	HF	0.52	0.96	0.96	0.76	0.84	0.79

An intersection of the "no-data"- layer with the gap validation dataset showed that only ca. 10 % cells of all visually, but not automatically identified gaps were actually classified as "no-data" cells (Table A 2-5). The assignement of new values to original no-data cells by means of interpolation from the neighbouring points during the image matching or raster transformation resulted in height values depending on the surrounding forest characteristics.

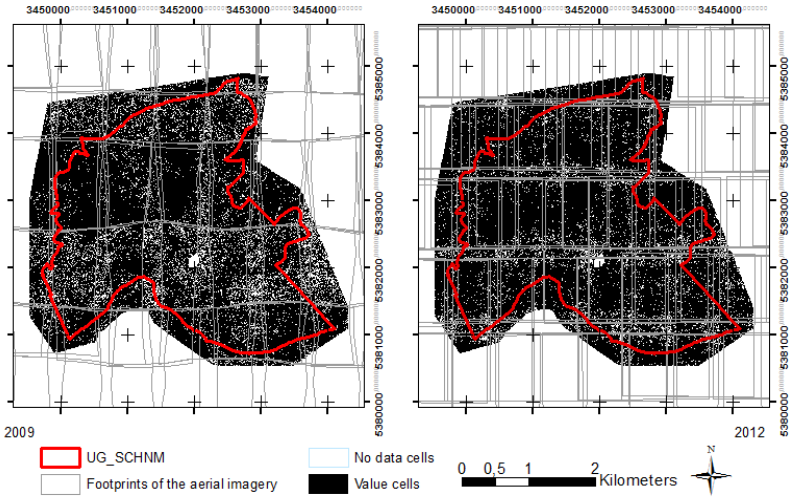

Figure 2-7 Distribution of "no-data" points (white) from eATE image matching algorithm in the study area in relation to aerial imagery footprints in 2009 (**left)** and 2012 (**right**).

2.3.3.3 Gap size and total area

In the study area, gap sizes ranged from 10 m² (predefined minimum size) to 19091 m² and 12556 m² in low forest (2009 and 2012 respectively) and to 2105 and 2495 m² in high forest (Table A 2-3). Despite the great difference in maximum sizes, median values ranged between 26 and 36 m². In 2009, gap size was significantly greater in LF than in HF (Wilcoxon rank sum test, p-value=0.0006) whereas in 2012 this characteristic was no longer pronounced (p-value=0.5644).

The most and the largest gaps were mapped in low stands, even though they constituted only about 20 % of the dense forest in both years. Moreover, the variance in gap size was most pronounced in LF, with standard deviations 2.5 – 3.2 times larger than for gaps in HF in the same study year. In high forest, number, mean size, median size and density of the gaps decreased between 2009 and 2012 amounting to a 36 % reduction of the total gap area in this class. In contrast, the amount and density of gaps in low forest increased from 13.8 gaps per ha in 2009 to 14.6 gaps per ha in 2012, with only minor increase of the total area.

Most gaps mapped in both stand types were very small (10 – 30 m²) or small (31 – 100 m²), together making up 75 - 81 % of all gaps and 13 - 23 % of the total gap area in all height classes and years (Figure 2-8). In low stands the greatest fraction of the total gap area (53 – 60 %) consisted of very large gaps (>1000 m²) whereas in high stands 58 - 59 % pertained to large gaps (101-1000 m²). In both low and high forest the number and area of smaller gaps increased whereas the large and very large gaps decreased from 2009 to 2012.

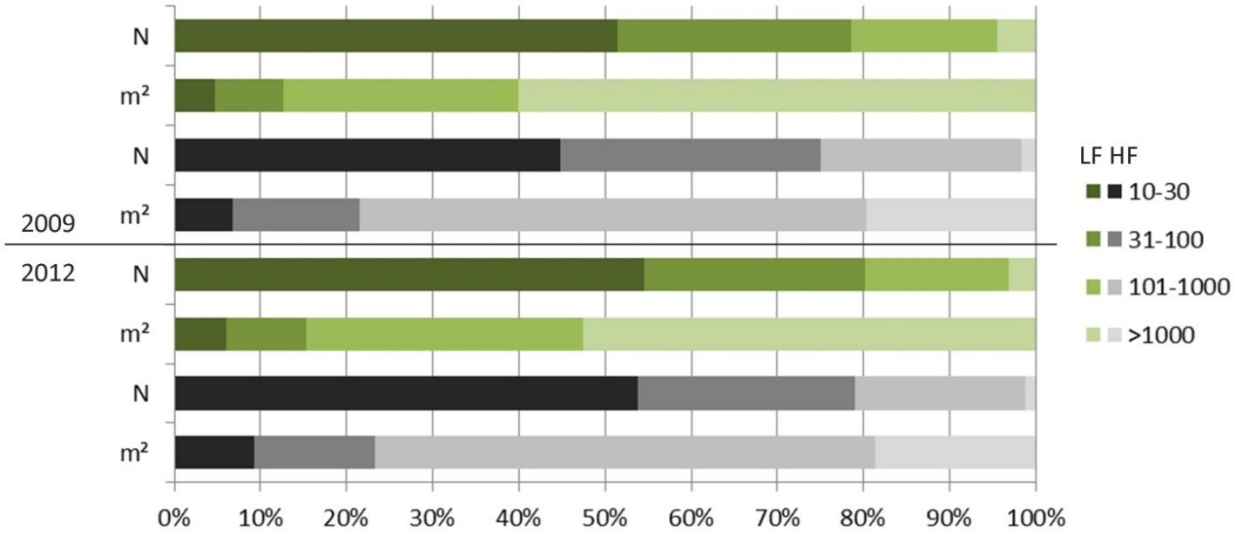

Figure 2-8 Number (N) and area (m²) of mapped gaps breakdown into size classes per year and forest height class (green scale – low forest LF, <8m height, grey scale – high forest HF, >8m height) given as percent of the total gap number or area in the respective class.

2.3.3.4 Gap changes

55% of the gaps recorded in low stands and 30 % of the gaps in high stands mapped in 2009 were also confirmed in 2012 (Table A 2-3, Persisting gaps 2009-2012, Figure 2-9). A substantial proportion (37 % of N, 45% of the total area) of gaps found in low forest in 2012 originated from open forest in 2009. Shifts between low and high forest were not that significant with 17 % of gaps in high forest of 2012 originating from gaps in low stands of 2009. The remaining differences in the amount of mapped gaps between the study years were due to displacement or shrinking of gaps.

2.3.3.5 Gaps on forest roads

Within the evaluation plots, 60 (30 %) gaps in 2009 and 85 (36 %) in 2012 were identified directly on a road or skidding trail, another 18 (9 %) and 17 (7 %) were found adjacent to these distinct linear features (Table A 2-6).

These figures were slightly higher than in the total study area where - depending on the mapping year and forest height class - 37 % (2009) and 25 % (2012) were located on or adjacent to a forest road (Table A 2-7). Even though not all these gaps were captured due to shadow occurrence and canopy closure above the road (Figure A 2-1), this gap type represented 67-80% of the total gap area each year and forest height class, with an average gap-size varying from 40 to 88m².

Excluding the gaps on or next to roads resulted in an average gap density of 10-11 gaps/ha in LF and 1-2 gaps/ha in HF and average gap-size of about 50 m^2 (Table A 2-8).

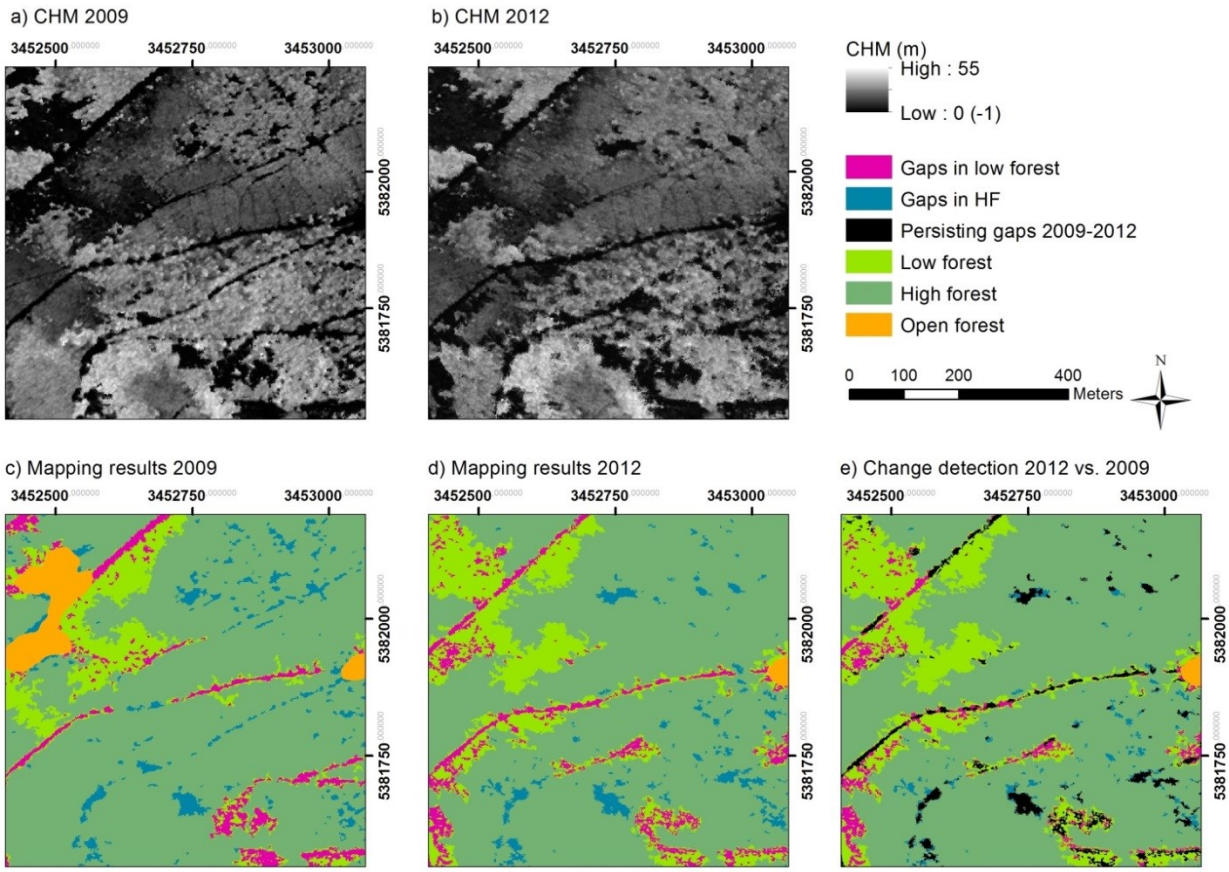

Figure 2-9 Example of gap mapping results: a) Canopy Height Model (CHM) of 2009, b) CHM of 2012, c) Mapping results of 2009, d) Mapping results of 2012, e) Change detection: gaps in 2012 vs. 2009. Gaps were only mapped in dense forest (> 60% canopy cover) classified into LF: low forest (<8m height) and HF: high forest (>=8m height). The remaining area is open forest (<60% canopy cover).

2.4 Discussion

Assessing forest gaps for biodiversity research purposes requires a clear definition and classification of gaps in relation to the research goal. The definition we adopted adhered to the fact that most species-habitat studies refer to gaps as canopy openings with a fixed maximum height of vegetation in a gap. Given the great variance in species-specific requirements regarding forms and types of gaps and in order to maintain a broad applicability for habitat assessments for various species, we applied a low threshold regarding minimum gap size and no *a priori* restrictions regarding shape or minimum diameter. With regard to gap-delineation based on remote-sensing this definition entails some general limitations which are related to the penetrability of the light through the tree canopy. In addition, compared to using LiDAR-based assessments, specific problems arise when using aerial imagery for deriving measures of vegetation height as a basis for gap-delineation.

2.4.1 Image matching and Canopy Height Models

Regularly updated and standardized aerial photographs from public flight mapping campaigns offer good possibilities for assessing forest structure in a cost-efficient way, especially when aiming at long-term monitoring. Primarily acquired to deliver high accuracy 3D earth surface measurements for general administration, economy and science applications these data - offered for public research at a special low cost - also provide a valid basis for mapping forest gaps with high accuracy. Even so, the image matching algorithms using aerial and satellite imagery for deriving DSMs still bear some potential for improvement, especially in rugged terrain and forest stands of complex structure (Hobi *et al.*, 2015). Wang *et al.* (2015b) indicate that their method provides a high degree of accuracy in managed mixed forest, with lower accuracies in mountainous forests, which can be explained by the mismatch between the generated DSMs as a result of different flight angles of the imagery from different flight campaigns. Similar situations can be observed in our study, due to the acquisition of the aerial imagery in different study years, where the data provider used two different cameras. Adler *et al.* (2014) observed that even in flat terrain different DSM matching algorithms produce different results, especially in highly structured canopy situations. Mountainous forests are likely more structured than intensively managed stands in the lowlands and thus particularly prone to shadow occurrence. In our study most of slopes were steep or very steep which definitely influenced the quality of the aerial imagery and the DSM accuracy.

The distribution of “no-data” cells points towards multiple sources of problems: first, inaccurate point matching in the outer areas of the camera viewing angle, second, shadow occurrence and third a possible inaccurate relative orientation of the stereo images.

The use of a “terrestrial bottom-up” gap-definition with predefined fixed (in contrast to a relative) maximum gap-vegetation height entails a significant effect of the DSM quality on the gap mapping performance, as inaccuracies in the surface heights in the order of magnitude of 1 m or more (Hobi and Ginzler, 2012; Ginzler and Hobi, 2015) significantly affect the delimitation of gaps with a maximum ground vegetation heights of 1 or 2 m.

Since the user’s influence on the acquisition process and quality of aerial imagery from standard flight campaigns of national or regional mapping agencies is limited, some shadows have to be accepted (Wang *et al.*, 2015b). Yet, it is crucial to know the accuracy of the input data as they influence the usability and reliability of the generated DSM (Hobi and Ginzler, 2012). A quality assessment of the aerial imagery concerning light conditions and associated shadow occurrence

could thus be beneficial. In our study, the details regarding flight time of acquisition of the aerial images were not available.

2.4.2 Forest classification and gap identification

DSMs derived from aerial imagery proved promising for forest gap identification as the results of canopy cover and forest gaps mapping were good. Moreover, important for application across large areas, gap extraction from a ready CHM was very fast (i.e. 170 – 250 ha per minute, depending on processor and memory), whereas the image matching was the most time-consuming part.

As one crucial step in the workflow the class of open forest was delineated. This is an important feature for many forest species and therefore a valuable side-product of our study. Canopy cover estimation both in entirely open areas as well as in a mixture of open and dense forest stands worked well, with uncertainties mostly occurring in areas with intermediate canopy cover (i.e. close to the predefined threshold for differentiation between open and dense forest of 60% cover). A sharp delimitation of naturally complex and continuous structures such as canopy cover is inherently difficult and can be considered as the main reason for misclassifications. In addition, some minor omission errors at the edges of the open areas were later captured and classified as gaps in the automated mapping process.

Forest gap mapping accuracy decreased with forest height and associated shadow occurrence. Presence of complete shadow strongly limited the method performance, where the areas of biggest mismatch between the automated detection and visual interpretation of gap features were observed. In areas with good visibility or with a partial shadow occurrence the method results were coupled with the height of the surrounding forest. Generally more gaps and bigger gap areas were automatically mapped in low forest stands, even though they constituted of only ca. 20 % of the dense forest in each study year. While the maximum height of 8 m of the low forest stands mostly allowed good insight in the inner parts of the stand, the results of gap mapping in the high stands, especially in 2012 where the relative shadow occurrence was higher, probably due to a later summer flight date, were not fully satisfying as gaps were underestimated.

Canopy gaps are an important structural attribute associated with variance in canopy cover (McElhinny *et al.*, 2005). In the aerial imagery this variance is represented by different spectral reflections, different texture and shadow occurrence in the obscured locations between trees. The latter affected not only the results of the automatic matching but also their verification, as the visual interpretation of gaps in shadowy areas was partially obstructed. In our case some uncertainties occurred during visual interpretation, due to the difficulty of ground identification, shadow

occurrence and not always orthogonal tree projection in 3D-view. As a consequence some potential reference gaps were probably omitted and the evaluation dataset was possibly incomplete. On the other hand, gaps on roads were potentially overestimated, when verifying shadowy canopy openings located along roads axes, influenced by the perception and automatic complementation of linear features by the visual interpreter.

We preferred visual assessment over field assessments for validation as the latter is less accurate due to errors caused by differences in human perception of a forest gap from the ground (Hobi *et al.*, 2015) and from the air, as well as to difficulties in gaining good position accuracy (Gaulton and Malthus, 2008). Nevertheless, an additional field check would be advisable as a control measure especially with regard to the vegetation height in the gap. However, good temporal agreement between the remote sensing data and the field assessment is crucial. Rapid vegetation growth following improved light conditions in canopy openings can bias the validation results, even when field assessments are performed only shortly after the remote sensing data had been gathered.

Gap mapping methods presented by other authors resulted in similar accuracies, although not directly comparable due to differences in validation methodology based on both visual and field measurements. For example, 82% of the gaps mapped from satellite imagery by Garbarino *et al.* (2012) were correctly classified when compared to visual assessments, while Hobi *et al.* (2015), also using satellite imagery as input data, achieved a producer´s accuracy of more than 65% compared to visually interpreted data. Focusing on the ecological aspects of gaps and their dynamics most of authors did not provide an explicit accuracy assessment of their gap mapping results. An exception are Vepakomma *et al.* (2010) who show a pictorial example revealing a strong similarity of the gaps delineated based on LiDAR with high-resolution images, and report a 96.5% match with field assessments.

2.4.3 Gap density and post-processing

The total gap density in the study area was similar in both study years with 4.9 and 4.7 gaps per ha in 2009 and 2012. 25 to 37 % of the mapped gap features and 67 to 80 % of the mapped gap area per forest height class of low or high forest and year were located on or next to forest roads. These gaps are characterized by specific environmental conditions and might thus be analyzed separately in ecological studies. The quantification of gap changes over time revealed clear trends in the gap dynamics, with forest height growth and densification leading to a decrease in gap area. However it is still difficult to judge, which changes in gap form and location were due to natural processes of forest growth and which result from technical difficulties such as inaccuracies in image matching

processes or different light conditions in the aerial imagery datasets. For a one-to-one analysis of gap dynamics (persistence, expansion, decline, displacement) and change detection, an additional assessment of the CHM quality is advisable (including date & time of the aerial images taken) and methods are required to automatically disentangle the mentioned sources of change.

2.4.4 Gaps as a parameter in the biodiversity studies

In biodiversity conservation context the variables representing forest structural complexity need to reflect observed relationships with faunal or floristic diversity (Zellweger *et al.*, 2013).

The characteristics of the gaps detected in our study such as: number, density, size, spatial coverage and form can be used directly as input into habitat models like Zellweger *et al.* (2013) does using forest gap density or Braunisch *et al.* (2014) calculating the number of gaps per ha, both to model the influence of forest structural complexity on multi species occurrence of four temperate mountain forest bird species: Capercaillie, Hazel Grouse (*Bonasa bonasia*), Three-toed woodpecker (*Picoides tridactylus*) and Pygmy Owl (*Glaucidium passerinum*). The mapped gap features can also serve derivation of suitable habitat indices e.g. gap area ratio that is used by Braunisch and Suchant (2013) for recommendations regarding forest management measures for Capercaillie conservation or calculation of desired gap metrics e.g. perimeter/area ratio or gap shape complexity index as used by Getzin *et al.* (2012) for assessment of floristic biodiversity of the forest understorey. Also canopy cover mapped as an interim step in our method was used as a model variable and one of management recommendations regarding habitat suitability for selected forest dwelling species e.g. Capercaille (Graf *et al.*, 2009; Bollmann *et al.*, 2013; Braunisch and Suchant, 2013).

Studies mentioned above proved that the parameters derived from LiDAR describing the canopy cover, its vertical variation and forest gaps are valuable input into habitat models and important structural attributes associated with occurrence of selected conservation-relevant species. Based on that knowledge we anticipate that the height information of the DSMs derived from image matching of stereo aerial imagery, although not as accurate as the LiDAR measurements but still achieving a high level of detail in comparison to satellite data, are suitable for gap detection for biodiversity studies at various, also large spatial scales.

2.5 Conclusions

The gap mapping method was developed for automated identification of biodiversity relevant forest structures at large spatial extents to support biodiversity studies and planning of forest conservation measures. Overall method performance was good, with very good results in low stands. In high

stands the results were moderate to insufficient depending on the study year. Main error sources we identified were linked to the quality of the input CHM, resulting from shadow occurrence and geometric limitations of stereo image matching.

Focusing on publicly available data, used without prior radiometric and geometric enhancement for fast and cost-efficient processing, we expected that remote sensing products from the public mapping agencies serve as reliable input data. Yet, the aerial images from two standard flight campaigns in Baden-Württemberg differed in quality, which affected the results. The influence of the spatial resolution and overlap of the stereo aerial images requires further research in order to optimize and standardize future flight campaigns, so as to deliver suitable material for reliable monitoring of gaps and other forest parameters.

We recommend a quality check of the input data prior to the gap extraction. Using shadow and "no-data" masks, as well as analysing the sun angle at the moment of the image acquisition is advisable to identify areas where the DSM values might be erroneous and where additional gaps can be expected. Changing the settings (e.g. maximum vegetation height in a gap) to more liberal may help identifying additional potential gaps in these areas.

Next to using aerial images of higher spatial resolution and/or higher overlap better mapping accuracies may be expected in flat terrain, where image matching algorithms perform better than in rugged mountainous topography (Ginzler and Hobi, 2015). Since time series analyses demand DSMs calculated using the same settings for all study years, to avoid variations in systematic errors from different image-matching algorithms (Adler *et al.*, 2014) quality reference standards for image matching as well as for outlier removal are required to improve the comparability of the results.

Terrestrial bottom-up gap definitions, as used in most ecological studies, entail some problems in combination with remote sensing data since a constant maximum vegetation height in a gap in contrast to continuous values of forest heights can be a one factor causing the omission of some potential gap cells. However, our method allows changes in gap mapping parameters and flexible application of thresholds depending on the ecological scope of the study in which the mapped gaps will be used. Moreover, the mapping workflow can be applied to any raster CHM delivering standardized results for a rapid forest gaps analysis.

2.6 Acknowledgments

The authors wish to thank Joao Paulo Pereira for technical support in the last phase of the project.

2.7 Author contributions

The method was developed together by Katarzyna Zielewska-Büttner and Petra Adler. Katarzyna Zielewska-Büttner also designed and carried out the visual stereoscopic validation, analyzed the data and wrote the manuscript. Michaela Ehmann formulated the gap definition and made important initial developments of the workflow. Veronika Braunisch was a scientific advisor and contributed significantly in the process of conceiving the method design, validation and writing.

Conflicts of Interest: The authors declare no conflict of interest.

2.8 Supplementary material

Figure A 2-1 Example for the verification of gaps mapped in 2012 on and next to forest roads (gaps intersecting 5 m buffer of the road centerline selected by location).

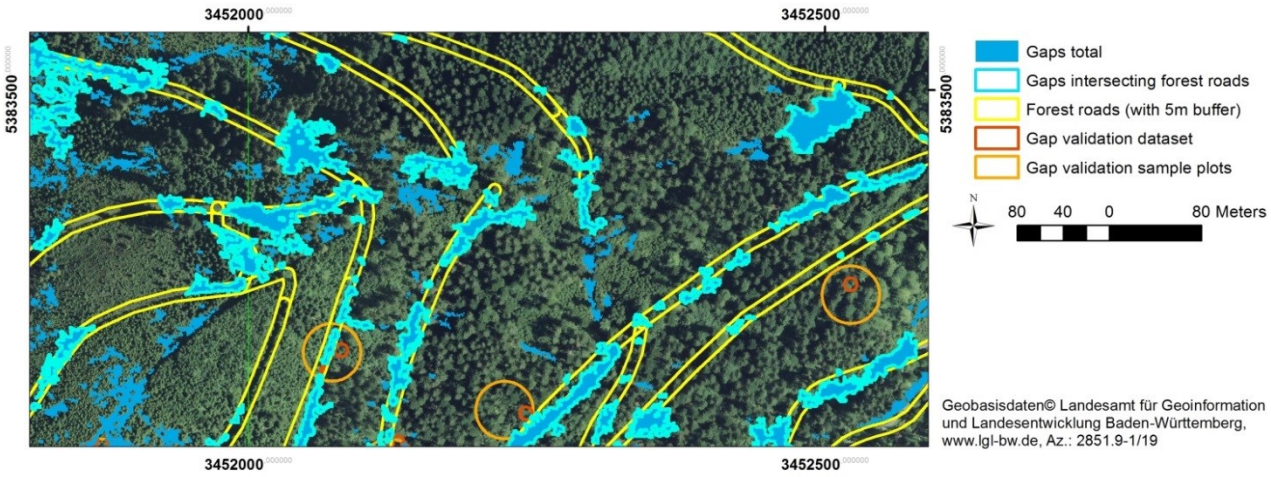

Figure A 2-2 Example of the results of delimiting open forest (delineated in light green) within a dense forest matrix in 2009 (right) and 2012 (left)

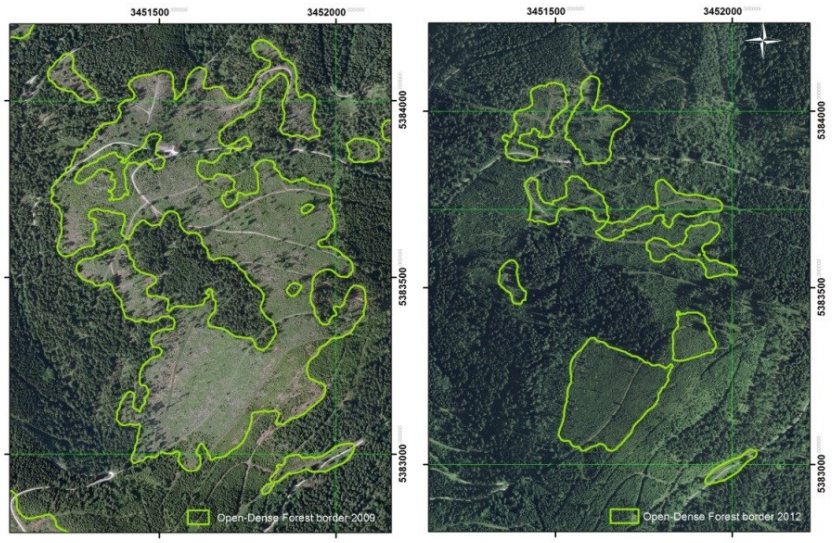

Table A 2-1 Confusion Matrix for evaluating the automated determination of open forest (OF) and dense forest (DF) with the results of visual classification

Automated mapping	Visual reference					
	2009			2012		
	OF	DF	Total	OF	DF	Total
OF	37	3	40	40	0	40
DF	3	37	40	6	34	40
Total	40	40	80	46	34	80

Table A 2-2 Descriptive statistics for low (LF<8m) and high (HF>= 8m) forest stands mapped in 2009 and 2012

Statistics	2009		2012	
	LF	HF	LF	HF
N	82	18	70	22
Minimum size (m²)	3020	3046	3126	3874
Maximum size (m²)	659404	6177173	834811	7383150
Mean size (m²)	21340	424257	30180	355155
Median size (m²)	6147	8957	5534	11478
Interquartile 25%	4237	3981	4283	5272
Interquartile 75%	12384	60830	17422	27214
SD (m²)	74429	1417558	105212	1533808
Sum area (m²)	1749919	7636625	2112599	7813413

Table A 2-3 Descriptive statistics of gap mapping results per year (including gaps persisting in both years) and forest type (low (LF) and high (HF) forest and in total)

	2009			2012			Persisting gaps 2009-2012		
Statistics	LF	HF	Total	LF	HF	Total	LF	HF	Total
N	2401	2174	4575	3088	1579	4667	1330	652	2765
Density (N/ha)	13.7	2.8	4.9	14.6	2.0	4.7	6.3	0.8	13.1
Min size (m²)	10	10	10	10	10	10	1	1	1
Max size (m²)	19091	2105	19091	12556	2495	12556	4129	1437	4129
Mean size (m²)	188	113	152	151	98	133	130	66	101
Median size (m²)	29	36	32	26	27	27	57	62	65
Interquartile 25%	16	17	16	15	15	15	18	22	20
Interquartile 75%	81	99	89	73	80	75	365	230	329
SD (m²)	699	221	530	545	215	461	367	137	283
Total area (m²)	450722	246026	696748	465853	155418	621271	173296	43169	279593
Coverage (m²/ha)	2576	322	742	2205	199	626	820	55	1323

Table A 2-4 Shadow occurrence statistics (yes=shadow, in division to “partial” and “full” shadow coverage) in areas of visually identified and not automatically mapped gaps in 2009 and 2012

Year	2009				2012			
Shadow occurrence	**no**	**shadow**			**no**	**shadow**		
		yes	*partial*	*full*		**yes**	*partial*	*full*
No of visually and not automatically identified gaps	**4**	**27**	*20*	*7*	**19**	**38**	*27*	*17*
% of visually and not automatically identified gaps	**13**	**87**	*21*	*74*	**30**	**70**	*27*	*43*

Table A 2-5 Statistics of “No-data” raster cells located within the evaluation plots for gap validation in 2009 and 2012

Year	**2009**	**2012**
“No-data” cells (no.) / % of total cells in evaluation plots	4107 (12.2 %)	3015 (8.8 %)
N of “no-data” cell groups (region group with 8 neighbors)	916	918
Max. no. of no cells in a group	77	74
Mean group size (N of no value cells)	4.5	4.5
Other raster cells	29484	31146
Total cells in the gap evaluation plots	33591	34161

Table A 2-6 Types of gaps (in regard to their location within a forest stand (0), on a storm throw (1), on a road (2), next to open forest (3), on a skidding trail (4) and next to a road or a skidding trail(5)) identified during the visual validation in 2009 and 2012

	2009		2012	
Gap type	No	%	No	%
Gap within a forest stand (0)	107	54	114	50
Gap on a storm throw (1)	1	0	13	6
Gap on a road (2)	40	20	54	23
Gap next to an open forest (3)	11	6	1	0
Gap on a skidding trail (4)	20	10	31	13
Gap next to road or skidding trail (5)	18	9	17	7
Gaps on or next to road or skidding trail (2,4,5)	*78*	*39*	*102*	*43*
Total	197	99	230	99

Table A 2-7 Statistics for gaps mapped on or next to forest roads (all gaps intersecting the 5 m buffer from the forest road line)

		Gaps		Gap area (m²)				
Year	Forest height class	N	*% of all gaps in class*	Sum	*% of total class area*	Mean	Range	SD
2009	LF	663	*28*	362328	*80*	87.6	0-6314	286
	HF	806	*37*	164628	*67*	44.5	0-1114	88
2012	LF	760	*25*	343053	*74*	72.3	0-3108	211
	HF	547	*35*	120369	*77*	40.2	0-1020	88

Table A 2-8 Basic statistics of gaps mapped not on or next to roads (solely within forest stands) in low (LF) and high (HF) forest height classes in 2009 and 2012

		Gaps		Gap area (m²)		
Year	Forest height class	N	*Gap density (N/ha)*	Sum	*Gap area per ha (m²/ha)*	Mean
2009	LF	1738	*9.9*	88650	*80*	51
	HF	1368	*1.8*	80274	*67*	59
2012	LF	2328	*11.0*	122846	*74*	53
	HF	1032	*1.3*	35130	*77*	34

3 CHAPTER II: PARAMETERS INFLUENCING FOREST GAP DETECTION USING CANOPY HEIGHT MODELS DERIVED FROM STEREO AERIAL IMAGERY

Chapter II was published as research article:

Zielewska-Büttner, K., Adler, P., Peteresen, M., Braunisch, V. (2016). Parameters Influencing Forest Gap Detection Using Canopy Height Models Derived From Stereo Aerial Imagery. In: Kersten, T.P. (Ed.), 3. Wissenschaftlich-Technische Jahrestagung der DGPF. Dreiländertagung der DGPF, der OVG und der SGPF. Publikationen der DGPF, Bern, Schweiz, pp. 405-416. URL: https://www.dgpf.de/src/tagung/jt2016/proceedings/papers/38_DLT2016_Zielewska-Buettner_et_al.pdf

Zusammenfassung: Lücken sind wichtige Strukturelemente für die Waldbiodiversität. Zur automatisierten Kartierung von Lücken in Relation zur umgebenden Bestandeshöhe und –bedeckung entwickelten wir eine Methode, welche auf von Stereo-Luftbildern abgeleiteten Kronenhöhenmodellen (CHMs) und einem LiDAR-Geländemodell beruht. Zur Evaluierung der Methode und der Bestimmung der wichtigsten Fehlerquellen wurden in einem 1021 ha großen Modellgebiet im Schwarzwald (Südwestdeutschland) die Kartierergebnisse aus drei Befliegungen (2009, 2012, 2014) verglichen. Die Befliegungen von 2009 und 2012 hatten eine Bodenauflösung von 20cm und eine Überlappung von 60 % in Flugrichtung und 30% quer. 2014 war die Bodenauflösung 10cm und Überlappung 80%, respektive 60%. Die Validierung erfolgte durch visuelle Stereointerpreation. Schattenvorkommen und die geometrischen Grenzen der Stereobildauswertung wurden als Hauptfehlerquellen erkannt.

Summary: Gaps in the canopy are important elements for forest biodiversity. We developed a method based on Canopy Height Models (CHMs) derived from stereoscopic aerial imagery and a LiDAR-based Digital Terrain Model (LiDAR DTM) to automatically delineate forest gaps in relation to height and cover of the surrounding forest. To evaluate the factors affecting the mapping accuracy, we compared the results from three different flight campaigns (2009, 2012 and 2014) in a 1021-ha model region in the Black Forest, Southwestern Germany. The public campaigns of 2009 and 2012 were taken with an overlap of 60% within stripe and 30% between stripes and an overall resolution on ground of 20cm. Data from 2014 had a 10cm resolution and an overlap of 80% within stripe and

60% between stripes. The validation was done by visual stereo-interpretation. Shadow occurrence and geometric limitations of the stereo aerial imagery were identified as main error sources.

3.1 Introduction

Forest gaps are considered important structural elements in forest ecology. They play a key role in forest regeneration processes (Getzin *et al.*, 2014) and provide suitable habitat structures for animal species that depend on semi open habitats (Sierro *et al.*, 2001; Müller and Brandl, 2009; Zellweger *et al.*, 2013). Canopy gaps are therefore of great interest for research in the fields of stand structure and regeneration dynamics as well as biodiversity and nature conservation. In addition to the widely used traditional field-data collection for identification and quantification of the canopy gaps in ecological studies, the use of remote sensing data has been recently recognized as a good source of suitable data enabling the analysis of the canopy structure at various, often broad spatial scales. The first method that is usually chosen for forest gap detection (VEPAKOMMA *ET AL.*, 2010; VEPAKOMMA, 2012) and habitat mapping for biodiversity and nature conservation purposes (Bässler *et al.*, 2010; Braunisch *et al.*, 2014; Seibold *et al.*, 2014) is Light Detection and Ranging (LiDAR) that is considered to deliver a more detailed picture of the horizontal and vertical forest structure than any other remote sensing system. However the recent technical advances in the field of digital photogrammetry demonstrate the great potential of the automatic image matching for the generation of Canopy Height Models (CHMs) and for deriving important forest parameters (Betts *et al.*, 2005; Straub *et al.*, 2013; Kotremba, 2014; Wang *et al.*, 2015b). Thus, to assess the viability of gap detection based on publicly available data we focused our research on CHMs derived from the standard stereo aerial imagery and the official LiDAR based Digital Terrain Model (LiDAR DTM), which are delivered in regular time intervals by the regional mapping agency of Baden-Württemberg (LGL). We aimed for a gap mapping tool which would deliver standardized and replicable results when applied on publicly available data either in form of original aerial imagery, point clouds or a raster CHM.

Gaps were detected and delineated in relation to height and cover of the surrounding forest in three steps: (1) open and dense forest are identified, (2) dense forest is classified into low and high forest and (3) gaps are extracted in the latter two classes. The method is described in Zielewska-Büttner *et al.* (2016a). In this conference paper we present parameters influencing the method performance with regard to canopy gaps detection (1). In addition we test in more detail the benefits of using a shadow mask (2) and discuss effects associated with variance in flight conditions (3). We also

consider the variance introduced by different image matching algorithms (4). Finally, the influence of spatial resolution and overlap of the stereo aerial images are presented comparing the results obtained with data of different flight campaigns (5).

3.2 Material and Method

3.2.1 Study area

The study area of 1021 ha (excluding the mountain lake surface of the Huzenbacher See) is located in the State of Baden-Württemberg, Southwestern Germany, in the northern Black Forest (8° 34' E, 48° 58' N). It is characterized by a heterogeneous topography with elevation ranging from 493 to 941 m, and a high variance in forest successional stages. Most slopes (77,5 %) are very steep (> 20°) or strongly inclined (10 - 20°) (AG Boden, 1996). Among the dominant tree species are Norway spruce (*Picea abies* L.) with admixture of Silver fir (*Abies alba* Mill.) and Scots pine (*Pinus sylvestris*). The broadleaved tree species account for less than 30 % in most (> 80 %) forest stands. The area is covered by a dense forest road network of 187 m/ha and underlying different protection regimes.

3.2.2 Remote sensing data

As primary input data for the method development, aerial imagery datasets from three flight campaigns (2009, 2012, 2014) were used (Table 3-1).

Table 3-1 Technical characteristics of the aerial image data used in the method development (2009, 2012) and the higher resolution and overlap data comparison (2014) (from ZIELEWSKA-BÜTTNER et al. 2016, modified)

Year	2009	2012	*2014*
Camera	UltraCamXp	DMC II 140 – 006	*UltraCamXp*
Panchromatic / color lens focal length	100 / 33 mm	92 mm	*100.5 mm*
Resolution	20 cm	20 cm	*10 cm*
Overlap	60 % / 30 %	60 % / 30 %	*80 % / 60 %*
Image type	Digital color infrared (RGB NIR)	Digital color infrared (RGB NIR)	*Pansharpened digital color infrared (RGB NIR)*
Angle-of-view from vertical, cross track (along track)	55° (37°)	50,7° (47,3°)	55° (37°)
No. of stripes in the block file	3	6	*4*
No. of pictures in the block file	23	48	*69*
Flight date	23.05.2009	01.08.2012	*17.07. – 19.07.2014*

Data (including the absolute orientation of the images) were provided by the state agency of spatial information and rural development of Baden-Württemberg (LGL) as pan sharpened, 4 channels (red, green, blue and near-infrared (RGB NIR)) stereo aerial images with radiometric resolution of 8 (2009) and 16 (2012 and 2014) bit. Data of 2014 originated from a special flight campaign of the Black Forest National Park. The overall spatial resolution of the imagery was 20 cm with an overlap of 60 % (end lap) and 30 % (side lap) in 2009 and 2012; and 10cm, 80% and 60% respectively, in 2014. In line with our goal of using only publicly available data, we limited the additional data used in the study to the products of the LGL (LiDAR DTM) or internal data of the forestry administration (forest road network dataset).

3.2.3 Gap mapping method

The gap mapping method was based on Canopy Height Models (CHMs) of 1 m ground resolution including the potential vegetation points of height between -1 and 55 m vs. the LiDAR DTM. The Digital Surface Models (DSMs) serving as basis for the CHMs generation were calculated from the stereoscopic aerial imagery using two image matching algorithms: Leica Photogrammetry Suite enhanced Automatic Terrain Extraction (LPS eATE (ERDAS 2012)) and Semi Global Matching (SGM XPro (Hexagon Geospatial 2015). As the two algorithms returned different point clouds partially complementing each other, in the initial study for the method development we decided, based on visual assessment, for a combination of three point clouds from eATE and SGM processed with the pyramid levels 0, 1 and 2 respectively to reach the best point coverage in a reasonable processing time. The detailed settings of both algorithms and the single processing steps are given in Zielewska-Büttner *et al.* (2016a). The point cloud editing was carried out with LAStools (Isenburg, 2014) whereas the LAS to a raster transformation was done in ArcGIS ("LasDataset to Raster"). For the gap detection a constantly closed surface was produced by filling the no-data areas with a including inverse distance weighting (IDW) interpolation method.

The gap detection was carried out in ArcGIS 10.3 (ESRI, 2014) (raster and vector based) in three steps: (1) identification of open and dense forest, (2) classification of dense forest into height classes of low and high forest and (3) gap extraction in the latter two classes. We defined gaps as canopy openings in dense forest (≥60% canopy cover) of at least 10 m² reaching through all forest strata down to maximum 2 m vegetation height in high forest stands (≥8 m height) and down to maximum 1 m in low forest stands (<8 m height). A minimum stand size of 0.3 ha is related to the size of the conventional minimum stand size in Baden-Württemberg (Mathow, 2015). Areas with canopy cover less than 60% and exceeding 0.5 ha were classified in line with Ahrens *et al.* (2004) as "open forest",

where the free spaces between the trees are considered as inherent stand characteristic and thus not mapped as gaps. 10 m² is the minimum size of a gap defined in line with Müller and Wagner (2003) and Schliemann and Bockheim (2011). The maximum gap-vegetation height was set to 2 m after Brokaw (1982) and adapted by the authors to 1 m in the lower stands.

3.2.4 Validation

To evaluate the gap mapping performance we compared the automatic mapping results with the visual stereo-interpretation of the original aerial imagery on an independent dataset of sample plots using Stereo Analyst for ArcGIS 10.2 (GEOSYSTEMS GmbH, 2014). As we expected the results to vary in relation to the terrain situation, 120 plots with a radius of 25 m (covering 2.4 % of the dense forest area) were placed according to a stratified random design into stands of three steepness classes (0-10°, 10-20°, >20° (AG Boden, 1996) and four aspect classes (N, E, S, W), resulting in 12 terrain classes represented by 10 sampling plots each. Gaps with an area of at least 10 m^2 inside the plot (168 in 2009 and 171 in 2012) were visually assessed, delineated and compared with the automatically mapped gaps located with at least 10 m² inside the evaluation plot. The gap–absence was evaluated on circles of 95 m² (mean size of the visually mapped gaps in both years) randomly placed in dense forest within the sampling plots in an amount equal to the visually verified gaps per year. At least 8 m² (80% of the minimum gap size) of overlap with the visually identified gaps was needed to confirm the correct classification of the automatically detected gaps or to classify a “non-gap” circle as incorrect. The agreement between visual and automatic mapping was then quantified in form of overall, producers´ and users´ accuracy as well as Cohen’s Kappa. An effect of selected parameters such as height of the surrounding forest, shadow occurrence (assessed visually), gap size, slope, aspect and gap location in relation to forest road, skidding trail or an open area (storm throw, open forest) on gap mapping results was tested using the Conditional Inference Trees (ctree) vignette of R-package “partykit” (Hothorn *et al.*, 2006).

To evaluate the influence of the missing original height information on the gap mapping performance, a no-data mask was generated as a raster of 1 m resolution from the final point clouds (combination of eATE and SGM pyramid 1 and 2 point clouds) of 2009 and 2012. It included only the raster cells, where no points were directly matched during the image matching process. As for the gap detection a constantly closed surface was used, by a comparison with the no-data mask the resulting improvement in accuracy was evaluated.

To quantify the effect of sun elevation on the image quality, we calculated a shadow mask for the data of 2009 and 2012. We defined as shadow an area without any textural differentiation. The

classification was done by a visually defined threshold. As the data from the two study years had different radiometric resolution, two different methods had to be used to calculate the shadow fraction in the aerial images. For the images from 2009 that had been resampled to 8-bit resolution we used for this year a Ratio S calculated according to Sarabandi *et al.* (2004) as S=arctan(Blue/max {Red/Green}). For 2012 data with 16-bit resolution we used the Intensity channel of the transformed images (Conrac Corp., 1980).

3.2.5 Comparison with data of higher overlap and resolution

To evaluate the potential influence of higher resolution and overlap of the aerial imagery on the method performance, Petersen (2015) applied the gap mapping method to a study polygon of 95 ha located in the south-western corner of the original research area (Figure 3-1) using data from a special flight campaign of the National Park Black Forest in 2014 (Table 3-1). Gap mapping results based on these pansharpened RGB NIR aerial imagery of 10 cm resolution and 80% and 60% end and side lap were compared with those obtained from the lower-resolution public data of 2012, using the eATE algorithm for point cloud generation. The CHMs used for gap extraction in 2014 were calculated based on the LiDAR derived DTM of the National Park Black Forest, as obtained from their own flight campaign in 2015.

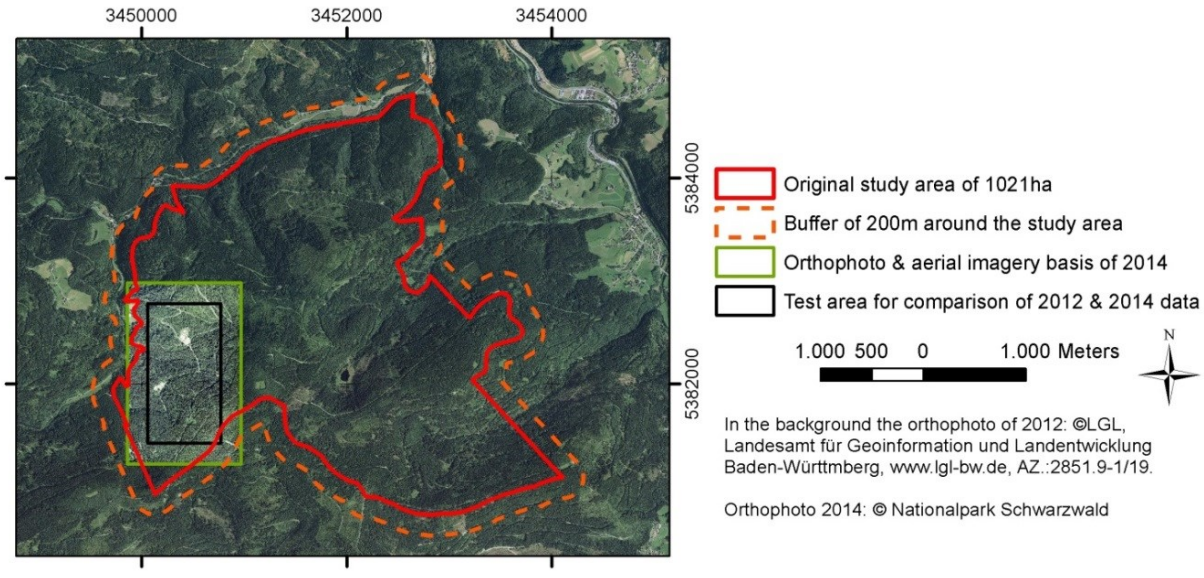

Figure 3-1 Location the test area for comparison of 2012 and 2014 data within the original study area presented on the background of the available orthophotos from 2012 and 2014.

3.3 Results

3.3.1 Gap mapping results

We detected 4575 (2009) and 4667 (2012) gaps in the dense forest of the study area using the automated method, what results in a total gap density of 4.9 gaps per ha (7.2 % of the dense forest area) in 2009 and 4.7 gaps per ha (6.3 %) in 2012. Considering the forest height classes, more gaps (13.7 and 14.6 N/ha in 2009 and 2012) covering a greater area (45 and 46 ha respectively) were mapped in the forest stands lower than 8 m compared to the higher forests with a gap density of 2.0 and 2.8 N/ha and mapped gap area of 25 and 16 ha in 2009 and 2012, respectively. The most (> 75%) of all detected gaps in both study years were very small or small (less than 100 m²) accounting for 13 % and 23% of the total gap area per year in 2009 and 2012, respectively. The visual validation resulted in an overall accuracy of 0.90 and 0.82 in 2009 and 2012 and the corresponding Kappa values of 0.80 and 0.66 (Table 3-2). Producer´s accuracies greater than 0.96 confirmed almost all automatically detected gaps as correctly classified. Yet, a fraction of the visually identified gaps were not detected during the automated mapping process, which is reflected in lower user´s accuracies of 0.84 in 2009 and 0.72 in 2012. However, more than 70 % of the visually but not automatically identified gaps in both study years were adjacent to the automatically mapped gaps, what suggest that gaps were correctly localized, but they were detected with a too small extent.

Table 3-2 Mapping accuracies of automatically generated gaps per year and forest high class derived from a comparison with the results of visual interpretation (accessed with 95 % confidence interval (CI)) (from ZIELEWSKA-BÜTTNER et al. 2016, modified)

	Producer´s accuracy	User´s accuracy	Producer´s accuracy	User´s accuracy	Kappa	Overall accuracy
	Gap	Gap	"Non-gap"	"Non-gap"		with 95 % CI
2009 DF	0.97	0.84	0.84	0.97	0.80	0.90
LF	0.98	0.93	0.68	0.89	0.73	0.93
HF	0.98	0.70	0.87	0.98	0.73	0.88
2012 DF	0.96	0.72	0.73	0.96	0.66	0.82
LF	0.98	0.85	0.59	0.94	0.93	0.86
HF	0.96	0.52	0.76	0.96	0.84	0.79

3.3.2 Shadow occurrence

Among the variables tested only the height of the surrounding forest and shadow occurrence significantly affected the gap mapping results. The occurrence of full shadow in the lower sections of the forest canopy was identified as the main cause for gap mapping omission errors in both years (ctree, $p<0.001$). This was confirmed also by means of visual verification, as the most of the visually identified but not automatically mapped gaps (70%–87%) were identified in areas of total or partial shadow. The height of the surrounding forest stands (LF and HF) is strongly linked to shadow occurrence as it determines the depth in the canopy, to which the light can penetrate. Despite

similar producer´s accuracies of 0.96-0.98 and overall accuracies of more than 0.79, gaps in LF were mapped with higher user´s accuracies than those in HF (0.93 vs. 0.70 in 2009 and 0.85 vs. 0.52 in 2012).

The shadow masks identifying complete shadow cells covered 29 % of the study area in 2009 and 16 % in 2012. However, the comparison with the location of automatically mapped gaps showed that only less than 5 % of the gaps were automatically detected in these areas. Shadow occurrence was mostly linked to steep slopes and exposition as well as to heterogeneous vertical structure and stand height (Figure 3-2), indicating a strong influence of the sun angle and associated time of data acquisition. The two flight campaigns of 2009 and 2012 were carried out in May and August, so the sun position at the time of data acquisition didn´t correspond which produced shadow in different areas (Figure 3-2).

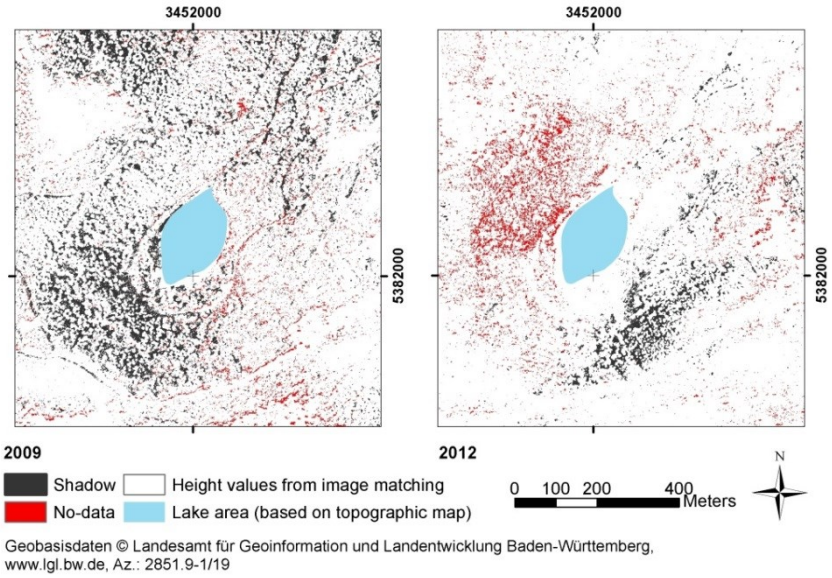

Figure 3-2 Example of complete shadow and no-data cells distribution in a steep part of the study area around the mountain lake “Huzenbacher See”

3.3.2.1 Image matching algorithm

The amount and distribution of no-data cells was influenced by the algorithms and pyramid levels of the images used for point matching. The area with no data ranged between 38% with SGM pyramid level 2 in 2012 and 9 % with SGM pyramid level 1 in 2009. Combining different algorithms and pyramid levels led to a reduction of no-data within the study area to less than 3%. Evaluating whether missing information in some raster cells could be a reason for a fraction of the undetected gaps, we found that only about 10 % of the visually, but not automatically identified gap cells (gap area) in both years belonged initially to the no-data cells.

The distribution of no-data and shadow raster cells (Figure 3-2) revealed that the points were mismatched not only in shadowy areas of the forest stands (8 % (2009) and 5 % (2012) of no-data cells intersected with the shadow mask) but also in low forest stands and on hilltops where aerial photographs should theoretically deliver good material for image matching. No-data cells were often located along flight strips (2009) or at the outer parts in the overlapping zone of the images (both years).

3.3.2.2 Image resolution and overlap

Comparing the results based on the original data from 2012 and the high-resolution dataset of 2014, a slightly larger amount of open forest (3 % in 2012 and 2 % in 2014) was mapped for 2012. Also the percentage of low forest was higher in 2012 (21 %) than in 2014 (14 %) (Figure 3-3).

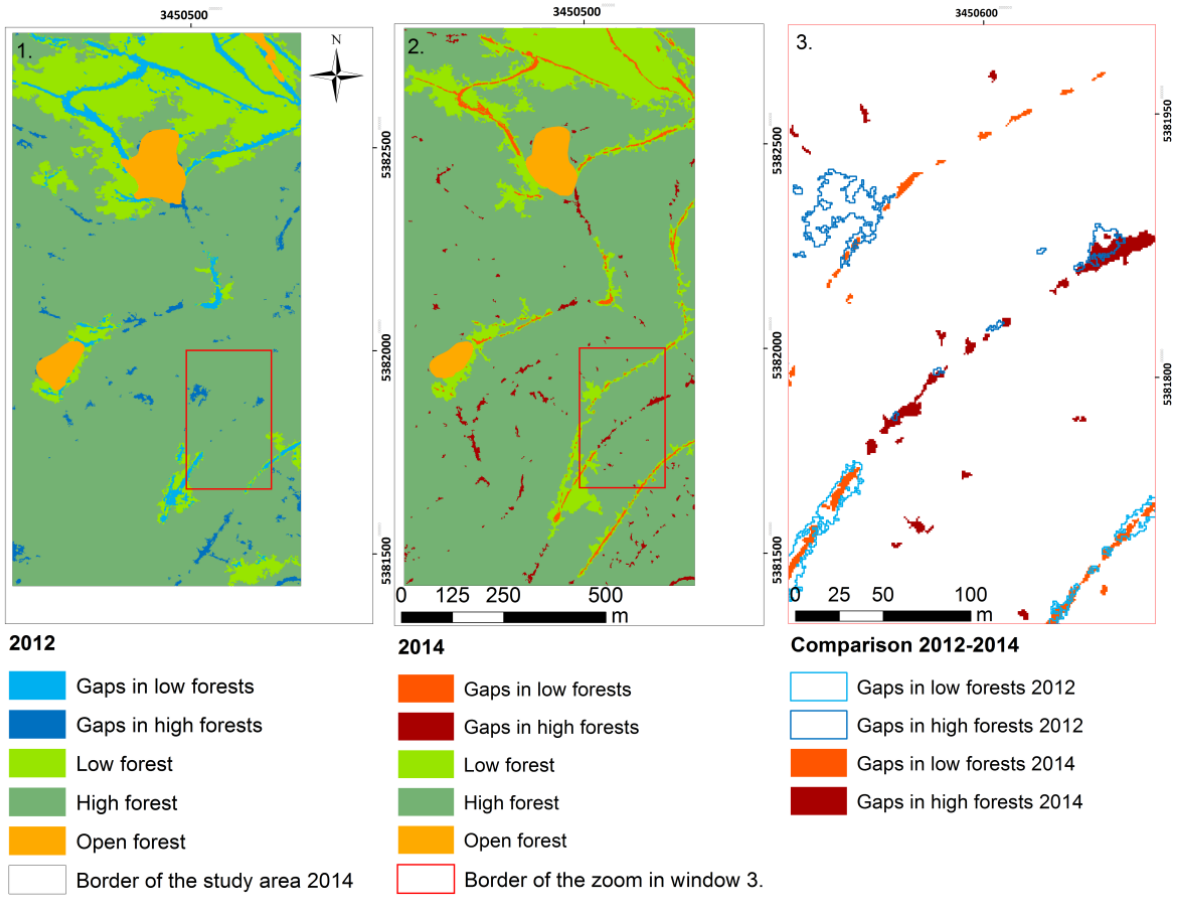

Figure 3-3 Results of the automated gap mapping in the test area for the comparison of data with different resolution and overlap: 1) results from 2012 (20 cm, overlap 60% /30%), 2) results from 2014 (10 cm, 80% /60%), 3) Zoom-in window as example for a comparison of 2012 and 2014 results.

To be able to compare the results of the gap mapping of both years the study area was reduced by the area that had been classified as open forest within either of the datasets. For the remaining area of 94 ha a larger total gap area was obtained with the dataset of 2012 (4.9 ha) compared to the

dataset of 2014 (2.5 ha) though a larger number of gaps was identified in the latter (2012: 240 gaps, 2014: 281 gaps). The reason for this can be found in the size of the mapped gaps. While more very small (10 m² - 30 m²) and small (31 m² - 100 m²) gaps were detected with the dataset of 2014 there were more large (100 m² - 1000 m²) and very large gaps with a size of more than 1000 m² mapped with the data of 2012 (Figure 3-4). The large and very large gaps were located mostly within the class of low forest or along forest tracks.

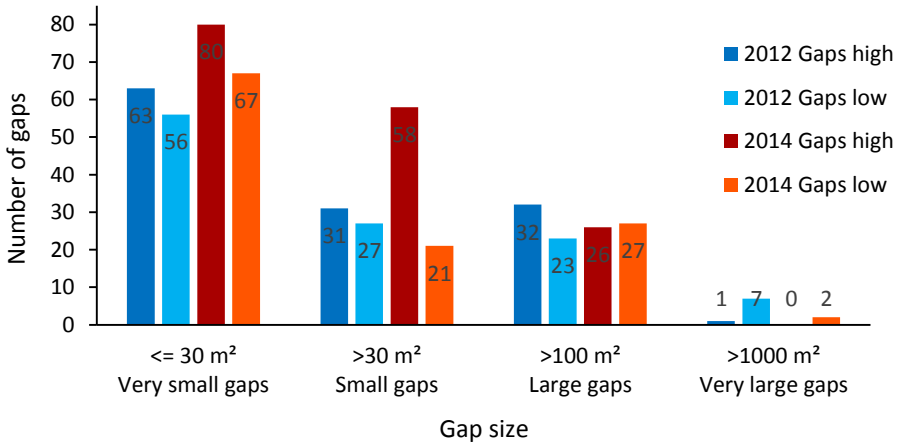

Figure 3-4 Distribution of gap sizes in the dataset of 2012 (blue bars) and 2014 (red/orange bars). “High” and “low” indicate high and low forest stands.

3.4 Discussion and Conclusions

Gap mapping from stereo aerial imagery with 20 cm resolution and 60/30% overlap proved to deliver promising results, with a good overall method performance and even very good results in low stands. Depending on the quality of the aerial imagery and the input CHM as well as the height of the surrounding forest and the associated shadow occurrence, the results in stands higher than 8 m were moderate to insufficient, depending on the study year. The mapping results might also depend on the topography and the structure of the forest stands. Ginzler and Hobi (2015) observed better mapping accuracies in a flat terrain than in rugged mountainous topography, which also characterised our study area, whereas Adler *et al.* (2014) found that even in flat terrain different DSM matching algorithms produce different results, especially in highly structured canopy situations. In addition, mountainous forests are likely more structured than intensively managed stands in the lowlands.

Shadow occurrence in aerial images is related to exposition, surface characteristics and caused by sun inclination and angle. Therefore the occurrence and distribution of shadow varies a lot between the different flight campaigns, especially in hilly areas comparable to our study area. Comparing the

overall amount of shadow within the images with the shadow pixels within the classified gaps, we see that only a very small portion of gaps was detected in the shadow areas. This can be influenced by a strong fragmentation of the shadow areas with single patches not bigger that 10m² (minimum gap size). It can also be interpreted, that shadow pixels may have influenced negatively the image correlation for point matching within stand surface openings. The latter argument was confirmed by the visual interpretation of the gaps as 70-80% of visually interpreted gaps that hadn't been detected automatically were located in partial or total shadow.

The superimposition of no-data areas with shadow areas showed no direct correlation. The appearance of no-data areas was more related to the geometric characteristics of the image, as they mainly occurred along image und flight strip borders.

By combining point clouds generated with two different image matching methods we expected a compensation effect and improvement of the point cloud structure in areas where no points were matched using only one of the algorithms. The results of our study underline the importance of the image matching method. Not all algorithms perform equally well with regard to specific mapping goals e.g. detection of canopy gaps, mapping of the tree tops or calculation of forest stand parameters. Developments in technology and image matching algorithms are rapid, which makes the choice of the "best" algorithm combination very difficult, with "best" being often only valid for the used data and software combination.

The data used to analyze the influence of image resolution and overlap originated from two different years. The images with 20 cm resolution and 60/30 % overlap were taken in 2012, whereas the images with 10 cm resolution and an overlap of 80/40 % were from 2014. However, as there were no disturbances in the two years between the flights, and the forest stands wasn't in an age-class where natural mortality causes the disappearance of single trees, a decrease in detected gaps would have been expected. Nevertheless, the number of forest gaps increased from 240 to 281 with simultaneous decrease in size. This change in average gap size could be either explained by vegetation growth, at the gap edges, which reduces gap size. The increasing number of very small and small gaps could be explained ingrowth of vegetation, partially closing larger forest gaps, leaving more and smaller gaps behind. A visual examination, however, showed that the many of these very small and small gaps detected in 2014 where not mapped in 2012. Especially within high forest stands the number of detected gaps rose by almost 30 % while the amount of high forest only increased by 8 % between the years. This increase can not only be explained by ingrowth but by a better insight into the canopy structure due to a higher image overlap and resolution in the 2014 data.

The results from different flight campaigns indicate shadow occurrence and geometric limitations of the aerial imagery as serious constraints, both bearing a high potential for improvement. Flight campaigns should consider the issues arising from varying flight time and associated solar altitude. Moreover, an increase in spatial resolution and overlap of the aerial images could considerably improve the spatial accuracy of the results. Further improvements can be expected from an amelioration of the image matching algorithms. The use of shadow and no-data masks proved useful for the interpretation and evaluation of the automatically produced gap maps and we recommend them especially for change detection. Further research on these topics could help to optimize and standardize future flight campaigns, so that they can be used for reliable monitoring of gaps and other forest structure parameters.

3.5 Acknowledgements

We thank Joao Paulo Pereira for his inputs into gap mapping and generation of the no data masks and Martin Denter for calculation of the shadow masks. The study was carried out at the Forest Research Institute Baden-Württemberg (FVA) with the data contribution from the Black Forest National Park © Nationalpark Schwarzwald and the State Agency of Spatial Information and Rural Development of Baden-Württemberg (“Geobasisdaten ©LGL, Landesamt für Geoinformation und landentwicklung Baden-Württmberg, www.lgl-bw.de, AZ.:2851.9-1/19.)

4 CHAPTER III: DETECTION OF STANDING DEADWOOD FROM STEREO AERIAL IMAGERY DERIVED ORTHOIMAGERY AND DIGITAL SURFACE MODELS. ADDRESSING DEADWOOD AND BARE GROUND MISSCLASSIFICATION ISSUE

Chapter III was published as research article:

Zielewska-Büttner, K., Adler, P., Kolbe, S., Beck, R., Ganter, L., Koch, B., Braunisch, V. Detection of Standing Deadwood from Aerial Imagery Products: Two Methods for Addressing the Bare Ground Misclassification Issue. Forests 2020, 11, 801. DOI: https://www.mdpi.com/1999-4907/11/8/801

Abstract: Deadwood mapping is of high relevance for studies on forest biodiversity, forest disturbance and dynamics. As deadwood predominantly occurs in forests characterized by a high structural complexity and rugged terrain, the use of remote sensing offers numerous advantages over terrestrial inventory. However, deadwood misclassifications can occur in the presence of bare ground, displaying a similar spectral signature. We tested the potential to detect standing deadwood (h>5m) using orthophotos of 0.5m and digital surface models (DSM) of 1m resolution, both derived from image matching of stereo aerial imagery of 0.2m resolution and 60/30 % overlap (end/side lap). Models were calibrated in a 600ha mountain forest area, rich in deadwood of various stages of decay. We employed Random Forest (RF) classification, followed by two approaches for addressing the deadwood-bare ground misclassification issue: 1) post-processing, with a mean neighborhood filter for "deadwood"-pixels and filtering out isolated pixels and 2) a "deadwood-uncertainty" filter, quantifying the probability of a "deadwood"-pixel to be correctly classified as a function of the environmental and spectral conditions in its neighborhood. RF model validation based on data partitioning delivered high user's (UA) and producer's (PA) accuracies (both >0.9). Independent validation, however, revealed a high commission error for deadwood mainly in areas with bare ground (UA=0.60, PA=0.87). Post-processing (1) and the application of the uncertainty filter (2) both improved the distinction between deadwood and bare ground and led to a more balanced relation between UA and PA (UA of 0.69 and 0.74, PA of 0.79 and 0.80, under (1) and (2), respectively). Deadwood-pixels showed 90% location agreement with manually delineated reference deadwood objects. With both alternative solutions deadwood mapping achieved reliable results however the highest accuracies were obtained with deadwood-uncertainty

filter. Since the information on surface heights was crucial for correct classification, enhancing DSM quality could substantially improve the results.

Keywords: deadwood detection, forest structure, remote sensing, orthophoto, RGBI, digital surface model, DSM, canopy height model CHM, Random Forest

4.1 Introduction

Deadwood is an important resource for more than 30 % of all forest species and thus of great relevance for forest biodiversity (Hahn and Christensen, 2004; Schuck *et al.*, 2004; Paillet *et al.*, 2010; Thorn *et al.*, 2019). Standing or laying, fresh or in later stages of decay it offers a variety of microhabitats for various species (Pechacek and Krištín, 2004; Müller *et al.*, 2005; Seibold *et al.*, 2014; Kortmann *et al.*, 2018b), provides substrate for lichens, mosses and fungi (Bader *et al.*, 1995; Baldrian *et al.*, 2016; Olchowik *et al.*, 2019), and nutrients for a new generation of trees. Effective biodiversity conservation in forest landscapes requires information about the amount and distribution of deadwood at relevant spatial scales (Braunisch, 2008; Stighäll *et al.*, 2011; Kortmann *et al.*, 2018a).

Mapping deadwood across large areas is therefore of general interest for biodiversity studies and nature conservation (Bouvet *et al.*, 2016), although the requirements regarding the detail of deadwood mapping may vary. While for assessing habitat quality for generalist species a rough approximation of deadwood amounts may be a sufficient proxy, for specialists a differentiation between standing and lying deadwood, various stages of decay, or even between different tree species may be required (Balasso, 2016; Zielewska-Büttner *et al.*, 2018). In this context, remote sensing offers numerous advantages for deadwood detection such as continuous spatial information, well-established visual interpretation keys (AFL, 2003; Ackermann *et al.*, 2012), as well as automated and standardized detection methods (Wulder *et al.*, 2006; Heurich *et al.*, 2015).

Detection of deadwood from remote sensing data relies on the spectral properties in the near-infrared region (NIR) of the light spectrum (0.7 - 1,3 µm) (Hildebrandt, 1996), that reflects best the difference between vital and non-vital vegetation tissues (Hildebrandt, 1996) as e.g. in desiccating leaves or dying trees (Kenneweg, 1970; Adamczyk and Bedkowski, 2006). Also the red edge gradient between the red and infrared bands (0.69 - 0.73 µm) and in some cases also bands from the short-wave-infrared region (SWIR ca 1.3 - 2.6 µm (Hildebrandt, 1996) or 1,1 – 3,0 µm (NASA Earth Observatory, 2014)) (Fassnacht *et al.*, 2014; Adamczyk and Osberger, 2015) (both not included in the

standard 4 channel (red, green, blue and near-infrared, RGBI) imagery can improve the detection of deadwood in an automated process. To diminish the influences and interdependencies between the bands, spectral indices based on algebraic combinations of reflectance in different bands were found to be helpful in mapping of different land cover and object classes (ENVI, 2019) among which is also the live, senescing and dead vegetation (Fassnacht, 2013; Waser *et al.*, 2014b).

Over decades deadwood has been mapped visually based on color-infrared (CIR) aerial imagery and applied in forest research and management e.g. for mapping bark beetle infestations (Heurich *et al.*, 2001; Wulder *et al.*, 2006; Zielewska, 2012), in forest tree health assessment (Commission, 2000), or in studies of forest dynamics (Ahrens *et al.*, 2004) and forest wildlife ecology (Bütler and Schlaepfer, 2004; Martinuzzi *et al.*, 2009). Nowadays, with the growing availability of digital optical data with very high resolutions (e.g. < 0.1 m from unmanned aerial vehicles (UAV), 0.1 - 0.2 m from aerial imagery, and < 10 m from satellite imagery (White *et al.*, 2016)), together with the availability of airborne laser scanning (ALS) data and the development of classification workflows, automated deadwood detection became possible. It brings the deadwood mapping to a higher level of detail and allows standardized processing of big datasets (Heurich *et al.*, 2015).

The suitability of remote sensing data for deadwood mapping differs. The spectral information from the infrared band of aerial or satellite imagery is indispensable to detect differences between the healthy, weakened and dead vegetation. It can be used as the only input to differentiate in an analog (visual) or automated way between the dead and live vegetation. The results differ depending on the study and the validation method with overall accuracies (OA) between 0.67 and 0.94 (Bütler and Schlaepfer, 2004; Pasher and King, 2009).

To enhance deadwood detection structural information on canopy heights is helpful. For automated analyses ALS data in combination with CIR aerial imagery showed the best results to date with OA of about 0.9 (Polewski *et al.*, 2015a; Kamińska *et al.*, 2018; Krzystek *et al.*, 2020). Detection of standing deadwood solely from ALS data was also tested and delivered heterogeneous results, depending on forest type and detection method (Maltamo *et al.*, 2014; Marchi *et al.*, 2018), with OAs from 0.65 - 0.73 (Yao *et al.*, 2012a; Korhonen *et al.*, 2016; Amiri *et al.*, 2019) to 0.86 - 0.92 (Martinuzzi *et al.*, 2009; Casas *et al.*, 2016).

In Germany, as in many other countries, up-to-date, area-wide ALS data is rarely available, whereas CIR aerial imagery is regularly updated by state surveys. As deadwood frequently occurs in rough terrain and forest stands with high structural complexity, the use of aerial imagery data imposes challenges on deadwood detection that need special addressing. Solar angle and viewing geometry

of aerial images cause shadow occurrence and limited insight into the canopy openings. These factors influence the derivation of correct canopy surface heights by image matching, especially in forest gaps and clearances or at the edges of forest roads (Zielewska-Büttner *et al.*, 2016a; White *et al.*, 2018; Ackermann *et al.*, 2020). These inaccuracies result in image and object distortions of derived "true-orthophotos".

This is where the correct separation of dead or senescing trees from bare ground becomes challenging (Meddens *et al.*, 2011; Fassnacht *et al.*, 2014). Bare ground, visible by eye through the canopy of open stands or at the border to forest roads, mimics the spectral signature of deadwood objects and is a source of misclassification in automated methods when vegetation heights are not reliable.

We used Random Forest (RF) models to classify standing deadwood among live and declining trees and bare ground. As input data vegetation heights from a canopy height model (CHM) derived from a digital surface model (DSM) from image matching of aerial images, and an ALS-based Digital Terrain Model (DTM) were used. The same aerial images and DSM were used to calculate a "true-orthophoto" (in the following termed "orthophoto"), from which spectral variables were generated. For improving the differentiation between "deadwood" and "bare ground" we developed and tested two alternative approaches: a post-processing procedure and the application of a "deadwood-uncertainty" filter. Based on the results we evaluated the suitability of regularly updated aerial imagery data of state surveys and the products thereof as a sole basis for reliable standing deadwood detection.

4.2 Materials and Methods

4.2.1 Study site

The study area of 600 ha is located on the northern slopes of Feldberg (1493 m a.s.l.), the highest mountain in the Black Forest mountain chain (Southwestern Germany). It encompasses 102 ha of a strictly protected forest reserve "Feldseewald" named from the mountain glacier lake "Feldsee" located at 1100 m a.s.l. within the reserve. The terrain of the study area is characterized by steep slopes with rock formations in the north-west of the lake and smoothly rising elevations from the lake to the east and north-east (Figure 4-1).

The reserve is surrounded by large, managed forest stands and some mountain meadows. The dominating tree species of the montane and subalpine conifer and mixed forests is Norway spruce (*Picea abies*) accompanied by Silver fir (*Abies alba*) and European beech (*Fagus sylvatica*). No

intervention policy since the creation of the forest nature reserve in 1993, natural disturbances and natural tree mortality caused a high abundance of deadwood in different forms and decay stages, which makes the area a suitable model region for developing and evaluating a deadwood detection method under difficult topographic conditions.

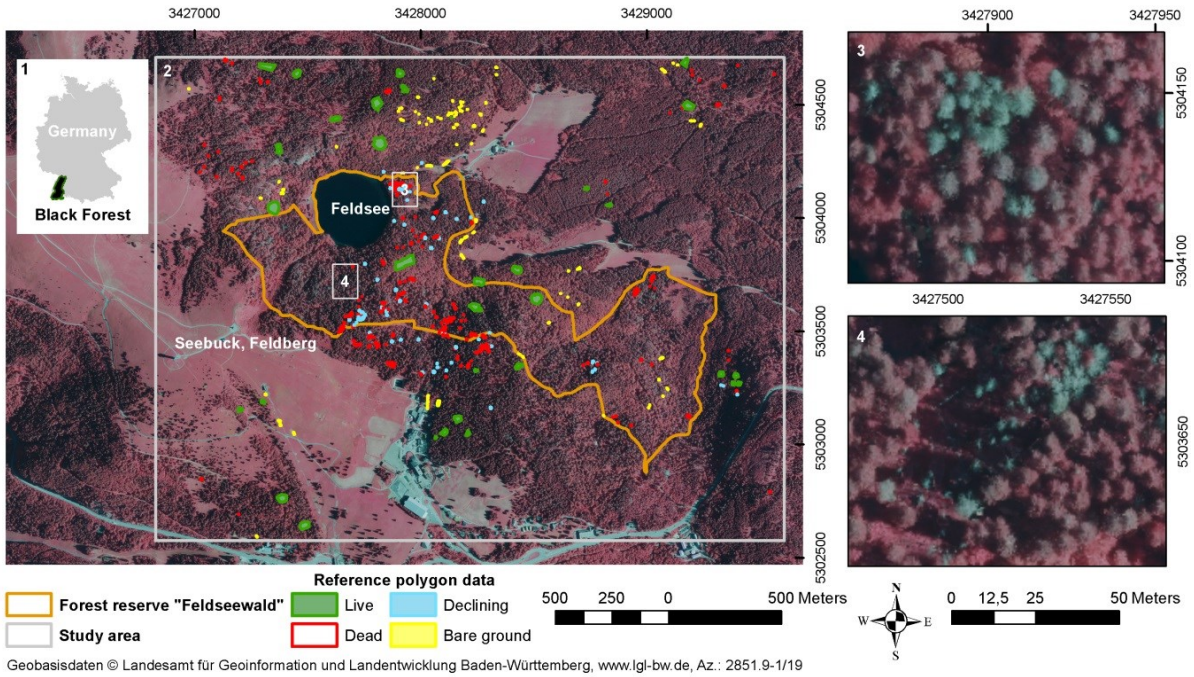

Figure 4-1 Location of the Black Forest in Germany (1); Study area (2) with the lake "Feldsee", the second top of Feldberg mountain "Seebuck" (1448 m a.s.l.), the "Feldseewald" strict forest reserve and the reference polygons for the 4 classes ("live", "dead", "declining" and "bare ground", see Figure 4-2) on the background of the color-infrared (CIR) orthophoto; Examples of standing dead trees (3, 4) and snags (4).

4.2.2 Remote sensing and GIS data

As a primary input the 4 channels (red, green, blue and near-infrared, RGBI) of stereo aerial imagery with a ground resolution of 0.2 m and overlap of 60/30 % (end/side lap) owned by the State Agency of Spatial Information and Rural Development (LGL) (Landesamt für Geoinformation und Landentwicklung Baden-Württemberg, 2020b) were used. The aerial imagery was acquired on 08 August 2016 between 07:12:08 - 07:41:37 with a UC-SXp-1-30019136 camera with a focal length of 100.5 mm. Orthophotos of 0.5 m resolution, as well as a DSM and CHM of 1 m resolution from the LGL (Landesamt für Geoinformation und Landentwicklung Baden-Württemberg, 2020b), all derived by image matching from the stereo aerial imagery in line with the methodology described in Schumacher *et al.* (2019), were used to deliver both spectral and surface height information for the modelling.

To avoid misclassifications with non-forest areas only land declared as “forest” (according to the forest-ownership GIS-layer administrated by the Department of Forest Geoinformation of Baden-Württemberg (Mathow, 2015)) was analyzed. Standing water was masked out based on a topographical GIS-layer produced by the State Authority Topographical and Cartographical Information System (ATKIS) (Landesamt für Geoinformation und Landentwicklung Baden-Württemberg, 2020a). A DTM of 1 m resolution (LGL) (Landesamt für Geoinformation und Landentwicklung Baden-Württemberg, 2020b) was used to derive slope for identifying steep rocks.

Shadow pixels were excluded from the classification to guarantee that only spectral information from the sunlit tree crowns was used. We generated two shadow masks based on hue (H) and value (V) from an HSV-transformation (hue, saturation, value) of the RGB bands and their histograms (calculated using the package “grDevices” implemented in the software R (R, 2019)). Deep (darkest) shadow pixels (H =≥0.51 or V ≤ 0.18) were removed during the data preparation. Partial shadow cells (H ≥ 0.37 or V ≤ 0.24) were used later in the post-processing.

All analyses were carried out on data with 0.5 m resolution to make best possible use of the high resolution information in the data. Raster-data with lower resolution were disaggregated to 0.5 m and polygon features were rasterized based on the resolution of the orthophoto and analyzed using the “raster” package in R (Hijmans, 2020). For polygon operations the “rgdal” (Bivand *et al.*, 2019) package in R was used.

4.2.3 Standing deadwood definition and model classes

The aim of our study was the detection of standing deadwood in different stages of decay, i.e. from recently dead trees with crown and needles to high snags (stages 3 to 6, according to Thomas *et al.* (1979) , Figure 4-2).

To exclude low stumps and avoid misclassifications with visible bare ground or lying deadwood, only pixels above 5 m in height according to the CHM were selected for the analysis. Considering the advantages of the infrared band in depicting differences in cell structure and water content in the vegetation, we did not only distinguish between “dead” and “live” (vital) vegetation, but considered also “declining” trees with signs of dieback, breakage or foliage discoloration. A fourth class “bare ground” was included in the model to account for pixels where the CHM was not accurate enough to exclude bare ground areas.

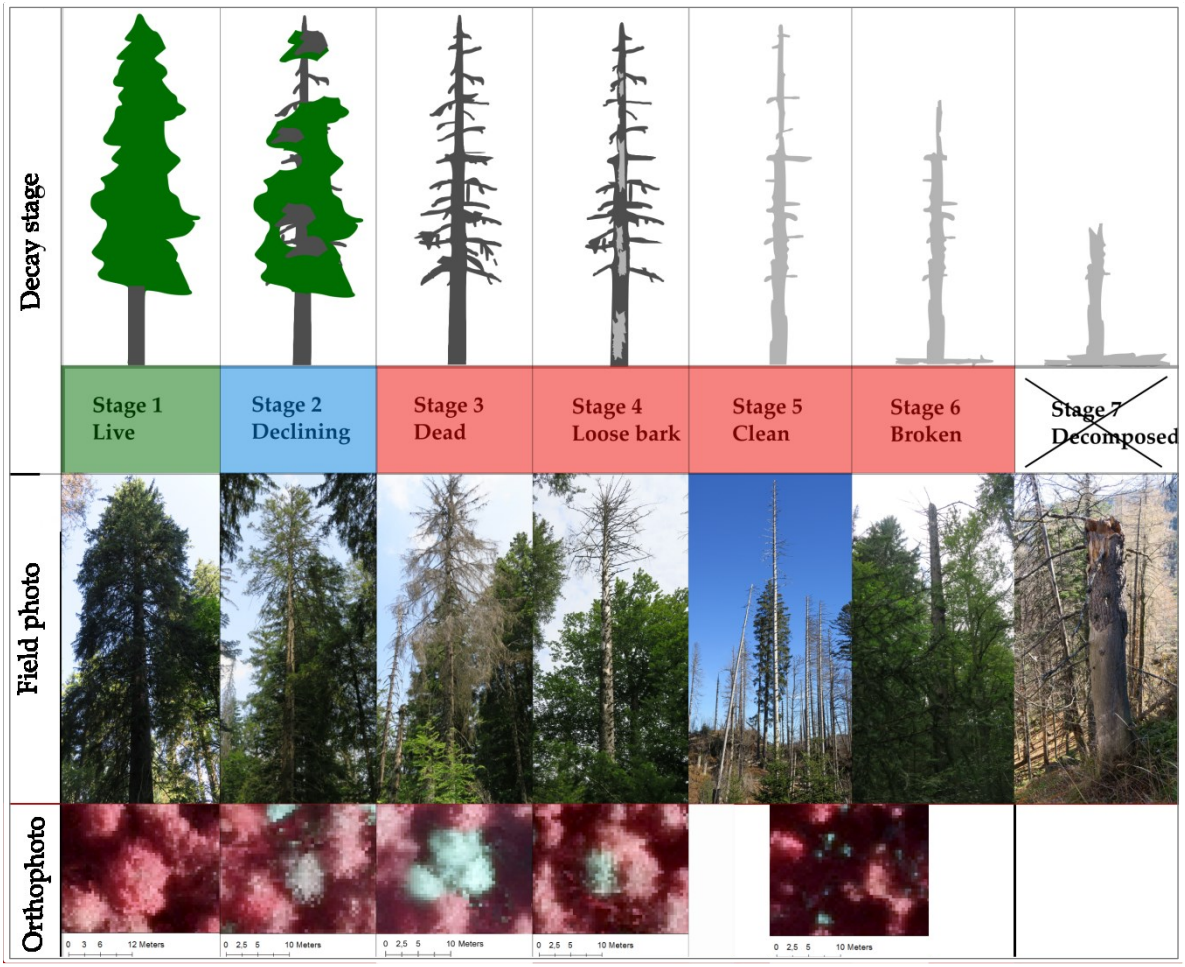

Figure 4-2 Classification of forest trees in three model classes ("live" – green, "declining" – blue, "dead"– red), the corresponding decay stages as adapted from Thomas *et al.* (1979) in Zielewska-Büttner *et al.* (2018), as well as their appearance photographed in the field (field photo) and from the air (orthophoto). Low snags and stumps (h < 5m) were excluded from the study.

4.2.4 Reference polygons for model calibration

515 reference polygons were digitized as a basis reference data pool for model training as well as for the validation on pure classes and a polygon-based validation (Table 4-1). The reference data was collected mainly from the forest reserve and adjacent stands, where selected trees of the classes "dead" and "declining" had been additionally verified in the field in 2017.

The reference polygons of the classes "dead" and "declining" were delineated as single tree objects, while "bare ground" and the "live" stand was mostly mapped as larger uniform areas to include potential partial shadows between trees standing close to each other. While delineating the reference data we made sure to create uniform object classes, while at the same time including the variability within the classes, e.g. selecting deadwood of various sizes and stages of decay. The

objects were also chosen from diverse spatial locations of the study area to account for regional differences and bidirectional reflection function effects (Fassnacht *et al.*, 2012).

The collected polygon data was rasterized with each pixel having its center inside the polygon assigned to the respective class.

The polygon sizes for the class "dead" varied from 0.1 (snags) to 65.9 m² (with a median of 11 m² (corresponding to a dead tree with branches of 1.5 - 2 m length). Declining trees had larger crowns and a minimum polygon size of 6.9 m² (median: 22.1 m²).

Table 4-1 Reference polygons, their number and size per class, as well as the amount of pixels available for training and validation on "pure classes" after converting polygon areas into raster maps with 0.5 m resolution.

Model class	N	Polygon area (m²)						No. of pixels
		Sum	Min	Max	Mean	Median	SD	
live	33	24789.7	1.2	2797	751.2	576.6	659.9	98137
dead	315	4295.7	0.1	65.9	13.6	11	12.1	17143
declining	64	1510.8	6.9	52	23.6	22.1	10.7	6048
bare ground	103	1208.9	0.5	178.7	11.7	4.2	22.3	4272

4.2.4.1 Deadwood detection method

The deadwood detection method was developed in 3 analysis steps as depicted in Figure 4-3. First, a RF model ("DDLG") was calibrated for predicting the model classes: "dead", "declining", "live" and "bare ground". The following two scenarios aimed at improving the differentiation between deadwood and bare ground: Firstly, a post-processing procedure (DDLG_P), estimating the probability of "deadwood"-pixel with a mean neighborhood filter and removing isolated pixels causing the so called "salt and pepper"-effect (Kelly *et al.*, 2011). Secondly, the application of a deadwood-uncertainty filter for identifying unreliable deadwood patches (DDLG_U).

4.2.4.2 Random forest model (DDLG)

The Random Forests (RF) algorithm (Breiman, 2001) implemented in the R-package "caret" (Kuhn *et al.*, 2018) was used in the first step (DDLG) as a classifier to distinguish standing deadwood from the three other model classes. We trained the RF model (DDLG) using 2000 pixels per class, randomly drawn from the reference polygons.

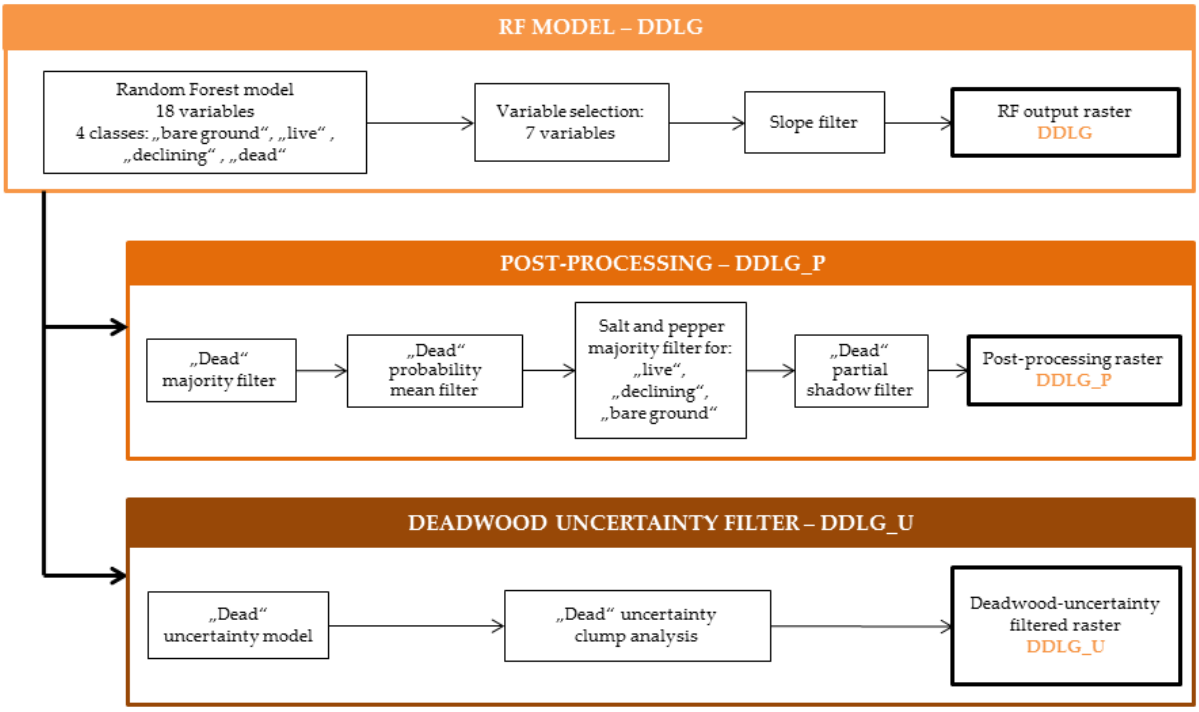

Figure 4-3 Methodological steps used for deadwood detection: First, a random forest model (DDLG) was calibrated, distinguishing between “dead”, “declining” and “live” trees, as well as “bare ground”. The model results were enhanced using two alternative approaches for addressing the deadwood - bare ground misclassification issue: (1) a chain of post-processing steps (DDLG_P) and (2) with the generation of a model-based deadwood-uncertainty filter (DDLG_U). Bold frames represent the classification results. The acronyms for the analysis steps correspond with the model classes: dead (D), declining (D), live (L), bare ground (G), as well as indicated post-processing (P) and uncertainty filter (U). For methodological details of the single analysis steps see 2.5.1-2.5.3.

The model was run 15 times using 3 repetitions and 5-fold cross-validation with 10 variables at each split, allowing 500 trees. Model input consisted of 18 variables: red (R), green (G), blue (B) and infrared (I) spectral bands of the orthophoto and ratios thereof (Table 4-2) complemented with hue, saturation and value (HSV) and information on vegetation height (CHM). We expected the latter to improve the differentiation between standing deadwood of more than 5m height and bare ground with expected heights close to 0 m.

To reduce model complexity, we selected the following uncorrelated (Spearman’s $r \leq |0.7|$) variables with the highest model contribution: Vegetation height (Vegetation_h), red-to-all band ratio (R_ratio), blue-to-infrared ratio (B_I_ratio), hue (H) and saturation (S). As RF algorithm can deal with correlated variables we also included the Normalized Difference Vegetation Index (NDVI), which was correlated with R_ratio and B_I_ratio, but is a standard variable used for studies on vegetation health and deadwood detection and the information of the blue spectral band (B) for potentially improving

bare ground recognition. The contributions of the individual variables to the full and the reduced RF model are shown in Table A 1.

Table 4-2 List of ratios tested as predictor variables for the Random Forest RF model. Variables selected in the final model are displayed in bold.

Predictor variables	Description or formula	Reference
R, G, **B**, I	Red, green, **blue**, infrared bands	-
H, S, V	**Hue, saturation**, value calculated with "rgb2hsv" function in "grDevices"	R-package "grDevices" (R, 2019)
Vegetation_h	**Vegetation height from CHM**	-
R_ratio	**R / (R + G + B + I)**	Ganz (2016)
G_ratio	G / (R + G + B + I)	
B_ratio	B / (R + G + B + I)	
I_ratio	I / (R + G + B + I)	
NDVI	**(I - R) / (I + R)**	Jackson and Huete (1991)
NDVI_green	(I - G) / (I + G)	Ahamed *et al.* (2011)
G_R_ratio	G / R	Waser *et al.* (2014b)
G_R_ratio_2	(G - R) / (G + R)	Gitelson *et al.* (1996)
B_ratio_2	(R / B) * (G / B) * (I / B)	self-developed after Waser *et al.* [11]
B_I_ratio	**B / I**	self-developed

Finally, to identify steep rocks and reclassify them to "bare ground", a slope-mask was used. Derived from the DTM and smoothed using the Gaussian filter in a 3-pixel neighborhood, it was applied to the model outcome, to reclassify "dead"-pixels to "bare ground" in areas with slopes > 50° and CHM-values < 15 m.

4.2.4.3 Post-processing of RF results (DDLG_P)

To enhance the results of the RF classification (DDLG) a post-processing procedure was developed to remove the salt and pepper effects (single pixels and groups of two) and to improve the differentiation between the classes "bare ground" and "dead" (Figure 4-3).

First, clumps of isolated deadwood pixels were identified (using the function "clump" of the "raster" package) and the amount of pixels in each clump ("dead" patch) was calculated. Clumps smaller than 0.5 m² (2 pixels) were considered unreliable and reclassified based on the most frequent pixel value occurring in its 3 x 3 pixel neighborhood (majority filter). In case isolated "dead" pixels were surrounded by NA values, they were reclassified to NA.

Hypothesizing that isolated deadwood pixels surrounded by pixels of the classes "dead" or "declining" had a higher probability to be correctly classified than when surrounded by "bare ground" or "live"-pixels, focal statistics was applied to categorize deadwood pixels based on their

surroundings. For this purpose, pixels of all classes were reclassified into: “NA”= 0 , “bare ground”= 1, “live” = 2 , “declining” = 3, “dead” = 4 and for each pixel the mean value k of the neighboring pixels within a 3 x 3 pixel window was calculated. Pixels of the classes “dead” and “bare ground” with $k \geq 3.1$ were classified as “dead”. The remaining “dead”-pixels were reclassified as follows: ”declining” with $2.8 \leq k < 3.1$, “live” with $1.4 \leq k < 2.8$ and “bare ground” with $k < 1.4$.

The majority-filter to remove the salt & pepper effect was then applied a second time, this time to three remaining pixel classes. Finally, a “partial shadow-filter” was applied. Clumps of deadwood pixels located entirely (> 99 % of the clump size area) in partial shadow (for details see data section 2.2) were reclassified to “bare ground”.

The steps of the post-processing procedure were calculated using packages: "raster", "igraph" (Csardi. and Nepusz, 2006), and "data.table” (Dowle and Srinivasan, 2019) in R. The package “tictoc” (Izrailev, 2014) was applied to monitor the processing time. The results were saved as geoTiff in unsigned integer raster format.

4.2.4.4 Deadwood uncertainty filter (DDLG_U)

As an alternative solution to improve the differentiation between “bare ground” and deadwood a deadwood-uncertainty filter was developed, based on a binomial generalized linear model (GLM) quantifying the probability of a “dead”-pixel to be correctly classified (1 = ”dead”, 0 = ”not dead”), as a function of the surrounding environmental and spectral conditions.

To generate the training and evaluation data for this model, a visual evaluation of the results of the deadwood model layer (DDLG) was carried out. All “dead” DDLG pixels were clumped into patches (3482) and converted to polygons in ArcGIS. A random selection of 2000 clumps was visually classified into “dead” (correctly classified = 1) or “not-dead” (misclassified = 0). Where no reliable classification was possible by visual interpretation, the respective polygon was dropped. Of the 762 verified and 1236 falsified deadwood patches consisting of 23119 and 5169 pixels respectively, 1000 pixels per class were then randomly selected for the training and four evaluation datasets respectively (i.e. consisting of 2000 pixels each).

Six predictor variables were entered in this model (Table 4-3): the clump size the deadwood pixel was embedded in, bare-ground occurrence and canopy cover within a 11.5 x 11.5 m (23 x 23 pixels) moving window corresponding roughly to a size of a dead tree’s crown, and three image texture variables: the curvature, as well as the mean value of curvature and the Mean Euclidean Distance (Irons and Petersen, 1981) both calculated in a 5 x 5 pixel moving window to explore the texture of smaller sections of deadwood objects, e.g. changing reflections in the infrared (I) band at the outer

parts of dead trees. Curvature was calculated using “Curvature” function of ArcMap (ESRI, 2018) and Mean Euclidean Distance was used as implemented ERDAS Imagine (HEXAGON, 2020).

Table 4-3 Predictor variables tested for the deadwood-uncertainty model with their description, hypothesized meaning and unit. Variables selected for the final model are presented in bold. I – infrared spectral band.

Variable	Description	Hypothesized meaning	Unit
Clump_size	Size of the “dead” pixel clumps grouped with 8 neighbors (1 pixel = 0.25 m²)	Very small and very big clumps are more likely to be falsely classified	N
Bare_ground	Proportion of bare ground within a 11.5 x 11.5 m (23 x 23 pixels) moving window	Occurrence of “bare ground” next to “dead” pixels may indicate a possible misclassifications of both classes	0-1
Canopy_cover	Proportion of pixels above 2 m vegetation height within a 11.5 x 11.5 m (23 x 23 pixels) moving window	Pixels with low canopy cover are likely to have false height values in transition areas between high and low vegetation	0-1
Curvature	Curvature values per pixel based on the I band	Form and direction of the I spectral signal may differ between “dead” and “bare ground” objects	Value (-∞) - ∞
Curvature_Mean	Mean curvature values within a 2.5 x 2.5 m (5 x 5 pixels) moving window based on the I band	Form and direction of the I spectral signal in a wider surrounding may show differences between “dead” and “bare ground” objects	Value (-∞) - ∞
Mean Euclidean Distance (Texture Features)	Mean Euclidean Distance values within a 2.5 x 2.5 m (5 x 5 pixels) moving window based on the I band	“Dead” and “bare ground” objects may show different texture characteristics in the I band	Value 0 - ∞

We followed a hierarchical variable selection procedure: First, variables were tested univariately and in their quadratic form. Uncorrelated (Spearman’s $r <= |0.7|$) variables which significantly contributed to distinguishing correctly and falsely classified “dead” pixels were retained (Table A 4-2). We then tested all possible combinations of these variables using the dredge-function (R-package MuMIN (Barton, 2019)) to select the best model based on Akaike’s Information Criterion (AIC). Model fit was measured by means of several evaluation metrics: the Area Under the Receiver Operating Characteristic Curve (AUC) as implemented in R package “AUC” (Ballings and Van den Poel, 2013) as well as sensitivity, specificity, positive prediction value (PPV), negative prediction value (NPV), overall accuracy (OA) and Cohen´s Kappa as implemented in the R package “caret” and described by Hosmer and Lemeshow (2000).

In addition, the uncertainty model was evaluated using four independent evaluation datasets (2000 pixels each), drawn without replacement and with an equal proportion of presence and absence observations in each set.

To analyze the influence of the single predictor variables, we plotted them against the target variable using the R-package “ggplot2” (Wickham, 2016).

Finally, to convert continuous values into a binary filter (deadwood-classification correct/false), different cut-off values were tested: The value at Kappa maximum and the value resulting in a maximum sensitivity with a specificity of at least 0.7 (identified using the multiple optimal cutpoint selection with increments of 0.05, R-package “cutpointr” (Thiele, 2019)), with the intention of keeping as many of the correctly classified “dead” pixels as possible while removing a large proportion of the falsely classified pixels.

4.2.5 Model validation

4.2.5.1 Visual assessment

As a first step, the outcome of all models was visually examined based on orthophoto, CHM and stereo aerial imagery using GIS (2D) and Summit Evolution (3D) (DAT/EM, 2012) to appraise the plausibility of the predictions in a real-world situation.

4.2.5.2 “Pure classes” validation

We evaluated the RF model (DDLG) using the validation dataset consisting of 2000 pixels per class, randomly drawn from the reference polygons.

The confusion matrix and associated accuracy measures, i.e. overall accuracy (OA) with a 95 percent confidence interval (95% CI), producer’s (PA) and user’s (UA) accuracy as well as Cohen´s Kappa were calculated for each class as implemented in the package “caret”, comparing each class factor level to the remaining levels (i.e. a "one versus all" approach).

4.2.5.3 Pixel-based validation based on a stratified random sample

In addition to the validation on “pure classes” an independent stratified random sample was collected. For this purpose, 750 pixels per class (“dead”, “declining”, “live”, “bare-ground”) with only 1 pixel randomly sampled per clump (defined based on the DDLG_P layer) were selected. Pixels were then classified by visual interpretation, with pixels of different classes randomized before interpretation to avoid any interpreters’ bias. For evaluation, the results of the visual classification

were compared with the results of the three model outcomes (DDLG, DDLG_P and DDLG_U) for generating the confusion matrices and associated accuracy measures.

4.2.5.4 Polygon-based deadwood validation

Finally, to estimate the accuracy of single tree detection of the three modelling outcomes, the results for the class "dead" were compared with the reference polygons of "dead" class. For this purpose an intersection analysis was conducted to assess to which extent the deadwood reference polygons intersected with pixels of the deadwood class identified by each model (DDLG, DDLG_P and DDLG_U). "Positive detection" was assigned, when at least one deadwood pixel (single "dead" pixels often representing deadwood in decay stages 5 or 6 (Figure 4-2)) intersected. In addition, we compared the overall area covered by all intersecting pixels with the area of the reference polygons.

4.3 Results

4.3.1 Random Forest model and pure classes' validation

The reduced Random Forest model based on 7 variables (DDLG) performed similar compared to the initial, full model including 18 variables, with a Cohen's Kappa of 0.92 and 0.93 and an overall accuracy of 0.95 and 0.94 respectively (Table 4-4). All classes were predicted with very good producer's and user's accuracy values (all around 0.9 or above).

Table 4-4 Results of the "pure classes" validation for the DDLG model with all 18 and the finally selected 7 variables respectively, measured by producer's, user's and overall (in bold) accuracies as well as Cohen's Kappa. Confusion matrices are presented in (Table A 4-1)

DDLG version	Accuracy measure	Class				Overall accuracy	Kappa
		Bare ground	Live	Declining	Dead		
18 variables	Producer's accuracy	0.99	0.97	0.90	0.92	**0.94**	**0.93**
	User's accuracy	0.99	0.94	0.89	0.95		
7 variables	Producer's accuracy	0.99	0.97	0.91	0.92	**0.95**	**0.92**
	User's accuracy	0.98	0.95	0.90	0.96		

The most important predictor variables were Vegetation height (CHM), R_ratio, NDVI, B_I_ratio and hue (Figure A 4-1). Vegetation heights were a key factor for separating pixels of the classes "bare ground" and "dead". NDVI and R_ratio were especially decisive for the recognition of "live" trees, and NDVI, hue and B_I_ratio were important for distinguishing between the classes "live", "declining" and "dead". Blue band and saturation showed only little contributions to the model.

4.3.2 Uncertainty model

The deadwood-uncertainty model included 5 of the 6 tested input variables (Table A 4-2), Clump_size and Bare_ground, both as linear and quadratic terms, Canopy_cover, Curvature and Curvature_Mean. All retained variables contributed significantly to the model. The effect plots (Figure A 4-2) show that correct classification of deadwood was associated with larger clump sizes, higher canopy cover and low amount of “bare ground” in the neighborhood. Moreover, deadwood was more likely to be correctly classified under higher texture parameter values (higher structural complexity).

With an AUC of 0.89 the model showed good predictive power. Cohen´s Kappa ranged between 0.58 to 0.60 and the overall accuracy between 0.79 and 0.80, depending on the selected threshold (Table 4-5). The Kappa maximum threshold (0.39) showed slightly better overall performance and better predictive power for identifying misclassified pixels. However, as we prioritised keeping a wrongly classified over discarding a correctly classified “dead” pixel, the maximum sensitivity by specificity of 0.7 - value (0.31) was selected to discriminate between “dead” and “not-dead”.

Table 4-5 Model fit and predictive performance of the “deadwood-uncertainty” model measured by sensitivity, specificity, positive prediction value (PPV), negative prediction value (NPV), overall accuracy and Cohen´s Kappa for thresholds based on Kappa maximum (0.39) and the maximum sensitivity by the specificity of 0.7 (0.31). In addition threshold-independent Area Under the ROC-Curve (AUC) was provided for different classes’ separation. Independent validation was performed on four independent validation datasets with their results calculated for the selected threshold of maximum sensitivity by specificity of 0.7 (0.31). The validation results are presented below for comparison with arithmetic mean and standard error values showing the amount of variation between the results of different folds.

Performance	Model fit		4 FOLDS validation Max sensitivity by specificity=0.7 (0.31)	
metrics	Kappa maximum (0.39)	Max sensitivity by specificity=0.7 (0.31)	Mean	Standard deviation
Sensitivity	0.82	0.88	0.89	0.007
Specificity	0.77	0.70	0.72	0.009
PPV	0.78	0.75	0.76	0.005
NPV	0.81	0.85	0.87	0.007
Overall accuracy	0.80	0.79	0.80	0.003
Cohen's Kappa	0.60	0.58	0.61	0.005
AUC	0.89		0.90	0.005

The results of the independent model validation, using four validation folds showed consistently good model performance for all metrics (Table 4-5), with an average AUC-value of 0.90, mean

Cohen's Kappa of 0.61, and mean value for overall accuracy of 0.80 across folds by standard deviation of less than 0.005.

4.3.3 Classification results

The different classification scenarios DDLG, DDLG_P and DDLG_U (Table 4-5) resulted in different amounts of pixels per class, but showed a consistent general pattern with 39.4% "live", 0.4 - 0.5% "dead", 5.2 - 5.5% "declining" and 0.2% "bare ground" areas. About 55% of the area was masked out as NA (Figure 4-4, Table 4-6).

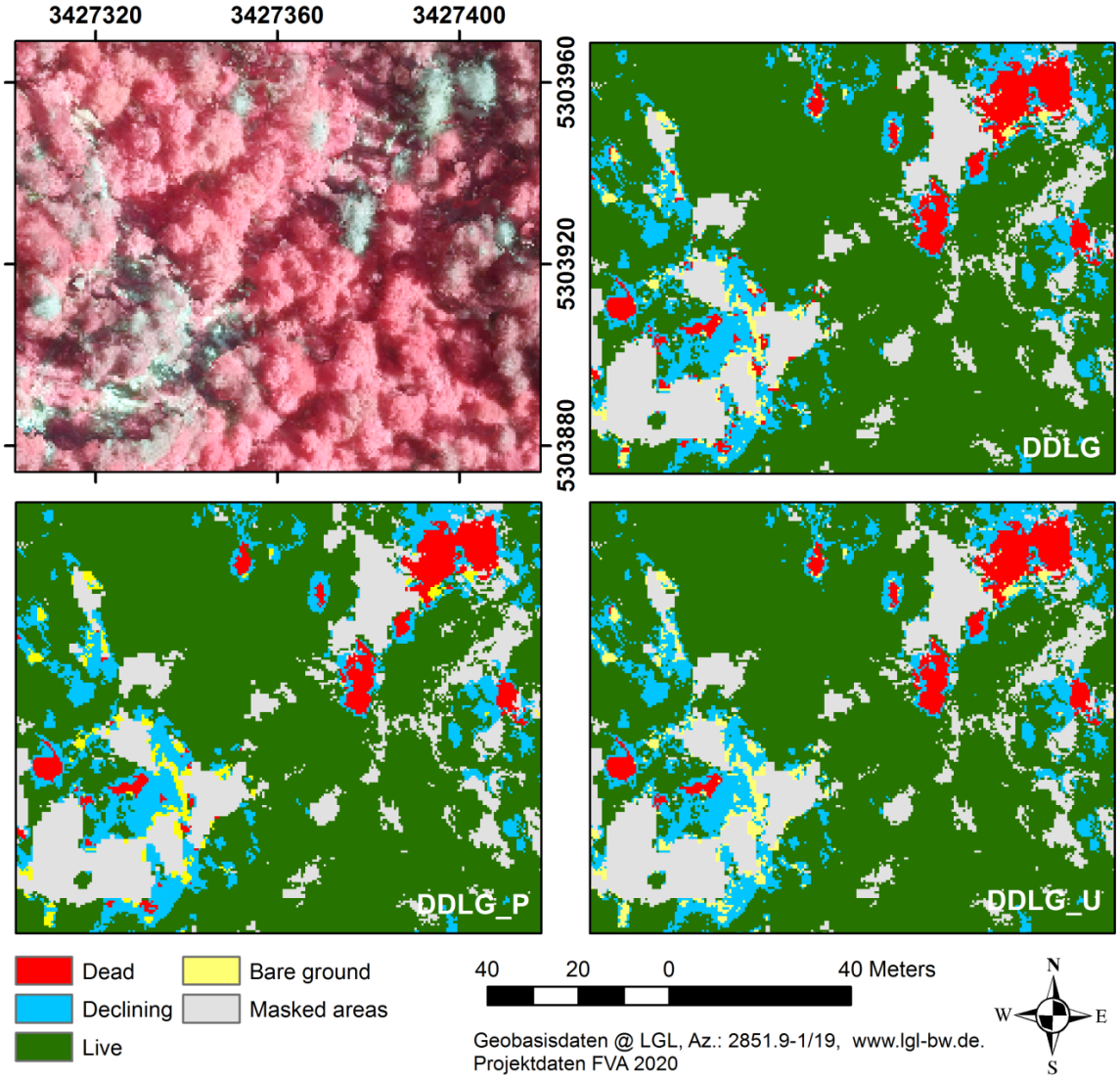

Figure 4-4 Examples of the results obtained with different classification scenarios: Random Forest (RF) classification (DDLG), RF classification with post-processing (DDLG_P) and with additional deadwood-uncertainty filter (DDLG_U), compared to the input CIR aerial imagery (upper left). Note the reduction of isolated pixels in DDLG_P and the improved "bare ground" recognition in DDLG_P and DDLG_U compared to DDLG (lower left corner).

With post-processing, the amount isolated pixels of the classes “dead”, “declining” and “bare ground” decreased, mostly in favour of “live” pixels (Table 4-6, Figure 4-4). The uncertainty filter targeting at a better differentiation between “dead” and “bare ground” changed the proportions of these two classes from about 3 / 1 to 2 / 1 (Table 4-6).

Table 4-6 Classification results per class in number and percent (%) of pixels (0.5 x 0.5m) for the three classification scenarios: Random Forest (RF) classification (DDLG), RF classification with post-processing (DDLG_P) and with additional deadwood-uncertainty filter (DDLG_U)

Class	DDLG		DDLG_P		DDLG_U	
	Pixel	%	Pixel	%	Pixel	%
Live	9341179	39.4%	9342529	39.4%	9341179	39.4%
Dead	119790	0.5%	105661	0.4%	102815	0.4%
Declining	1274349	5.4%	1237793	5.2%	1274349	5.4%
Bare ground	35690	0.2%	36265	0.2%	52665	0.2%
NA	12933862	54.6%	12982622	54.8%	12933862	54.6%
Total	*23704870*	100.0%	*23704870*	100.0%	*23704870*	100.0%

The number of deadwood clumps (“dead”-pixels consolidated to patches) (Table 4-7) decreased successively from almost 10000 (DDLG) to 3482 in DDLG_P and 3139 in DDLG_U, while their total area decreased from ca. 3 ha to 2.64 and 2.57 ha respectively. In all cases small deadwood patches dominated with a median size of 0.5 for DDLG and 2.25 - 3 m² for DDLG_P and DDLG_U, a minimum size of 0.25 m² (1 pixel) and a maximum size of over 800 m² (a large group of dead trees aggregated to one patch).

Table 4-7 Classification results for deadwood patches (clumps of pixels classified “dead”) expressed in number of pixels (size 0.5 x 0.5m) per classification scenario: Random Forest (RF) classification (DDLG), RF classification with post-processing (DDLG_P) and with “deadwood-uncertainty” filter (DDLG_U).

	DDLG		DDLG_P		DDLG_U	
	Pixel	m²	Pixel	m²	Pixel	m²
N	9868		3482		3139	
SUM	119790.00	29947.50	105661.00	26415.25	102815.00	25703.75
MEAN	12.14	3.04	30.34	7.59	32.75	8.19
MEDIAN	2.00	0.50	10.00	2.50	12.00	3.00
MIN	1.00	0.25	1.00	0.25	1.00	0.25
MAX	3281.00	820.25	3258.00	814.50	3281.00	820.25
SD	53.82	13.45	87.30	21.82	91.98	22.99

4.3.4 Model validation

4.3.4.1 Visual assessment

The visual assessment, carried out parallel to the statistical validation, didn´t confirm the high accuracy values of the pure classes validation of the DDLG model. Visual control identified rocks and bare ground within the forest stands and on forest stand borders being misclassified as “dead”, not conforming to the very high accuracy values for predicting this class and to the almost 100 % accuracy for the class “bare ground”.

4.3.4.2 Pixel-based validation

For all three classification scenarios, validation on an independent, stratified random sample of pixels showed lower accuracies per class than that obtained with pure classes’ validation on the DDLG. Cohen’s Kappa (0.59 - 0.65) and overall accuracies (0.70 - 0.74) (Table 4-8) were of similar magnitude for all three scenarios, with the best results for DDLG_U.

Table 4-8 Results of the validation on an independent stratified random sample of 750 pixels per class for the three classification scenarios Random Forest (RF) classification (DDLG), RF classification with post-processing (DDLG_P) and with deadwood-uncertainty filter (DDLG_U). Presented are producer’s, user’s and overall accuracy and Cohen’s Kappa. Detailed confusion matrices with the amount of validated pixels per class are shown in Table A 4-3.

Model scenario	Accuracy measure	Class				Overall accuracy	Kappa
		Bare ground	Live	Declining	Dead		
DDLG	User's accuracy	0.82	0.77	0.67	0.60	**0.70**	**0.60**
	Producer's accuracy	0.57	0.79	0.56	0.87		
DDLG_P	User's accuracy	0.75	0.73	0.61	0.69	**0.70**	**0.59**
	Producer's accuracy	0.66	0.79	0.55	0.79		
DDLG_U	User's accuracy	0.76	0.77	0.66	0.74	**0.74**	**0.65**
	Producer's accuracy	0.82	0.77	0.56	0.80		

The greatest balance between producer’s and user’s accuracies were consistently achieved for the class “live” with PA of 0.79 for the DDLG and 0.77 for the two other scenarios and UA of 0.77 (DDLG, DDLG_U) and 0.73 (DDLG_P). The drop in PA after post-processing was probably caused by the majority filter applied to smooth the results. The class “live” had the most misclassifications with the class “declining”, for which classification was generally least reliable (PA of 0.55 - 0.56 and UA of 0.61 - 0.67), and additional misclassifications occurred with the class “dead”. “Bare ground” classified by DDLG achieved PA = 0.57 and UA = 0.82 and was almost exclusively misclassified as “dead”. This

improved with post-processing to PA = 0.66 and to PA = 0.82 after applying the uncertainty filter. Simultaneously, the UA dropped from 0.82 to 0.75 (DDLG_P) and 0.76 (DDLG_U).

The classification of "dead" pixels showed the best PA=0.87 in the first scenario (DDLG). On the other hand a low UA = 0.60 indicated a high commission error, with misclassifications especially in the classes "bare ground" (283 pixels) and "declining" (138 pixels) (Table A 4-3). Post processing and the application of the deadwood-uncertainty filter, both led to a more balanced PA to UA relationship. UA increased significantly from 0.60 (DDLG) to 0.69 (DDLG_P) and 0.74 (DDLG_U) whereas PA decreased from 0.87 to 0.79 and 0.80 for the same scenarios.

4.3.4.3 Polygon based deadwood validation

The polygon-based validation confirmed good detection of standing deadwood objects with 91 - 96 % of the reference deadwood-patches and 90 % of their area being detected in all classification scenarios (Table 4-9). Mean (12.8-13.4) and median (10.4-10.6) patch-size, and their standard deviation (11.5) showed similar values for both the intersected and the reference polygons, indicating that detected deadwood patches correctly depicted the "real" deadwood occurrence in most cases.

Table 4-9 Results of the polygon-based validation. Basic statistics (N, % of N, area sum and percent (%), area mean, median, maximum and standard deviation) for the deadwood patches identified by the three classification scenarios: Random Forest (RF) classification (DDLG), RF classification with post-processing (DDLG_P) and with a deadwood-uncertainty filter (DDLG_U), that were validated (Intersected) and not validated (Not intersected) when compared with the reference deadwood polygons.

Polygon data	DDLG		DDLG_P		DDLG_PU	
	Intersected	**Not intersected**	**Intersected**	**Not intersected**	**Intersected**	**Not intersected**
N	303	12	287	22	291	24
N (% of reference)	**96%**	**4%**	**91%**	**7%**	**92%**	**8%**
AREA SUM (m²)	3868.5	7.5	3844.7	23.1	3855.2	22.3
AREA (% of reference)	**90%**	**0%**	**90%**	**1%**	**90%**	**1%**
AREA MEAN (m²)	12.8	0.6	13.4	0.8	13.2	0.9
AREA MEDIAN (m²)	10.4	0.1	10.6	0.7	10.6	0.5
AREA MAX (m²)	64.9	4.3	65.1	4.3	64.9	4.3
AREA SD (m²)	11.5	1.2	11.5	0.9	11.5	1.1

The intersection of the deadwood reference polygons with the patches constructed from pixels classified as "dead" showed that their total area exceeded the total area of the reference polygons

by 40% in all three classification scenarios: DDLG, DDLG_P and DDLG_U (Table A 4-4). The maximum area of a single deadwood-patch of 811-813.8 m² (identified by all 3 scenarios) compared to the maximum size of a single reference polygon of 65.9 m² indicated grouping of several deadwood-objects into one patch.

For DDLG, the number of intersecting deadwood-patches (323) was larger than those of the reference polygons (315). For DDLG_P and DDLG_U the number of intersecting deadwood-patches dropped to 76 % (238) and 90 % (285) of the reference polygon numbers (Table A 4-4). Given detection rates of more than 90% (Table 4-9) this again indicates clustering of pixels of several dead trees into a larger patch. The number of omitted (i.e. not detected) polygons (Table 4-9) was lowest for DDLG and highest for DDLG_P, with an increasing trend of omitting small polygons for DDLG_U and DDLG_P. The mean area of the not detected polygons was less than 1 m² and the median less than 0.7 m², corresponding to 1 - 3 pixel and the total area of omitted deadwood did not exceed 1 % in either scenario.

4.4 Discussion

4.4.1 Deadwood detection

With Random Forest classification, we used a standard procedure to detect standing deadwood and distinguish it from living and declining trees, as well as bare ground. Although the validation on pure classes appeared promising, with very high accuracies above 0.9, visual assessment revealed grave misclassifications of “bare ground” as “deadwood”. This result was confirmed when applying an independent, random sampling validation, revealing a low UA of 0.60 (Table 4-8). The latter improved with post-processing (UA = 0.69) and the application of a deadwood uncertainty filter (UA = 0.74), but for the price of decreasing PA from 0.87 to 0.79 and 0.80, a reliable, and therefore satisfactory level. OA remained constant for DDLG and DDLG_P at 0.7 and increased to 0.74 for DDLG_U. This level of accuracy places our method in line with visual methods based on CIR aerial imagery and methods for detecting snags using solely ALS data, e.g. Yao *et al.* (2012a) with OA of 0.7 - 0.75. Combining CIR and ALS data delivered mostly better results with OA between 0.83 (Kantola *et al.*, 2010) and > 0.9 (Polewski *et al.*, 2015a; Kamińska *et al.*, 2018) depending on the algorithm used.

The polygon-based validation, with more than 90 % of the deadwood-patches and their area correctly identified, proved a very good detectability of single dead trees. Not-detected polygons with a median area of 1 - 3 pixels in all classification scenarios indicate the biggest problems in the

detection of snags and small dead crowns. This is in line with Wing *et al.* (2015), who showed detection reliability rising with the tree's diameter at breast height (DBH) and Krzystek *et al.* (2020) who found lower accuracies for snags (UA= 0.56, PA = 0.66) than for dead trees (UA and PA > 0.9). Although our method was pixel-based, the deadwood-detection accuracy corresponds with the accuracy of 0.71 - 0.77 (by 1 to 1 pixel correspondence) achieved by Polewski *et al.* (2015c) using object detection methods based on ALS and CIR aerial imagery.

The larger overall area of our classified deadwood patches compared to the area of the reference polygons partially resulted from aggregating pixels to coarse clumps encompassing several neighbouring dead trees. However, for many ecological questions and applications in practical forestry identifying single deadwood objects and quantifying their size is important and can give a hint e.g. on the decay stage of a dead tree (Zielewska-Büttner *et al.*, 2018). Our pixel-based method produced information on the location and area of standing deadwood together with a probability that a pixel was correctly classified. Adding object detection would thus be a valuable extension of our method.

Adamczyk and Bedkowski (2006) underlined the difficulty in deadwood detection, as spectral differences between the classes are very fluent and influenced by light conditions, the location of the tree, crown geometry and individual trees coloring (Adamczyk and Bedkowski, 2006). We decided to use declining trees as a supporting class, having in mind that especially in the outer parts of crowns there is no sharp transition between a healthy crown and bare ground or the live stand. As expected, the PAs for this class were constantly the lowest (0.55 - 0.56) across all scenarios as this class was not targeted for improvement. Although not highly reliable (UA between 0.61 and 0.67) the trees identified as "declining" still have a potential to be used in forestry practice for identifying trees differing from the rest of the stand, e.g. by showing dry branches, breakage or lichens in the crown, or being weakened and thus potentially prone to or in early stage of insect (e.g. bark beetle) infestation.

4.4.2 Bare ground issue

The class "bare ground" occurred to be the key to the optimization of our deadwood detection method. Problems with discriminating between soil and deadwood were also pointed out by Fassnacht *et al.* (2014) and Meddens *et al.* (2011), who observed that misclassifications occurred mostly in sunned parts of dead trees. Most studies mapping senescent or dead trees from remotely sensed data neglect the possible confusion with bare ground. The magnitude of this issue largely depends on the amount of bare ground in the study area. Forest regeneration regime and soil

productivity also play a role, when areas remain non-vegetated for long times after disturbance events (Fassnacht *et al.*, 2014). Given the high proportion (38 %) of "bare ground" pixels misclassified as "dead" in the DDLG raster, which dropped to 21 % (DDLG_P) and 14 % (DDLG_U), we claim that for reliable deadwood mapping this potential error needs to be addressed, especially if the results are intended for nature conservation measures, forestry operations or field campaigns which would incur a waste of resources if planned where no dead trees are present (Wulder *et al.*, 2005). On the other hand increasing "bare ground" detection on the cost of reducing PA of deadwood could be disadvantageous, when the goal was the identification of dead trees e.g. for traffic safety, where detection of every dead tree is important (Stereńczak *et al.*, 2017).

Decreasing the image resolution from 0.3 to 2.4 m enabled Meddens *et al.* (2011) resolving the "bare ground" vs. "dead" misclassification problem. This underlines the necessity of using data of a resolution that matches the resolution of the analyzed objects. Hengl (2006) proposed a minimum of four pixels for representing the smallest circular objects and at least two pixels for representing the narrowest objects as vital for reliably detecting an object in an image, while Dalponte *et al.* (2015) recommended the spatial resolution of the imagery to match the expected minimum size of the tree crowns in the scene. Exploring the optimal spatial resolution of multispectral satellite images for detecting single dead trees in forest areas Pluto-Kossakowska *et al.* (2017) found 0.5 - 1 m to be the best pixel size. In that respect the 0.5 m resolution in our study seems to be a good choice, when aiming at mapping all standing deadwood including single snags without branches (i.e. corresponding to one to a few pixels in size).

Resampling images of lower resolution didn't suffice to achieve good results in single tree detection. However a pixel size of > 2.5 m can be enough if the goal of the study is the detection of deadwood-patches, not single trees, as already used in some applications, e.g. for planning forest operations (Kamińska *et al.*, 2018). Quantifying the effect of decreasing the resolution (e.g. to 1 x 1 m) on the classification results would be an important future research topic, as this would strongly reduce processing time and the amount of data. Still, the intended practical use of the model results will always be a critical factor for defining the appropriate method.

4.4.3 Canopy height information

As we limited our scope to the detection of standing deadwood while neglecting lying deadwood, a 5 m height mask based on the CHM was included in the model set-up at the very beginning to mask out all areas close to the ground,. The same was proposed by Fassnacht *et al.* (2014) for a better separation of forest from non-forest areas. They suggested using vegetation height information

provided by the spaceborne mission TanDEM-X or stereo-photogrammetry of overlapping aerial photographs in combination with an accurate DTM from ALS data. Our results, based on the second option, show that the CHM was insufficient for detecting small forest openings with bare ground which could possibly be detected when using ALS data (White *et al.*, 2018).

The accuracy of digital surface models is highly related to the point density acquired either by ALS or by the matching of overlapping aerial images, with the former achieving much higher point densities. The amount of points matched from stereo aerial imagery depends on numerous factors e.g. image resolution, overlap between neighboring images, image geometry, light and weather conditions at the time of data acquisition (Ackermann *et al.*, 2020). In shaded areas and near the ground surface with surrounding higher vegetation matching success is limited (Straub *et al.*, 2013; Zielewska-Büttner *et al.*, 2016b).

The aerial imagery material we used was acquired in August at very early hours (7 - 9 am) and thus image quality was negatively affected by grave occurrence of shadow and varying spectral signals. Controlling the flight times to limit shadow occurrence, as well as increasing the resolution and overlap of the stereo imagery, would certainly enhance the quality of the orthophotos and DSMs derived from the data, and consequentially enhance the accuracy of both spectral and structural predictor variables and classification results.

Information on vegetation height was among the most important predictor variables in both, our RF model and the deadwood-uncertainty model. We expect that using ALS data for deriving DSM and CHM would bear the greatest potential for model improvement. In many countries, e.g. in Scandinavia (Trier *et al.*, 2018) or Canada (White *et al.*, 2016), ALS data is already a standard element of the mapping services provided by the public authorities and widely used in forestry, as delivering accurate information on canopy heights, tree species and timber volume for forest management.

4.4.4 Deadwood detection algorithms

In the last two decades various machine learning (ML) algorithms have been used for image classification (Valbuena *et al.*, 2016; Liu *et al.*, 2018) in the field of forest ecology. Also in deadwood detection ML algorithms, such as Maximum Likelihood (Pluto-Kossakowska *et al.*, 2017; Stereńczak *et al.*, 2017), RF (Kamińska *et al.*, 2018) or Supported Vector Machines (SVM) (Fassnacht *et al.*, 2014), were applied.

We used RF as it demands little parametrization, being at the same time robust to large datasets and not requiring a-priori assumptions on statistical distributions (Wegmann *et al.*, 2016). Even though RF can deal with correlated variables we reduced the number of predictors from 18 to 7 variables to

save processing time. The results of both models showed similar - very high - accuracies, when validated on the pure classes' dataset, our reason for focusing on improving the classification results by post-processing and extra filtering instead of further optimizing the RF model.

After vegetation height, other important variables were R_ratio, NDVI, B_I_ratio and hue, what confirms the higher suitability of ratios and indices for image classification than the use of pure bands (Jackson and Huete, 1991; Waser *et al.*, 2014b) and that the crucial spectral information is found in red, infrared and blue bands.

Both alternative solutions applied to enhance the RF output (DDLG) improved the classification results in the targeted classes "dead" and "bare ground". Post-processing (DDLG_P) incorporated a mean neighborhood filter for "dead" pixels assuming a lower accuracy of dead pixels in the neighborhood of "bare ground" and a "salt and pepper effect" filter removing isolated pixels of all classes, which are considered as most prone to errors. This process enhanced the separation of the classes "dead" and "bare ground" and the overall classification results to acceptable accuracies of UA=0.69 by PA=0.79.

The best results, however, were achieved when applying the deadwood uncertainty filter with UA=0.74 and PA=0.80 for "dead" and UA=0.76 and PA=0.82 for "bare ground" (DDLG_U). Texture patterns of the infrared band and structural variables (canopy cover and neighboring "bare ground" pixels) included in the deadwood-uncertainty model were crucial for separating correctly classified "dead"-pixels from misclassified ones. However, since the texture variables needed extra pre-processing and the uncertainty model itself required time for the generation of new training data and model calibration, this approach was more costly compared to post-processing.

In recent years deep learning (DL) algorithms have become increasingly popular for analyzing remote sensing data (Paoletti *et al.*, 2019). In deadwood mapping they showed very good results for identifying windthrow areas (Hamdi *et al.*, 2019) or detecting deadwood objects from very high resolution (VHR) CIR aerial imagery (Jiang *et al.*, 2019). Convolutional neural networks (CNN), which use different levels of generalization of the same data (O'Shea and Nash, 2015) could possibly help to correctly delineate deadwood objects that are characterized by smooth transition edges. The variables Curvature and Curvature_mean for example, which both significantly contributed to the deadwood-uncertainty model, represent different aggregation levels of the same structure and suggest a potential benefit of using CNNs. Exploring the capability of DLAs to deal with large datasets of high resolution (0.5 - 1 m) for large-scale deadwood detection is thus a promising future research direction.

Our method using solely RGBI and CHM data could potentially be transferred to other areas, for which similar spectral and structural digital information is available. However, the requirements and possibilities for model transferability to areas with different quality aerial imagery and other forest types need to be evaluated. The method could also be tested on satellite imagery data, with additional attention in this case needed to be paid to proper data pre-processing including atmospheric correction, accurate georeferencing and co-registration with the DSM and subsidiary data.

4.5 Conclusions

We presented two alternative methods for enhancing pixel-based standing deadwood detection based on RF classification, using either post-processing or a deadwood-uncertainty filter. Both methods proved to deliver satisfactory results in a standardized automated manner, but the best accuracies were achieved when applying the deadwood-uncertainty filter. Problems with differentiating between deadwood and bare ground at forest borders and in areas with heterogeneous vegetation heights were addressed and partially solved, leading to more balanced accuracies for “deadwood” and “bare ground” classification. In this context, we also show the misleading results of pure-classes validation and highlight the need for various independent validation methods including visual appraisal.

Our methods were solely based on spectral variables and vegetation heights derived from RGBI spectral bands and the CHM and can potentially be used for other datasets containing this information. For further improvement we suggest using ALS as a source for reliable surface heights or stereo aerial imagery with higher resolution and overlap. The latter becoming successively more and more available could deliver more detailed DSMs and accurate “true-orthophotos”. Finally, object based image analysis enabling the mapping of single dead tree polygons could be an additional step in our analysis and added value for forest ecology studies and management applications based on these data, e.g. for habitat suitability modelling, monitoring of deadwood and forest development or for the evaluation of deadwood enrichment programs.

4.6 Author Contributions

Conceptualization, K.Z-B., P.A., V.B.; methodology, K.Z-B., S.K., P.A., R.B., B.K., V.B.; validation, K.Z-B., L.G., R.B., S.K., P.A.; formal analysis, K.Z-B., S.K., P.A., V.B.; investigation, K.Z-B., S.K. R.B., L.G.; resources, V.B., P.A.; data curation, K.Z-B., S.K.; writing—original draft preparation, K.Z-B..; writing—review and editing, V.B., P.A., S.K., L.G., R.B., B.K.; visualization, K.Z-B.; supervision, P.A., V.B.

4.7 Acknowledgments

Thanks a lot to Anne-Sophie Stelzer for her statistical advice, to Johannes Brändle for his technical support in calculation the last results and for translating the model script into an algorithm for processing large datasets across large spatial scales together with Sven Kolbe.

Conflicts of Interest: The authors declare no conflict of interest.

4.8 Appendix A

1) 2)

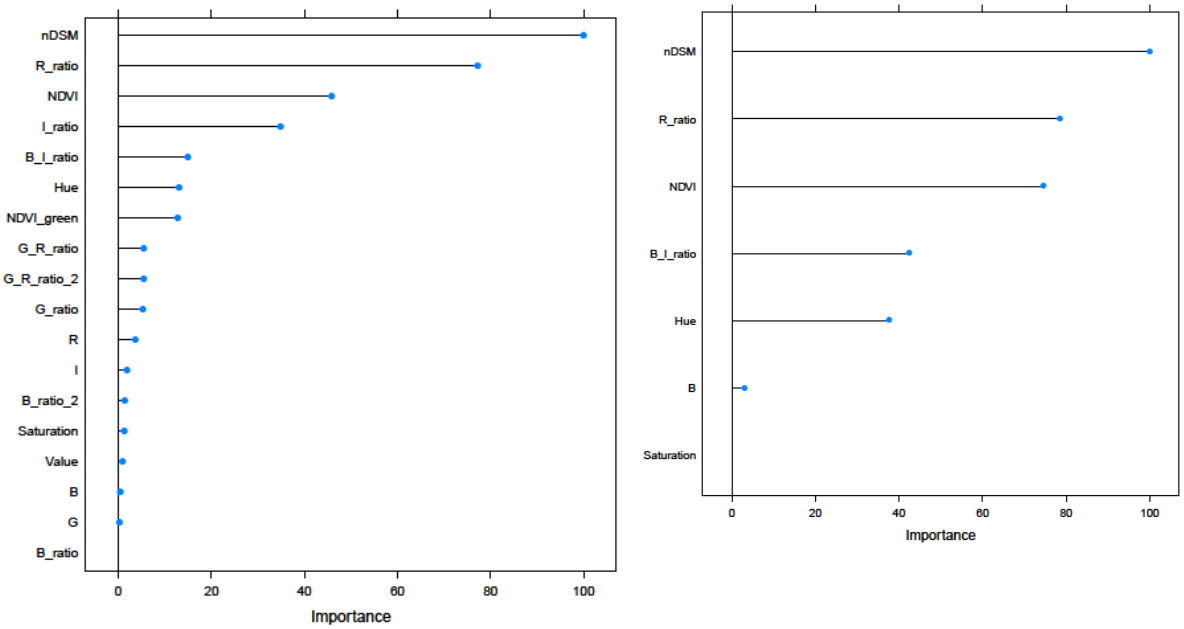

Figure A 4-1 Variable importance in a Random Forest model (DDLG) including all 18 predictor variables (1) and a model reduced to 7 predictor variables (2). (For variable abbreviations see Table 4-2).

Table A 4-1 Confusion matrix presenting the pure class validation results of the Random Forest model (DDLG) with 1) 18 variables vs. 2) 7 variables

	DDLG		Reference				Predicted total	User's accuracy
			Bare ground	Live	Declining	Dead		
18 variables	Predicted	Bare ground	1971	1	8	14	1994	0.99
		Live	1	1940	112	4	2057	0.94
		Declining	10	59	1792	145	2006	0.89
		Dead	18	0	88	1837	1943	0.95
	Reference total		2000	2000	2000	1986	7540	
	Producer's accuracy		0.99	0.97	0.90	0.92		***0.94***
7 variables	Predicted	Bare ground	1989	0	12	22	2023	0.98
		Live	0	1930	104	4	2038	0.95
		Declining	4	66	1812	131	2013	0.90
		Dead	7	4	72	1843	1926	0.96
	Reference total		2000	2000	2000	2000	7574	
	Producer's accuracy		0.99	0.97	0.91	0.92		***0.95***

Table A 4-2 Variables tested and retained (in bold) in the "deadwood-uncertainty model", a generalized linear model GLM predicting the probability of standing deadwood being correctly classified. Variables are presented with their mean and standard deviation (SD) for correctly (PRES) and falsely (ABS) classified deadwood pixels. Also provided are the p-value and AIC of univariate models including the linear (l) and quadratic (q) term of the variable. Variable codes and descriptions are listed in Table 4-3.

	PRES_mean	PRES_SD	ABS_mean	ABS_SD	p_l	AIC_l	p_q	AIC_q
Clump_size	634.17	1121.12	27.81	33.21	0.00	1791.67	0.00	1792.66
Bare_ground	0.01	0.02	0.02	0.06	0.00	2680.88	0.01	2678.66
Canopy_cover	0.97	0.08	0.91	0.13	0.00	2633.00	0.00	2601.77
Curvature	504964.4	5138583.2	-510916.8	6535890.7	0.0	2761.7	NA	NA
Curvature_mean	101697.8	546521.5	-169517.6	520512.3	0.0	2650.9	NA	NA
Mean_Eucklidean _Distance	4945.2	2088.6	5078.5	3116.0	0.3	2775.3	NA	NA

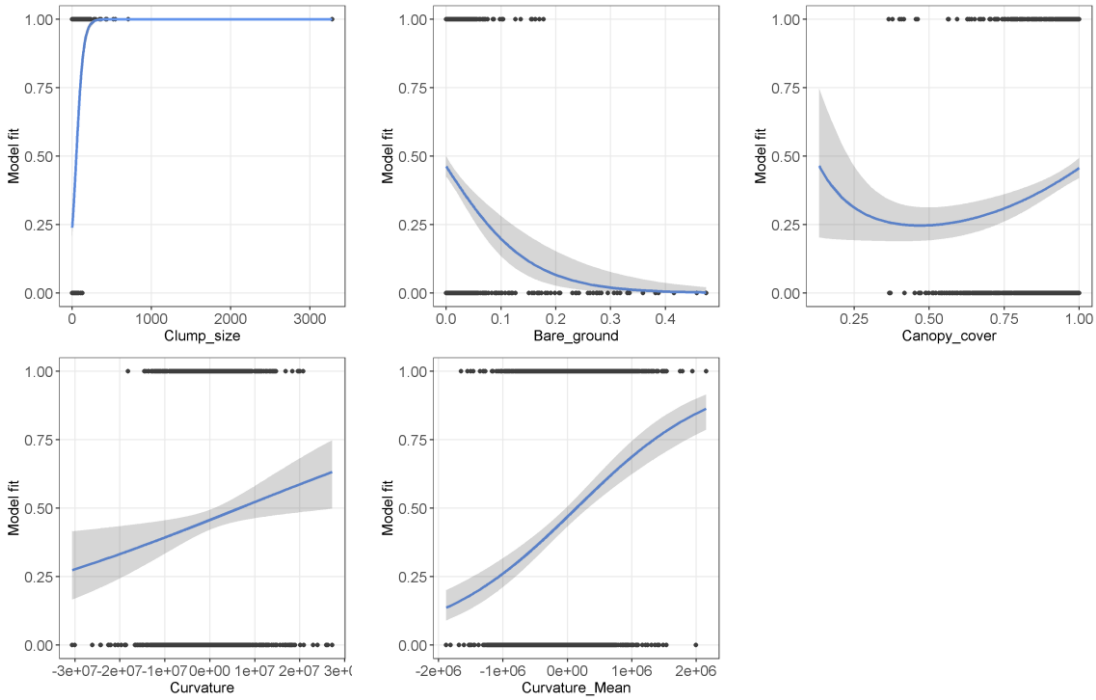

Figure A 4-2 Effect plots showing probability of a deadwood-pixel to be correctly classified as "dead" as a function of the predictor variables included in the deadwood-uncertainty model (Table A 4-2). The blue line indicates the estimated smoothing parameter of a given variable, while keeping all other variables set to their median value. Shadowed areas indicate the 95 % confidence intervals conditional on the estimated smoothing parameter. Variable codes and descriptions are listed in Table 4-3.

Table A 4-3 Results of the validation of the three deadwood classification models Random Forest (RF) classification (DDLG), RF classification with post-processing (DDLG_P) and after applying a deadwood-uncertainty filter (DDLG_U) based on a stratified random sample (750 pixels per class). Results are presented as confusion matrix, user's and producer's accuracy and the overall accuracy in italics. (Table continues on the next page)

			Reference				Total predicted	User's accuracy
			Bare ground	Live	Declining	Dead		
DDLG	Predicted	Bare ground	427	4	26	64	521	**0.82**
		Live	8	590	163	3	764	**0.77**
		Declining	32	148	423	30	633	**0.67**
		Dead	283	7	138	653	1081	**0.60**
	Total reference		750	749	750	750	2093	
	Producer's & *overall* accuracy		**0.57**	**0.79**	**0.56**	**0.87**		***0.70***
DDLG_P	Predicted	Bare ground	492	7	51	110	660	**0.75**
		Live	29	595	186	7	817	**0.73**
		Declining	71	146	410	42	669	**0.61**
		Dead	158	2	103	591	854	**0.69**
	Total reference		750	750	750	750	2088	
	Producer's & *overall* accuracy		**0.66**	**0.79**	**0.55**	**0.79**		***0.70***

			Reference				Total predicted	User's accuracy
			Bare ground	Live	Declining	Dead		
DDLG_U	Predicted	Bare ground	612	8	67	119	806	**0.76**
		Live	3	581	167	3	754	**0.77**
		Declining	30	155	421	28	634	**0.66**
		Dead	105	6	95	600	806	**0.74**
	Total reference		750	750	750	750	2214	
	Producer's & *overall* accuracy		**0.82**	**0.77**	**0.56**	**0.80**		***0.74***

Table A 4-4 Basic statistics summary (number and area) of deadwood-patches, identified by the three classification scenarios: Random Forest (RF) classification (DDLG), RF classification with post-processing (DDLG_P) and with additional deadwood-uncertainty filter (DDLG_U), compared to the visually delineated reference polygons used for validation

	Reference polygons	DDLG	DDLG_P	DDLG_U
N	315	323	238	285
AREA SUM (m²)	4295.7	6034.8	6024.5	6013.5
% of reference polygons	100%	145%	145%	144%
AREA MEAN (m²)	13.6	18.7	25.3	21.1
AREA MEDIAN (m²)	11.0	5.2	11.0	6.5
AREA MAX (m²)	65.9	813.8	811.0	813.8
AREA SD (m²)	12.1	56.6	64.6	59.8

5 CHAPTER IV: REMOTELY SENSED SINGLE TREE DATA ENABLE THE DETERMINATION OF HABITAT THRESHOLDS FOR THE THREE-TOED WOODPECKER (PICOIDES TRIDACTYLUS)

Chapter IV was published as a following research paper:

Zielewska-Büttner, K.; Heurich, M.; Müller, J.; Braunisch, V. (2018). Remotely Sensed Single Tree Data Enable the Determination of Habitat Thresholds for the Three-Toed Woodpecker (Picoides tridactylus). Remote Sens., 10, 1972. DOI: 10.3390/rs10121972.

Abstract: Forest biodiversity conservation requires precise, area-wide information on the abundance and distribution of key habitat structures at multiple spatial scales. We combined airborne laser scanning (ALS) data with color-infrared (CIR) aerial imagery for identifying individual tree characteristics and quantifying multi-scale habitat requirements using the example of the three-toed woodpecker (Picoides tridactylus) (TTW) in the Bavarian Forest National Park (Germany). This bird, a keystone species of boreal and mountainous forests, is highly reliant on bark beetles dwelling in dead or dying trees. While previous studies showed a positive relationship between the TTW presence and the amount of deadwood as a limiting resource, we hypothesized a unimodal response with a negative effect of very high deadwood amounts and tested for effects of substrate quality. Based on 104 woodpecker presence or absence locations, habitat selection was modelled at four spatial scales reflecting different woodpecker home range sizes. The abundance of standing dead trees was the most important predictor, with an increase in the probability of TTW occurrence up to a threshold of 44–50 dead trees per hectare, followed by a decrease in the probability of occurrence. A positive relationship with the deadwood crown size indicated the importance of fresh deadwood. Remote sensing data allowed both an area-wide prediction of species occurrence and the derivation of ecological threshold values for deadwood quality and quantity for more informed conservation management.

Keywords: deadwood; standing deadwood; dead tree; snags; three-toed woodpecker (*Picoides tridactylus*), habitat suitability model (HSM), habitat requirements; airborne laser scanning (ALS), CIR aerial imagery

5.1 Introduction

Effective biodiversity conservation in managed forest landscapes requires knowledge about the distribution of key habitat features at relevant scales (Müller et al., 2009; Stighäll et al., 2011). This knowledge is essential for assessing species' habitat selection, deriving threshold values for key features, and evaluating habitat quality across large spatial scales. Habitat suitability models (HSMs) (Guisan and Thuiller, 2005) and their spatially explicit variant, species distribution models (SDMs), have been widely employed in the last decades to predict species occurrence (Magg et al., 2015), abundance, or richness (Lesak et al., 2011; Vogeler et al., 2014; Zellweger et al., 2016) based on environmental variables (Hirzel and Le Lay, 2008). Given their need for area-wide environmental information across large spatial scales, SDMs have mostly been based on publicly available topographic, climatic, or land-cover variables, which are often too coarse-grained and imprecise for reliably assessing habitat characteristics and quality for forest-dwelling species.

Forests, especially those with natural stand characteristics, are habitats with a high vertical and horizontal structural complexity (Jayathunga et al., 2018) and are difficult to characterize with simultaneously high precision and the required generalization. Traditionally, forest structure is described based on plot-based forest inventories or high-resolution mapping in the field, which are costly (White *et al.*, 2016) and therefore often carried out at limited spatial extents (Zellweger, 2013). Moreover, they do not deliver continuous spatial information. The rapid development of remote sensing techniques and efficient methods for data processing make information originating from airborne and satellite surveys increasingly attractive for forest ecology and biodiversity research, conservation and management (Lausch *et al.*, 2016; Vogeler and Cohen, 2016). These techniques and methods allow detailed and area-wide structural analyses, alleviating the trade-off between precision and extent (Zellweger, 2013; Lindberg *et al.*, 2015).

Initially forest structural and compositional parameters used in conservation studies predominantly originated from passive remote sensing such as aerial and satellite imagery and were obtained using manual or semi-automatic mapping methods (Ahrens *et al.*, 2004; Bütler and Schlaepfer, 2004). Current trends increasingly turn towards active remote sensing with airborne laser scanning (ALS, also referred to as airborne Light Detection and Ranging or LiDAR) and the fusion of data from different sources enabling the combination of structural and spectral information (White *et al.*, 2016). With its ability to penetrate through the canopy, ALS provides information on vegetation heights at and below the forest surface, allowing a precise, high-resolution description of the vertical and horizontal vegetation structure (Müller *et al.*, 2010; Rechsteiner *et al.*, 2017). ALS-based

structural information has been shown to perform well in predicting the habitat selection of various forest species, especially bats and birds (Graf *et al.*, 2009; Martinuzzi *et al.*, 2009; Lesak *et al.*, 2011; Zellweger, 2013; Braunisch *et al.*, 2014; Froidevaux *et al.*, 2016; Rechsteiner *et al.*, 2017; Kortmann *et al.*, 2018b) using three-dimensional habitat structures. The fusion of ALS data with satellite or aerial imagery combines accurate measurements of vertical structure with the advantages of using spectral information (e.g., for identifying tree species (Persson et al., 2004; Dalponte et al., 2008; Heinzel et al., 2008; Säynäjoki et al., 2008; Heinzel and Koch, 2012; Amiri et al., 2016), distinguishing between living and dead trees (Dalponte et al., 2008; Polewski et al., 2015c, b) or analyzing forest structural complexity (Latifi et al., 2016; Jayathunga et al., 2018). Such information can be highly relevant for analyzing and predicting the habitat requirements of forest species linked to specific tree-characteristics and for determining their abundance across large spatial scales (Vogeler and Cohen, 2016).

The three-toed woodpecker (TTW) is a forest bird typical for boreal and mountainous natural spruce dominated forests with a high amount of standing deadwood. Although globally red-listed with a status of least concern and stable population size (BirdLife, 2016), this species is regionally rare and vulnerable (Głowaciński *et al.*, 2002) or even threatened with extinction (Hölzinger and Mahler, 2001; Südbeck *et al.*, 2007; Bauer *et al.*, 2016). The TTW is frequently selected as a focal species of forest biodiversity conservation programs, as its occurrence is associated with a high forest bird diversity (Mikusiński *et al.*, 2001). It functions as a key-stone species (sensu Thompson and Angelstam (1999)) (Bütler *et al.*, 2004b) as it provides breeding opportunities for a variety of cavity-breeding species (Saari and Mikusinski, 1996; Virkkala, 2006). Feeding mainly on larvae of bark and wood-boring insects (Fayt, 2003; Pechacek and Krištín, 2004), the TTW is highly dependent on dying and dead conifer (mostly spruce) trees (Braunisch *et al.*, 2014) and is therefore considered an umbrella species for the saproxylic species community (Angelstam *et al.*, 2003).

The habitat variables determining TTW home range selection in its boreo-alpine distribution range (Mikusiński *et al.*, 2018; Mollet *et al.*, 2018) correspond to the attributes of mature, spruce dominated, hemiboreal, boreal, or mountain forests. Spruce-dominated natural old-growth forests with a high variability in tree diameters (diameter at breast height, DBH) as well as a high abundance and diversity of deadwood provide suitable conditions for a continuous woodpecker presence, as they host stable populations of spruce bark and longhorn beetles, its staple food (Pechacek and Krištín, 1996; Fayt, 2003; Pechacek and d'Oleire-Oltmanns, 2004; Pechacek and Krištín, 2004). In other habitats, woodpecker breeding density varies greatly with the abundance of insect prey (Fayt, 2003).

Spruce trees infested by bark beetles as well as standing deadwood (Pechacek and Krištín, 1996) are key habitat components for both TTW subspecies: *Picoides tridactylus alpinus* inhabiting mountainous conifer and mixed forests and *Picoides tridactylus tridactylus* inhabiting hemi- and boreal lowland mixed and spruce forests. Deadwood diversity, i.e., the presence of various stages of decay, allows woodpeckers to adjust their diet to varying external conditions and energetic needs (Pechacek and Krištín, 1993, 1996, 2004). Kratzer *et al.* (2009) showed a significantly higher abundance of deadwood in the early stages of decay (comparable to stage three to four according to Thomas *et al.* (1979), Figure 5-1) at sites with woodpecker presence compared to absence sites. Also, Balasso (2016) underlined the preference of TTW for fresh snags, especially recently dead spruce with loose but attached bark, still inhabited by large numbers of bark beetles.

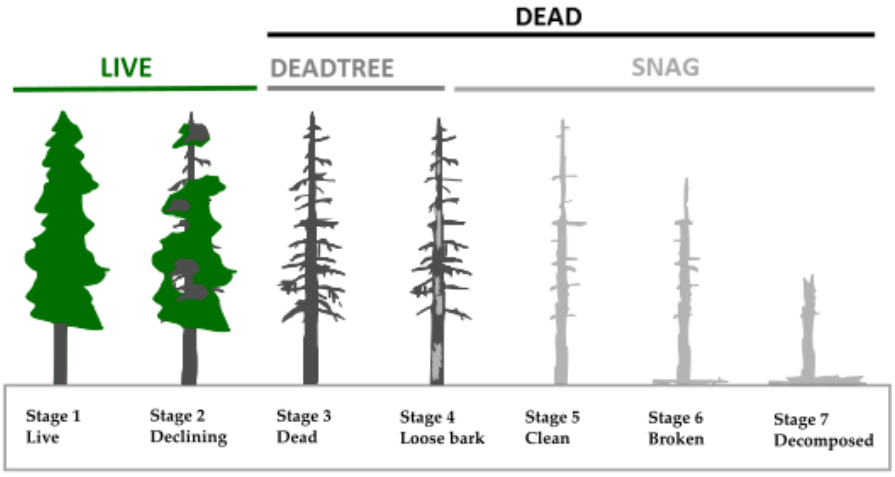

Figure 5-1 For the purpose of this study, trees were classified as: living trees (LIVE) and standing deadwood objects (DEAD), which were further divided into dead trees (DEADTREE) and snags (SNAG) representing the stages of conifer tree decomposition after Thomas *et al.* (1979). Note the shrinking of the horizontal extension of the tree crown during the progress in decay.

In addition, various authors showed the bird's preference for old-growth stands (Imbeau and Desrochers, 2002; Pakkala *et al.*, 2002; Fayt, 2003; Südbeck, 2005; Pugacewicz, 2011; Kajtoch *et al.*, 2013a; Amcoff and Eriksson, 1996), with TTW territories documented mostly in stands older than 60 years (Matysek and Kajtoch, 2010a; Kajtoch *et al.*, 2013a), 80 years (Romero-Calcerrada and Luque, 2006; Matysek and Kajtoch, 2010b), or 100 years (Bütler *et al.*, 2004a; Bütler *et al.*, 2004c), and with a high abundance of veteran trees (Pechacek and d'Oleire-Oltmanns, 2004; Kajtoch *et al.*, 2013a; Kajtoch and Figarski, 2014).

Outside of the boreal zone, TTW occurrence mostly coincides with a high protection status, as in Białowieża National Park (Walankiewicz *et al.*, 2011; Kajtoch *et al.*, 2013b; Czeszczewik *et al.*, 2015),

in the Polish Carpathians (Kajtoch, 2009; Matysek and Kajtoch, 2010b) or other protected areas (Andris and Kaiser, 1995; Kratzer *et al.*, 2009; Senitza and Gutzinger, 2010; Kajtoch *et al.*, 2013a; Kajtoch *et al.*, 2013b). In these areas, the bird's home range sizes are smallest ranging from 16 ha (Pechacek, 2006) to 40–60 ha (Dorka, 1996; Pechacek and Krištín, 1996; Pugacewicz, 2011; Kajtoch *et al.*, 2013b), while home range sizes in managed forests, with lower densities of the required habitat requisites, are larger (i.e., between 100 and 400 ha (Pechacek and d'Oleire-Oltmanns, 2004; Amcoff and Eriksson, 1996). Territory density is lower in managed forest landscapes with 0.2–0.7 territories per 100 ha compared to 1–5 territories per 100 ha in natural old growth and unmanaged forests (Pakkala *et al.*, 2002; Matysek and Kajtoch, 2010a, b; Kajtoch *et al.*, 2013b).

Due mainly to harvesting and sanitation cutting, deadwood, to which TTW occurrence is closely linked, is an especially limited resource in managed forest ecosystems (Müller and Bütler, 2010; Kajtoch *et al.*, 2013a; Braunisch *et al.*, 2014; Kajtoch and Figarski, 2014; Czeszczewik *et al.*, 2015). Deadwood thresholds of European forest-dwelling species range from 10 to 150 m3/ha with values of 20–50 m3/ha given for the majority of species as reviewed by Müller and Bütler (2010). This corresponds well with the 15–18 m3/ha to 30 m3/ha given for TTW occurrence (Bütler *et al.*, 2004b; Bütler *et al.*, 2004c; Kajtoch *et al.*, 2013a; Kajtoch and Figarski, 2014). Higher densities of deadwood are rare in Europe and occur only locally, mainly in protected areas (Hahn and Christensen, 2004; Müller and Bütler, 2010), so that an upper deadwood limit could not be determined yet. However, the existence of a deadwood-optimum is likely, as a share of living trees would be necessary to allow for a continuous provision of dying and freshly dead trees.

In this study, we test the usability of remotely sensed single tree data for analyzing habitat selection and predicting area-wide occurrence of the TTW, identifying the most important variables explaining home range selection at multiple spatial scales, and deriving threshold values for conservation management. We test the hypothesis that extremely high amounts of deadwood lead to a decrease in the probability of TTW occurrence and assess the influence of deadwood quality on habitat selection.

5.2 Materials and Methods

5.2.1 Study Area

The study was conducted in the Bavarian Forest National Park. Founded in 1970 as the first German National Park, it initially covered an area of 13,300 ha which was extended to 24,218 ha in 1998. The park is located in southeastern Bavaria (Germany) and borders the Šumava National Park (69,030 ha),

Czech Republic to the East. The park covers a large part of the Bavarian Forest mountain chain with an elevational gradient ranging from 600 to 1453 m a.s.l. Depending on elevation, the mean annual temperature (1972–2001) varies from 3.5 to 7.0 °C, and the total annual precipitation varies from 1300 to 1900 mm (Bässler *et al.*, 2008). The predominant vegetation is mountainous spruce and mixed forest with a share of Norway spruce (*Picea abies*) of 67.0%, European beech (*Fagus sylvatica*): 24.5%, Silver fir (*Abies alba*): 2.6%, and other tree species: 5.9% (Cailleret *et al.*, 2014).

Following its non-intervention policy, the National Park authority allowed for natural forest dynamics in the core zone (currently encompassing 68% of the park area), with massive bark beetle outbreaks after severe storm and windthrow events in 1983 and 1984. This resulted in a dieback of spruce forests at an unprecedented rate in Central Europe in recent decades (Lausch *et al.*, 2011).

5.2.2 Remote Sensing Data

Habitat variables were extracted from a full, remote sensing-based tree inventory (Heurich *et al.*, 2015). Full waveform ALS data was acquired on the 24th/26th/27th of July 2012 through the Milan Flug GmbH, using a Riegl LMS-Q 600i laser scanner of 350 KHz. A nominal point density of 30–40 points/m^2 was obtained from data recorded at a 0.32 m footprint. CIR aerial images were acquired in August 2012 using a DMC camera and a ground sampling distance of 20 cm. The images are composed of 3 spectral bands: near infrared, red, and green.

The preprocessing of the raw ALS data to the georeferenced three-dimensional (3D) point cloud, including the derivation of the intensity and the pulse width values using a sum of Gaussian functions, is described in Reitberger *et al.* (2008) and Yao *et al.* (2012b). Single tree detection and delineation was carried out with a 3D segmenting method solely based on ALS data and the geographical position and top height (H) were calculated for each segmented tree (Yao *et al.*, 2014). This resulted in a dataset containing 12,106,320 trees, consisting of two types of geographical data, point data for tree tops and polygons for crown delineation. In the next steps, for each tree, the tree type (conifer, broadleaf, or deadwood), projected crown area (C), crown base height and crown volume, were derived using both types of remote sensing data. Spectral information from CIR aerial imagery fused with segmented ALS point cloud data was used for tree species classification based on Reitberger *et al.* (2008) and for the detection of snags and standing deadwood in line with Polewski *et al.* (2015c) and Polewski *et al.* (2015a). The crown base height and the crown volume originated from a 3D Alpha-Shape-triangulation of the segmented ALS point cloud. Diameter at breast height (DBH), basal area (BA) and volume (VOL) were also calculated for live trees in an extra modelling step based on a calibration with an extensive ground reference database (Heurich, 2008).

In addition to the automatically derived, tree-based information, we tested independent data of yearly visual assessment of deadwood areas based on the CIR aerial imagery (Heurich, 2008), dated 2010–2015 (Table A 5-1).

5.2.3 Species Data and Sampling Design

Presence locations of the TTW originated from the database of the Bavarian Forest National Park, including data from the biological monitoring, various research projects, and chance observations by trained park staff (Figure 5-2). Locations of TTW, either observed directly or through sound identification, were recorded with a GPS. Data were collected in two time periods (2007–2008 and 2012–2014), however, to achieve a temporal synchronization with the remote sensing data from 2012, we only used the observations from the latter sampling period (N = 115).

To study habitat selection at different relevant scales, we generated circular sample plots around each presence location, with sizes reflecting the area requirements of the species reported under different conditions:

- R = 100 m to evaluate the habitat characteristics in close vicinity of the TTW presence locations.
- R = 250 m (19.6 ha) representing the minimum reported home range of an individual TTW under excellent habitat conditions (ca. 16–19 ha (Pechacek and d'Oleire-Oltmanns, 2004));
- R = 450 m (63.6 ha) depicting the average minimum home range size reported for areas with presumably good conditions such as protected areas (Goggans *et al.*, 1989; Fayt, 2003; Kajtoch *et al.*, 2013a; Kajtoch *et al.*, 2013b);
- R = 600 m (113 ha) corresponding to the average home range size reported by various authors (Pechacek and Krištín, 1996; Angelstam *et al.*, 2004; Pechacek, 2004; Kajtoch *et al.*, 2013b).

The presence locations showed spatial clumping in some regions, indicating multiple observations originating from the same individual. To avoid pseudoreplication, we thinned the initial set of presence locations allowing a maximum 18% overlap of the sampling plots at the largest scale (R = 600 m), after Pechacek (2004) who reported average territory overlaps of 17.6% (±3.9). Using R-package "Spatstat" package (Baddeley *et al.*, 2018) to discard all presence locations that fell below the resulting minimum distance of 840 m, resulted in a final set of 52 presence locations.

In addition, we randomly created a similar number of pseudo-absence locations (in the following referred to as "absence") with the same minimum distance to any presence location and to each other.

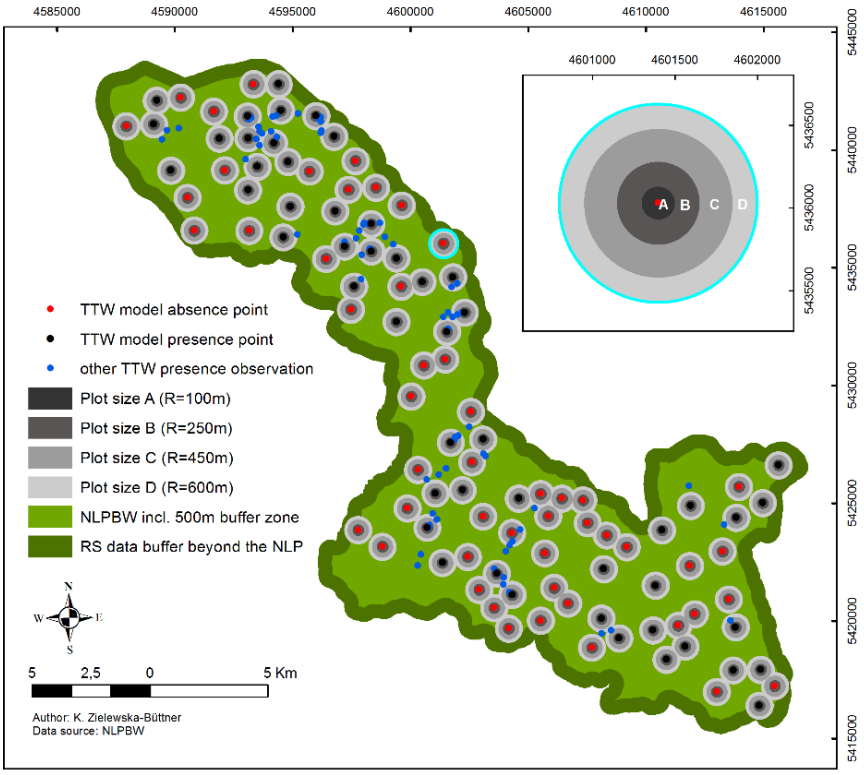

Figure 5-2 Study area (Bavarian Forest National Park) and the locations with TTW presence (black points) and absence (red points) used for the analysis. Presence locations closer than 840 m to the next location were discarded to avoid using multiple observations of the same bird (blue points). Grey buffers represent different home range sizes with radii of 100 (A), 250 (B), 450 (C), and 600 m (D) (inset).

5.2.4 Predictor Variables

Predictor variables were generated for each of the four sampling plot scales and encompassed three classes: general forest stand characteristics, specific tree features, as well as topographic information (Table 5-1).

Based on a literature review, predictor variables describing general forest stand characteristics were selected according to their hypothesized ecological relevance for the species. Forest cover per plot was defined as the share of the horizontal plot area covered by all trees' crowns. The proportion of forest cover attributed to trees higher than 15 m was assessed as a proxy for mature forest, and the proportion the sampling plot covered by crowns of standing deadwood, as an indicator for areal deadwood availability. We also included a similar variable derived from the standard visual mapping (CIR): the proportion of area with standing deadwood originating from the period 2010–2015. This data was compared with the available ALS and CIR based data. In addition, the number and proportion of living trees (i.e., conifers, deciduous trees, and all trees) were calculated for each plot size, as well as the average height (H), diameter (DBH), and volume (VOL) and the variance thereof.

Specific tree features such as dead, “resource” or “veteran” trees have been observed to be important for the TTW. We defined resource trees (RESOURCE) as all living trees with a DBH > 30 cm, based on Pechacek and d’Oleire-Oltmanns (2004), Kajtoch and Figarski (2014) and Kajtoch *et al.* (2013a). To approximate the different decay stages of deadwood in adherence to Thomas *et al.* (1979) (Figure 5-1), and to distinguish between potential foraging trees (stages 2–4) and other dead trees (stages 5–7) as proposed by Bütler *et al.* (2004c), we subdivided the deadwood (category DEAD including all standing deadwood objects) into snags (SNAG) and dead trees (DEADTREE). The category SNAG encompassed all deadwood with either a crown area of C < 4 m^2 (1st Quartile of the DEAD crown area values) or deadwood with C ≥ 4 m^2 but a height of H < 15 m. DEADTREE objects were characterized as C ≥ 4 m^2 and H ≥ 15 m. The threshold of 15 m was chosen because in our study area, living spruce trees of that height had an approximate DBH of 20 cm (Figure A 5-1), allowing a direct comparison with DBH-based classifications of deadwood used by other authors (Bütler *et al.*, 2004c). Finally, we calculated the mean crown area of the trees in the respective classes (DEAD, DEADTREE, and SNAG) per plot to obtain a continuous metric of the crown status as a proxy of the stage of decay.

All structural predictors, except the variable derived from visual interpretation (DEADCIR_part), were thus calculated based on the single tree data originating from the ALS and CIR remote sensing dataset, either used directly to describe specific tree features or aggregated to describe forest stand related characteristics.

In addition, topographic variables were generated using a digital terrain model (DTM) with a 25 × 25 m resolution and included altitude, slope, eastern (sine of aspect), and northern (cosine of aspect) exposition as well as solar radiation, calculated using the Solar Analyst module in ArcGIS (ESRI, 2018). We also included latitude and longitude to test for random spatial clustering of the woodpecker observations.

The preparation and calculation of variables with a horizontal dimension (i.e., referring to the proportion of the plot area) was carried out in ArcMap 10.4.1. (ESRI, 2016). The processing and calculation of the remaining variables was carried out in RStudio (RStudio, 2016) using R (R Core Team, 2017) with the packages: “Raster” (Hijmans *et al.*, 2017) and “Rgdal” (Bivand *et al.*, 2017).

Table 5-1 Tested predictor variables each calculated for circular sampling plots of r = 100, 200, 450, and 600 m respectively, with their potential ecological relevance for the model species. (BB = bark beetle, DBH = diameter at breast height, RS = remote sensing).

Category	Variable	Description	Ecological Meaning	Unit
Forest stand characteristics	FCOVER_part	Proportion of forest cover per plot based on crown area	Stand structure and shelter function	0–1
	STANDH15_partF	Proportion of crown cover of trees with H > 15 m to forest cover	Stand structure: mature trees	0–1
	DEADCIR_part	Proportion of deadwood area per plot (2010–2016 aerial imagery)	Feeding potential for BB/Option for cavities	0–1
	DEADRSI_part	Proportion of deadwood area per plot (2012 RS tree inventory)	Feeding potential for BB/Option for cavities	0–1
	LIVE_Nha	Amount of living trees per ha	Forest stand density and tree shelter function	N/ha
	LIVE_VOLha	Total volume of live trees per ha	Forest stand structure	m^3/ha
	LIVE_BAha	Mean basal area of live trees per plot	Proxy for stand mass and forest age	m^2/ha
	LIVE_BAvar	Variance of live tree basal area per plot	Proxy for stand age heterogeneity	m^2/ha
	LIVE_Hmean	Mean height of live trees per plot	Proxy for stand vertical structure and age	m
	LIVE_Hvar	Variance of live tree height per plot	Proxy for vertical structure/age heterogeneity	m
	CONIF_Npart	Proportion of conifer trees (N) in all live trees	Forest type and potential food resources	0-1
	CONIF_VOLpart	Proportion of conifers (Volume) in all live trees	Forest type and resources food resources	0-1
	DECID_VOLha	Volume of deciduous trees per ha	Forest type and shelter function	m^3/ha
Specific tree features	RESOURCE_Nha	Amount of trees with DBH > 30 cm per ha	Feeding potential for BB/Option for cavities	N/ha
	DEAD_Nha	Amount of all standing deadwood per ha	Feeding potential for BB/Option for cavities	N/ha
	DEAD_Hmean	Mean height of all standing deadwood per plot	Feeding potential for BB/Option for cavities	m
	DEAD_Cmean	Mean crown area of all standing deadwood per plot	Feeding potential for BB/Option for cavities	m^2
	SNAG_Nha	Amount of snags per ha	Old deadwood (rather unsuitable)	N/ha
	SNAG_Hmean	Snags mean height per plot	Old deadwood (rather unsuitable)	m
	SNAG_Cmean	Snags mean crown area per plot	Old deadwood (rather unsuitable)	m^2
	DEADTREE_Nha	Amount of all standing dead trees per ha	Deadwood with BB potential	N/ha
	DEADTREE_Hmean	Mean H of all standing dead trees per plot	Deadwood with BB potential	m
	DEADTREE_Cmean	Mean crown area of all standing dead trees per plot	Deadwood with BB potential	m^2
Topography	ALTITUDE_mean	Mean altitude a.s.l. of a sampling plot	Proxy for climate	m
	SLOPE_mean	Mean slope of a sampling plot	Proxy for terrain	Degree
	EAST	Easting (sine of aspect) of a sampling plot	Sun exposure	(−1)–1
	NORTH	Northing (cosine of aspect) of a sampling plot	Sun exposure	(−1)–1
	SOLAR_mean	Yearly mean of solar radiation per plot	Proxy for climate	h

5.2.5 Statistical Analysis

We modelled species occurrence as a function of the environmental variables using General Additive Models (GAM) facilitated in the R-package "mgcv" (Wood and Augustin, 2002; Wood, 2004; Wood, 2018). GAMs combine General Linear Models with smoothing splines (Dormann and Kühn, 2012), thereby allowing to fit the response curves "as closely as possible" to the data, within a permitted level of smoothing.

For each plot size we selected the best explaining variables following a hierarchical procedure. First, we ran univariate models for each variable, also testing their quadratic term. Predictor variables which significantly explained woodpecker occurrence ($p \leq 0.05$) or showed a trend ($p \leq 0.1$) and were significant in other studies (such as information on amount and volume of conifers and amount of live trees per plot) were retained. To avoid collinearity among variables in the multivariate models, we removed from any pair of correlated variables (Spearman's $r \geq |0.7|$)(Dormann *et al.*, 2004) the "weaker" predictor based on Akaike's Information Criterion (AIC) (Burnham and Anderson, 2002).

In a first step, a common initial set of input variables (i.e., all variables retained at any of the four scales) was used for model calibration on all plot sizes. In addition to the environmental variables smoothed with a smooth term s(), a tensor smooth for the spatial location te(x, y) was added to account for effects of random spatial clustering of the TTW data (Figure A 5-2).

To avoid overfitting, as it was observed when running the model with automatic settings, we set the upper limit of the degrees of freedom associated with a smooth term to k = 3, as Guisan *et al.* (2017) recommends after Hastie *et al.* (2009) to use lower degrees of freedom ($df < 4$) for deductive species distribution and habitat modelling, while avoiding degrees of smoothing higher than 4 or 5 for predictive purposes. We used automatic variable selection (function "select=TRUE" in mgcv) which indicates variables that do not contribute to the model and can therefore be dismissed with $p = 1$. After the removal of these variables, the models were recalibrated and variables were again removed until no $p = 1$ occurred. In a second step, we used chi-square test statistics for assessing the significance of the smooth terms and removed variables with $p < 1$ but with chi-square equal 0 as not contributing to the model. At each step we compared the AIC of the resulting model with the previous step until no further reduction was achieved This way, we obtained one "best model" for each of the 4 plot sizes.

The models' fit was evaluated using 5-fold cross validation with 20% of the observations held back randomly with a condition of an equal proportion of presence and absence observations in folds. Multiple evaluation metrics, i.e., sensitivity, specificity, correctly classified rate, and Cohen's Kappa (all using the threshold 0.5), as well as the area under the receiver operating characteristics (ROC) curve (AUC) were calculated using the "caret" package in "R" (Kuhn *et al.*, 2018) and evaluated according to Hosmer and Lemeshow (2000). The best model was then used to predict TTW occurrence probability across the entire National Park.

To analyze the model results, we plotted the single predictor variables against their smooths (function “gam.check” in the “mgcv” package) and against the target variable using the packages “mgcv” and “ggplot2” (Wickham and Chang, 2016).

Finally, we calculated conditional inference trees (CTREEs), as implemented in the R-package “party” (Hothorn *et al.*, 2017), to obtain thresholds for the most important variables for practical management recommendations. Trees based on maximally selected rank statistics were fitted using the Bonferroni correction for multiple testing and a minimum sum of weights in a node to be considered for splitting of 20 (minsplit = 20). All variables selected for the respective “best” GAM at each scale were included in the multivariate trees. In addition, univariate trees were fitted for variables with a significant split in the multivariate tree.

5.3 Results

5.3.1 Habitat Selection

Univariate models revealed eight environmental variables that significantly contributed to explaining woodpecker presence at least one of the four scales and were retained for calibrating multivariate models (Table 5-2). With the exception of altitude all of the significant variables described stand and tree-related habitat characteristics. Three additional variables (DEAD_Nha, DEADTREE_Cmean, and DEADRSI_part) were significant but discarded as correlated with retained variables.

Table 5-2 Retained predictor variables for modelling the occurrence of the three-toed woodpecker and their univariate (simple and quadratic) *p*-value (<0.1) on the four plot sizes. Variables with $p < 0.05$ are bold. Mean values and the standard deviation (SD) of these variables at presence, absence and both study plots are listed in Table A 5-1.

	R = 100 m		**R = 250 m**		**R = 450 m**		**R = 600 m**	
Variables $p < 0.05/0.1$	**Linear**	**Quadratic**	**Linear**	**Quadratic**	**Linear**	**Quadratic**	**Linear**	**Quadratic**
Altitude_mean	**0.040**		**0.042**		**0.043**		**0.045**	
CONIF_Nha			0.063		**0.025**		**0.031**	
DEAD_Cmean	**0.003**		**0.006**		**0.028**		0.096	
DEADTREE_Nha	**0.025**	**0.000**	**0.034**	**0.005**	**0.035**	0.066	0.091	0.089
SNAG_Cmean		0.052		**0.043**		0.063		
LIVE_Nha	0.081		0.076		0.07			
CONIF_VOLpart		0.051		0.096				
DEADCIR_part		**0.007**		0.064				

The final models consisted of 4 to 6 variables, depending on the plot scale (Table 5-3). The amount of dead trees was the only variable with a significant contribution at all scales. Altitude and the mean crown diameter of all standing deadwood were also included in all models, but the former was only significant at the two smaller scales, while the latter was only significant at the two intermediate scales. The proportional volume of conifer trees was included at 3 scales and the mean crown diameter of snags only on sampling plots with a 250 m radius, but neither of them had a significant

contribution. The spatial location was also included in all models, suggesting a spatially clustered distribution of the woodpecker observations. The two preselected variables representing the living stand (the amount of living trees per ha and the amount of conifers per ha), although univariately significant at 3 scales, did not contribute to any of the multivariate GAMs.

Table 5-3 General Additive Models (GAMs) explaining the occurrence of the three-toed woodpecker (TTW) as a function of remote sensing-based forest inventory variables and altitude at four sampling scales, i.e., within different radii (R) around TTW sampling locations. Parametric coefficients and approximate significance of the smooth terms (effective degrees of freedom (edf), *p*-value) are given for the variables selected in the best model for each scale. Variable codes and descriptions are listed in Table A 5-1. Bold figures indicate significant variables ($p < 0.05$).

	R = 100 m		**R = 250 m**		**R = 450 m**		**R = 600 m**	
	edf	***p*-Value**	**edf**	***p*-Value**	**edf**	***p*-Value**	**edf**	***p*-Value**
Intercept estimate	0.134		0.035		0.013		0.006	
Standard error	0.249		0.227		0.208		0.205	
Z-Value	0.537		0.156		0.064		0.032	
Pr(>|z|)	0.591		0.876		0.949		0.975	
s(Altitude_mean)	**0.817**	**0.049**	**0.929**	**0.020**	0.681	0.076	0.605	0.105
s(DEAD_Cmean)	0.167	0.239	**0.947**	**0.018**	**0.784**	**0.038**	0.627	0.103
s(DEADTREE_Nha)	**1.000**	**0.000**	**0.906**	**0.007**	**0.953**	**0.021**	**0.855**	**0.027**
s(SNAG_Cmean)			0.790	0.099				
s(CONIF_VOLpart)	0.620	0.114	1.571	0.107			0.176	0.252
te(x,y)	**1.795**	**0.045**	1.742	0.154	**1.509**	**0.033**	**1.640**	**0.037**

The most meaningful variable at all scales was the amount of dead trees (DEADRTREE_Nha). The response plots (Figure 5-3 and Table A 5-2) indicate a unimodal response with adverse effects on woodpecker presence when the amount of dead trees increased beyond a threshold of 40–55 trees per hectare. However, these results need to be interpreted with caution due to only a few plots with extremely high numbers of dead tree driving this trend (i.e., two sample plots with DEADTREE_Nha > 90 on R = 100 m and R = 250 m and three sample plots with DEADTREE_Nha > 70 on R: 250, 450, and 600 m).

Another deadwood variable, the mean crown area of all standing deadwood (Dead_Cmean), showed a significant positive effect on TTW occurrence at the two intermediate scales (R = 250 and R = 450 m), suggesting a preference for deadwood with large crowns, i.e., in the early stages of decay (Figure 5-1). This is in line with the species' opposite response trend to the mean crown area of snags (SNAG_Cmean) at the intermediate scale (R = 250 m). Finally, the share of conifers in the total volume of living trees (CONIF_VOLpart) showed a slightly unimodal, but non-significant relationship with TTW presence, with the highest occurrence probabilities in stands with about 50–80% conifers, depending on the sampling scale. Altitude was included in all models and significant at the two smallest scales, with higher probabilities of TTW presence at higher altitudes.

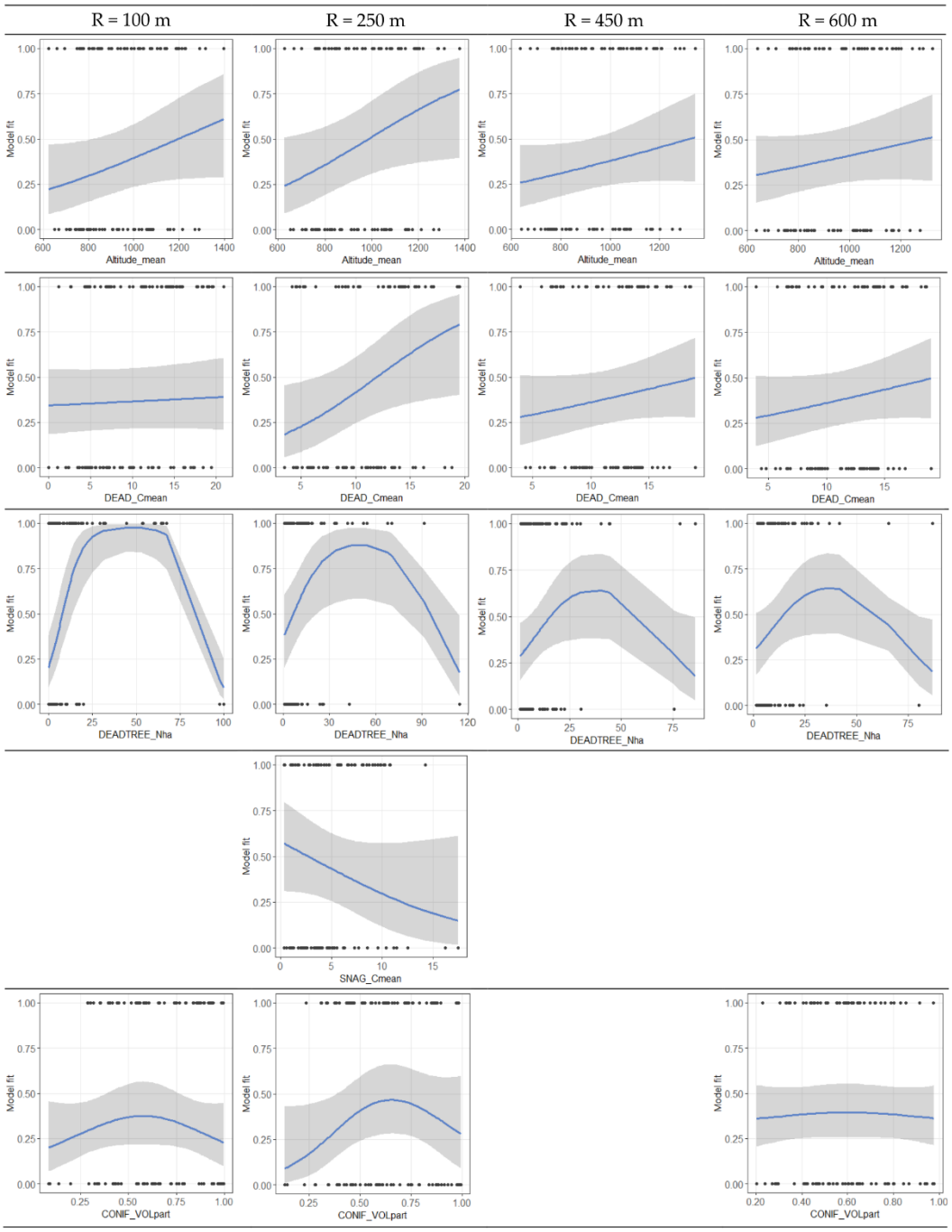

Figure 5-3 Effect plots showing predicted TTW occurrence as a function of the environmental predictors included in the best models at different plot scales (Table 5-3). The blue line indicates the estimated smoothing parameter of a given variable, while keeping all other variables set on the median. Shadowed areas indicate the 95% confidence intervals conditional on the estimated smoothing parameter. Variable codes and descriptions are listed in Table 5-1.

5.3.2 Model Performance

Model performance decreased with increasing sampling scale. This trend applied to both model fit and predictive performance over the 5-fold cross validation replicates and was consistent across all evaluation metrics (Table 5-4). Based on the AUC, our final models showed a good to excellent fit at the two small scales (R = 100 m and R = 250 m, AUC > 0.8) and an acceptable fit at the two larger scales (R = 450 and 600, 0.7 < AUC < 0.8) (Hosmer and Lemeshow, 2000). Five-fold cross validation

confirmed an acceptable predictive performance of the models at the two smallest scales (AUC > 0.7), but less so at the two larger scales (0.6 < AUC < 0.7). Similar trends were found for the other evaluation metrics R-Square (Adjusted), Correct Classification Rate (CCR), and Cohen's Kappa (Table 5-4). Sensitivity was generally higher than specificity at all scales indicating better detection and prediction of TTW presence than of absence locations. Complete results of the cross validation are presented in Appendix A, Table A 5-2.

Table 5-4 Fit of the final models (Fit) and the averaged results of the 5-fold cross-validation (CV, in italics) at four spatial scales: Akaike's Information Criterion (AIC), R-Square adjusted (R-sq. adj.), and Area Under the ROC-Curve (AUC), Sensitivity, Specificity, Correct Classification Rate (CCR), and Cohen's Kappa. Variable codes and descriptions are listed in Table 5-1.

	R = 100 m			**R = 250 m**			**R = 450 m**			**R = 600 m**		
	Model Fit	***CV***		**Model Fit**	***CV***		**Model Fit**	***CV***		**Model Fit**	***CV***	
		Mean	***SD***		***Mean***	***SD***		***Mean***	***SD***		***Mean***	***SD***
R-sq.(adj.)	0.33	*0.34*	*0.04*	0.25	*0.25*	*0.06*	0.14	*0.15*	*0.04*	0.11	*0.12*	*0.03*
AUC	0.85	*0.77*	*0.10*	0.82	*0.71*	*0.08*	0.74	*0.63*	*0.09*	0.72	*0.61*	*0.10*
Sensitivity	0.85	*0.75*	*0.14*	0.83	*0.66*	*0.06*	0.75	*0.58*	*0.13*	0.71	*0.54*	*0.07*
Specificity	0.73	*0.67*	*0.24*	0.69	*0.65*	*0.13*	0.64	*0.52*	*0.17*	0.60	*0.58*	*0.12*
CCR	0.79	*0.71*	*0.12*	0.76	*0.65*	*0.08*	0.69	*0.55*	*0.12*	0.65	*0.56*	*0.06*
Cohen's Kappa	0.58	*0.41*	*0.24*	0.52	*0.31*	*0.15*	0.39	*0.10*	*0.24*	0.31	*0.12*	*0.12*

5.3.3 Model Prediction

The model calibrated at the smallest scale (R = 100 m) was employed to predict TTW occurrence throughout the National Park. The results are shown for a raster of 100 × 100 m (Figure 5-4), with the occurrence probability of each raster cell calculated based on the conditions within R = 100 m around the grid cell center. When using a presence probability of 0.5 as a threshold for occurrence, 36% of the park area was classified as potentially suitable TTW habitat.

5.3.4 Variable Thresholds

The results of the conditional inference trees (Figure 5-5) revealed significant thresholds for two variables, the mean crown area and the amount of standing deadwood per plot. Multivariate trees were only found at the two smallest scales, with a first split indicating the highest TTW presence probability (>0.7) when deadwood with large crowns (>11–13 m^2) was available, intermediate probabilities (>0.5) when the abundance of dead trees per hectare was at least 4–5 (R = 100) or 3 (R = 250) respectively, and a low probability when none of the two variables exceeded these thresholds. These results indicate substrate selection with a first priority for fresh and then for other deadwood. No split was observed for variables measured on plots of 450 m radius or larger. Univariate models of the two variables with significant splits showed a TTW-presence probability of 0.7–0.8 when more than 8 dead trees per hectare were present in the surrounding of 100 and 250 m, respectively, or when the mean crown size DEAD_Cmean was larger than 11 m^2 (R = 100 m) to 13 m^2 (R = 250).

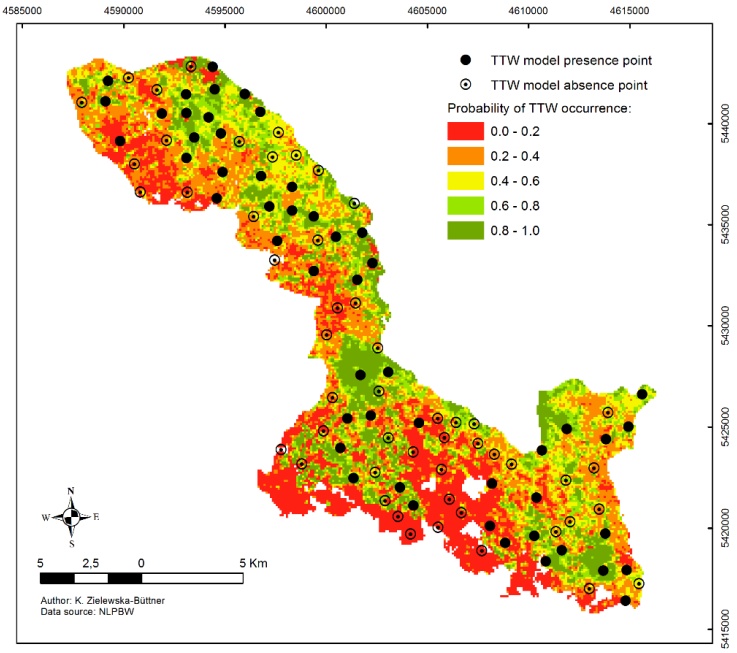

Figure 5-4 Predicted probability of three-toed woodpecker (TTW) occurrence for the Bavarian Forest National Park using the best GAM model according to Table 5-3 (calibrated for R = 100 m). The occurrence probability is shown for a 100 × 100 m raster, with the value of each cell calculated based on the environmental conditions within R = 100 m around the grid cell center. Black and transparent circles indicate the TTW presence and absence locations used for model calibration.

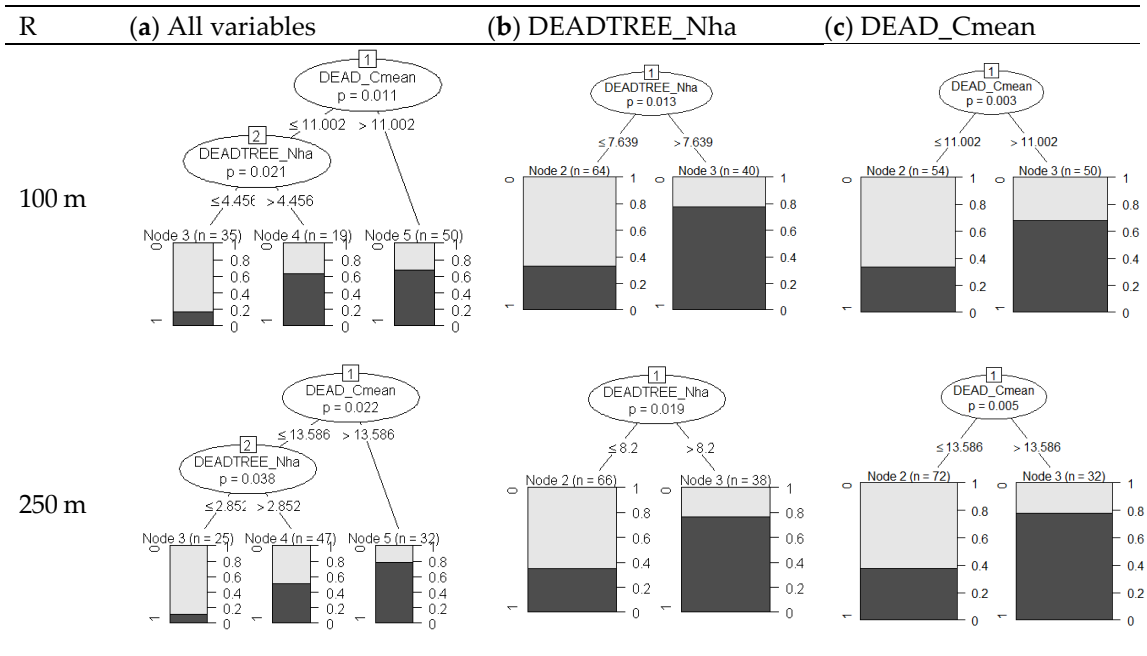

Figure 5-5 Multivariate (a) conditional inference trees (CTREEs) constructed from the variables selected into the best Generalized Additive Models (GAMs) at four sampling scales (R = 100 m, 250 m, 450 m, 600 m, see Table 5-3), and univariate trees (b) constructed from the variables with a significant split in (a). Each node of the trees represents one split of the data into significantly different partitions, with variables ranked according to their importance, until no further split is possible. The significance of the split (*p*-values after Bonferroni correction) is indicated in the splitting nodes. The *Y*-axis shows the predicted probability of TTW occurrence (1—presence; 0—absence) under the given combination of variable values. The variable values splitting the datasets are indicated on the tree branches. DEAD_Cmean: mean crown area of all standing deadwood, DEADTREE_Nha: number of dead trees per hectare. No significant splits were obtained for variables included at the two larger scales (R = 450 m, 600 m).

5.4 Discussion

Our analysis shows the usability of area-wide, remote-sensing-based, single tree data for modelling the habitat selection of an endangered and highly specialized forest species such as the three-toed woodpecker. Combining remote sensing information from different sources with a comprehensive set of species observation data enabled finding species-relevant predictor variables and thresholds for practical forest management and species conservation.

5.4.1 Remote Sensing Data

The fusion of multiple sources of remote sensing data, especially ALS and aerial imagery technologies, has high potential for complementing traditional, field-based forest inventories (White *et al.*, 2016). Although original ALS point clouds deliver more detailed information on tree height and forest structure (Farrell *et al.*, 2013) and are widely used as input data for habitat modelling (Davies and Asner, 2014), the combination of ALS data with aerial imagery for deriving single tree-related information proved crucial for our purpose: While ALS data enabled accurate mapping of single trees and their projected crown areas with subsequent modelling of tree volume, multispectral data allowed deadwood detection and — in combination with the structural information — the detection of specific deadwood characteristics, such as fresh deadwood and snags. This approach offered two additional advantages: First, by summarizing structural information at the tree-level, our variables refer to a species-relevant ecological scale of habitat selection. Second, other than abstract point-cloud metrics, our data describe environmental features that can be directly translated into target values for conservation management.

Our deadwood variables at the tree scale outperformed the deadwood information (area-percentage of deadwood per plot, DEADCIR_part, Table 5-3) obtained from the yearly visual assessment of aerial imagery. Although univariately significant at the smallest plot size, it did not enter the final model. Only new deadwood areas were mapped each year (Rall and Martin, 2002; Heurich *et al.*, 2010), thereby neglecting forest dynamics such as ingrowth and regeneration in the dieback areas of previous years. Complete mapping of standing deadwood for a given year may therefore have improved the performance of this variable.

The corresponding variable based on remote sensing tree inventory data, the area percentage of deadwood per plot (DEADRSI_part), showed better explanatory power (lower AIC than DEADCIR) on 100 and 250 m plot sizes, but was correlated with the number of dead trees (DEADTREE_Nha), our most important predictor. It was therefore discarded. Nevertheless, the relationship of the two variables with TTW occurrence shows some potential for the planar mapping of standing deadwood areas when single tree crown delineation is not possible.

We show the usability of remotely sensed single tree data and derived variables using the example of the TTW, a keystone species of boreal and mountainous spruce dominated forests. However, these data could also be of high relevance for modelling the habitat of other species or species assemblages of that forest types (Mikusiński *et al.*, 2001; Braunisch *et al.*, 2014). Information on deadwood features and their quality (dead trees, snags and stumps) could be vital for species

depending on deadwood in different decay stages either for food, shelter, or roosting such as saproxylic beetles (Økland *et al.*, 1996), birds (Mollet *et al.*, 2018), or bats (Bouvet *et al.*, 2016; Tillon *et al.*, 2016) and crown delineation, allowing the determination of canopy cover and forest gaps, could be used in studies deriving habitat thresholds for species responding to these structures e.g., capercaille (Braunisch and Suchant, 2008) or hazel grouse (Zellweger *et al.*, 2013).

5.4.2 Species Data

TTW presence data originated from three survey projects, including non-systematically collected chance observations of park staff. Despite thinning the original data according to the expected home range for one pair of birds, the models still indicated a clustering of the observations and a spatial correlation of the model performance with the locations of the observations. This may reflect a bias in sampling intensity, e.g., related to the road and walking paths network in the National Park, or be caused by a species-relevant environmental variable not included in the model. Our final models showed notably higher sensitivity than specificity, indicating a better classification of presence than absence data. This may be because of the random generation of pseudo-absence data outside the TTW presence areas, where false absences could not be ruled out.

We used species observations from three consecutive years starting in year one of the remote sensing data acquisition. At this time, the area of the National Park offered a large range of conditions, including optimal TTW habitat of mountainous, spruce dominated forests with a large amount of standing deadwood in different stages of decay. As both species and environmental data originated within a limited period of time and a unique environment, our models reflect only a snapshot of the species–habitat relationship (Guisan and Thuiller, 2005). The time lag of two years between the acquisition of remote sensing and species data we consider negligible, as also demonstrated by Vierling *et al.* (2014), since no significant changes due to disturbance events were recorded in the respective period and the National Park is not subjected to regular harvesting. Moreover, our models showed a high predictive performance, with results largely conforming to those of other studies. This makes us confident that they captured TTW habitat requirements with a high level of generality.

5.4.3 Modelling Approach

GAMs are increasingly used in ecological modelling, especially when species–habitat relationships are complex and not easily fitted with the standard parametric functions of the predictors (Guisan *et al.*, 2017). Using GAMs for the exploratory analysis of predictor variables is advantageous as GAMs fit the data in the most exact way possible (Dormann and Kühn, 2012). However, being data-driven, they are prone to overfitting. We applied stronger smoothing to address this issue. The most important feature of GAMs for our study was the possibility of including a multidimensional smoother (Guisan *et al.*, 2017) for the spatial location (x,y) of TTW observations to account for spatial clumping of the data.

Although useful for identifying key variables and describing the species response, GAMs do not provide threshold values which are frequently required in ecology and forestry to define

conservation targets (Toms and Villard, 2015). We used conditional inference trees for this purpose as Müller and Bütler (2010) found them particularly useful among a variety of methods (Andersen *et al.*, 2009). The simplicity of the underlying model and the visualization of the results facilitate the development of applicable guidelines.

5.4.4 TTW Habitat Selection

From the initial broad set of environmental predictors (Table 5-1), only four structural variables indicating food resources, cavities, and altitude affected the occurrence of the TTW in our study area. Dead tree abundance was the most important variable. The species had a preference for deadwood in the early stages of decay when the abundance of insect food is highest (Hogstad, 1976, 1977). Dying and dead spruce trees provide the major food sources of the TTW due to bark beetles (esp. *Ips typographus*) and wood-boring longhorn beetles inhabiting them. Müller and Bütler (2010) showed the probability of TTW presence increasing from 0.1 to 0.9 when more than 0.81 (0.56–1.22, Switzerland) and 0.44 (0.25–0.62, Sweden) m^3/ha basal area of standing deadwood corresponding to approx. seven and four dead trees with DBH ≥ 21 were present. Our results of 8 or more dead trees per hectare resulting in an 80% probability of TTW presence are in accordance with these findings.

In contrast with previous findings focusing on the minimum deadwood threshold, we show that very high amounts of deadwood, especially of late decay stages with little foraging value, negatively affect TTW occurrence probability. The detection of this tendency was made possible by very few observations at the extreme end of the gradient (i.e., sites with up to 120 trees per hectare), stemming from the large-scale area-wide bark beetle infestations. The lack of suitable research areas in Europe exhibiting the full possible gradient of deadwood abundance may be the reason that this effect has remained undetected, although Scherzinger (2006) observed a recession in TTW occurrence, a few years after a significant increase following the bark beetle outbreak. This implies that a patchy distribution of bark-beetle infested trees and tree groups in the forest landscape is favorable compared to large-scale area-wide dieback, which is more likely in homogeneous, even-aged stands. Such heterogeneous deadwood distributions may be furthered by natural topographic complexity and increasing forest structural variability through active management or strict protection (Senf and R., 2017), as structural heterogeneity is expected to increase in unmanaged forests (Donato *et al.*, 2012).

We also found a positive effect of the mean crown area of the dead trees per plot, indicating the availability of fresh deadwood with still complete tree crowns. This variable was selected into all models, although only significant at the two intermediate scales. Conditional inference trees indicated high probabilities (0.7–0.8) of woodpecker occurrence when the mean crown area per plot was larger than 11 m^2 (R = 100 m) or 13–13.5 m^2 (R = 250–450 m), respectively, corresponding to an average branch length of about 2 m. These findings are in line with Balasso (2016), who found that the presence of TTW was related to abundance of fresh snags, and Scherzinger (2006), who reported an initial increase in TTW occurrence shortly after bark beetle infestations with a subsequent decrease after some years. Nevertheless, the relationship between remotely sensed crown parameters and bark conditions needs further research.

In most field-based studies, deadwood is classified into standing dead trees, snags, and logs, representing different decay stages to account for TTW's prey diversity. In our study, the input data was limited to information that can be derived from the air. The first limitation was the omission of logs, the recognition of which, although theoretically possible by using ALS data from scanning in leaf-off conditions (Polewski *et al.*, 2014), was impossible with our data. Studies relying on field data often included this variable in HSMs (Bütler *et al.*, 2004b; Kajtoch *et al.*, 2013a), however it was rarely significant (Kratzer *et al.*, 2009). In addition, our remote sensing data could not provide information about the DBH, basal area (BA) and volume (Vol) of deadwood objects as often used in other studies (Roberge *et al.*, 2008; Kratzer *et al.*, 2009; Müller and Bütler, 2010; Kajtoch *et al.*, 2013a; Balasso, 2016). This was due to the difficulty of modelling these values without reliable height measurements of the tree tops that are often broken in standing deadwood.

Similar to the findings of Braunisch *et al.* (2014), our study suggested a positive, but non-significant correlation of TTW occurrence with the presence of conifers. In the Bavarian Forest National Park, conifer trees are predominantly Norway spruce, the primary host tree of *Ips typographus* which is the staple food of the TTW (Hohlfeld, 1997). Scherzinger (2006) concluded that not the pure amount of deadwood, but a permanent occurrence of dying and freshly dead trees originating from a continuous share of live spruce stands are crucial for the presence of TTW in the area. Mapping still alive, but degenerating spruce trees (the so called green attack stage) that were not detectable from our data and that remain a challenge for the remote sensing research (Lausch *et al.*, 2013; Ortiz *et al.*, 2013; Immitzer and Atzberger, 2014) could potentially be of high explanatory value for TTW habitat selection. Further research using hyperspectral data could bring important progress here (Waser *et al.*, 2014b; Abdullah *et al.*, 2018a; Abdullah *et al.*, 2018b). Resource trees that were an important variable in other studies (Pechacek and d'Oleire-Oltmanns, 2004; Kajtoch *et al.*, 2013a; Kajtoch and Figarski, 2014) did not correlate with TTW occurrence in our study, due to a similar, very high resource supply in both presence and absence plots over the entire study area.

Decreasing model performance from the smallest to the largest sampling scale indicates habitat conditions, especially the amount and quality of deadwood, in the surrounding approximately 20 ha are most decisive for the TTW's habitat choice (Rechsteiner *et al.*, 2017). As species' area requirements depend on habitat quality, TTW home range sizes have been shown to vary considerably among regions and foraging conditions (Pechacek, 2004; Südbeck, 2005; Romero-Calcerrada and Luque, 2006; Mikusiński *et al.*, 2018). Bütler *et al.* (2004c) reports TTW ranges vary between 44 and 176 ha, depending on food availability and snag abundance. Kajtoch *et al.* (2013b) suggests at least 100 ha with optimal conditions and 200 ha in suboptimal stands are necessary, conforming to the results of other studies (Goggans *et al.*, 1989; Fayt, 2003; Angelstam *et al.*, 2004; Pechacek, 2004; Amcoff and Eriksson, 1996). Our study area, with its consistently high abundance of patchily distributed deadwood in different stages of decay therefore seems to represent an optimal habitat for the TTW.

5.4.5 Management Recommendations

Effective forest and biodiversity management requires habitat thresholds at a scale and resolution that are ecologically relevant to the species and can be practically implemented (Farrell *et al.*, 2013). Bütler *et al.* (2004c) recommended a precautious 1.6 m^2 (basal area), corresponding to 5% of all standing trees or 14 standing dead trees with a DBH ≥ 21 cm per ha. We show the best response of TTW to habitat features within 100 to 250 m, i.e., related to a surrounding of up to 20 hectares. Within this area, at least eight dead trees per hectare should be retained, focusing on fresh deadwood in the early stages of decay, indicated by an average branch length of at least 2 m. Pechacek and Krištín (2004) give similar management recommendations claiming that "dead trees should not be removed within a 250 m circle from nests".

To favour the coexistence of alternative prey for TTW and ensure a constant input of fresh deadwood, retaining and restoring dead coniferous trees in different stages of decay and a substantial portion of live spruce trees is required. At the landscape scale, Bütler *et al.* (2004b) showed an effect of the spatial arrangement and density of deadwood rich patches, and recommended a network of forest stands with high deadwood densities embedded in a forest landscape with lower deadwood densities. As bark beetle spread was revealed to be strongly distance dependent with the most new infestations occurring within a 250 m radius of the previous year's infestation and 95% thereof in 500 m (Kautz *et al.*, 2011), safeguarding a wide enough inter-patch distance is crucial for preventing of bark beetle outbreak. Patches of declining and dead trees large enough to host bark beetle populations but disconnected from each other, would therefore aid forest managers in effectively controlling bark beetle dispersion (Seidl *et al.*, 2016), while at the same time promoting woodpecker habitat.

Our map showing current TTW habitat suitability allows distinguishing deadwood rich versus deadwood poor areas, so as to accurately target conservations measures.

5.5 Conclusions

Our study highlights the value of remote sensing, especially the fusion of ALS data with digital aerial imagery, for generating a full inventory of live and dead standing trees for large-scale, area-wide habitat analyses. Combining structural and spectral data enabled not only the identification of deadwood, but also of deadwood characteristics, which is indispensable for reliably modelling the habitat requirements of species highly specialized on particular types of standing deadwood. While our habitat analysis confirms the amount of standing dead trees as a key predictor of TTW occurrence, and the species' preference for fresh deadwood characterized by large and intact crowns, our study is the first showing a negative impact of very high deadwood amounts, with a tipping point at about 40–55 standing dead trees per ha. Moreover, we highlight the importance of resource diversity including also snags and live conifers. Based on tree-related remote sensing information, we were able to draw management recommendations. For example, keeping at least eight dead trees in the early stages of decay per hectare within 20 ha (corresponding to a small woodpecker's home range) leads to an increase in habitat suitability for the TTW.

Our models show a high predictive power, nevertheless, they may be improved by a more precise separation of fresh and old deadwood or even a further differentiation of decay stages or deadwood quality obtainable from field studies. Comparing decay stages from field assessments with time series of remote sensing data, and using hyperspectral imagery to detect tree decline in an early stage (e.g., the first *stage* of a *bark beetle* infestation), may further advance the set of predictors and aid foresters to better identify and carry out effective management measures to support biodiversity.

5.6 Author Contributions

Conceptualization, J.M. and V.B.; Data curation, K.Z.-B., M.H. and J.M.; Formal analysis, K.Z.-B.; Investigation, K.Z.-B.; Methodology, K.Z.-B., M.H., J.M. and V.B.; Supervision, V.B.; Visualization, K.Z.-B.; Writing—original draft, K.Z.-B.; Writing—review & editing, M.H., J.M. and V.B.

5.7 Acknowledgments

We thank Peter Krzystek (University of Applied Sciences Munich) for performing the tree segmentation, Barbara Koch (Chair of Remote Sensing and Landscape Information Systems, University of Freiburg) for her support and constructive remarks on the manuscript, Anne-Sophie Stelzer (Dept. of the Biometry and Informatics, FVA) for statistical advice, Miguel Kohling (Dept. of the Biometry and Informatics, FVA) for help with tree polygon data wrangling and Lena Maria Carlson (Dept. of Forest Nature Conservation, FVA) for language proofreading.

Conflicts of Interest: The authors declare no conflict of interest.

5.8 Appendix A

Table A 5-1 Environmental variables with their mean and standard deviation (SD) at presence, absence and all study plots. Variable codes and descriptions are listed in Table 5-1. (Table continues on the next page)

R	Variable	Unit	All Plots		Presence		Absence	
			Mean	SD	Mean	SD	Mean	SD
100	Altitude_mean	m a.s.l.	953.84	182.37	990.93	187.98	916.74	170.36
	CONIF_Nha	N/ha	172.96	91.54	159.96	90.21	185.95	91.89
	DEAD_Cmean	m^2	10.35	5.32	11.92	5.13	8.78	5.09
	DEADTREE_Nha	N/ha	12.75	19.74	17.55	19.56	7.95	18.91
	SNAG_Cmean	m^2	4.76	4.28	5.19	4.01	4.34	4.53
	LIVE_Nha	N/ha	299.55	134.15	276.43	137.98	322.66	127.35
	CONIF_VOL	%	0.65	0.24	0.66	0.22	0.65	0.27
	DEADCIR_part	%	0.04	0.09	0.05	0.09	0.03	0.09
250	Altitude_mean	m a.s.l.	953.53	180.50	989.86	184.95	917.20	170.00
	CONIF_Nha	N/ha	178.28	78.48	163.82	75.10	192.73	79.84
	DEAD_Cmean	m^2	11.01	4.13	12.16	4.14	9.86	3.82

R	Variable	Unit	All Plots		Presence		Absence	
			Mean	SD	Mean	SD	Mean	SD
250	DEADTREE_Nha	N/ha	12.58	18.97	16.94	20.03	8.21	16.93
	SNAG_Cmean	m^2	5.02	3.63	5.48	3.33	4.56	3.89
	LIVE_Nha	N/ha	311.07	116.69	290.57	119.85	331.57	110.81
	CONIF_VOLpart	%	0.63	0.22	0.63	0.21	0.63	0.24
	DEADCIR_part	%	0.04	0.08	0.05	0.08	0.03	0.08
450	Altitude_mean	m a.s.l.	952.71	176.60	987.99	179.23	917.44	168.31
	CONIF_Nha	N/ha	184.81	71.52	168.79	69.50	200.84	70.54
	DEAD_Cmean	m131	11.52	3.61	12.31	3.76	10.73	3.30
	DEADTREE_Nha	N/ha	11.77	15.01	15.24	17.31	8.30	11.43
	SNAG_Cmean	m^2	5.56	3.44	5.87	3.12	5.25	3.74
	LIVE_Nha	N/ha	329.25	108.90	309.69	113.58	348.81	101.35
	CONIF_VOLpart	%	0.60	0.19	0.59	0.18	0.61	0.21
	DEADCIR_part	%	0.37	0.65	0.47	0.73	0.28	0.56
600	Altitude_mean	m a.s.l.	951.77	173.45	986.13	174.79	917.41	166.72
	CONIF_Nha	N/ha	187.38	70.91	172.16	67.59	202.60	71.51
	DEAD_Cmean	m131	11.76	3.47	12.33	3.62	11.19	3.26
	DEADTREE_Nha	N/ha	11.96	14.24	14.50	15.71	9.43	12.24
	SNAG_Cmean	m^2	5.69	3.18	5.90	2.91	5.49	3.45
	LIVE_Nha	N/ha	335.78	105.28	319.20	112.90	352.35	95.29
	CONIF_VOLpart	%	0.58	0.18	0.57	0.16	0.59	0.20
	DEADCIR_part	%	0.04	0.06	0.04	0.06	0.03	0.06

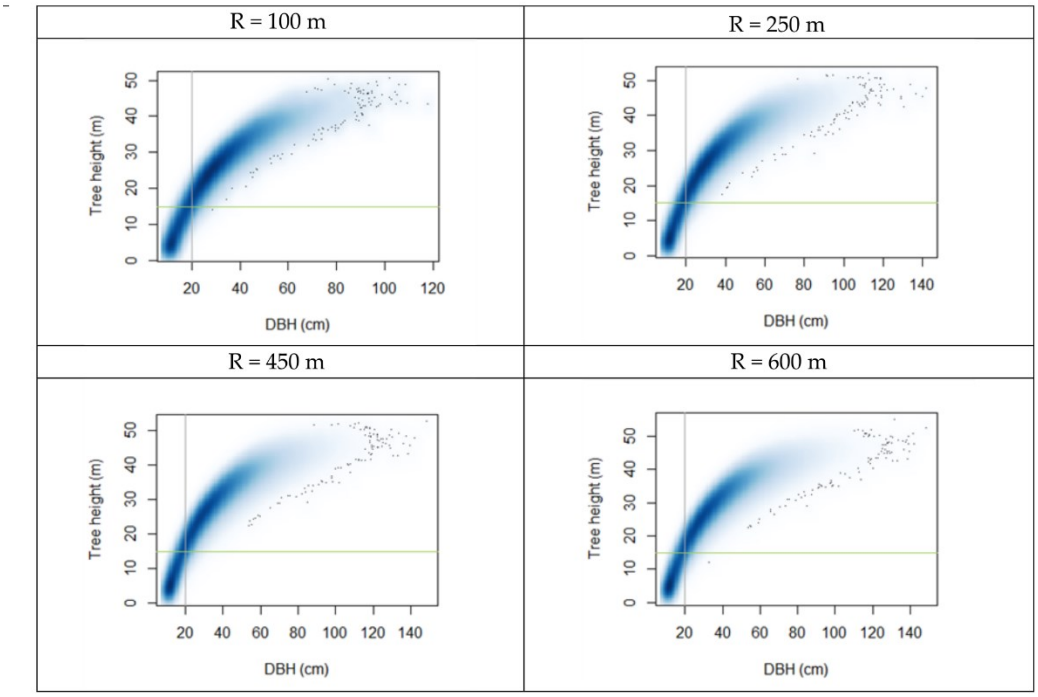

Figure A 5-1 Scatter plots showing the relationship between the diameter at breast height (DBH in cm) and the height (m) of live conifer trees on various plot sizes. The green horizontal line shows the threshold of H = 15 m. The vertical blue line shows the DBH = 20 cm.

Table A 5-2 Performance of the four models including the predictors at 4 spatial scales (i.e., within different radii R, in meters), measured for each of the 5-fold cross-validation replicates as well as for their mean (and standard deviation (SD)). The following evaluation metrics are shown: AIC: Akaikes Information Criterion, R-Sq. (adj.): Adjusted R-Squared, AUC: Area under the ROC curve, Sensitivity, Specificity, Correct Classification Rate (measured with a threshold of 0.5), and Cohen's Kappa.

R	Model Fit Measures	Fold_1	Fold_2	Fold_3	Fold_4	Fold_5	Mean	SD
100	AIC	91.00	93.32	91.55	87.59	83.49	89.39	3.49
	R-sq.(adj.)	0.31	0.28	0.35	0.37	0.40	0.34	0.04
	AUC	0.80	0.89	0.84	0.74	0.59	0.77	0.10
	Sensitivity	0.91	0.82	0.50	0.70	0.80	0.75	0.14
	Specificity	0.73	0.91	0.90	0.50	0.30	0.67	0.24
	Correct Class. Rate	0.82	0.86	0.70	0.60	0.55	0.71	0.12
	Cohen's Kappa	0.64	0.73	0.40	0.20	0.10	0.41	0.24
250	AIC	98.43	97.17	106.73	104.61	91.30	99.65	5.52
	R-sq.(adj.)	0.25	0.28	0.18	0.18	0.35	0.25	0.06
	AUC	0.65	0.74	0.83	0.71	0.60	0.71	0.08
	Sensitivity	0.55	0.64	0.70	0.70	0.70	0.66	0.06
	Specificity	0.55	0.82	0.80	0.60	0.50	0.65	0.13
	Correct Class. Rate	0.55	0.73	0.75	0.65	0.60	0.65	0.08
	Cohen's Kappa	0.09	0.46	0.50	0.30	0.20	0.31	0.15
450	AIC	104.04	105.93	113.38	109.05	104.26	107.33	3.51
	R-sq.(adj.)	0.18	0.16	0.09	0.13	0.19	0.15	0.04
	AUC	0.55	0.63	0.76	0.70	0.51	0.63	0.09
	Sensitivity	0.36	0.64	0.70	0.70	0.50	0.58	0.13
	Specificity	0.55	0.55	0.80	0.40	0.30	0.52	0.17
	Correct Class. Rate	0.46	0.59	0.75	0.55	0.40	0.55	0.12
	Cohen's Kappa	−0.09	0.18	0.50	0.10	−0.20	0.10	0.24
600	AIC	106.22	109.15	113.70	113.15	108.39	110.12	2.87
	R-sq.(adj.)	0.17	0.12	0.09	0.09	0.15	0.12	0.03
	AUC	0.50	0.63	0.71	0.71	0.49	0.61	0.10
	Sensitivity	0.46	0.64	0.50	0.60	0.50	0.54	0.07
	Specificity	0.55	0.46	0.80	0.60	0.50	0.58	0.12
	Correct Class. Rate	0.50	0.55	0.65	0.60	0.50	0.56	0.06
	Cohen's Kappa	0.00	0.09	0.30	0.20	0.00	0.12	0.12

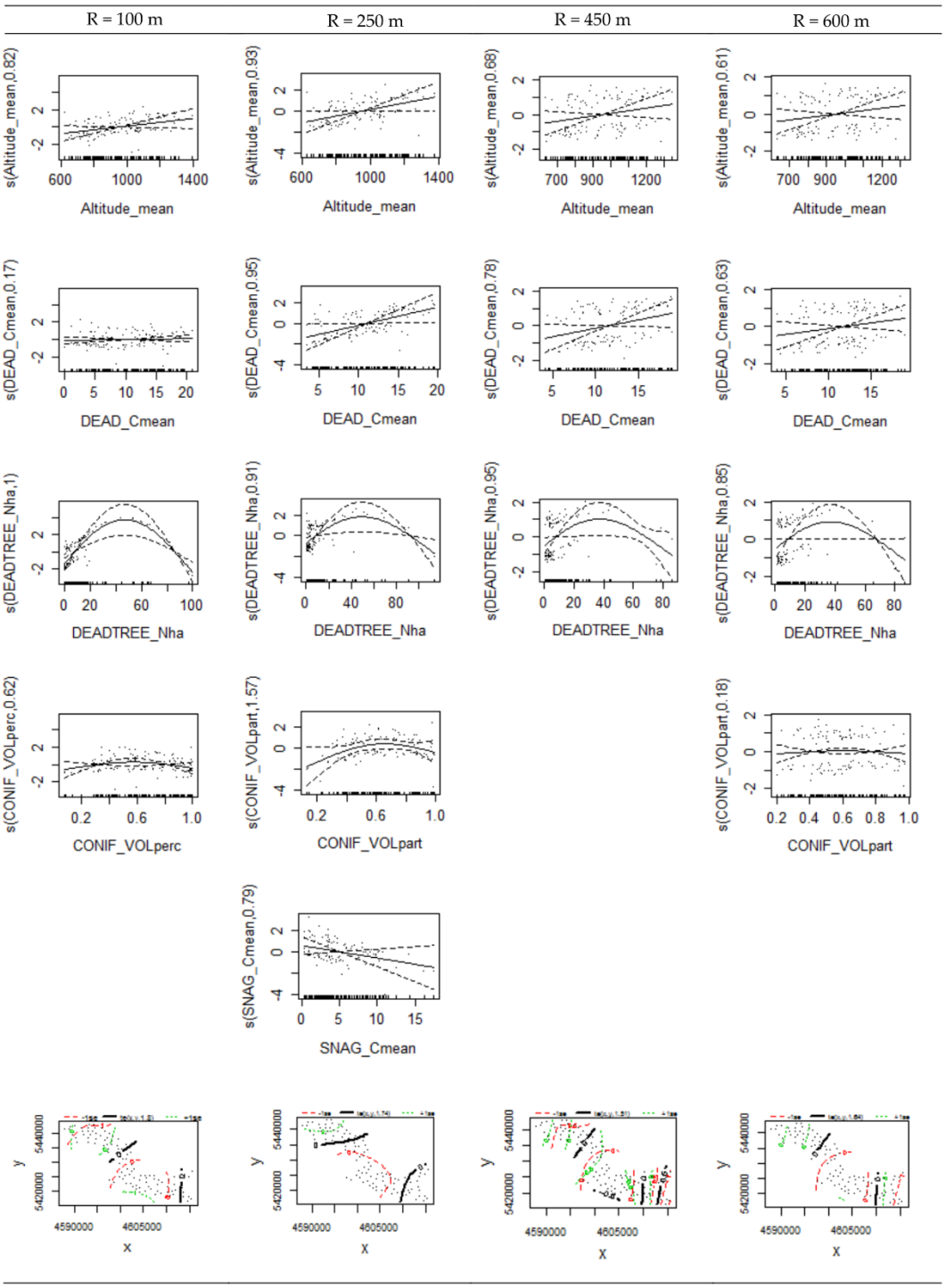

Figure A 5-2 Variable smooth effect plots for the predictor variables at all spatial scales produced using "gam.check". In brackets on y-axis: variables' edf (the estimated degrees of freedom of the smooth') from the GAM model. Variable codes and descriptions are listed in Table 5-1.

6 SYNTHESIS

6.1 Main findings and contributions

The following main findings related to the three research questions (see 1.7) have been identified as a result of this thesis:

RQ1: The aerial imagery can deliver reliable but limited information on vertical vegetation structure. Single objects of open forest structures and standing deadwood can be derived only with limited accuracy and inaccurate object extents.

RQ2: The resolution and overlap of the aerial imagery, the forest structure, the topography as well as the day and time of the data acquisition with the related shadow occurrence are the main factors influencing the detail and accuracy of the CHMs derived from image matching. Using aerial imagery with higher resolution and overlap, taken at times of highest possible solar elevation or employing the ALS data can improve the detection of forest structures.

RQ3: Forest structure parameters based solely on aerial imagery or aerial imagery combined with ALS data enable the quantification and characterization of meaningful habitat variables for predicting the occurrence of the focal species. Area-wide data coverage and standardized automated procedures open new perspectives for forest and conservation planning.

6.1.1 Novel aspects

Several novel aspects were addressed in my thesis. In the methodological part aerial imagery data and products thereof (orthophotos and CHMs) were used and evaluated for automatized derivation of biodiversity relevant forest structure parameters. So far, ecology studies were mainly based on variables derived using visual assessment from aerial imagery and orthophotos or using automatized procedures from ALS data (Müller and Brandl, 2009; Zellweger, 2013; White *et al.*, 2018).

The gap mapping method (Chapter I) was implemented in an automated tool allowing the adjustment of mapping thresholds for gaps and forest types if required by the user. The method, aiming at area-wide analyses, was based solely on the vegetation heights from the aerial imagery based CHM. I obtained good overall results, but also revealed limitations regarding data accuracy in high forests stands. These limitations could be improved when using CHMs derived from ALS (White *et al.*, 2018) or aerial imagery of higher resolution (Chapter II) (Petersen, 2015).

As an intermediate product in the hierarchic image segmentation algorithm of the gap detection method canopy cover was also calculated and delineated. This forest structure parameter has been considered an important attribute in forest ecology as it determines the light and thermal regime on the ground and affects the occurrence and diversity of many conservation-relevant forest taxa (e.g. bats (Russo *et al.*, 2007; Bouvet *et al.*, 2016), birds (Graf *et al.*, 2009; Bollmann *et al.*, 2013), saproxylic beetles (Vogel *et al.*, 2020) or butterflies (Bergman, 2001; Freese *et al.*, 2006)).

Stereo aerial imagery is currently the only available high resolution data source that simultaneously provides both spectral and structural (in course of image matching) information at an operational

scale. To evaluate the potential of combining this information was one of the objectives of this thesis. My deadwood detection method (Chapter III) combined the spectral information from orthophotos and the vegetation heights (CHM) originating from the same aerial imagery which assures appropriate spatial alignment of the different spatial variables at the pixel level.

A further novel aspect of the deadwood detection method (Chapter III) was resolving the bare ground and deadwood misclassification issue. Although a well-known problem, it is rarely addressed and enhancement-methods are lacking (Meddens *et al.*, 2011; Fassnacht *et al.*, 2014). I explored the reasons for the misclassification issues and presented two alternative solutions for addressing them, one based on morphological analyses of the RF results and the second employing an additional deadwood uncertainty filer, developed based on a linear regression model (Chapter III).

Finally, extracting large-scale, area-wide habitat variables, especially on deadwood quantity and quality, from RS-data combining CIR aerial imagery and ALS (Chapter IV) allowed addressing new ecological questions. All habitat models for the Three-toed woodpecker developed so far predicted habitat suitability to increase steadily with a growing amount of dead wood within the bird's home range (Pechacek and Krištín, 1996; Bütler *et al.*, 2004a; Müller and Bütler, 2010). Referring to Scherzinger (2006) we hypothesized and were able to confirm that this relationship is unimodal, i.e. that bird's habitat suitability decreases after reaching an optimum of 44-50 dead trees per ha, which makes a significant contribution to the knowledge on TTW ecology.

6.1.2 Developed methods

The development of remote sensing-based methods for the area-wide detection of forest gaps and standing deadwood was the goal of the methodological part of this thesis. I aimed at automated, flexible and cost-efficient methods that can be adjusted to the various requirements of ecological research questions, but also standardized for long-term monitoring programs. The selection of methods was based on the overall goal, to focus on aerial imagery data from state surveys. Given the need for and the problems associated with processing very large aerial imagery datasets the choice was also influenced by the given technical possibilities and limitations. Obviously, some aspects of the methodology could have benefitted from other, newer or just emerging solutions.

To map forest gaps (Chapter I) and detect their changes over time across large spatial extents I developed a hierarchic image segmentation procedure combining point- and region-based threshold value analyses. Following the structure of a decision tree, including pixel-based threshold- and neighborhood analyses, model objects were delineated. The object-class "open forest", potentially of high relevance for forest biodiversity, was delineated with high overall accuracy OA = 0.92. Despite good overall performance (OA ≥ 0.82 for two different datasets), the gap mapping method showed problems in high stands (height ≥ 8m) indicating the limitations of aerial imagery data and derived CHMs.

Different image matching software: Leica Photogrammetry Suite enhanced Automatic Terrain Extraction (LPS eATE (ERDAS 2012)) and Semi Global Matching (SGM XPro (Hexagon Geospatial 2015) were employed in Chapters I and II for point clouds derivation, whereas in deadwood detection (Chapter III) DSMs based on the SURE algorithm (Rothermel *et al.*, 2012; Kirchhoefer *et al.*, 2017)

were used. Different algorithms delivered diverging results (Chapter I, II) (Ackermann *et al.*, 2020). The suitability of the software therefore often depends on the goal of the vegetation height analysis (e.g. single object vs. area estimation, or top canopy measurements vs. derivation of heights in complex structured stands and close to the ground) and some limitations need to be accepted.

To detect standing deadwood above 5m height in mountainous stands of the Black Forest pixel-based RF classification was applied in the first step. The vegetation heights (CHM) were the most important predictor variable followed by vegetation indices: NDVI, R_ratio (Eq. 2) (Ganz, 2016) and B_I_ratio (Eq. 3) (self-developed). R_ratio was based on the R-band capabilities to differentiate between different chlorophyll content. B_I_Ratio was developed based on the different spectral reflections of the vegetation and bare ground in the blue and infrared band. All three ratios showed in the study area "Feldseewald" good separation between the different vegetation classes: live, declining and dead. However, the recognition of bare ground pixels remained difficult as the ratios' values of this class showed similar values to another classes, especially these of the dead vegetation (Figure 6-1).

$$R\_ratio = R/(R+G+B+I) \qquad (Eq.\ 2)$$

$$B\_I\_ratio = B/I \qquad (Eq.\ 3)$$

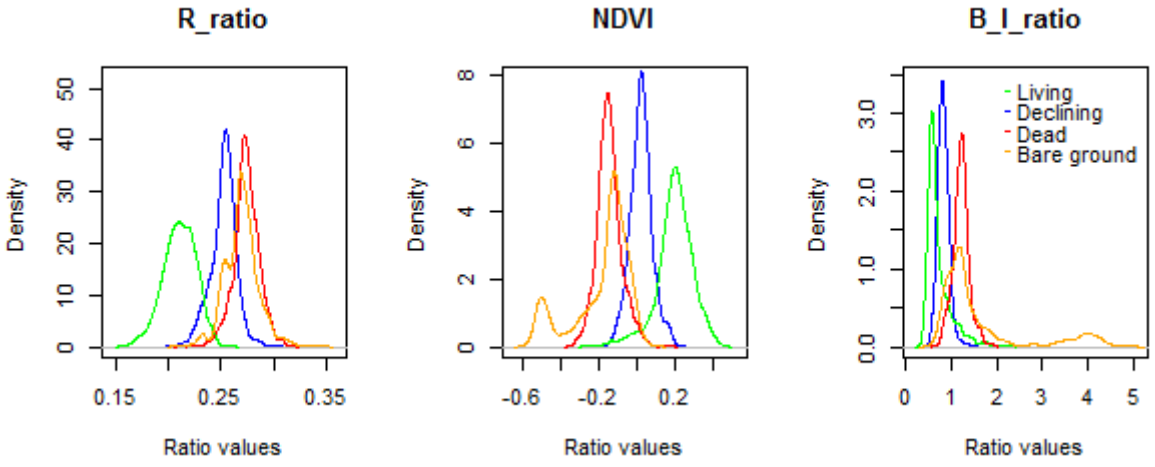

Figure 6-1 Distribution of values per class (Live, Dead and Declining (trees) and Bare ground) for three vegetation indices (R_ratio, NDVI, B_I_ratio) used in the deadwood detection method (Chapter III) based on the training data pixels (2000 pixels per class) used for training of Random Forest model in the study area "Feldseewald".

Hue was among the most significant variables predicting deadwood (Chapter III), which confirms the added value of the HSV-transformation for image analysis.

Hue and Value were also used for shadow detection in Chapter III. Remarkably, my deadwood mapping method included two shadow masks, 1) a deep shadow mask to exclude shadow areas from the analysis and 2) a newly developed special partial shadow mask to identify potentially unreliable deadwood pixels for additional filtering based on additional rules. I also used Ratio S calculated according to SARABANDI et al. (2004) (Eq. 4) and the Intensity channel of the transformed images

(CONRAC CORP. 1980) to identify shadow areas in the aerial imagery. The shadow pixels could be a reason for problems in image matching and erroneous surface heights in derived DSMs, which in turn deliver inaccurate CHMs and causes misclassifications in the subsequent analyses (Chapter II).

$$S = arctan(Blue/max\ \{Red/Green\}) \quad \text{(Eq. 4)}$$

The selection of all thresholds for defining shadow was based on visual assessment of the shadow fraction in the orthophotos and the distribution of values in the selected bands. This is a common practice in remote sensing studies (Shahtahmassebi *et al.*, 2013; Waser *et al.*, 2014a), along with visual delineation of big dark shadow areas (Piermattei *et al.*, 2019) or shadow modelling approaches (Sarabandi *et al.*, 2004; Polewski *et al.*, 2015c) as shadow thresholds depend on data and differ between flights and study areas according to the site and flight conditions.

To describe the texture of the aerial imagery I used Mean Euclidean Distance (Irons and Petersen, 1981) as implemented in ERDAS Imagine (HEXAGON, 2020) and the "Curvature" function in ArcMap (ESRI, 2018) As in the topographical concept of curvature, I hypothesized a similar contribution of the spectral information from the infrared band to the description of the spatial form of single deadwood objects. Both curvature and mean curvature, calculated at two aggregation levels, contributed significantly to deadwood recognition in the deadwood uncertainty model.

Addressing the bare ground-misclassification issue with 1) morphological post-processing and 2) a deadwood uncertainty filter including structural and textural information from the pixel's neighborhood, both applied on top of the RF classification, improved the discriminating between deadwood and bare ground pixels. Both solutions led to deadwood mapping results with a more balanced ratio between user's and producer's accuracy (i.e. a UA of 0.69 and 0.74 and PA of 0.79 and 0.80, under (1) and (2), respectively). The deadwood uncertainty filter delivered better results, but was also the more time and resource consuming procedure. The accuracy of my results correspond to that of other deadwood detection studies either based on visual interpretation of CIR aerial imagery (Bütler and Schlaepfer, 2004) or on methods using solely ALS data (Yao *et al.*, 2012a).

6.1.3 Potential and limitations of aerial imagery data

A thorough analysis of the meta-data and aerial imagery properties (Chapter I) pointed at shadow occurrence and geometric limitations of the source data being the limiting factor for the quality and accuracy of the derived CHMs. By focusing on data from state surveys, used without prior radiometric and geometric enhancement for fast and cost-efficient processing, reliable input data was expected. However, the aerial imagery originated from different flight campaigns differed in quality, especially in the amount of shadow, due to the date and time of data acquisition, which affected the results.

The results of Chapter II, comparing data from three different surveys, confirmed the findings of Chapter I. Introducing and keeping standards for flight time and solar altitude, so as to assure a low level of shadow occurrence and a good insight between the trees, should be seriously considered as bringing significant benefits for the successive data analyses, especially in complex surface situations.

Forest stand characteristics and topography were important parameters influencing the results of the gap mapping, with low reliability in high forest stands (Chapter I). This is in line with Adler *et al.* (2014) and Hobi *et al.* (2015), who observed a higher image matching success in plain or smooth terrain and even-aged homogenous stands compared to rugged terrain and forest of complex structure. Using aerial imagery with higher resolution and overlap for image matching can improve the detail and accuracy of the CHMs (Ganz *et al.*, 2019) and derived gap structures (Petersen, 2015) as proven in Chapter II. The number of detected gaps increased with the overlap and resolution of the data, with simultaneous decrease in size of the detected gaps pointing to higher spatial detail and accuracy achieved with the enhancement of the input data. Aerial imagery with higher resolution and overlap are recommended where possible over the data with corresponding lower parameters with an ultimate choice of ALS data, if available.

Knowing the drawbacks of the aerial imagery based DSMs and CHMs based on the DTMs from state surveys, which are especially prone to errors in complex or open structured stands and in mountainous rugged topography, a minimum threshold of 5 m height for detection of standing deadwood (Chapter III) was applied a-priori. However, it was not able to eliminate the bare ground pixels, known for their varying reflectance pattern depending on surface roughness and wetness as well as the angle of view in relation to the angle of illumination (Jones and Vaughan, 2010). Specific solutions were required to solve the bare ground and deadwood misclassification issue.

The primary input data for the ecological study on Three toed woodpecker habitat suitability (Chapter IV), combining the ALS structural data and spectral information from the color-infrared aerial imagery, allowed the mapping of single tree polygons and the calculation of tree-related attributes among which the tree type, tree height and crown area occurred to be decisive for the TTW's habitat selection. The available data, with the CIR component being crucial for differentiation between live and dead vegetation, did not only deliver information on the occurrence of standing deadwood but also enabled the estimation of different decay stages, which is relevant for many forest species (e.g. Balasso (2016)).

6.1.4 Model Validation

In this thesis I used stratified random sampling of both point objects (Chapter III) and areas (Chapter I, II) to generate quantitative validation data with minimal operator bias and good representation of all mapped classes. The calculation of a confusion matrix and associated accuracy metrics for multi-class classifications allowed the assessment of model performance (Chapters I-III) and the comparison between the different models and validation datasets (Chapter III).

In Chapter III, I showed a major drawback of generating validation data by partitioning the reference data revealed, as they can deliver too optimistic results not representing the actual situation. Collecting the training and reference data at the same time is not advisable and may lead to biased results (Fassnacht, 2013) potentially due to over-fitting the classifier to the sample (Kuhn and Johnson, 2013) or to the fact that validation data collected only from "pure class'" pixels do not account for problematic inter-class similarities.

An additional polygon based validation was applied similar to Fassnacht *et al.* (2014) to estimate the accuracy of the pixel-based approach in the detection of single dead tree objects (Chapter III). The results of the deadwood detection were intersected with the deadwood reference polygons with positive detection assigned to an overlap of at least one deadwood pixel. The analysis of the intersected area allowed an estimation of the spatial extent of the correct deadwood recognition.

Although the level of automatization in the modelling and validation is growing, visual assessment still remains an important validation element to gain a full understanding of the characteristics of the data and the associated problems. The visual inspection on the occurrence of outliers, missing data or false results is essential, especially during method development and optimization of algorithms while testing different settings. Orthophotos, CHMs and stereo aerial imagery are well suited for that purpose.

6.1.5 Practical use of the data products

For this doctoral thesis two forest structural elements: canopy gaps and standing deadwood, both being key habitat elements in forests and affecting the occurrence of many plant and animal species, were selected and methods for their detection were developed. A reliable detection of these structures is expected to support research and management in various fields of forestry such as forest growth and regeneration (Yamamoto, 2000; Diaci *et al.*, 2005; Nagel *et al.*, 2009) or species-habitat relationships and forest nature conservation (Angelstam *et al.*, 2003; Suchant *et al.*, 2009; Vihervaara *et al.*, 2017).

Information on deadwood occurrence can be valuable for bark beetle prevention and management (Kautz *et al.*, 2011) or for planning of traffic safety operations (Stereńczak *et al.*, 2017). Moreover, it can support the evaluation of deadwood enrichment programs (Schaber-Schoor, 2010) or other forest conservation plans and strategies (Schaber-Schoor *et al.*, 2015).

Forest structure detection based on automated processing methods also allows the generation of time series from aerial imagery of multiple flight campaigns. Analyzing deadwood occurrence and dynamics in protected and not protected forests (Rall and Martin, 2002; Zielewska, 2012) or observing the forest gaps' dynamics (Vepakomma, 2008; Rugani *et al.*, 2013) is of significant value both for forest managers developing or optimizing forest management plans, and for researchers investigating ecological processes in forests.

6.2 Limitation of this study and perspectives for future research

All methodological studies (Chapters I, II and III) showed limitations with regard to the accuracy of the vegetation heights derived from image matching. The aerial imagery data used was not sufficient to provide reliable values in low areas between trees and at the borders between high and low surfaces e.g. at the borders to forest roads or between stands.

Technical development and advances in aerial imagery data acquisition with increasing availability of data with higher resolution and overlap make further research necessary examining potential of these data for deriving more accurate surface heights. Furthermore, cost-benefit studies comparing

the ALS-based CHMs with these derived from image matching of aerial imagery, similar to study of Eid *et al.* (2004), are required to rate the real potential of both data sources and may deliver arguments for integrating regularly updated ALS data into the product-portfolio of large scale public services. There are good examples from Scandinavia where ALS is the main data source for forest inventories (Kangas *et al.*, 2018). However it needs to be taken into consideration that an increase in the spatial extent of the ALS campaigns also inflates the variation within the scanned areas and in the quality of the resulting data.

More accurate data on surface heights could aid detection of small forest gaps and deadwood objects in various stages of decay and possibly also reduce misclassifications with bare-ground areas with low surface height. In addition, the detection of single dead trees and snags (objects, polygons), which provide valuable habitat information for specialized species (Chapter IV), would benefit from more accurate vegetation heights.

VHR stereoscopic satellite imagery such as WorldView-3 (European-Space-Imaging, 2018a), WorldView-4 (European-Space-Imaging, 2018b) or Pléiades (Coeurdev and Gabriel-Robe, 2012) imagery data might be an alternative to aerial images for mapping high-resolution forest structures such as deadwood or canopy gaps, especially when the methods are intended to be used at bigger spatial scales (Pluto-Kossakowska *et al.*, 2017; Piermattei *et al.*, 2019). More research is required on the combined use of satellite stereoscopic data for the generation of both spectral and structural information for analyses and applications in ecology.

Taking into consideration the rapid methodological development and first successful small scale studies on deadwood detection using DL algorithms (Jiang *et al.*, 2019), further research in this field is necessary to examine the potential of these techniques for accurate classification and segmentation of forest structures across large areas. In Chapter III of this thesis, two curvature variables calculated at different aggregation levels were fed into the deadwood uncertainty model to separate bare ground from deadwood pixels. Their positive contribution to the model suggests a potential benefit of using the DL structures, such as e.g. convolutional neural networks (CNN), for mapping of deadwood objects and thus a promising research direction.

The study on TTW habitat suitability (Chapter IV) shows the value of combining aerial imagery with ALS data, allowing not only the detection of standing deadwood but also the separation of fresh and old deadwood. Further analyses of decay stages observed in the field with time series of remote sensing data, including hyperspectral data for the detection of early stage vegetation tissue damage and tree decline (Abdullah *et al.*, 2019) may advance the studies on deadwood dynamics and allow more accurate predictor variables for ecological studies and effective forest nature conservation.

6.3 Final remarks

Remotely sensed data and mapping techniques are valuable for biodiversity studies, as they provide continuous data and can be used to derive ecologically relevant variables on vertical and horizontal structural dimensions across large spatial scales. Such data are not only relevant for analyzing and

predicting species occurrence patterns but also for deriving ecological threshold values and to distinguish between suitable and unsuitable areas for targeted conservation measures.

This work confirms that public aerial imagery and the data products thereof such as orthophotos and DSMs enable the detection of forest structures; it does, however, have limits. Although more accurate information on vegetation heights can be derived from other sources especially from ALS, aerial images remain the most flexible data that provides both spectral information and the possibility of obtaining structural information with image matching technique.

The quality of the structural information from DSMs was a drawback, since this thesis targeted fine forest structures located in-between tall trees and between high and low vegetation. Main possibilities for improvement are in using aerial imagery of higher resolution and overlap, as they enable better insight in-between the trees and allow image matching with higher accuracy. The standards of data from state surveys have been changing in the last years and aerial imagery and the products thereof have successively become more accurate and detailed, the benefit of which needs to be evaluated.

The deadwood detection method optimized for a better separation of bare ground and deadwood shows that new approaches combining different methods and data at different aggregation levels can unveil valuable information. Although there are so many RS data types available on the market, aerial imagery data shall still be explored further as it might bear a potential to deliver additional useful information resulting from new technical developments.

LIST OF FIGURES

Supplementary material / Appendix A

LIST OF TABLES

Supplementary material / Appendix A

REFERENCES

Abdullah, H., Darvishzadeh, R., Skidmore, A.K., Groen, T.A., Heurich, M., 2018a. European spruce bark beetle (Ips typographus, L.) green attack affects foliar reflectance and biochemical properties. International Journal of Applied Earth Observation and Geoinformation 64, 199-209.

Abdullah, H., Skidmore, A.K., Darvishzadeh, R., Heurich, M., 2018b. Sentinel-2 accurately maps green-attack stage of European spruce bark beetle (Ips typographus, L.) compared with Landsat-8. Remote Sensing in Ecology and Conservation, 1-21.

Abdullah, H., Skidmore, A.K., Darvishzadeh, R., Heurich, M., 2019. Timing of red-edge and shortwave infrared reflectance critical for early stress detection induced by bark beetle (Ips typographus, L.) attack. international Journal of Applied Earth Observation and Geoinformation 82, 101900, p. 13.

Ackermann, J., Adler, P., Aufreiter, C., Bauerhansl, C., Bucher, T., Franz, S., Engels, F., Ginzler, C., Hoffmann, K., Jütte, K., Kenneweg, H., Koukal, T., Martin, K., Oehmichen, K., Rüffer, O., Sagischewski, H., Seitz, R., Straub, C., Tintrup, G., Zielewska-Büttner, K., 2020. Oberflächenmodelle aus Luftbildern für forstliche Anwendungen. Leitfaden AFL 2020. WSL Berichte 87, p. 60.

Ackermann, J., Adler, P., Bauerhansl, C., Brockamp, U., Engels, F., Franken, F., Ginzler, C., Gross, C.-P., Hoffmann, K., Jütte, K., Kenneweg, H., Koukal, T., Martin, K., Regner, B., Seitz, R., Troycke, A., 2012. Das digitale Luftbild. Ein Praxisleitfaden für Anwender im Forst- und Umweltbereich. Universitätsverlag Göttingen, Göttingen, 7, p. 79.

Adamczyk, J., Bedkowski, K., 2006. Digital analysis of relationships between crown colours on aerial photographs and trees health status. In, Roczniki Gomatyki. Polskie Towarzystwo Informacji Przestrzennej, SGGW Warszawa, 4, 4, pp. 47-54.

Adamczyk, J., Osberger, A., 2015. Red-edge vegetation indices for detecting and assessing disturbances in Norway spruce dominated mountain forests. International Journal of Applied Earth Observation and Geoinformation 37, 90-99.

Adler, P., Naake, T., Peters, S., Ginzler, C., Bauerhansl, C., Stepper, C., 2014. Reliability of forest canopy height extraction from digital aerial images. In, ForestSAT Conference, Riva del Garda (TN), Italy.

AFL, Arbeitsgruppe Forstlicher Luftbildinterpreten, 2003. Luftbildinterpretationsschlüssel – Bestimmungsschlüssel für die Beschreibung von strukturreichen Waldbeständen im Color-Infrarot-Luftbild. In: Troyke, A., Habermann, R., Wolff, B., Gärtner, M., Engels, F., Brockamp, U., Hoffmann, K., Scherrer, H.-U., Kenneweg, H., Kleinschmit, B., Adler, P., Dees, M., Gross, C.-P., Banko, G., Koukal, T. (Eds.). Landesforstpräsidium (LFP) Freistaat Sachsen, Pirna, p. 48.

AG Boden, Ad-hoc-Arbeitsgruppe Boden der Geologischen Landesämter und der Bundesanstalt für Geowissenschaften und Rohstoffe der Bundesrepublik Deutschland, 1996. Bodenkundliche Kartieranleitung. Bundesanstalt für Geowissenschaften und Rohstoffe und Geologische Landesämter, Hannover, p. 392.

Ahamed, T., Tian, L., Zhang, Y., Ting, K.C., 2011. A review of remote sensing methods for biomass feedstock production. Biomass Bioenergy 35, 2455–2469.

Ahrens, W., 2001. Analyse der Waldentwicklung in Naturwaldreservaten auf Basis digitaler Orthobilder. In, Forstwissenschaftliche Fakultät. Albert-Ludwigs-Universität, Freiburg i. Brsg., p. 143.

Ahrens, W., Brockamp, U., Pisoke, T., 2004. Zur Erfassung von Waldstrukturen im Luftbild. Arbeitsanleitung für Waldschutzgebiete Baden-Württemberg. Waldschutzgebiete Baden-Württemberg 5, p. 54.

Albrecht, L., 1991. Die Bedeutung des toten Holzes im Wald. Forstwissenschaftliches Centralblatt vereinigt mit Tharandter forstliches Jahrbuch 110, 106-113.

Amcoff, M., Eriksson, P., 1996. Occurrence of three-toed woodpecker Picoides tridactylus at the scales of forest stand and landscape. Ornis Svecica 6 107-119.

Amiri, N., Krzystek, P., Heurich, M., Skidmore, A.K., 2019. Classification of Tree Species as Well as Standing Dead Trees Using Triple Wavelength ALS in a Temperate Forest. Remote Sensing 11, 2614.

Amiri, N., Polewski, P., Yao, W., Heurich, M., Krzystek, P., Skidmore, A.K., 2016. Feature relevance assessment for single tree species classification using ALS point clouds and aerial imagery. In, Young Professionals Conference on Remote Sensing, Oberpfaffenhofen, Germany, p. 4.

Andersen, T., Carstensen, J., Hernández-García, E., Duarte, C.M., 2009. Ecological thresholds and regime shifts: approaches to identification. Trends in Ecology and Evolution 24, 49-57.

Andris, K., Kaiser, H., 1995. Wiederansiedlung des Dreizehenspechtes (Picoides tridactylus) im Südschwarzwald. Naturschutz südl. Oberrhein 1, 3-10.

Angelstam, P., Bütler, R., Lazdinis, M., Mikusinski, G., Roberge, J.-M., 2003. Habitat thresholds for focal species at multiple scales and forest biodiversity conservation — dead wood as an example. Ann. Zool. Fennici 40, 473-482.

Angelstam, P., Roberge, J.-M., Lõhmus, A., Bergmanis, M., Brazaitis, G., Dönz-Breuss, M., Edenius, L., Kosinski, Z., Kurlavicius, P., Lārmanis, V., Lūkins, M., Mikusiński, G., Račinskis, E., Strazds, M., Tryjanowski, P., 2004. Habitat modelling as a tool for landscape-scale conservation – a review of parameters for focal forest birds. Ecological Bulletins 51, 427-453.

Aschoff, T., Spiecker, H., Holdenried, M.W., 2006. Terrestrische Laserscanner und akustische Ortungssysteme: Jagdlebensräumen von Fledermäusen. AFZ-DerWald 4, 172-175.

Baddeley, A., Turner, R., Rubak, E., 2018. Package 'spatstat'. Spatial Point Pattern Analysis, Model-Fitting, Simulation, Tests. In. R package version 1.55-1; Available online: https://cran.r-project.org/web/packages/spatstat/spatstat.pdf (accessed on 14.04.2018).

Bader, P., Jansson, S., Jonsson, B.G., 1995. Wood-inhabiting fungi and substratum decline in selectively logged boreal spruce forests. Biol. Conserv. 72, 355–362.

Balasso, M., 2016. Ecological requirements of the threetoed woodpecker (Picoides tridactylus L.) in boreal forests of northern Sweden In, Department of Wildlife, Fish, and Environmental studies, Faculty of Forest Science. Swedish University of Agricultural Sciences, Umeå, p. 30.

Baldrian, P., Zrůstová, P., Tláskal, V., Davidová, A., Merhautová, V., Vrška, T., 2016. Fungi associated with decomposing deadwood in a natural beech-dominated forest. Fungal Ecology 23, 109-122.

Ballings, M., Van den Poel, D., 2013. AUC: Threshold independent performance measures for probabilistic classifiers. R package version 0.3.0.

Baltsavias, E., Gruen, A., Eisenbeiss, H., Zhang, L., Waser, L.T., 2008. High-quality image matching and automated generation of 3D tree models. International Journal of Remote Sensing 29, 1243-1259.

Bannari, A., Morin, D., Bonn, F., Huete, A.R., 1995. A review of vegetation indices. Remote Sensing Reviews 13, 95-120.

Barbet-Massin, M., Jiguet, F., Albert, C.H., Thuiller, W., 2012. Selecting pseudo-absences for species distribution models: how, where and how many? Methods in Ecology and Evolution 3, 327-338.

Barlow, J., Lennox, G.D., Ferreira, J., Berenguer, E., Lees, A.C., Nally, R.M., Thomson, J.R., Ferraz, S.F.d.B., Louzada, J., Oliveira, V.H.F., Parry, L., Ribeiro de Castro Solar, R., Vieira, I.C.G., Aragão, L.E.O.C., Begotti, R.A., Braga, R.F., Cardoso, T.M., de Oliveira Jr, R.C., Souza Jr, C.M., Moura, N.G., Nunes, S.S., Siqueira, J.V., Pardini, R., Silveira, J.M., Vaz-de-Mello, F.Z., Veiga, R.C.S., Venturieri, A., Gardner, T.A., 2016. Anthropogenic disturbance in tropical forests can double biodiversity loss from deforestation. Nature 535, 144-147.

Barton, K., 2019. MuMIn: Multi-Model Inference. R package version 1.43.15. In. https://CRAN.R-project.org/package=MuMIn (accessed on 10.01.2020)

Basile, M., Asbeck, T., Jonker, M., Knuff, A., Bauhus, J., Braunisch, V., Mikusiński, G., Storch, I., 2020. What do tree-related microhabitats tell us about the abundance of forest-dwelling bats, birds, and insects? Journal of Environmental Management 264, 110401.

Bässler, C., Förster, B., Moning, C., Müller, J., 2008. The BIOKLIM project: Biodiversity research between climate change and wilding in a temperate montane forest–the conceptual framework. Waldökologie, Landschaftsforschung und Naturschutz 7, 21–33.

Bässler, C., Stadler, J., Müller, J., Förster, B., Göttlein, A., Brandl, R., 2010. LiDAR as a rapid tool to predict forest habitat types in Natura 2000 networks. Biodiversity and Conservation 20, 456-481.

Bässler, C.M., J., 2015. Selbst naturnahe Waldwirtschaft stört biologische Prozesse. AFZ-Der Wald 3, 42-43.

Bauer, H.-G., Boschert, M., Förschler, M.I., Hölzinger, J., Kramer, M., Ulrich, M., 2016. Rote Liste und kommentiertes Verzeichnis der Brutvogelarten Baden-Württembergs. 6. Fassung. Stand: 31.12.2013. Naturschutz-Praxis Artenschutz 11. LUBW Landesanstalt für Umwelt, Messungen und Naturschutz Baden-Württemberg, Karlsruhe, p. 239.

Beatty, C.R., Cox, N.A., Kuzee, M.E., 2018. Biodiversity guidelines for forest landscape restoration opportunities assessments. First edition. IUCN, Gland, Switzerland, p. 43.

Bergman, K.-O., 2001. Population Dynamics and the Importance of Habitat Management for Conservation of the Butterfly Lopinga achine. Journal of Applied Ecology 38, 1303-1313.

Bergseng, E., Ørka, H.O., Næsset, E., Gobakken, T., 2015. Assessing forest inventory information obtained from different inventory approaches and remote sensing data sources. Annals of Forest Science 72, 33-45.

Betts, H.D., Brown, L.J., Stewart, G.H., 2005. Forest canopy gap detection and characterisation by use of high-resolution Digital Elevation Models. New Zealand Journal of Ecology 29, 95-103.

Betts, M.G., Wolf, C., Ripple, W.J., Phalan, B., Millers, K.A., Duarte, A., Butchart, S.H.M., Levi, T., 2017. Global forest loss disproportionately erodes biodiversity in intact landscapes. Nature 547, 441-444.

BirdLife, I., 2016. European Red List of Birds. Office for Official Publications of the European Communities, Luxembourg, p. 67.

Bivand, R., Keitt, T., Rowlingson, B., 2019. Package ‘rgdal’. Bindings for the 'Geospatial' Data Abstraction Library. R package version 1.4-3. https://CRAN.R-project.org/package=rgdal. (accessed on 05.05.2019).

Bivand, R., Keitt, T., Rowlingson, B., Pebesma, E., Sumner, M., Hijmans, R., Rouault, E., 2017. Package ‘rgdal’. Bindings for the 'Geospatial' Data Abstraction Library. Version 1.2-16. http://www.gdal.org, (accessed on 02.02.2018).

Blaschke, T., Burnett, C., Pekkarinen, A., 2004. Image Segmentation Methods for Object-based Analysis and Classification. In: S.M.D., J., F.D.V., M. (Eds.), Remote Sensing Image Analysis: Including The Spatial Domain. Remote Sensing and Digital Image Processing. Springer, Dordrecht, pp. 211-236.

Bollmann, K., Mollet, P., Ehrbar, R., 2013. Das Auerhuhn Tetrao urogallus im Alpinen Lebensraum: Verbreitung, Bestand, Lebensraumansprüche und Förderung. Vogelwelt 134, 19 – 28.

Boncina, A., 2011. Conceptual Approaches to Integrate Nature Conservation into Forest Management: A Central European Perspective. International Forestry Review 13, 13-22.

Bouvet, A., Paillet, Y., Archaux, F., Tillon, L., Denis, P., Gilg, O., Gosselin, F., 2016. Effects of forest structure,management and landscape on bird and bat communities. Environmental Conservation 43, 148-160.

Braunisch, V., 2008. Spacially explicit species-habitat models for large-scale conservation planning. Modelling habitat potential and habitat connectivity for capercaillie (Tetrao urogallus). In, Faculty of Forest and Environmental Sciences. Albert-Ludwigs-Universität Freiburg im Breisgau, p. 245.

Braunisch, V., Coppes, J., Arlettaz, R., Suchant, R., Zellweger, F., Bollmann, K., 2014. Temperate mountain forest biodiversity under climate change: compensating negative effects by increasing structural complexity. PloS one 9, e97718.

Braunisch, V., Suchant, R., 2008. Using ecological forest site mapping for long-term habitat suitability assessments in wildlife conservation-Demonstrated for capercaillie (Tetrao urogallus). Forest Ecology and Management 256, 1209-1221.

Braunisch, V., Suchant, R., 2010. Predicting species distributions based on incomplete survey data: the trade-off between precision and scale. Ecography 33, 826-840.

Braunisch, V., Suchant, R., 2013. Aktionsplan Auerhuhn *Tetrao urogallus* im Schwarzwald: Ein integratives Konzept zum Erhalt einer überlebensfähigen Population. Vogelwelt 134, 29-41.

Breiman, L., 2001. Random Forests. Machine Learning 45, 5-32.

Brokaw, N.V.L., 1982. The Definition of Treefall Gap and Its Effect on Measures of Forest Dynamics. Biotropica 14, 158-160.

Bundesministerium für Umwelt, Naturschutz, Bau und Reaktorsicherheit (BMUB), 2007. Nationale Strategie zur biologischen Vielfalt. Kabinettsbeschluss vom 7. November 2007. In: Referat N I 1, Küchler-Krischun.J.D., Walter A. M. (Ed.), Berlin, p. 179.

Burnham, K.P., Anderson, D.R., 2002. Model Selection and Multimodel Inference. A Practical Information-Theoretic Approach. Springer-Verlag, New York.

Bütler, R., Angelstam, P., Ekelund, P., Schlaepfer, R., 2004a. Dead wood threshold values for the three-toed woodpecker presence in boreal and sub-Alpine forest. Biological Conservation 119, 305-318.

Bütler, R., Angelstam, P., Ekelund, P., Schlaepfer, R., 2004b. Dead wood threshold values for the three-toed woodpecker presence in boreal and sub-Alpine forests. Biological Conservation 119, 305-318.

Bütler, R., Angelstam, P., Schlaepfer, R., 2004c. Quantitative snag targets for the three-toed woodpecker, Picoides tridactylus. Ecological Bulletins 51, 219-232.

Bütler, R., Lachat, T., Larrieu, L., Paillet, Y., 2013. Habitat trees: Key elements for forest biodiversity. Integrative Approaches as an Opportunity for the Conservation of Forest Biodiversity. European Forest Institute, Joensuu, 84-91.

Bütler, R., Schlaepfer, R., 2004. Spruce snag quantification by coupling colour infrared aerial photos and a GIS. Forest Ecology and Management 195, 325-339.

Cailleret, M., Heurich, M., Bugmann, H., 2014. Reduction in browsing intensity may not compensate climate change effects on tree species composition in the Bavarian Forest National Park. Forest ecology and management 328, 179-192.

Carr, A., Zeale, M.R.K., Weatherall, A., Froidevaux, J.S.P., Jones, G., 2018. Ground-based and LiDAR-derived measurements reveal scale-dependent selection of roost characteristics by the rare tree-dwelling bat Barbastella barbastellus. Forest Ecology and Management 417, 237-246.

Casas, Á., García, M., Siegel, R.B., Koltunov, A., Ramírez, C., Ustin, S., 2016. Burned forest characterization at single-tree level with airborne laser scanning for assessing wildlife habitat. Remote Sensing of Environment 175, 231-241.

Chehata, N., Orny, C., Boukir, S., Guyon, D., 2011. Object-based forest change detection using high resolution satellite images. In: Stilla, U.e.a. (Ed.), Photogrammetric Image Analysis PIA11. International Archives of Photogrammetry, Remote Sensing and Spatial Information Sciences 38 (3/W22), Munich, Germany, pp. 49-54.

Coeurdev, L., Gabriel-Robe, C., 2012. Pléiades Imagery-User Guid. In. Astrium GEO-Information Services, Toulouse, France, p. 118.

Cohen, J., 1960. A coefficient of agreement for nominal scales. Educational and Psychological Measurement 20, 37-46.

Conchedda, G., Durieux, L., Mayaux, P., 2008. An object-based method for mapping and change analysis in mangrove ecosystems. ISPRS Journal of Photogrammetry and Remote Sensing 63, 578-589.

Congalton, R.G., 1991. A Review of Assessing the Accuracy of Classifications of Remotely Sensed Data. Remote Sensing of Environment 37, 35-46.

Conrac Corp., C.D., 1980. Raster Graphics Handbook. In. Conrac Corp, Covina, California.

Corbane, C., Lang, S., Pipkins, K., Alleaume, S., Deshayes, M., García Millán, V.E., Strasser, T., Vanden Borre, J., Toon, S., Michael, F., 2015. Remote sensing for mapping natural habitats and their conservation status – New opportunities and challenges. International Journal of Applied Earth Observation and Geoinformation 37, 7-16.

Csardi., G., Nepusz, T., 2006. The igraph software package for complex network research. In, InterJournal, Complex Systems.

Czeszczewik, D., Sahel, M., Zub, K., Kapusta, A., Stanski, T., Walankiewicz, W., 2015. Effects of forest management on bird assemblages in the Bialowieza Forest, Poland. iForest – Biogeosciences and Forestry 8, 377-385.

Dalponte, M., Bruzzone, L., Gianelle, D., 2008. Fusion of Hyperspectral and LIDAR Remote Sensing Data for Classification of Complex Forest Areas. IEEE Transactions on Geoscience and Remote Sensing 46, 1416-1427.

Dalponte, M., Reyes, F., Kandare, K., Gianelle, D., 2015. Delineation of Individual Tree Crowns from ALS and Hyperspectral data: a comparison among four methods. European Journal of Remote Sensing 48, 365-382.

DAT/EM Systems International, 2012. Summit Evolution. Release 7.3., https://www.datem.com/summit-evolution/ (accessed on 08.06.2020)

Davies, A.B., Asner, G.P., 2014. Advances in animal ecology from 3D-LiDAR ecosystem mapping. Trends in Ecology & Evolution 29, 681-691.

Diaci, J., Pisek, R., Boncina, A., 2005. Regeneration in experimental gaps of subalpine Picea abies forest in the Slovenian Alps. European Journal of Forest Research 124, 29-36.

Dietmaier, A., McDermid, G.J., Mustafizur Rahman, M., Linke, J., Ludwig, R., 2019. Comparison of LiDAR and Digital Aerial Photogrammetry for Characterizing Canopy Openings in the Boreal Forest of Northern Alberta. Remote Sensing 11, 22.

Djupstrom, L., Perhans, K., Weslien, J., Schroeder, M., Gustafsson, L., Wikberg, S., 2010. Co-variation of lichens, bryophytes, saproxylic beetles and dead wood in Swedish boreal forests. Systematics and Biodiversity 8.

Donato, D.C., Campbell, J.L., Franklin, J.F., 2012. Multiple successional pathways and precocity in forest development: can some forests be born complex? Journal of Vegetation Science 23, 576-584.

Dorka, U., 1996. Aktionsraumgröße, Habitatnutzung sowie Gefährdung und Schutz des Dreizehenspechtes (Picoides tridactylus) im Bannwaldgebiet Hoher Ochsenkopf (Nordschwarzwald) nach der Wiederansiedlung der Art. Naturschutz südl. Oberrhein 1, 159-168.

Dormann, C., Blaschke, T., Lausch, A., Schröder, B., Sondgerath, D., 2004. Habitatmodelle - Methodik, Anwendung, Nutzen. Tagungsband zum Workshop vom 8-10. Oktober 2003. UFZ-Berichte 9/2004.

Dormann, C.F., Kühn, I., 2012. Angewandte Statistik für die biologischen Wissenschaften. 2., durchgesehene, aktualisierte, überarbeitete und erweiterte Auflage. Helmholtz Zentrum für Umweltforschung-UFZ, Leipzig, p. 245.

Dowle, M., Srinivasan, A., 2019. data.table: Extension of `data.frame`. R package version 1.12.8. https://CRAN.R-project.org/package=data.table (accessed on 10.01.2020)

Ehbrecht, M., Schall, P., Ammer, C., Seidel, D., 2017. Quantifying stand structural complexity and its relationship with forest management, tree species diversity and microclimate. Agricultural and Forest Meteorology 242, 1-9.

Eid, T., Gobakken, T., Næsset, E., 2004. Comparing stand inventories for large areas based on photo-interpretation and laser scanning by means of cost-plus-loss analyses. Scandinavian Journal of Forest Research 19, 512-523.

ENVI, 2019. Vegetation Indices. © 2020 Harris Geospatial Solutions, Inc. http://www.harrisgeospatial.com/docs /VegetationIndices.html (accessed on 01.12.2019)

ERDAS, I.C., 2012. LPS eATE. From Image to Point Clouds: Model Your World Like Never Before. Product Sheet. 5/12 GEO-US-0033A-ENG. ©Intergraph Corporation.

ESA, European Space Agency, 2020. Sentinel 2. © ESA 2000 – 2020, https://sentinel.esa.int /web/sentinel /missions/sentinel-2 (accessed on 02.07.2020)

ESRI, E.S.R.I., 2014. ArcMap 10.3, Redlands, California.

ESRI, E.S.R.I., 2016. ArcMap 10.4.1., Redlands, California.

ESRI, E.S.R.I., 2018. ArcGIS Desktop 10.5.1., Redlands, California.

European Commission, 2000. Remote Sensing Applications for Forest Health Status Assessment. Second Edition. In, European Union scheme on the protection of forests against atmospheric pollution. Office for Official Publications of the European Communities, Luxembourg, p. 216.

European-Space-Imaging, 2018a. WorldView-3. Data Sheet. In. European Space Imaging, Munich, https://www.euspaceimaging.com/wp-content/uploads/2018/06/EUSI-WorldView-3-2018.pdf (accessed 05.06.2020)

European-Space-Imaging, 2018b. WorldView-4. Data Sheet. In. European Space Imaging, Munich, https://www.euspaceimaging.com/wp-content/uploads/2018/06/EUSI_WorldView-4.pdf (accessed 05.06.2020)

FAO, Food and Agriculture Organisation of the United Nations, 2018. The State of the World's Forests 2018 - Forest pathways to sustainable development. Licence: CC BY-NC-SA 3.0 IGO. Rome, p. 118.

Farrell, S.L., Collier, B.A., Skow, K.L., Long, A.M., Campomizzi, A.J., Morrison, M.L., Hays, K.B., Wilkins, R.N., 2013. Using LiDAR-derived vegetation metrics for high-resolution, species distribution models for conservation planning. Ecosphere 4(3), 18.

Fassnacht, F., Koch, B., 2012. Review on forestry oriented multi-angular remote sensing techniques. International Forestry Review 14, 285-298.

Fassnacht, F.E., 2013. Assessing the potential of imaging spectroscopy data to map tree species composition and bark beetle-related tree mortality. In, Chair of Remote Sensing and Landscape Information Systems. Faculty of Environment and Natural Resources, Albert-Ludwigs-University, Freiburg, p. 99.

Fassnacht, F.E., Latifi, H., Ghosh, A., Joshi, P.K., Koch, B., 2014. Assessing the potential of hyperspectral imagery to map bark beetle-induced tree mortality. Remote Sensing of Environment 140, 533-548.

Fassnacht, F.E., Latifi, H., Koch, B., 2012. An angular vegetation index for imaging spectroscopy data—Preliminary results on forest damage detection in the Bavarian National Park, Germany. International Journal of Applied Earth Observation and Geoinformation 19, 308-321.

Fayt, P., 2003. Population ecology of the Three-toed Woodpecker under varying food supplies. In, PhD Dissertations in Biology. University of Joensuu, p. 126.

Felton, A., Löfroth, T., Angelstam, P., Gustafsson, L., Hjältén, J., Felton, A.M., Simonsson, P., Dahlberg, A., Lindbladh, M., Svensson, J., Nilsson, U., Lodin, I., Hedwall, P.O., Sténs, A., Lämås, T., Brunet, J., Kalén, C., Kriström, B., Gemmel, P., Ranius, T., 2019. Keeping pace with forestry: Multi-scale conservation in a changing production forest matrix. Ambio, p. 15.

Freese, A., Benes, J., Bolz, R., Cizek, O., Dolek, M., Geyer, A., Gros, P., Konvicka, M., Liegl, A., Stettmer, C., 2006. Habitat use of the endangered butterfly Euphydryas maturna and forestry in Central Europe. Animal Conservation 9, 388-397.

Frey, J., 2019. Evaluating close range remote sensing techniques for the retention of biodiversity-related forest structures. In, Chair of Remote Sensing and Landscape Information Systems Albert-Ludwigs-Universität Freiburg Freiburg, p. 103.

Frey, J., Joa, B., Schraml, U., Koch, B., 2019. Same Viewpoint Different Perspectives—A Comparison of Expert Ratings with a TLS Derived Forest Stand Structural Complexity Index. . Remote Sensing 11, 17.

Froidevaux, J.S.P., Zellweger, F., Bollmann, K., Jones, G., Obrist, M.K., 2016. From field surveys to LiDAR: Shining a light on how bats respond to forest structure. Remote Sensing of Environment 175, 242-250.

Ganz, S., 2016. Automatische Klassifizierung von Nadelbäumen basierend auf Luftbildern. Automatic classification of coniferous tree genera based on aerial images. In, Fakultät für Umwelt und Natürliche Ressourcen. Albert-Ludwigs-Universität Freiburg, Freiburg, p. 84.

Ganz, S., Käber, Y., Adler, P., 2019. Measuring Tree Height with Remote Sensing—A Comparison of Photogrammetric and LiDAR Data with Different Field Measurements. Forests 10, 14.

Garbarino, M., E., B.M., E., L., Nagel, T.A., Dukić, V., Govedar, Z., Motta, R., 2012. Gap disturbances and regeneration patterns in a Bosnian old-growth forest: a multispectral remote sensing and ground-based approach. Annals of Forest Science 69, 617-625.

Gaulton, R., Malthus, T., J. , 2008. LiDAR mapping of canopy gaps in continuous cover forests; a comparison of a canopy height model and point cloud based techniques. SilviLaser 2008, Edinburgh, UK, 407-416.

GEOSYSTEMS GmbH, I.C., 2014. Stereoauswertung mit Erdas extensions für ArcGIS®. Germering, http://www.geosystems.de/produkte/pdf/SAfAG_Flyer_dt_10-2014.pdf (accessed on 2.11.2015)

Getzin, S., Nuske, R.S., Wiegand, K., 2014. Using Unmanned Aerial Vehicles (UAV) to Quantify Spatial Gap Patterns in Forests. Remote Sensing 6, 6988-7004.

Getzin, S., Wiegand, K., Schöning, I., 2012. Assessing biodiversity in forests using very high-resolution images and unmanned aerial vehicles. Methods in Ecology and Evolution 3, 397–404.

Ginzler, C., Hobi, M.L., 2015. Countrywide Stereo-Image Matching for Updating Digital Surface Models in the Framework of the Swiss National Forest Inventory. Remote Sensing, 4343-4370.

Ginzler, C., Hobi, M.L., 2016. Das aktuelle Vegetationshöhenmodell der Schweiz: spezifische Anwendungen im Waldbereich. Schweizerische Zeitschrift fur Forstwesen 167, 128-135.

Ginzler, C., Price, B., Bösch, R., Fischer, C., Hobi, M.L., Psomas, A., Rehush, N., Wang, Z., Waser, L.T., 2019. Area-Wide Products. In: Fischer, C., Traub, B. (Eds.), Swiss National Forest Inventory - Methods and Models of the Fourth Assessment. Springer, Cham, pp 125-142.

Gitelson, A.A., Kaufman, Y., Merzlyak, M.N., 1996. Use of green channel in remote sensing of global vegetation from EOS-MODIS. Remote Sensing of Environment 58, 289–298.

Głowaciński, Z., Makomaska-Juchiewicz, M., Połczyńska-Konior, G. (Eds.), 2002. Red List of Threatened Animals in Poland. Polish Academy of Sciences, Institude of Nature Conservation, Cracow.

Goggans, R., Dixon, R.D., Seminara, L.C., 1989. Habitat Use by Three-toed and Black-backed Woodpeckers: Deschutes National Forest, Oregon. Technical Report #87-3-02. Oregon Department of Fish and Wildlife, Nongame Wildlife Program. USDA Deschutes National Forest, 1989. Available online: https://digital.osl.state.or.us/islandora/object/osl:18053 (accessed on 12 July 2018), p. 43.

Gosh, A., 2014. A framework for mapping tree species combining hyperspectral and LiDAR data: Role of selected classifiers and sensor across three spatial scales. International Journal of Applied Earth Observation and Geoinformation, 26, 49-63.

Graf, R.F., Mathys, L., Bollmann, K., 2009. Habitat assessment for forest dwelling species using LiDAR remote sensing: Capercaillie in the Alps. Forest Ecology and Management 257, 160-167.

Guisan, A., Thuiller, W., 2005. Predicting species distribution: offering more than simple habitat models. Ecology Letters 8, 993–1009.

Guisan, A., Thuiller, W., Zimmermann, N.E., 2017. Habitat Suitability and Distribution Models With Applications in R. Cambridge University Press, Cambridge.

Gustafsson, L., Baker, S.C., Bauhus, J., Beese, W.J., Brodie, A., Kouki, J., Lindenmayer, D.B., Lõhmus, A., Pastur, G.M., Messier, C., Neyland, M., Palik, B., Sverdrup-Thygeson, A., Volney, W.J.A., Wayne, A., Franklin, J.F., 2012. Retention Forestry to Maintain Multifunctional Forests: A World Perspective. BioScience 62, 633-645.

Hahn, K., Christensen, M., 2004. Dead Wood in European Forest Reserves - A reference for Forest Management. In, EFI Proceedings No. 51. Monitoring and Indicators of Forest Biodiversity in Europe - From Ideas to Operationality. European Forest Institue, pp. 181-191.

Hamdi, Z.M., Brandmeier, M., Straub, C., 2019. Forest Damage Assessment Using Deep Learning on High Resolution Remote Sensing Data. Remote Sensing 11.

Haralick, R., Shanmugam, K., Dinstein, I., 1973. Textural Features for Image Classification. IEEE Trans Syst Man Cybern SMC-3, 610-621.

Hastie, T., Tibshirani, R., Friedman, J., 2009. The Elements of Statistical Learning. Data Mining, Inference,and Prediction. Springer, Berlin.

Heinzel, J., Koch, B., 2012. Investigating multiple data sources for tree species classification in temperate forest and use for single tree delineation. International Journal of Applied Earth Observation and Geoinformation 18, 101-110.

Heinzel, J., Weinacker, H., Koch, B., 2008. Full automatic detection of tree species based on delineated single tree crowns - a data fusion approach for airborne laser scanning data and aerial photographs. In, SilviLaser, Edinburgh, UK, p. 10.

Hengl, T., 2006. Finding the right pixel size. Computers & Geosciences 32, 1283-1298.

Hernando, A., Tiede, D., Albrecht, F., Lang, S., 2012. Spatial and thematic assessment of object-based forest stand delineation using an OFA-matrix. International Journal of Applied Earth Observation and Geoinformation 19, 214-225.

Herrmann, S., Bauhus, J., 2010. Totholz - Bedeutung, Situation, Dynamik. In. Wald-und-Klima.net, p. 5. http://www.waldundklima.net/wald/totholz_bauhus_herrmann_20100126.php (accessed on 25.10.2019)

Heurich, M., 2008. Automatic recognition and measurement of single trees based on data from airborne laser scanning over the richly structured natural forests of the Bavarian Forest National Park. Forest Ecology and Management 255, 2416-2433.

Heurich, M., Fahse, L., Reinelt, A., 2001. Die Buchdruckermassenvermehrung im Nationalpark Bayerischer Wald. In: Waldentwicklung im Bergwald nach Windwurf und Borkenkäferbefall. Wissenschaftliche Schriftenreihe der Nationalparkverwaltung Bayerischer Wald 16.

Heurich, M., Krzystek, P., Polakowsky, F., Latifi, H., Krauss, A., Müller, J., 2015. Erste Waldinventur auf Basis von Lidardaten und digitalen Luftbildern im Nationalpark Bayerischer Wald. Forstliche Forschungsberichte München 214, 101-113.

Heurich, M., Ochs, T., Andresen, T., Schneider, T., 2010. Object-orientated image analysis for the semi-automatic detection of dead trees following a spruce bark beetle (Ips typographus) outbreak. European Journal of Forest Research 129, 313-324.

HEXAGON Geospatial, 2020. ERDAS IMAGINE. Copyright 1990~2019. All Rights Reserved. Intergraph Corporation.

HEXAGON Geospatial, 2014. ERDAS IMAGINE Help. XPro Semi-Global Matching. Intergraph Corporation. https://hexagongeospatial.fluidtopics.net/en/book#!book;uri=f2790e0ca81311531f1a57c6b7bc80b2;breadcrumb=23b983d2543add5a03fc94e16648eae7-b70c75349e3a9ef9f26c972ab994b6b6-572fc16c2299fb0cf9dea36da3f6df73-77e5f6815e5da847bab34f6d88a2efec-895bc642e4bd922f332936d584d19af7 (accessed on 02.11.2015)

Hijmans, J.R., 2020. raster: Geographic Data Analysis and Modeling. R package version 3.0-12. https://CRAN.R-project.org/package=raster (accessed on 12.02.2020)

Hijmans, R.J., van Etten, J., Cheng, J., Mattiuzzi, M., Sumner, M., Greenberg, J.A., Lamigueiro, O.P., Bevan, A., Racine, E.B., Shortridge, A., Ghosh, A., 2017. Package 'raster'. Geographic Data Analysis and Modeling. R package version 2.6-7, https://cran.r-project.org/web/packages/raster/raster.pdf (accessed on 18.02.18).

Hildebrandt, G., 1996. Fernerkundung und Luftbildmessung für Forstwirtschaft, Vegetationskartierung und Landschaftsökologie. Wichmann Verlag, Heidelberg, p. 676.

Hirzel, A.H., Le Lay, G., 2008. Habitat suitability modelling and niche theory. Review. Journal of Applied Ecology 45, 1372-1381.

Hobi, M.L., Commarmot, B., Ginzler, C., Bugmann, H., 2015. Gap pattern of the largest primeval beech forest of Europe revealed by remote sensing. Ecosphere, 1-15.

Hobi, M.L., Ginzler, C., 2012. Accuracy assessment of digital surface models based on WorldView-2 and ADS80 stereo remote sensing data. Sensors 12, 6347-6368.

Hofstetter, L., Arlettaz, R., Bollmann, K., Braunisch, V., 2015. Interchangeable sets of complementary habitat variables allow for flexible, site-adapted wildlife habitat management in forest ecosystems. Basic and Applied Ecology 500868, 14.

Hogstad, O., 1976. Sexual dimorphism and divergence in winter foraging behaviour of Three-toed woodpeckers *Picoides tridactylus*. Ibis 118, 41-50.

Hogstad, O., 1977. Seasonal Change in Intersexual Niche Differentiation of the Three-Toed Woodpecker *Picoides tridactylus*. Ornis Scandinavica (Scandinavian Journal of Ornithology) 8, 101-111.

Hohlfeld, F., 1997. Vergleichende ornithologische Untersuchungen in je sechs Bann- und Wirtschaftswäldern im Hinblick auf die Bedeutung des Totholzes für Vögel. In, Ornithologische Jahreshefte für Baden-Württemberg. Einstein, J., Hölzinger, J., Knötsch, G., Kroymann, B., Mahler, U., Opitz, H., Schmid, W., Freiburg, p. 127.

Holopainen, M., Vastaranta, M., Hyyppä, J., 2014. Outlook for the Next Generation's Precision Forestry in Finland. Forests 5, 7, 1682-1694.

Hölzinger, J., Mahler, U., 2001. Die Vögel Baden-Württembergs. Bd. 2 Nicht-Singvögel. 3 Pteroclididae (Flughühner) - Picidae (Spechte), p. 547.

Hosmer, D.H., Lemeshow, S., 2000. Applied logistic regression. John Wiley & Sons, New York, p. 375.

Hothorn, T., Hornik, K., Strobl, C., Zeileis, A., 2017. Package 'party'. A Laboratory for Recursive Partytioning. Package version 1.2-4. 2017. Available online: https://cran.r-project.org/web/packages/party/vignettes/party.pdf (accessed on 5.05. 2018).

Hothorn, T., Hornik, K., Zeileis, A., 2006. Unbiased Recursive Partitioning: A Conditional Inference Framework. Journal of Computational and Graphical Statistics 15, 651-674.

Hothorn, T.; Zeileis, A., 2015. Partykit: A modular toolkit for recursive partytioning in R. Reference Manual. Available online: https://cran.r-project.org/web/packages/partykit/partykit.pdf (accessed on 3.08.2015).

Hytteborn, H., Verwijst, T., 2013. Small-scale disturbance and stand structure dynamics in an old-growth Picea abies forest over 54 yr in central Sweden. Journal of Vegetation Science, 25, 100-112.

Imbeau, L., Desrochers, A., 2002. Area sensitivity and edge avoidance: the case of the Three-toed Woodpecker (Picoides tridactylus) in a managed forest. Forest Ecology and Management 164, 249-256.

Immitzer, M., Atzberger, C., 2014. Early detection of bark beetle infestation in Norway spruce (Picea abies, L.) using worldView-2 data. Photogrammetrie. Fernerkundung. Geoinformation 5, 351–367.

IPBES, 2019. Addendum: Summary for policymakers of the global assessment report on biodiversity and ecosystem services of the Intergovernmental Science-Policy Platform on Biodiversity and Ecosystem Services. In: Diaz, S., Settele, J., Brondizio, E. (Eds.), Report of the Plenary of the Intergovernmental Science-Policy Platform on Biodiversity and Ecosystem Services on the work of its seventh session. Intergovernmental Science-Policy Platform on Biodiversity and Ecosystem Services, Bonn: IPBES, p. 45.

Irons, J.R., Petersen, G.W., 1981. Texture transforms of remote sensing data. Remote Sensing of Environment 11, 359-370.

Isenburg, M., 2014. Rapid lasso - fast tools to catch reality. In: GmbH, R. (Ed.), GERMANY.

Izrailev, S., 2014. tictoc: Functions for timing R scripts, as well as implementations of Stack and List structures.. R package version 1.0., https://CRAN.R-project.org/package=tictoc (accessed 10.11.2019)

Jackson, R.D., Huete, A.R., 1991. Interpreting vegetation indices. Preventive veterinary medicine 11, 185-200.

Jayathunga, S., Owari, T., Tsuyuki, S., 2018. Analysis of forest structural complexity using airborne LiDAR data and aerial photography in a mixed conifer–broadleaf forest in northern Japan. Journal of Forest Research 29, 479–493.

Jiang, S., Yao, W., Heurich, M., 2019. Dead wood detection based on semantic segmentation of vhr aerial cir imagery using optimized fcn-densenet. ISPRS - International Archives of the Photogrammetry, Remote Sensing and Spatial Information Sciences XLII-2/W16, 127-133.

Johann, E., 2006. Historical development of nature-based forestry in Central Europe. In: Diaci, J. (Ed.), Nature-based forestry in central Europe. Alternatives to Industrial Forestry and Strict Preservation. Studia Forestalia Slovenica Nr. 126. Department of Forestry and Renewable Forest Resources - Biotechnical Faculty, Ljubljana, p. 167.

Jones, H.G., Vaughan, R.A., 2010. Remote Sensing of Vegetation. Principles, Techniques and Applications. Oxford University Press, p. 284.

Kajtoch, Ł., 2009. Występowanie dzięciołów: trójpalczastego Picoides tridactylus i białogrzbietego Dendrocopos leucotos w Beskidzie Wyspowym. Notatki Ornitologiczne 50, 85-96.

Kajtoch, Ł., Figarski, T., 2014. Stenotopowe gatunki dzięciołów jako wskaźnik pożądanych ilości drewna martwych i zamierających drzew w karpackich lasach. Studia i Materiały CEPL w Rogowie 16, 116-130.

Kajtoch, Ł., Figarski, T., Pełka, J., 2013a. The role of forest structural elements in determining the occurrence of two specialsit woodpecker species in the Carpathians, Poland. Ornis Fennica 90, 23-40.

Kajtoch, Ł., Skierczyński, M., Czeszczewik, D., 2013b. Dzięcioł trójpalczasty Picoides tridactylus. In: Zawadzka, D., Ciach, M., Figarski, T., Kajtoch, Ł., Rejt, Ł. (Eds.), Materiały do wyznaczania i określania stanu zachowania siedlisk ptasich w obszarach specjalnej ochrony ptaków Natura 2000. GDOŚ, Warszawa, pp. 87-92.

Kamińska, A., Lisiewicz, M., Stereńczak, K., Kraszewski, B., Sadkowski, R., 2018. Species-related single dead tree detection using multi-temporal ALS data and CIR imagery. Remote Sensing of Environment 219, 31-43.

Kangas, A., Astrup, R., Breidenbach, J., Fridman, J., Gobakken, T., Korhonen, K.T., Maltamo, M., Nilsson, M., Nord-Larsen, T., Næsset, E., Olsson, H., 2018. Remote sensing and forest inventories in Nordic countries – roadmap for the future. Scandinavian Journal of Forest Research 33, 397-412.

Kantola, T., Vastaranta, M., Yu, X., Lyytikainen-Saarenmaa, P., Holopainen, M., Talvitie, M., Kaasalainen, S., Solberg, S., Hyyppa, J., 2010. Classification of Defoliated Trees Using Tree-Level Airborne Laser Scanning Data Combined with Aerial Images. Remote Sensing 2, 2665-2679.

Kathke, S., Bruelheide, H., 2010. Gap dynamics in a near-natural spruce forest at Mt. Brocken, Germany. Forest Ecology and Management 259, 624-632.

Kautz, M., Dworschak, K., Gruppe, A., Schopf, R., 2011. Quantifying spatio-temporal dispersion of bark beetle infestations in epidemic and non-epidemic conditions. Forest Ecology and Management 262, 598-608.

Kelly, M., Blanchard, S.D., Kersten, E., Koy, K., 2011. Terrestrial Remotely Sensed Imagery in Support of Public Health: New Avenues of Research Using Object-Based Image Analysis. Remote Sensing 3, 2321-2345.

Kempeneers, P., Sedano, F., Seebach, L., Strobl, P., San-Miguel-Ayanz, J., 2012. Data Fusion of Different Spatial Resolution Remote Sensing Images Applied to Forest-Type Mapping. Geoscience and Remote Sensing, IEEE Transactions on 49, 4977-4986.

Kenneweg, H., 1970. Auswertung von Farbluftbildern für die Abgrenzung von Schädigungen an Waldbeständen. Bildmessung u. Luftbildwesen, 283-290.

Kirchhoefer, M., Schumacher, J., Adler, P., Kändler, G., 2017. Considerations towards a Novel Approach for Integrating Angle-Count Sampling Data in Remote Sensing Based Forest Inventories. Forests 8, 18.

Korhonen, L., Salas, C., Østgård, T., Lien, V., Gobakken, T., Næsset, E., 2016. Predicting the occurrence of large-diameter trees using airborne laser scanning. Canadian Journal of Forest Research 46, 461-469.

Kortmann, M., Heurich, M., Latifi, H., Rösner, S., Seidl, R., Müller, J., Thorn, S., 2018a. Forest structure following natural disturbances and early succession provides habitat for two avian flagship species, capercaillie (Tetrao urogallus) and hazel grouse (Tetrastes bonasia). Biological Conservation 226.

Kortmann, M., Hurst, J., Brinkmann, R., Heurich, M., Silveyra González, R., Müller, J., Thorn, S., 2018b. Beauty and the beast: how a bat utilizes forests shaped by outbreaks of an insect pest. Animal Conservation 21, 21-30.

Kotremba, C., 2014. Hochauflösende fernerkundliche Erfassung von Waldstrukturen im GIS am Beispiel der Kernzone "Quallgebiet der Wieslauter" im Pfälzerwald. AFZ-DerWald, 12-15.

Koukoulas, S., Blackburn, G.A., 2004. Quantifying the spatial properties of forest canopy gaps using LiDAR imagery and GIS. International Journal of Remote Sensing 25, 3049–3071.

Kratzer, R., Straub, F., Dorka, U., Pechacek, P., 2009. Totholzschwellenwertanalyse für den Dreizehenspecht (Picoides tridactylus) im Schwarzwald. Schriftenreihe Nationalpark Kalkalpen 10, 79-88.

Krzystek, P., Serebryanyk, A., Schnörr, C., Červenka, J., Heurich, M., 2020. Large-Scale Mapping of Tree Species and Dead Trees in Šumava National Park and Bavarian Forest National Park Using Lidar and Multispectral Imagery. Remote Sens. 2020, 12, 661. Remote Sensing 12, 22.

Kuhn, M., Johnson, K., 2013. Applied Predictive Modeling. © Springer Science+Business Media New York, p. 600.

Kuhn, M., Wing, J., Weston, S., Williams, A., Keefer, C., Engelhardt, A., Cooper, T., Mayer, Z., Kenkel, B., the R Core Team, Benesty, M., Lescarbeau, R., Ziem, A., Scrucca, L., 2015. Package 'caret'. Classification and Regression Training. Version 6.0–52. Reference Manual. https://cran.r-project.org/web/packages/caret/caret.pdf (accessed on 3.08.2015).

Kuhn, M., Wing, J., Weston, S., Williams, A., Keefer, C., Engelhardt, A., Cooper, T., Mayer, Z., Kenkel, B., the R Core Team, Benesty, M., Lescarbeau, R., Ziem, A., Scrucca, L., Tang, Y., Candan, C., Hunt, T., 2018. Package 'caret'. Classification and Regression Training. Version 6.0-79. Reference Manual. https://github.com/topepo/caret/ (accessed on 20.09.2019).

Lambeck, R.J., 1997. Focal species: a multi-species umbrella for nature conservation. Conservation biology : the journal of the Society for Conservation Biology, 849–856.

Lanaras, C., Baltsavias, E., Schindler, K., 2015. A Comparison and Combination of Methods for Co-Registration of Multi-Modal Images. In, 35th Asian Conference on Remote Sensing (ACRS 2014), Nay Pyi Taw, Myanmar, October 27-31, 2014. Curran, p. 746.

Landesamt für Geoinformation und Landentwicklung Baden-Württemberg, LGL, 2015a. ATKIS® - Amtliches Topographisch-Kartographisches Informationssystem. Stuttgart, http://www.lgl-bw.de/lgl-internet/opencms/de /05_Geoinformation/AAA/ATKIS/ (accessed on 30.10.2015).

Landesamt für Geoinformation und Landentwicklung Baden-Württemberg, LGL, 2015b. Digitale Geländemodelle (DGM). Stuttgart, https://www.lgl-bw.de/lgl-internet/opencms/de/05_Geoinformation /Geotopographie/Digitale_Gelaendemodelle/ (accessed on 30.10.2015).

Landesamt für Geoinformation und Landentwicklung Baden-Württemberg, LGL, 2015c. Geobasisdaten © www.lgl-bw.de Az.: 2851.9-1/19.

Landesamt für Geoinformation und Landentwicklung Baden-Württemberg, LGL, 2020a. ATKIS® - Amtliches Topographisch-Kartographisches Informationssystem. Stuttgart. https://www.lgl-bw.de/unsere-themen/ Geoinformation/AFIS-ALKIS-ATKIS/ATKIS/index.html (accessed on 03.01.2020)

Landesamt für Geoinformation und Landentwicklung Baden-Württemberg, LGL, 2020b. Geodaten. Stuttgart, https://www.lgl-bw.de/unsere-themen/Produkte/Geodaten (accessed on 03.01.2020)

Latifi, H., Heurich, M., Hartig, F., Müller, J., Krzystek, P., Jehl, H., Dech, S., 2016. Estimating over- and understorey canopy density of temperate mixed stands by airborne LiDAR data. Forestry: An International Journal of Forest Research 89, 69-81.

Lausch, A., Bannehr, L., Beckmann, M., Boehm, C., Feilhauer, H., Hacker, J.M., Heurich, M., Jung, A., Klenke, R., Neumann, C., Pause, M., Rocchini, D., Schaepman, M.E., Schmidtlein, S., Schulz, K., Selsam, P., Settele, J., Skidmore, A.K., Cord, A.F., 2016. Linking Earth Observation and taxonomic, structural and functional biodiversity: Local to ecosystem perspectives. Ecological indicators 70, 317-339.

Lausch, A., Fahse, L., Heurich, M., 2011. Factors affecting the spatio-temporal dispersion of Ips typographus (L.) in Bavarian Forest National Park: A long-term quantitative landscape-level analysis. Forest Ecology and Management 261, 233-245.

Lausch, A., Heurich, M., Gordalla, D., Dobner, H.-J., Gwillym-Margianto, S., Salbach, C., 2013. Forecasting potential bark beetle outbreaks based on spruce forest vitality using hyperspectral remote-sensing techniques at different scales. Forest Ecology and Management 308, 76-89.

Law, K., 1980. Textured Image Segmentation. Dissertation. 80 L 425, University of Southern California, Los Angeles, USA, p. 178.

Leberger, R., Rosa, I.M.D., Guerra, C.A., Wolf, F., Pereira, H.M., 2020. Global patterns of forest loss across IUCN categories of protected areas. Biological Conservation 241, 108299.

Lesak, A.A., Radeloff, V.C., Hawbaker, T.J., Pidgeon, A.M., Gobakken, T., Contrucci, K., 2011. Modeling forest songbird species richness using LiDAR-derived measures of forest structure Remote Sensing of Environment 115, 2823–2835.

Lindberg, E., Roberge, J.-M., Johannsson, T., Hjältén, J., 2015. Can Airborne Laser Scanning (ALS) and Forest Estimates Derived from Satellite Images Be Used to Predict Abundance and Species Richness of Birds and Beetles in Boreal Forest? Remote Sensing 7, 4233-4252.

Lindenmayer, D.B., Franklin, J.F., 2002. Conserving Forest Biodiversity: A Comprehensive Multiscaled Approach., Washington.

Lindenmayer, D.B., Franklin, J.F., Fischer, J., 2006. General management principles and a checklist of strategies to guide forest biodiversity conservation. Biological Conservation 131, 433-445.

Lindenmayer, D.B., Margules, C.R., Botkin, D.B., 2000. Indicators of Biodiversity for Ecologically Sustainable Forest Management. Conserv Biology 14, 941–950.

Liu, Z., Peng, C., Timothy, W., Candau, J.-N., Desrochers, A., Kneeshaw, D., 2018. Application of machine-learning methods in forest ecology: Recent progress and future challenges. Environmental Reviews 26.

Magg, N., Ballenthien, E., Braunisch, V., 2019. Faunal surrogates for forest species conservation: A systematic niche-based approach. Ecological Indicators 102, 65-75.

Magg, N., Müller, J., Heibl, C., Hackländer, K., Wölfl, S., Wölfl, M., Bufka, L., Cervený, J., Heurich, M., 2015. Habitat availability is not limiting the distribution of the Bohemian–Bavarian lynx Lynx lynx population. Oryx, 1-11.

Maltamo, M., Kallio, E., Bollandsås, O.M., Næsset, E., Gobakken, T., Pesonen, A., 2014. Assessing Dead Wood by Airborne Laser Scanning. In: Maltamo, M., Næsset, E., Vauhkonen, J. (Eds.), Forestry Applications of Airborne Laser Scanning: Concepts and Case Studies. Springer Netherlands, Dordrecht, pp. 375-395.

Mantel, K., 1990. Wald und Forst in der Geschichte : ein Lehr- und Handbuch. Mit e. Vorw. von Helmut Brandl. Hannover: Schaper, Alfeld.

Marchi, N., Pirotti, F., Lingua, E., 2018. Airborne and Terrestrial Laser Scanning Data for the Assessment of Standing and Lying Deadwood: Current Situation and New Perspectives. Remote Sensing 10.

Martinuzzi, S., Vierling, L.A., Gould, W.A., Falkowski, M.J., Evans, J.S., Hudak, A.T., Vierling, K.T., 2009. Mapping snags and understory shrubs for a LiDAR-based assessment of wildlife habitat suitability. Remote Sensing of Environment 113, 2533-2546.

Mathow, T., 2015. Personal communication. ForstBW. Regierungspräsidium Freiburg, Forstdirektion. Referat 84 Forsteinrichtung und Forstliche Geoinformation, Freiburg.

Matysek, M., Kajtoch, Ł., 2010a. Dzięcioły białogrzbiety Dendrocopos leucotos i dzięcioł trójpalczasty Picoides tridactylus w Beskidzie Średnim. Ornis Polonica 3, 230-234.

Matysek, M., Kajtoch, Ł., 2010b. Wystepowanie dzieciołów: trójpalczastego Picoides tridactylus i bialogrzbietego Dendrocopos leucotos w Beskidzie Wyspowym. Ornis Polonica 51, 230-234.

McElhinny, C., Gibbons, P., Brack, C., Bauhus, J., 2005. Forest and woodland stand structural complexity: Its definition and measurement. Forest ecology and management 218, 1-24.

Meddens, A.J.H., Hicke, J.A., Vierling, L.A., 2011. Evaluating the potential of multispectral imagery to map multiple stages of tree mortality. Remote Sensing of Environment 115, 1632-1642.

Messier, C., Puettmann, J.K., Coates, D.K., 2015. Managing Forests as Complex Adaptive Systems. Building Resilience to the Challenge of Global Change. Routledge.

Meyer, P., Janda, P., Mikoláš, M., Trotsiuk, V., Krumm, F., Mrhalová, H., Synek, M., Lábusová, J., Kraus, D., Brandes, J., Svoboda, M., 2017. A matter of time: self-regulated tree regeneration in a natural Norway spruce (Picea abies) forest at Mt. Brocken, Germany. European Journal of Forest Research 136, 907-921.

Mikusiński, G., Gromadzki, M., Chylarecki, P., 2001. Woodpeckers as Indicators of Forest Bird Diversity. Conservation Biology 15, 208-217.

Mikusiński, G., Roberge, J., Fuller, R.E., 2018. Ecology and Conservation of Forest Birds (Ecology, Biodiversity and Conservation). Cambridge University Press, Cambridge.

Mitchell, M., Wilson, R., Twedt, D., Mini, A., James, J., 2016. Object-Based Forest Classification to Facilitate Landscape-Scale Conservation in the Mississippi Alluvial Valley. Remote Sensing Applications: Society and Environment 4, 55-60.

Mollet, P., Bollmann, K., Braunisch, V., Arlettaz, R., 2018. Subalpine Coniferous Forests of Europe. Avian Communities in European High-Altitude Woodlands. In: Mikusiński, G., Roberge, J.M., Fuller, R. (Eds.), Ecology and Conservation of Forest Birds. Cambridge University Press, Cambridge, p. 566.

Moosmayer, H.U., 1972. Ausscheidung von Waldschutzgebieten: hier: Schonwald "Kleemiss" im Forstbezirk Klosterreichenbach. In: Ministerium für Ernährung, L., Weinbau und Forsten Baden-Württemberg (Ed.), V 794.2/1 - 4, Stuttgart, p. 2.

Müller, D., Schröder, B., Müller, J., 2009. Modelling habitat selection of the cryptic Hazel Grouse Bonasa bonasia in a montane forest. J Ornithol 150, 717–732.

Müller, J., Brandl, R., 2009. Assessing biodiversity by remote sensing in mountainous terrain: the potential of LiDAR to predict forest beetle assemblages. Journal of Applied Ecology 46, 897-905.

Müller, J., Bußler, H., Bense, U., Brustel, H., Flechtner, G., Fowles, A., Kahlen, M., Möller, G., Mühle, H., Schmidl, J., Zabransky, P., 2005. Urwald relict species – Saproxylic beetles indicating structural qualities and habitat tradition. Waldoekologie-online. AFSV Naturnähe-Indikatoren und Naturwaldreservatsforschung. 2, 106 - 113.

Müller, J., Bütler, R., 2010. A review of habitat thresholds for dead wood: a baseline for management recommendations in European forests. European Journal of Forest Research 129, 981-992.

Müller, J., Stadler, J., Brandl, R., 2010. Composition versus physiognomy of vegetation as predictors of bird assemblages: The role of lidar. Remote Sensing of Environment 114, 490–495.

Müller, K.H., Wagner, S., 2003. Störungslücken in Fichtenbeständen des Erzgebirges: Initiale eines Waldumbaues. Forst und Holz, 58. Jahrgang 13/14, 407-411.

Nagel, T.A., Svoboda, M., Rugani, T., Diaci, J., 2009. Gap regeneration and replacement patterns in an old-growth Fagus–Abies forest of Bosnia–Herzegovina. Plant Ecology 208, 307-318.

Nicodemus, F.E., Richmond, J.C., Hsia, J.J., Ginsberg, J.W., Limperis, T., 1977. Geometrical Considerations and Nomenclature for Reflectance. NBS Monogr., No. 160. In. National Bureau of Standards, U.S., Department of Commerce, Washington, D.C., p. 52.

Noss, R.F., 1990. Indicators for Monitoring of Biodiversity. A Hierarchical Approach. Conserv Biology 4, 355-364.

Noss, R.F., 1999. Assessing and monitoring forest biodiversity: a suggested framework and indicators. Forest Ecology and Management 115, 135-146.

O'Shea, K., Nash, R., 2015. An Introduction to Convolutional Neural Networks. ArXiv e-prints: arXiv:1511.08458v2 [cs.NE] (accessed on 20.01.2020)

Nasa Earth Observatory, 2014. Observing in Infrared. In, NASA Goddard Space Flight Centre. https://earthobservatory.nasa.gov/features/FalseColor/page5.php (accessed on 29.03.2020)

Økland, B., Bakke, A., Hågvar, S., Kvamme, T., 1996. What factors influence the diversity of saproxylic beetles? A multiscaled study from a spruce forest in southern Norway. Biodiversity & Conservation 5, 75-100.

Olchowik, J., Hilszczanska, D., Bzdyk, R., Studnicki, M., Malewski, T., Borowski, Z., 2019. Effect of Deadwood on Ectomycorrhizal Colonisation of Old-Growth Oak Forests. Forests 10, 480.

Ortiz, S.M., Breidenbach, J., Kändler, G., 2013. Early Detection of Bark Beetle Green Attack Using TerraSAR-X and RapidEye Data. Remote Sensing 5, 1912-1931.

Paillet, Y., Berges, L., Hjalten, J., Odor, P., Avon, C., Bernhardt-Romermann, M., Bijlsma, R.J., De Bruyn, L., Fuhr, M., Grandin, U., Kanka, R., Lundin, L., Luque, S., Magura, T., Matesanz, S., Meszaros, I., Sebastia, M.T., Schmidt, W., Standovar, T., Tothmeresz, B., Uotila, A., Valladares, F., Vellak, K., Virtanen, R., 2010. Biodiversity differences between managed and unmanaged forests: meta-analysis of species richness in Europe. Conservation biology : the journal of the Society for Conservation Biology 24, 101-112.

Pakkala, T., Hanski, I., Tomppo, E., 2002. Spatial Ecology of the Three-Toed Woodpecker in Managed Forest Landscapes. Silva Fennica 36, 279-288.

Paoletti, M.E., Haut, J.M., Plaza, J., Plaza, A., 2019. Deep learning classifiers for hyperspectral imaging: A review. ISPRS Journal of Photogrammetry and Remote Sensing 158, 279-317.

Pasher, J., King, D.J., 2009. Mapping dead wood distribution in a temperate hardwood forest using high resolution airborne imagery. Forest Ecology and Management 258, 1536-1548.

Patriquin, K., J., Barclay, R.M.R., 2003. Foraging by bats in cleared, thinned and unharvested boreal forest Journal of Applied Ecology 40, 646-657.

Pechacek, P., 2004. Spacing behavior of Eurasian Three-toed Woodpeckers *(Picoides tridactylus)* during the breeding season in Germany. The Auk 121, 58-67.

Pechacek, P., 2006. Breeding performance, natal dispersal, and nest site fidelity of the three-toed woodpecker in the German Alps. Ann. Zool. Fennici 43, 165-176.

Pechacek, P., d'Oleire-Oltmanns, W., 2004. Habitat use of the three-toed woodpecker in central Europe during the breeding period. Biological Conservation 116, 333-341.

Pechacek, P., Krištín, A., 1993. Nahrung der Spechte im Nationalpark Berchtesgaden. Vogelwelt 114, 165-177.

Pechacek, P., Krištín, A., 1996. Zur Ernährung und Nahrungsokologie des Dreizehenspechts Picoides tridactylus während der Nestlingsperiode. Der Ornithologische Beobachter 93, 259-266.

Pechacek, P., Krištín, A., 2004. Comparative diets of adult and young Threetoed Woodpeckers in a european alpine forest community. Journal of Wildlife Management 68, 683-693.

Pekkarinen, A., Seebach, L., Strobl, P., 2009. Pan-European forest/non-forest mapping with Landsat ETM plus and CORINE Land Cover 2000 data. ISPRS Journal of Photogrammetry and Remote Sensing 64, 171-183.

Persson, Å., Holmgren, J., Söderman, U., Olsson, H., 2004. Tree species classification of individual trees in Sweden by combining high resolution laser data with high resolution near-infrared digital images. International Archives of Photogrammetry, Remote Sensing and Spatial InformationSciences 36 - 8/W2, 204-207.

Petersen, M., 2015. Influence of Different Aerial Datasets on the Characterisation of Vertical and Horizontal Forest Stand Structure. In, Chair of Remote Sensing and Landscape Information Systems. Faculty of Environment and Natural Resources. . Albert-Ludwigs Universiy, Freiburg, p. 65.

Pfeifer, M., Lefebvre, V., Peres, C., Banks-Leite, C., Wearn, O., Marsh, C., Butchart, S., Arroyo-Rodríguez, V., Barlow, J., Cerezo Blandón, A., Cisneros, L., D'Cruze, N., Faria, D., Hadley, A., Harris, S.M., Klingbeil, B., Kormann, U., Lens, L., Medina Rangel, G., Ewers, R., 2017. Creation of forest edges has a global impact on forest vertebrates. Nature 551.

Piermattei, L., Marty, M., Ginzler, C., Pöchtrager, M., Karel, W., Ressl, C., Pfeifer, N., Hollaus, M., 2019. Pléiades satellite images for deriving forest metrics in the Alpine region. International Journal of Applied Earth Observation and Geoinformation 80, 240-256.

Pluto-Kossakowska, J., Osinska-Skotak, K., Stereńczak, K., 2017. Determining the spatial resolution of multispectral satellite images optimal to detect dead trees in forest areas. Sylwan 161, 395-404.

Polewski, P., Yao, W., Heurich, M., Krzystek, P., Stilla, U., 2014. Detection of fallen trees in ALS point clouds by learning the Normalized Cut similarity function from simulated samples. ISPRS Annals of Photogrammetry, Remote Sensing and Spatial Information Sciences II-3, 111-118.

Polewski, P., Yao, W., Heurich, M., Krzystek, P., Stilla, U., 2015a. Active learning approach to detecting standing dead trees from ALS point clouds combined with aerial infrared imagery. In: (CVF), C.V.F. (Ed.), CVPR Workshop, Boston, pp. 10-18.

Polewski, P., Yao, W., Heurich, M., Krzystek, P., Stilla, U., 2015b. Combining Active and Semisupervised Learning of Remote Sensing Data Within a Renyi Entropy Regularization Framework. IEEE Journal of Selected Topics in Applied Earth Observations and Remote Sensing.

Polewski, P., Yao, W., Heurich, M., Krzystek, P., Stilla, U., 2015c. Detection of single standing dead trees from aerial color infrared imagery by segmentation with shape and intensity priors ISPRS Annals of the Photogrammetry, Remote Sensing and Spatial Information Sciences Volume II-3/W4, 2015 PIA15+HRIGI15 - Joint ISPRS conference 2015, 25-27 March 2015, Munich, Germany, 181-188.

Pugacewicz, E., 2011. Ocena liczebności dzięcioła białogrzbietego *Dendrocopos leucotos* i dzięcioła trójpalczastego *Picoides tridactylus* na powierzchni fizjograficznej w Puszczy Białowieskiej metodą aktywnej penetracji terenu. Dubelt 3, 45-75.

Qinghong, L., Hytteborn, H., 1991. Gap Structure, Disturbance and Regeneration in a Primeval Picea abies Forest. Journal of Vegetation Science, 2, 391-402.

R Core Team, 2019. R: A language and environment for statistical computing. R Foundation for Statistical Computing. In. R Foundation for Statistical Computing, Vienna, Austria.

Rall, H., Martin, K., 2002. Luftbildauswertung zur Waldentwicklung im Nationalpark Bayerischer Wald 2001-Ein neues Verfahren und seine Ergebnisse zur Totholzkartierung. In, Berichte aus dem Nationalpark. Nationalparkverwaltung Bayerischer Wald, Grafenau, p. 21.

Rechsteiner, C., Zellweger, Z., Gerber, A., Breiner, F.T., Bollmann, K., 2017. Remotely sensed forest habitat structures improve regional species conservation. Remote Sensing in Ecology and Conservation, 1-12.

Regnery, B., Couvet, D., Kubarek, L., Julien, J.-F., Kerbiriou, C., 2013. Tree microhabitats as indicators of bird and bat communities in Mediterranean forests. Ecological Indicators 34, 221-230.

Reitberger, J., Krzystek, P., Stilla, U., 2008. Analysis of full waveform LIDAR data for the classification of deciduous and coniferous trees. International Journal of Remote Sensing 29, 1407-1431.

Roberge, J.-M., Angelstam, P., Villard, M.-A., 2008. Specialised woodpeckers and naturalness in hemiboreal forests – Deriving quantitative targets for conservation planning. Biological Conservation 141, 997–1012.

Romero-Calcerrada, R., Luque, S., 2006. Habitat quality assessment using Weights-of-Evidence based GIS modelling: The case of Picoides tridactylus as species indicator of the biodiversity value of the Finnish forest. Ecological Modelling 196, 62-76.

Rossiter, D.G., 2014. Technical Note: Statistical methods for accuracy assesment of classified thematic maps. In, Enschede (NL): International Institute for Geo-information Science & Earth Observation (ITC).

Rothermel, M., Wenzel, K., Fritsch, D., Haala, N., 2012. Sure: Photogrammetric surface reconstruction from imagery. Proceedings In, LC3D Workshop, Berlin

RStudio, Team., 2016. RStudio: Integrated Development for R. Version 1.0.143. RStudio, Inc. PBC, Boston, MA. http://www.rstudio.com/

Rugani, T., Diaci, J., Hladnik, D., 2013. Gap dynamics and structure of two old-growth beech forest remnants in Slovenia. PloS one 8, e52641.

Runkel, V., 2008. Mikrohabitatnutzung syntoper Waldfledermäuse. Ein Vergleich der genutzten Strukturen in anthropogen geformten Waldbiotopen Mitteleuropas. In, Der Naturwissenschaftlichen Fakultät Friedrich-Alexander-Universität Erlangen-Nürnberg, Erlangen-Nürnberg, p. 167.

Runkle, J.R., 1981. Gap Regeneration in Some Old-growth Forests of the Eastern United States. Ecology 62, 1041-1051.

Russo, D., Cistronec, L., Jones, G., 2007. Emergence time in forest bats: the influence of canopy closure. Acta oecologica 31, 119-126.

Saari, L., Mikusinski, G., 1996. Population fluctuations of woodpecker species on the Baltic island of Aasla, SW Finland. Ornis Fennica 73, 168-178.

Sarabandi, P., Yamazaki, F., Matsuoka, M., Kiremidjian, A., 2004. Shadow Detection and Radiometric Restoration in Satellite High Resolution Images. In, Geoscience and Remote Sensing Symposium, 2004. IGARSS '04. Proceedings. IEEE International, Anchorage, Alaska, pp. 3744-3747.

Säynäjoki, R., Packalén, P., Maltamo, M., Vehmas, M., Eerikäinen, K., 2008. Detection of Aspens Using High Resolution Aerial Laser Scanning Data and Digital Aerial Images. Sensors 8, 5037-5054.

Schaber-Schoor, G., 2010. Fachliche Anforderungen, Ziele und Handlungsansätze verschiedener Alt- und Totholzkonzepte. AFZ-Der Wald 65. Jahrg., 8-9.

Schaber-Schoor, G.E., Betz, B., Vonarb, S., Wirth, K., 2015. Gesamtkonzeption Waldnaturschutz ForstBW. In: ForstBW (Ed.). Landesbetrieb ForstBW, Stuttgart, p. 60.

Scherzinger, W., 1996. Naturschutz im Wald: Qualitätsziele einer dynamischen Waldentwicklung. Ulmer, Stuttgart, p. 447.

Scherzinger, W., 2006. Reaktionen der Vogelwelt auf den großflächigen Bestandeszusammenbruch des montanen Nadelwaldes im Inneren Bayerischen Wald. Vogelwelt 127, 209 – 263.

Schiewe, J., 2012. Segmentation of high-resolution remotely sensed data - Concepts, applications and problems. International Archives of Photogrammetry and Remote Sensing 34.

Schliemann, S.A., Bockheim, J.G., 2011. Methods for studying treefall gaps: A review. Forest Ecology and Management 261, 1143-1151.

Schuck, A., Meyer, P., Menke, N., Lier, M., M., L., 2004. Forest biodiversity indicator: dead wood-a proposed approach towards operationalising the MCPFE indicator. In: M., M. (Ed.), EFI Proceedings 51. Monitoring and Indicators of Forest Biodiversity in Europe - From Ideas to Operationality. EFI, Joensuu, pp. 49-77.

Schumacher, J., Rattay, M., Kirchhöfer, M., Adler, P., Kändler, G., 2019. Combination of Multi-Temporal Sentinel 2 Images and Aerial Image Based Canopy Height Models for Timber Volume Modelling. Forests 10, 19.

Seebach, L., 2013. Deriving harmonised forest information in Europe using remote sensing methods. Potentials and limitations for further applications., 141.

Seibold, S., Brandl, R., Buse, J., Hothorn, T., Schmidl, J., Thorn, S., Müller, J., 2014 Association of extinction risk of saproxylic beetles with ecological degradation of forests in Europe. Conserv Biology 0, 1-9.

Seidl, R., Müller, J., Hothorn, T., Bässler, C., Heurich, M., Kautz, M., 2016. Small beetle, large-scale drivers: how regional and landscape factors affect outbreaks of the European spruce bark beetle. Journal of Applied Ecology 53, 530-540.

Senf, C., R., S., 2017. Natural disturbances are spatially diverse but temporally synchronized across temperate forest landscapes in Europe. Glob Change Biology, 1-11.

Senitza, E., Gutzinger, R., 2010. Kartierung der Spechte und Eulen im Nationalpark Hohe Tauern Tirol. Nationalparkverwaltung Tirol, Nationalpark Hohe Tauern.

Shahtahmassebi, A., Yang, N., Wang, K., Moore, N., Shen, Z., 2013. Review of shadow detection and de-shadowing methods in remote sensing. Chin. Geogr. Sci. 23, 403–420.

Sierro, A., Arlettaz, R., Naef-Daenzer, B., Strebel, S., Zbinden, N., 2001. Habitat use and foraging ecology of the nightjar (Caprimulgus europaeus) in the Swiss Alps: towards a conservation scheme. Biological Conservation 98, 325-331.

Silleos, G., Alexandridis, T., Gitas, I., Perakis, K., 2006. Vegetation indices: Advances made in biomass estimation and vegetation monitoring in the last 30 years.

Smith, G.F., Gittings, T., Wilson, M., French, L., Oxbrough, A., O'Donoghue, S., O'Halloran, J., Kelly, D.L., Mitchell, F.J.G., Kelly, T., Iremonger, S., McKee, A.-M., Giller, P., 2008. Identifying practical indicators of biodiversity for stand-level management of plantation forests. Biodiversity and Conservation 17, 991-1015.

Stehman, S.V., Czaplewski, R.L., 1998. Design and Analysis for Thematic Map Accuracy Assessment: Fundamental Principles. Remote Sensing Of Environment 64, 331-344

Stepper, C., Straub, C., Pretzsch, H., 2014. Assessing height changes in a highly structured forest using regularly acquired aerial image data.

Stereńczak, K., Kraszewski, B., Mielcarek, M., Piasecka, Z., 2017. Inventory of standing dead trees in the surroundings of communication routes – The contribution of remote sensing to potential risk assessments. Forest Ecology and Management, 76-91.

Stereńczak, K., Kraszewski, B., Mielcarek, M., Piasecka, Ż., 2017. Inventory of standing dead trees in the surroundings of communication routes – The contribution of remote sensing to potential risk assessments. Forest Ecology and Management 402, 76-91.

Stighäll, K., Roberge, J.-M., Andersson, K., Angelstam, P., 2011. Usefulness of biophysical proxy data for modelling habitat of an endangered forest species: The white-backed woodpecker Dendrocopos leucotos. Scandinavian Journal of Forest Research 26, 576-585.

Story, M., Congalton, R.G., 1986. Accuracy assessment: a user's perspective. Photogrammetric Engineering and Remote Sensing 52, 397-399.

Straub, C., Stepper, C., Seitz, R., Waser, L.T., 2013. Potential of UltraCamX stereo images for estimating timber volume and basal area at the plot level in mixed European forests. Canadian Journal of Forest Research 43, 731-741.

Suchant, R., Braunisch, V., Erlacher, J., 2009. Aktionsplan Auerhuhn. Kurzfassung. In: (FVA), F.V.-u.F.B.-W. (Ed.), Freiburg, p. 14.

Südbeck, P., 2005. Artsteckbriefe. Dreizehenspecht. In: Südbeck, P. (Ed.), Methodenstandards zur Erfassung der Brutvögel Deutschlands. . Mugler Druck-Service GmbH, Radolfzell, pp. 462-463.

Südbeck, P., Bauer, H.-G., Boschert, M., Boye, P., Knief, W., Vögel), N.G.R.L., 2007. Rote Liste der Brutvögel Deutschlands. 4. Fassung. Berichte zum Vogelschutz 44.

R Core Team, 2017. R: A language and environment for statistical computing. R Foundation for Statistical Computing. In. R Foundation for Statistical Computing, Vienna, Austria.

Thibaud, E., Petitpierre, B., Broennimann, O., Davison, A.C., Guisan, A., 2014. Measuring the relative effect of factors affecting species distribution model predictions. Methods in Ecology and Evolution 5, 947-955.

Thiele, C., 2019. cutpointr: Determine and Evaluate Optimal Cutpoints in Binary Classification Tasks. R package version 1.0.1., https://CRAN.R-project.org/package=cutpointr (accessed on 05.12.2020).

Thomas, J.W., Anderson, R.G., Black, H.J., Bull, E.L., Canutt, P.R., Carter, B.E., Cromack, K.J., Hall, F.C., Martin, R.E., Maser, C., Miller, R.J., Pedersen, R.J., Rodiek, J.E., Scherzinger, R.J., Wick, H.L., Williams, J.T., 1979. Wildlife habitats in managed forests--the Blue Mountains of Oregon and Washington. Agriculture Handbook No. 553. U.S. Department of Agriculture. Forest Service.

Thompson, I.D., Angelstam, P., 1999. Special species. In: Hunter, M.L. (Ed.), Maintaining Biodiversity in Forest Ecosystems. Cambridge University Press, Cambridge, pp. 434–459.

Thorn, S., Müller, J., Leverkus, A.B., 2019. Preventing European forest diebacks. Science 365 (6460):.

Thüringer Landesamt für Bodenmanagement und Geoinformation, TLBG, 2020. Digitale Oberflächenmodelle (DOM), Freistaat Thüringen, https://www.thueringen.de/th9/tlbg/geoinformation/3d-informationen/dom/index.aspx (accessed on 02.07.2020).

Tillon, L., Bouget, C., Aulagnier, S., Paillet, Y., 2016. How does deadwood structure temperate forest bat assemblages? European Journal of Forest Research, 17.

Toms, J.D., Villard, M.-A., 2015. Threshold detection: matching statistical methodology to ecological questions and conservation planning objectives. Avian Conservation and Ecology 10, 8.

Trier, Ø.D., Salberg, A.-B., Kermit, M., Rudjord, Ø., Gobakken, T., Næsset, E., Aarsten, D., 2018. Tree species classification in Norway from airborne hyperspectral and airborne laser scanning data. European Journal of Remote Sensing 51, 336-351,.

Ullah, S., Dees, M., Datta, P., Adler, P., Schardt, M., Koch, B., 2019. Potential of Modern Photogrammetry Versus Airborne Laser Scanning for Estimating Forest Variables in a Mountain Environment. Remote Sensing 11.

Valbuena, R., Maltamo, M., Packalen, P., 2016. Classification of forest development stages from national low-density lidar datasets: a comparison of machine learning methods. Revista de Teledetección 45, 15-25.

Vepakomma, U., 2008. Spatiotemporal charaterlsation of gap dynamics and boreal forest responses using multi-temporal lidar data. Dissertation, UNIVERSITÉ DU QUÉBEC À MONTRÉAL, p. 202.

Vepakomma, U., 2012. Spatial contiguity and continuity of canopy gaps in mixed wood boreal forests: persistence, expansion, shrinkage and displacement. Journal of Ecology 100, 1257-1268.

Vepakomma, U., Kneeshaw, D., Fortin, M.-J., 2010. Interactions of multiple disturbances in shaping boreal forest dynamics: a spatially explicit analysis using multi-temporal lidar data and high-resolution imagery. Journal of Ecology 98 526-539.

Vierling, K.T., Swiftb, C.E., Hudak, A.T., Vogelerd, J.C., Vierling, L.A., 2014. How much does the time lag between wildlife field-data collection and LiDAR-data acquisition matter for studies of animal distributions? A case study using bird communities. Remote Sensing Letters 5, 185–193.

Vihervaara, P., Auvinen, A.-P., Mononen, L., Törmä, M., Ahlroth, P., Anttila, S., Böttcher, K., Forsius, M., Heino, J., Heliölä, J., Koskelainen, M., Kuussaari, M., Meissner, K., Ojala, O., Tuominen, S., Viitasalo, M., Virkkala, R., 2017. How Essential Biodiversity Variables and remote sensing can help national biodiversity monitoring. Global Ecology and Conservation 10, 43-59.

Virkkala, R., 2006. Why study woodpeckers? The significance of woodpeckers in forest ecosystems. Ann. Zool. Fennici 43, 82-85.

Vogel, S., Gossner, M.M., Mergner, U., Müller, J., Thorn, S., 2020. Optimizing enrichment of deadwood for biodiversity by varying sun exposure and tree species: an experimental approach. Journal of Applied Ecology n/a.

Vogeler, J.C., Cohen, W.B., 2016. A review of the role of active remote sensing and data fusion for characterizing forest in wildlife habitat models. Revista de Teledetección 45, 1-14.

Vogeler, J.C., Hudak, A.T., Vierling, L.A., Evans, J., Green, P., Vierling, K.T., 2014. Terrain and vegetation structural influences on local avian species richness in two mixed-conifer forests. Remote Sensing of Environment 147, 13–22.

Walankiewicz, W., Czeszczewik, D., Tumiel, T., Stański, T., 2011. Woodpeckers abundance in the Białowieża Forest – a comparison between deciduous, strictly protected and managed stands. Ornis Polonica 52, 161-168.

Wang, Z., Ginzler, C., Waser, L.T., 2015a. A novel method to assess short-term forest cover changes based on digital surface models from image-based point clouds. Forestry: An International Journal of Forest Research 88, 429-440.

Wang, Z., Waser, L.T., Ginzler, C., 2015b. A novel method to assess short-term forest cover changes based on digital surface models from image-based point clouds. Forestry, 1-12.

Waser, L., Küchler, M., Jütte, K., Stampfer, T., 2014a. Evaluating the Potential of WorldView-2 Data to Classify Tree Species and Different Levels of Ash Mortality. Remote Sensing 6, 4515-4545.

Waser, L.T., Ginzler, C., Kuechler, M., Baltsavias, E., Hurni, L., 2011. Semi-automatic classification of tree species in different forest ecosystems by spectral and geometric variables derived from Airborne Digital Sensor (ADS40) and RC30 data. Remote Sensing of Environment 115, 76-85.

Waser, L.T., Küchler, M., Jütte, K., Stampfer, T., 2014b. Evaluating the Potential of WorldView-2 Data to Classify Tree Species and Different Levels of Ash Mortality. Remote Sensing 6, 4515-4545.

Wegmann, M., Leutner, B., Dech, S.e., 2016. Remote Sensing and GIS for Ecologists: Using Open Source Software. Pelagic Publishing, Exeter, UK, p. 352.

White, J., Tompalski, P., Coops, N., Wulder, M., 2018. Comparison of airborne laser scanning and digital stereo imagery for characterizing forest canopy gaps in coastal temperate rainforests. Remote Sensing of Environment 208, 1-14.

White, J.C., Coops, N.C., Wulder, M.A., Vastaranta, M., Hilker, T., Tompalski, P., 2016. Remote Sensing Technologies for Enhancing Forest Inventories: A Review. Canadian Journal of Remote Sensing 42, 619-641.

White, J.C., Wulder, M.A., Vastaranta, M., Coops, N.C., Pitt, D., Woods, M., 2013. The Utility of Image-Based Point Clouds for Forest Inventory: A Comparison with Airborne Laser Scanning. Forests 4, 518-536.

Wickham, H., 2016. ggplot2: Elegant Graphics for Data Analysis. Springer Verlag, New York, p. 260.

Wickham, H., Chang, W., 2016. Package 'ggplot2'. Create Elegant Data Visualisations Using the Grammar of Graphics. R package version 2.2.1, ©RStudio; 2016. https://cran.r-project.org/web/packages/ggplot2/ggplot2.pdf (accessed on 14 April 2018).

Wing, B.M., Ritchie, M.W., Boston, K., Cohen, W.B., Olsen, M.J., 2015. Individual snag detection using neighborhood attribute filtered airborne lidar data. Remote Sensing of Environment 163, 165-179.

Wood, S., 2004. Stable and efficient multiple smoothing parameter estimation for generalized additive models. Journal of the American Statistical Association 99, 673-686.

Wood, S., Augustin, N.H., 2002. GAMs with integrated model selection using penalized regression splines and applications to environmental modelling. Ecological modelling 157, 157-177.

Wood, S.N., 2018. Package 'mgcv'. Mixed GAM Computation Vehicle with Automatic Smoothness Estimation. In. simon.wood@r-project.org.

Wrbka, T., Szerencisits, E., Peterseil, J., Thurner, B., Eds., 2015; SINUS Kulturlandschaft—Methoden.Kulturlandschaftskartierung. Abteilung für Vegetationsökologie und Naturschutzforschung. Institut für Ökologie und Naturschutz, UniversitätWien: Wien, Österreich. http://131.130.59.133/projekte/sinus/klkart10/methoden/kartierung.htm (accessed on 20 February 2015).

Wulder, M.A., Dymond, C.C., White, J.C., Leckie, D.G., Carroll, A.L., 2006. Surveying mountain pine beetle damage of forests: A review of remote sensing opportunities. Forest Ecology and Management 221, 27-41.

Wulder, M.A., White, J.C., Bentz, B., 2005. Detection and mapping of mountain pine beetle red attack: matching information needs with appropriate remotely sensed data. Proceedings of the Joint 2004 Annual General Meeting and Convention of the Society of American Foresters and the Canadian Institute of Forestry. . In. Society of American Foresters, Bethesda, Maryland, Edmonton, Alberta.

Yamamoto, S.-I., 2000. Forest Gap Dynamics and Tree Regeneration. Journal of Forest Research 5, 223-229.

Yao, W., Krull, J., Krzystek, P., Heurich, M., 2014. Sensitivity Analysis of 3D Individual Tree Detection from LiDAR Point Clouds of Temperate Forests. Forests 5, 1122-1142.

Yao, W., Krzystek, P., Heurich, M., 2012a. Identifying standing dead trees in forest areas based on 3D single tree detection from full waveform Lidar data. In, ISPRS Annals of the Photogrammetry. Remote Sensing and Spatial Information Sciences ISPRS, Melbourne, Australia, pp. 359-364.

Yao, W., Krzystek, P., Heurich, M., 2012b. Tree species classification and estimation of stem volume and DBH based on single tree extraction by exploiting airborne full-waveform LiDAR data. Remote Sensing of Environment 123, 368–380.

Zellweger, F., Baltensweiler, A., Ginzler, C., Roth, T., Braunisch, V., Bugmann, H., Bollmann, K., 2016. Environmental predictors of species richness in forest landscapes: abiotic factors versus vegetation structure Journal of Biogeography (J. Biogeogr.), 1-11.

Zellweger, F., Braunisch, V., Baltensweiler, A., Bollmann, K., 2013. Remotely sensed forest structural complexity predicts multi species occurrence at the landscape scale. Forest Ecology and Management 307, 303-312.

Zellweger, F., Braunisch, V., Morsdorf, F., Baltensweiler, A., Abegg, M., Roth, T., Bugmann, H., Bollmann, K., 2015. Disentangling the effects of climate, topography, soil and vegetation on stand-scale species richness in temperate forests. Forest Ecology and Management 349, 36-44.

Zellweger, F.M., F.; Purves, R. S.; Braunisch, V.; Bollmann, K., 2013. Improved methods for measuring forest landscape structure: LiDAR complements field-based habitat assessment. Biodiversity and Conservation 23, 289-307.

Zielewska-Büttner, K., Adler, P., Ehmann, M., Braunisch, V., 2016a. Automated Detection of Forest Gaps in Spruce Dominated Stands Using Canopy Height Models Derived from Stereo Aerial Imagery. Remote Sensing 8 (3).

Zielewska-Büttner, K., Adler, P., Ehmann, M., Braunisch, V., 2017. Erratum: Zielewska-Büttner, K.; Adler, P.; Ehmann, M.; Braunisch, V. Automated Detection of Forest Gaps in Spruce Dominated Stands Using Canopy Height Models Derived from Stereo Aerial Imagery. Remote Sens. 2016, 8, 175. Remote Sensing 9 (5), 1-2.

Zielewska-Büttner, K., Adler, P., Peteresen, M., Braunisch, V., 2016b. Parameters Influencing Forest Gap Detection Using Canopy Height Models Derived From Stereo Aerial Imagery. In: Kersten, T.P. (Ed.), 3. Wissenschaftlich-Technische Jahrestagung der DGPF. Dreiländertagung der DGPF, der OVG und der SGPF. . Publikationen der DGPF, Bern, Schweiz, pp. 405-416.

Zielewska-Büttner, K., Heurich, M., Müller, J., Braunisch, V., 2018. Remotely Sensed Single Tree Data Enable the Determination of Habitat Thresholds for the Three-Toed Woodpecker (Picoides tridactylus). Remote Sensing 10, 1-25.

Zielewska, K., 2012. Ips Typographus. Ein Katalysator für einen Waldstrukturenwandel. WSG Baden-Württemberg 15, 19-42.

Zimmermann, S., Hoffmann, K., 2017. Accuracy Assessment of Normalized Digital Surface Models from Aerial Images Regarding Tree Height Determination in Saxony, Germany. PFG – Journal of Photogrammetry, Remote Sensing and Geoinformation Science 85, 257-263.